

INFORMATION TO USERS

This manuscript has been reproduced from the microfilm master. UMI films the text directly from the original or copy submitted. Thus, some thesis and dissertation copies are in typewriter face, while others may be from any type of computer printer.

The quality of this reproduction is dependent upon the quality of the copy submitted. Broken or indistinct print, colored or poor quality illustrations and photographs, print bleedthrough, substandard margins, and improper alignment can adversely affect reproduction.

In the unlikely event that the author did not send UMI a complete manuscript and there are missing pages, these will be noted. Also, if unauthorized copyright material had to be removed, a note will indicate the deletion.

Oversize materials (e.g., maps, drawings, charts) are reproduced by sectioning the original, beginning at the upper left-hand corner and continuing from left to right in equal sections with small overlaps.

Photographs included in the original manuscript have been reproduced xerographically in this copy. Higher quality 6" x 9" black and white photographic prints are available for any photographs or illustrations appearing in this copy for an additional charge. Contact UMI directly to order.

ProQuest Information and Learning
300 North Zeeb Road, Ann Arbor, MI 48106-1346 USA
800-521-0600

UMI[®]

University of Alberta

**Solvent Uptake and Swelling by a PS-DVB Column Packing
and Metal Ion Speciation by Microdrop Solvent Extraction**

by

Ying Wang



**A thesis submitted to the Faculty of Graduate Studies and Research in partial
fulfillment of the requirements for the degree of Doctor of Philosophy**

Department of Chemistry

Edmonton, Alberta

Fall 2000



**National Library
of Canada**

**Acquisitions and
Bibliographic Services**

**395 Wellington Street
Ottawa ON K1A 0N4
Canada**

**Bibliothèque nationale
du Canada**

**Acquisitions et
services bibliographiques**

**395, rue Wellington
Ottawa ON K1A 0N4
Canada**

Your file Votre référence

Our file Notre référence

The author has granted a non-exclusive licence allowing the National Library of Canada to reproduce, loan, distribute or sell copies of this thesis in microform, paper or electronic formats.

The author retains ownership of the copyright in this thesis. Neither the thesis nor substantial extracts from it may be printed or otherwise reproduced without the author's permission.

L'auteur a accordé une licence non exclusive permettant à la Bibliothèque nationale du Canada de reproduire, prêter, distribuer ou vendre des copies de cette thèse sous la forme de microfiche/film, de reproduction sur papier ou sur format électronique.

L'auteur conserve la propriété du droit d'auteur qui protège cette thèse. Ni la thèse ni des extraits substantiels de celle-ci ne doivent être imprimés ou autrement reproduits sans son autorisation.

0-612-59693-1

Canada

University of Alberta

Library Release Form

Name of Author: Ying Wang
Title of Thesis: Solvent Uptake and Swelling by a PS-DVB Column
Packing and Metal Ion Speciation by Microdrop
Solvent Extraction
Degree: Doctor of Philosophy
Year this Degree Granted: 2000

Permission is hereby granted to the University of Alberta Library to reproduce single copies of this thesis and to lend or sell such copies for private, scholarly or scientific research purposes only.

The author reserves all other publication and other rights in association with the copyright in the thesis, and except as herein before provided, neither the thesis nor any substantial portion thereof may be printed or otherwise reproduced in any material form whatever without the author's prior written permission.




19B, 15-8, Tong Zhi Jie
Changchun, Jilin
P.R.China 130061

Date: Sept. 29, 2000


University of Alberta

Faculty of Graduate Studies and Research

The undersigned certify that they have read, and recommended to the Faculty of Graduate Studies and Research for acceptance, a thesis entitled Solvent Uptake and Swelling by a PS-DVB Column Packing and Metal Ion Speciation by Microdrop Solvent Extraction submitted by Ying Wang in partial fulfillment of the requirements for the degree of Doctor Philosophy.



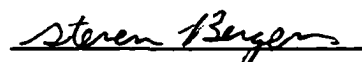
Dr. Frederick F. Cantwell



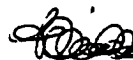
Dr. Gary Horlick



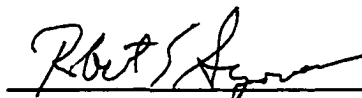
Dr. Norman J. Dovichi



Dr. Steve H. Bergens



Dr. Len Wiebe



Dr. Robert E. Synovec

Date: Sept. 29, 2000

Abstract

This work consists of two parts. Part I, from Chapter 1 to Chapter 4, studies the solvent uptake and swelling by a PS-DVB column packing; Part II, from Chapter 5 to Chapter 9 investigates a novel metal ion speciation technique using microdrop solvent extraction.

It has been realized that not only the surface of the polymer matrix of the polymeric HPLC packing materials is involved in the chromatographic behavior, but also the bulk mass of the polymer matrix itself. The purpose of Part I of the present work is to investigate the process by which “good” solvents such as THF enhance the column efficiency. The sorbent Hamilton PRP- ∞ is employed because it is nominally non-porous and therefore can represent the polymer matrix. The combined experimental results of solvent uptake and swelling by PRP- ∞ reveal that the interaction between THF and the permanent micropores in PS-DVB polymer matrix gives rise to the increase of sample diffusion and thereby good chromatographic performance.

Based on a previously developed micro-drop solvent extraction technique^{1,2} the objective of Part II of the present work is to explore the feasibility of a new metal speciation technique, which can be applied to speciation studies in the presence of kinetically labile species.

In this work a 1 μ L solution of a metal-chelating extractant, Lix63, in n-octane is employed as the organic phase suspended at the tip of a microsyringe needle in a stirred aqueous solution. Therefore, free-metal species that can complex with the metal-chelating agent in n-octane are extracted into the organic drop. The analysis of this organic drop by

ICP/MS with a direct sample insertion device (DSID) then provides a measure of the free metal ion species.

Perturbation is an inherent problem in speciation studies in the presence of kinetically labile species, which requires that the analysis procedure should not disturb the original equilibrium in the system. The conventional perturbation problem caused by the removal of analyte from the aqueous phase due to the extraction is essentially eliminated in micro-drop extraction as used in this work. However, the unwanted extraction of the Lix63 into aqueous phase, due to the small organic/aqueous phase ratio required by the micro-extraction system, and/or to inadequate hydrophobicity of the extractant, introduces an additional source of perturbation.

In this work, a perturbation model was established, which embodies criteria for perturbation conditions including the kinetic contribution resulting from not waiting until equilibrium is reached. This perturbation model permits a quantitative prediction of the extent of perturbation for a given combination of the experimental parameters. The experimental data corrected by using the perturbation model were in good agreement with the theoretical data.

¹ Jeannot, Michael A.; Cantwell, Frederick F. *Anal. Chem.* 1997, 69, 235-239.

² Jeannot, Michael A.; Cantwell, Frederick F. *Anal. Chem.* 1997, 69, 2935-2940.

**This thesis is dedicated to my wonderful parents
Their love and their faith in me are the driving forces of
my entire Ph.D. study**

Acknowledgements

I would like to express my deep gratitude to my research supervisor, Dr. Frederick F. Cantwell, for his precious guidance throughout this work. I have benefited not only from his many helpful ideas and insightful suggestions for this work, but also from his rigorous approach in research and his understanding and caring character, which have set a good example for his students. I am also deeply grateful to the generosity of Dr. Gary Horlick for allowing the use of ICP/MS, without which the work of Part II would not be possible. Moreover, I would like to thank Barbara Ells for her work on the investigation of the effect of THF on sample sorption isotherms and kinetics, which is used in Part I of this thesis as a helpful aid in the discussion.

My gratitude also to my husband, Jeff Lu, who has given his love and full support during my entire Ph.D. study, especially, in my writing of the C language computer program presented in this work.

Finally, I would like to thank the Department of Chemistry at University of Alberta for financial assistance.

TABLE OF CONTENTS

	Page	
Chapter 1	Introduction to Part I	1
Chapter 2	Theory for Part I	
2.1	Polymerization and Polymer Structure of PS-DVB	7
2.2	Solubility Parameter and Solvent Effect on Polymer Structure	10
2.3	Sorption Isotherms and Capillary Condensation	11
2.4	Polymer Swelling	17
2.5	Sample Diffusion in Polymer Matrix	18
2.6	Activity Considerations	20
Chapter 3	Experimental Section for Part I	
3.1	Sorbent and Chemicals	26
3.2	Apparatus	26
3.2.1	Isotherm and Polymer Density Measurement	26
3.2.2	Polymer Swelling Measurement	31
3.3	Measurement Procedures	33
3.3.1	Measurement of Hold-up Volume	33
3.3.2	Measurement of Polymer Density	34
3.3.3	Measurement of Sorption Isotherm	35
3.3.4	Measurement of Polymer Swelling	36
3.4	Optimum Experimental Conditions	40

Chapter 4	Results and Discussion for Part I	
4.1	Solvent Sorption Isotherms	44
4.2	Polymer Swelling	47
4.3	Swelling <i>versus</i> Solvent Sorption	50
4.4	Effect of THF on Sample Sorption Isotherms and Sample Sorption Kinetics	53
4.5	Summary of the Effect of THF on Polymer Matrix	54
4.6	Conclusions and Future Work	59
Chapter 5	Introduction to Part II	
5.1	Metal Speciation	61
5.1.1	Role of Metal Speciation	62
5.1.2	Methods for Metal Speciation	63
5.1.3	Lability of Metal Species	65
5.1.4	Non-Perturbing Speciation Techniques	66
5.1.4.1	Computational Methods	66
5.1.4.2	Electroanalytical Methods	66
5.1.4.3	Ion Exchange Methods	70
5.1.4.4	Extraction Methods	71
5.1.4.5	Electrospray Mass Spectrometry	74
5.2	Metal Solvent Extraction and Chelating Extractant Lix63	75
5.3	Solvent Micro-extraction Techniques	78
5.4	Direct Sample Insertion Device for ICP/MS	82
5.5	Objective of the Present Work	86

Chapter 6	Theory for Part II	
6.1	Introduction	88
6.2	Equilibrium Consideration	88
6.2.1	Equilibria in Metal Solvent Extraction Systems and Criteria for Speciation Measurement	88
6.2.2	Relationship between $[ML_2]_o$ and $C_{M,aq}$	93
	6.2.2.1 EDTA, Glycine and Citrate Systems	93
	6.2.2.2 Phthalate System	96
6.2.3	Calibration Curve	97
6.3	Discussion of Perturbation at Equilibrium	100
6.4	Extraction Kinetics	108
6.4.1	Extraction Regime and Its Identification	109
6.4.2	Kinetic Considerations in the present work	111
	6.4.2.1 Chemical Kinetic Control	112
	6.4.2.2 Diffusional Control	117
6.5	Discussion of Perturbation Before Equilibrium	119
6.6	Calculation of Metal Species Distribution	125
Chapter 7	Characterization of Microdrop Solvent Extraction – Direct Sample Insertion (DSI) - ICP/MS	
7.1	Introduction	128
7.2	Experimental Section	128
	7.2.1 Chemicals	128
	7.2.2 Purification of Lix63	129

7.2.3	Reagents and Test Solution Preparation	132
7.2.4	Apparatus for Microdrop Solvent Extraction	133
7.2.5	Direct Sample Insertion Device for ICP	135
7.2.6	Experimental Procedures	136
7.3	Measurement by DSI – ICP/MS	137
7.3.1	Operating Conditions of DSI - ICP/MS	137
7.3.2	Choice of Internal Standard	139
7.3.3	Data Treatment and Calibration Curve	141
7.4	Investigation of Kinetic Mechanism	143
7.4.1	Effect of Stirring Speed and Organic Drop Size on Initial Rate	143
7.4.2	First Order Rate Curve Fit with Respect to Copper	147
7.4.3	Conclusions Regarding Extraction Kinetics	149
7.5	Extraction Calibration Curve	149
Chapter 8	Free Copper Ion Determination by Microdrop Solvent Extraction – DSI – ICP/MS in the Presence of Complexing Ligands	
8.1	Introduction	151
8.2	Experimental Section	151
8.2.1	Chemicals	151
8.2.2	Reagents	152
8.2.3	Preparation of Test Solutions	152
8.3	Results and Discussion	153
8.3.1	Free Copper Ion Determination in the Presence of EDTA	157

8.3.2	Free Copper Ion Determination in the Presence of Glycine, Phthalate, or Citrate	160
8.4	Conclusions	170
Chapter 9	Comments and Future Work for Part II	
9.1	Comments	172
9.2	Future Work	173
	Bibliography	175
Appendix 1	Size of blue dextran molecule	189
Appendix 2	Comparison of the real particle size and particle image size	190
Appendix 3	C Program for Calculation of Metal Species Distribution	195
Appendix 4	Macro for ICP/MS Data Treatment	201
Appendix 5	Data for Figures	203

LIST OF TABLES

Tables	Page
4.1 The effect of THF on swelling	50
4.2 The results of the sorption of THF by PRP- ∞	57
6.1 Constants used in the calculation of copper species distribution	127
7.1 Parameters used for DSI-ICP/MS	138
8.1 Average f values	157
8.2 Comparison of theoretical data and experimental data corrected by Perturbation Factor ($X = \text{Glycine}$)	168
8.3 Comparison of theoretical data and experimental data corrected by Perturbation Factor ($X = \text{Phthalate}$)	169
8.4 Comparison of theoretical data and experimental data corrected by Perturbation Factor ($X = \text{Citrate}$)	169
A2.1 Schematic diagram of image formation in a microscope	192
A2.2 Light spot in microscope fitted with $\times 3.5$ objective	193
A2.3 Schematic diagram for calculation	194

LIST OF FIGURES

Figures	Page
2.1 PRP- ∞ polymerization process	9
2.2 Polymer structure change in solvent	12
2.3 Giles's sub-classification of L-type isotherm	13
2.4 Cylindrical capillary pore	16
2.5 Change in activity coefficients with change in weight-volume concentrations in aqueous solution for MeOH (A) and THF (B)	24
2.6 Change in mole fraction with change in weight-volume concentrations in aqueous solution for MeOH (A) and THF (B)	25
3.1 Column equilibration set-up	27
3.2 Column	28
3.3 Degassing equipment	30
3.4 Flow-through cell for polymer swelling measurement	32
3.5 The image of particle under high power microscope	38
3.6 Loading curve	41
3.7 Elution curve	42
3.8 Swelling curve	43
4.1 Sorption isotherm for MeOH (A) and THF (B) on PRP- ∞ using Solution phase activities	45
4.2 Swelling of PRP- ∞ produced by the sorption of MeOH (A) and THF (B) at different solution phase activities.	49
4.3 Swelling produced by sorbed volume of MeOH on PRP- ∞	51
4.4 Swelling produced by sorbed volume of THF on PRP- ∞	52
4.5 Sample sorption isotherm of naphthalene on PRP- ∞ from different	

	Compositon solvents	55
4.6	Sample sorption rate curves of naphthalene on PRP- ∞ from different Compositon solvents	56
5.1	Diagram of basic component of set-up for DSI-ICP/MS	84
5.2	Schematic diagram of DSI	85
6.1	Equilibrium Perturbation Factor versus Log $K_{f, MX'}$ at the various values of $C_{X, aq} / C_{M, aq}$	103
6.2	Equilibrium Perturbation Factor versus Log $K_{f, MX'}$ at the various values of $K_{f, ML}^+ [L]$	104
6.3	Equilibrium Perturbation Factor versus Log $K_{f, MX'}$ at the various values of $\log K_2$	105
6.4	Perturbation Factor versus Log (1-exp(- $k_{SAMP} t$)) for EDTA system	121
6.5	Perturbation Factor versus Log (1-exp(- $k_{SAMP} t$)) for glycine system	122
6.6	Perturbation Factor versus Log (1-exp(- $k_{SAMP} t$)) for citrate system	123
6.7	Perturbation Factor versus Log (1-exp(- $k_{SAMP} t$)) for phthalate system	124
7.1	Microdrop solvent extraction apparatus	134
7.2	Modified graphite electrode	136
7.3	Typical ICP/MS signals of Cu^{63} and internal standard Ga^{69}	140
7.4	Typical calibration curve on ICP/MS	142
7.5	Initial rate curves with varying stirring speeds	144
7.6	Initial rate curves with varying organic drop size	145
7.7	Plot of initial rate vs. stirring speed and organic drop size	146
7.8	First order rate curve fitting	148
7.9	Extraction calibration curve	150
8.1	Effect of EDTA on free copper determination	158

8.2	Perturbation Factor versus $\text{Log } K_{f, \text{Cu-X}'}$ at the various values of $C_{\text{EDTA, aq}} / C_{\text{Cu, aq}}$	159
8.3	Effect of glycine on free copper determination	162
8.4	Perturbation Factor versus $\text{Log } K_{f, \text{Cu-X}'}$ at the various values of $C_{\text{glycine, aq}} / C_{\text{Cu, aq}}$	163
8.5	Effect of phthalate on free copper determination	164
8.6	Perturbation Factor versus $\text{Log } K_{f, \text{Cu-X}'}$ at the various values of $C_{\text{phthalate, aq}} / C_{\text{Cu, aq}}$	165
8.7	Effect of citrate on free copper determination	166
8.8	Perturbation Factor versus $\text{Log } K_{f, \text{Cu-X}'}$ at the various values of $C_{\text{citrate, aq}} / C_{\text{Cu, aq}}$	167

List of Symbols and Abbreviations

a_1	Activities
A_{12}	Constants from the literature, eq. 2.7
A_{21}	Constants from the literature, eq. 2.7
AN	Acetonitrile
ASV	Anodic stripping voltammetry
C_1	Weight-volume concentrations of organic modifier in aqueous solution (g/mL)
$C_{b,f}$	Concentration of blue dextran in the eluate, eq. 3.1
$C_{L,o}$	Concentration of total extractant L species in organic phase
C_m	Concentration of the organic solution, eq. 3.1
$C_{M,aq}$	Concentration of total metal species in aqueous phase
$C_{m,E}$	Concentration of organic modifier in the eluate, eq. 3.3 (g/mL), eq. 3.3
$C_{m,S}$	Concentration of organic modifier sorbed per gram of PRP- ∞ (g/g), eq. 3.3
$C_{o,e}$	Concentration of extracted copper at equilibrium
$C_{o,t}$	Concentration of extracted copper at time t
$C_{X,aq}$	Concentration of total ligand X species in aqueous phase
CME	Chemically modified electrode
D	Diffusion coefficient of a solute in the polymer matrix in the presence of solvent, eq. 2.4
D_p	Diffusion coefficient of a solute in in the dry polymer matrix, eq. 2.4
DBC	Dibenzo-18-crown-6
E_i^v	Molar cohesive energy, eq. 2.1

f	Constant defined in eq. 8.5
F	Fraction of the equilibrium amount of sample sorbed at time t ; eq. 2.3
G_{12}	Constants from the literature, eq.2.7
G_{21}	Constants from the literature, eq.2.7
HDEHP	Di-(2-ethylhexyl) phosphoric acid
HMDE	Hanging mercury drop electrode
ISE	Ion selective electrode
k	Chemical reaction rate constant
K_1	Constant defined in eq. 6.6
K_2	Constant defined in eq. 6.6a
K_a	Acid dissociation constant
K_f	Formation constant
K_f'	Conditional formation constant
LLE	Liquid-liquid extraction
m	An integer, eq. 2.3
m_1	Molar masses of organic modifier, eq. 2.11
m_2	Molar masses of water, eq. 2.11
	Gram molecular weight of the organic modifier, eq. 3.4
MB	Methylene blue
MeOH	Methanol
n_{gel}	Sorption capacities of the gel region, eq.2.5 and 2.6
n_t	Moles of sample sorbed per dry gram of PRP- ∞ at time t , eq. 2.3
n_{μ}	Sorption capacities of the micropore region, eq.2.5 and 2.6

n_{∞}	Moles of sample sorbed per dry gram of PRP- ∞ at equilibrium, eq. 2.3
N_{av}	Avogadro's number
NA	Naphthalene
p	Saturation vapor pressure within the pore, eq. 2.2
p_0	Saturation vapor pressure of the solvent on a flat surface, eq. 2.2
PF	Perturbation Factor
PS-DVB	Poly(styrene-divinylbenzene)
r	Radius of the particle, eq. 2.3
r_p	Radius of a straight capillary pore, Figure 2.4
R_g	Gas constant
SPE	Solid phase extraction
SPME	Solid phase micro-extraction
t	time
T	Temperature
TFE	Thin mercury-film electrode
THF	Tetrahydrofuran
V	Molar volume
V_1	Initial volume of the organic modifier, eq. 2.10
V_2	Volume of water (g)
V_{aq}	Volume of aqueous phase
V_b	Volume of the volumetric flask, eq. 3.1
V_{mix}	Volume of the mixture of water and organic modifier (g)
V_o	Volume of organic phase

$V_{o,m}$	Hold-up volume of the system, eq. 3.1
\bar{v}_m	Volume of one molecule of organic modifier
ΔV_p	Volume change per gram of PRP- ∞ , eq. 3.1
W_1	Weight of the organic modifier (g), eq. 2.10
W_2	Weight of water (g)
α_x	Fraction of component X
β	Cumulative formation constant
χ_1	Mole fraction of the organic modifier, eq.2.7
χ_2	Mole fraction of water, eq.2.7
δ	Solubility parameter, eq. 2.1
γ	Surface tension, eq. 2.2
γ_1	Activity coefficient of the organic modifier, eq.2.7
κ	Distribution coefficient
λ	Ratio of the hindrance parameters, eq. 2.4
θ	Contact angle, Figure 2.4
θ	Ratio of tortuosities, in the presence and absence of solvent, eq. 2.4
ρ_1	Density of the pure modifier, eq. 2.10
ρ_2	Density of pure water, eq. 2.11
ρ_{mix}	Density of the solution, eq. 2.13
$\rho_{PRP-\infty}$	Density of PRP- ∞
τ_{12}	Constants from the literature, eq.2.7
τ_{21}	Constants from the literature, eq.2.7

Chapter 1

Introduction to Part I

Reversed-phase high performance liquid chromatography (RP-HPLC) is a mode of HPLC, which utilizes a non-polar stationary phase and a polar mobile phase. It is the most widely applied mode among modern liquid chromatography techniques.¹ Stationary phase materials employed in RP-HPLC include silica-based packings, polymer-based packings, graphitized carbon packing materials, charge-transfer-type packing materials, and so on,² among which silica-based and polymer-based packing materials are the most commonly used. Although a polymeric packing material was employed in the first application of modern liquid chromatography back in 1954,³ its use is not as popular as silica-based packing materials, which were introduced commercially in the mid-1970s and have dominated the HPLC field ever since. This is because silica-based packings have good mechanical strength, good chromatographic performance, and a large range of particle size, pore size, surface modifications and surface areas.⁴ However, there is increasing interest in polymeric packings in HPLC in recent years due to the following reasons: first, improvements in making modern polymeric packing materials have been made, such as improvement in polymer rigidity;⁵ second, more applications are developed for these packing materials; and third, their retention characteristics are becoming better understood.

The polymeric packing materials are conventionally employed as alternatives for silica-based packings, where silica-based packings have certain limitations. These limitations include the lack of stability in aqueous mobile phases with high pH, the poor column efficiency and column-to-column variability for their applications to basic compounds, due to the presence of residual silanols on their particle surface,⁴ and the lack of compatibility with the biological activities of some proteins.⁶ Polymeric packing materials possess the advantages of chemical inertness and the homogeneity of the hydrophobic surface due to the absence of strong binding sites, such as silanol groups.

They also exhibit exceptional lot-to-lot reproducibility. Furthermore, a wide variety of surface modifications of polymeric materials to give phase ranging from hydrophobic to hydrophilic is possible.^{7, 8} In addition to these advantages, there are selectivity differences from that of silica-based packings, and higher capacity for sample, which are also reasons for the choice of polymer-based packings in HPLC.⁶

Polymeric packing materials for HPLC are commercially prepared by suspension polymerization, a technique in which the polymerization reaction takes place in organic droplets suspended in water.⁹ The organic droplets mainly contain: (1) a mono-functional monomer; (2) a poly-functional monomer, also called cross-linking agent, the amount of which determines the cross-linking degree of the polymer, and consequently, the mechanical rigidity and physical flexibility of the polymer; (3) an initiator for the polymerization, and (4) sometimes, a diluent, which is also called a "porogen". The commonly used monomers are styrene, vinyl alcohol, alkyl methacrylate, hydroxylalkyl methacrylate, hydroxylalkyl acrylate, and so on.⁶ The most prominent poly-functional monomer is divinylbenzene.

Benson and Woo⁵ have classified the polymeric structures of the polymer-based packings into two types: microporous and macroporous, in terms of whether or not the "porogen" has been employed in the course of synthesis of the packing materials. The "porogen" is a compound soluble in the monomer and insoluble in the polymer. When there is "porogen" present in the organic droplets during suspension polymerization, the resultant polymer will contain large voids or pores due to the spaces taken by the inert "porogen" diluent in the course of polymerization. This technique of making so-called macroporous polymers was discovered during the 1950's and was developed to be able to control the nature of the pore structure in the synthesis process during the 1960's.^{10, 11, 12, 13, 14} Most of the commercially available polymeric packings are of this type. The porosity of the polymer is determined by the crosslinking degree, which is in turn determined by the amount of crosslinking monomer added in the polymerization process. The less the crosslinking monomer is utilized, the larger the spaces between polymeric chains, and the softer the polymer. In a single macroporous polymer bead, there are

permanent macro- and mesopores, which are separated by solid polymer matrix. Macro- and meso- pores have widths $\geq 50\text{nm}$ and between 2nm and 50nm , respectively.¹⁵

If the polymer bead is composed of polymer matrix alone without large pores (macro- and mesopores), then it is usually called a non-porous polymer. The non-porous polymers are synthesized without using the “porogen”. However, porosity is a term of relative meaning. In this case, the non-porous polymers also contain so-called micropores ($\leq 2\text{nm}$)¹⁵, which are the spaces between polymeric chains, and this type of polymer is called a microporous polymer. The existence of these micropores has been proven by size exclusion chromatography¹⁶ and their pore size distributions have been measured by nitrogen adsorption.¹⁷ It has been gradually realized that not only the surface of the polymer matrix (or walls of the large pores) is involved in the chromatographic behavior, but also the bulk mass of polymer matrix itself (micropores).^{16,18}

Poly(styrene-divinylbenzene) (PS-DVB) copolymers are synthesized by copolymerizing styrene with divinylbenzene as the crosslinking agent. Since the first synthesis of PS-DVB by Moore in 1964,¹⁹ PS-DVB and modified PS-DVB packing materials have been used for organic phase gel permeation chromatography.²⁰ More recently they have been used for reversed phase chromatography,²¹ and have since become by far the most popular stationary phases for RP-HPLC among all the polymeric packings. The development of PS-DVB packing materials has primarily focused on the improvement of polymer rigidity and column efficiency.⁶ The previous type of PS-DVB, namely Amberlite XAD-2 and XAD-4, are semirigid gels, which were ground into irregular particles and then sieved for use in HPLC. From the late 1970's on, major improvements have been made in the development of modern PS-DVB. The problem of pressure instability has been overcome and the column efficiency has also been improved. More reliable commercial PS-DVB packings have since appeared, such as the PRP series (Hamilton, Reno, Nevada, U.S.A.), including PRP- ∞ , PRP-1, PRP-2 and PRP-3; the PLRP-S series (Polymer Laboratories, Church Stretton, U.K.); the Shodex series (Showa Denko, Tokyo, Japan); and Finepak Gel (JASCO, Tokyo, Japan). All of

them except for PRP- ∞ are macroporous polymers. PRP- ∞ is a nominally non-porous polymer.²²

As for other polymeric packing materials, PS-DVB packings have been primarily applied in RP-HPLC when the separation of analytes on silica-based packings experiences difficulty due to the presence of silanols. The types of analytes which interact with silanols include a wide range of compounds, particularly the relatively polar samples such as phenols, carboxylic acids and organic amines.^{23, 24, 25} Another feature of PS-DVB packing, which has certainly broadened its application, is that the phenyl rings can be derivatized to produce cation or anion exchange functionality,⁷ or to produce special functional groups so as to gain compatibility for biologically active samples.^{22, 26, 27} PS-DVB packings have thus been widely used with biological samples, such as proteins,²⁸ peptides,²⁹ and pharmaceuticals.^{30, 31, 32} The non-porous PRP- ∞ and C₁₈ alkylated PRP- ∞ have been applied to the separation of plasmids, nucleic acids, DNA fragments and oligonucleotides.^{33, 34, 35, 36}

While PS-DVB packings have all the aforementioned advantages, they suffer from the disadvantage of yielding lower chromatographic efficiencies than silica-based reversed phase packing materials of the same particle size. Since aromatic compounds, especially, polynuclear aromatic hydrocarbons (PAHs) have shown severe tailing on PS-DVB in RPLC, the strong interaction of π -electrons in the polymer with the solute was often accepted as the reason for the peak asymmetry.⁵ However, alkyl-type packing materials without aromatic functionality have also shown asymmetric chromatographic peaks for PAHs of a certain size.^{37, 38} In addition, structural features of the sample compounds such as planarity and rigidity also influence column efficiency.^{16, 39} Moreover, it has been found⁴⁰ that the surface area of PS-DVB packings was not associated with the sorption capacity. There is extra sorption that takes place in addition to the usual process of adsorption onto the walls of larger pores (macropores).^{16, 41, 42} Furthermore, the peak tailing is not correlated with the capacity factor, k' , of the solute,⁴³ while it does show solvents and temperature dependence.^{16, 43} The solvents that have solubility parameters (δ) more comparable to that of PS-DVB (i.e. $\delta=18.6$ -

$19.0(\text{MPa})^{1/2}$)^{39,44} provide better separation efficiency than do those with very different δ .³⁹ And also, the composition of the aqueous/organic mobile phase can have a significant effect on the extent to which excessive bandbroadening and tailing occur with PS-DVB packings.^{7, 18,39,45,46,47} It is known that for the three commonly used organic modifiers, the tail-suppressing effect increases and are thus often marked from “poor solvent” to “good solvent”, in the order: methanol (MeOH) < acetonitrile (AN) < tetrahydrofuran (THF), for which the solubility parameters (δ) are 29.7, 24.7, and 18.6 (MPa)^{1/2}, respectively.^{16, 48,49} For comparison, $\delta = 47.9$ for water¹⁶ which is a non-sorbed solvent in RPLC. It was found⁴⁵ that all the compounds gave poor column efficiencies with PRLP-S in MeOH-water, while the separation in AN-water and THF-water gave much better efficiencies and peak shapes. It has also been found the use of a ternary mixture of water, a “poor” solvent, and even a small amount of a “good” solvent with δ near that of PS-DVB, such as 5% THF in methanol/water, can significantly improve the observed peak shape.⁴³

All these phenomena can be understood by taking the distinctive polymer structure into account. Most of the PS-DVB polymer used as reversed phase sorbents in LC are in the “macroporous” polymer category, as discussed earlier. It is commonly accepted that the low column efficiency is due to slow diffusion of solute molecules within the polymer matrix.^{6,16, 21, 39, 43, 41, 50,51} It has generally been inferred that it is solvent-induced swelling of the polymer matrix by adsorbed “good” solvent that is responsible for decreases in sample peak bandwidth and tailing, because diffusion of the sample compound is less hindered in the swollen polymer.^{39,43, 45, 46, 47} In addition, “selective binding” of the “good” solvent by micropores, which would otherwise bind the sample compound, has been proposed as an additional reason for improved sample peak shape.³⁹ Therefore, the study of the polymer matrix in terms of its solvation and swelling property may reveal the chromatographic performance characteristics of PS-DVB packing.

The purpose of the present first four chapters is to investigate the process by which “good” solvents such as THF enhance the column efficiency. The sorbent

Hamilton PRP- ∞ is employed because it is nominally non-porous and is composed of only polymer matrix, free of macropores.⁴¹ Binary and ternary aqueous/organic solvent mixtures are used which contain MeOH and /or THF as the organic modifier. The following relationships are measured: equilibrium sorption isotherms of the solvent components MeOH and THF from aqueous solution, and equilibrium swelling of PRP- ∞ as a function of the concentrations of MeOH and THF in aqueous solution.

Chapter 2

Theory for Part I

2.1 Polymerization and Polymer Structure of PS-DVB

As described earlier, PS-DVB copolymers are synthesized by suspension polymerization of vinyl monomers and divinyl crosslinkers in water.^{52,53,54} Normally present in the suspension are also the polymerization initiator, the solvent- and porogen-diluents, and some other agents for buffering, stabilizing and so on. After being initiated, the polymerization proceeds in a large number of organic droplets under stirring. The presence of divinylbenzene as the crosslinker in the synthesis process results in a three dimensional network which forms the rigid skeleton of the polymer. Whether or not permanent pores are present, their pore size, and their geometry can be controlled by whether or not a diluent is used and by the choice of the diluent. Polymers such as PRP- ∞ , which are synthesized in the absence of both solvent- and porogen- diluents, are considered to be composed of a solid, nominally non-porous matrix.

Figure 2.1 is a diagram of the synthesis process of PRP- ∞ proposed on the basis of polymerization literature.^{14,52,53,55,56,57,58} At an early stage, polymerization of the PS and DVB monomers yields many highly crosslinked nuclei (Figure 2.1a). The reactivity ratio for copolymerization of styrene and divinylbenzene is somewhat lower than unity.⁵⁹ In other words, divinylbenzene with two functional groups is more reactive than styrene with only one functional group. This will result in an initially formed polymer which is preferentially rich in divinylbenzene, while the polymer formed later is rich in styrene. Hence, the resulting polymer matrix will be rather heterogeneous in nature. As polymerization proceeds, these nuclei gradually grow larger and larger, while the crosslinking degree decreases gradually due to the faster depletion of the more reactive DVB crosslinkers. Hence, there is a crosslinking gradient existing around each nucleus. And the nuclei are covalently connected to one another in the lower crosslinked chains.

(Figure 2.1b) During the polymerization, within the forming polymer beads, the two monomers act as the solvent and fully solvate the precipitated polymer chains at the early stage. The monomers (solvent) is progressively removed as it becomes converted into the polymer. This results in entanglement among the growing chains (Figure 2.1c).

In the final stage of the polymerization process, as the last portion of monomers are removed by polymerization, the initially solvated and consequently expanded polymer network collapses (Figure 2.1d). It is apparent that the regions of a lower degree of crosslinking, which is associated with a larger flexibility of structure, are easier to collapse than regions of higher crosslinking degree. However, this last collapsing step in the polymerization process is reversible. Since the network was originally formed in a solvating environment, with the addition of a good solvating agent, it would be able to re-expand from the collapsed state to the swollen state.

Since the polymerization is initiated at random, the crosslinking process must be very complex. It is unavoidable that some vinyl groups of divinylbenzene remain unreacted after polymerization, particularly for the polymer with a high degree of crosslinking.¹⁶ Therefore, the finally formed PRP- ∞ particle has the following described structure^{12,16,56,57,60}: throughout the polymer particle is a very large number of very small and closely spaced nuclei. The crosslinking density and chain entanglements are highest within the nuclei and decrease with distance from the nuclei. Thus, there is a gradient of crosslinking density from the center of each nucleus to the inter-nuclear region. Regions of the matrix having higher crosslinking density contain larger and more numerous permanent spaces between the chains, i.e., the permanent micropores. Regions with lower crosslinking density are called gel.

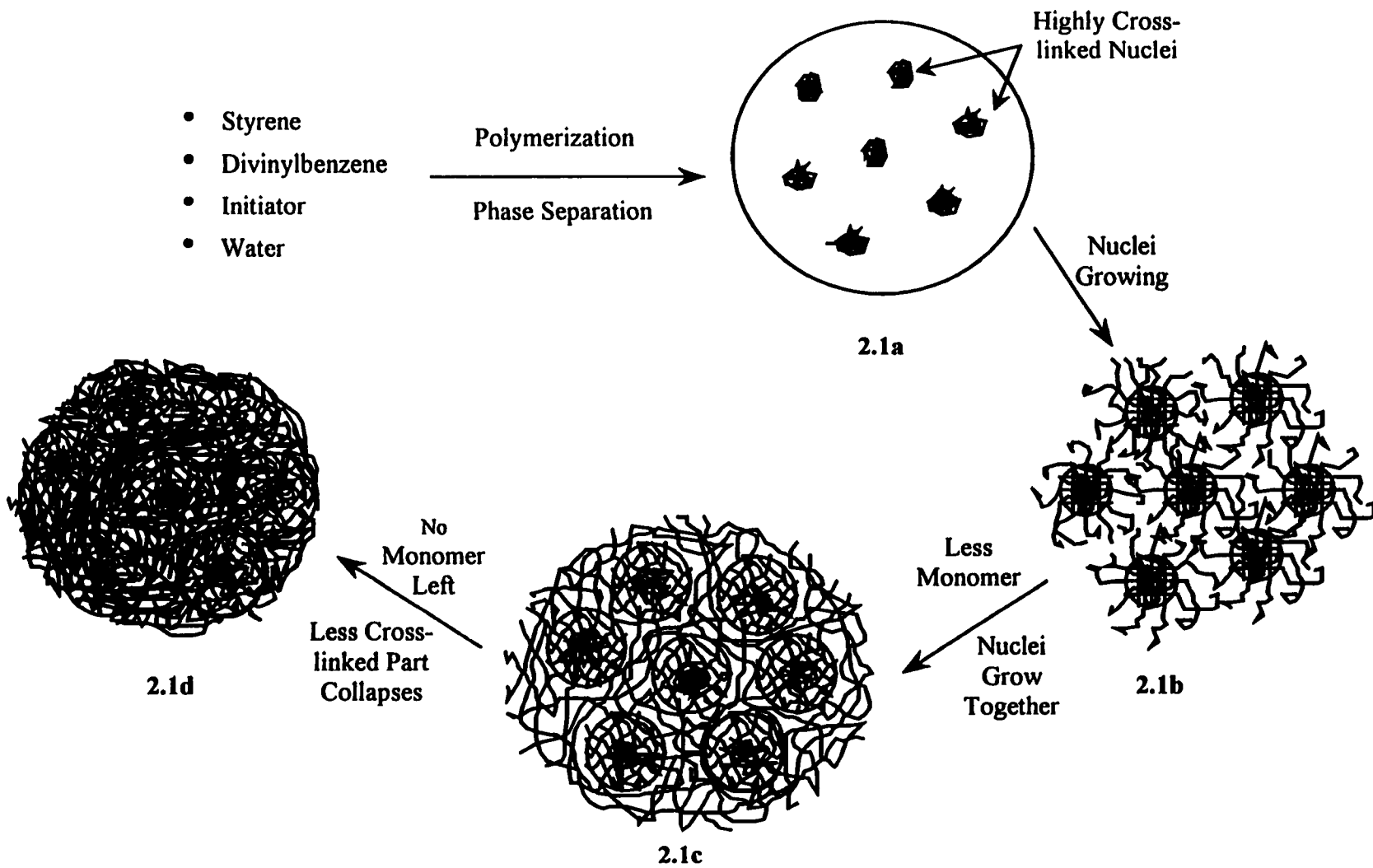


Figure 2.1 PRP-∞ polymerization process

2.2 Solubility Parameter and Solvent Effect on Polymer Structure

The solubility parameter, δ , of a substance is defined in the equation:

$$\delta_i = \left(\frac{-\Delta E_i^v}{V_i} \right)^{1/2} \quad (2.1)$$

where $-E_i^v$ is molar cohesive energy and V_i is molar volume.^{61, 62} The solubility parameter indicates the ability of a substance to participate in dispersion, dipole and hydrogen bonding interactions, and is one of the most useful concepts in polymer science for predicting solvents, swelling agents and additives for polymeric material.⁶³ If the solubility parameter of a reagent is close to that of the polymer, such as is the case with THF and PS-DVB, the reagent is a good solvent for the polymer and is able to extensively swell the polymer. On the other hand, in a poorly solvating system in the presence of a reagent with a solubility parameter not close to that of the polymer, as methanol with respect to PS-DVB, the reagent is not able to completely wet the polymer and swelling in the polymer is minimal.

Polymer swelling depends not only on the swelling ability of the solvent, but also the structural characteristics of the polymer itself. The different regions of a polymer matrix behave differently in good solvents, as shown in Figure 2.2. The highly crosslinked (micropore) regions have greater rigidity because they have entirely or partially lost the ability to move during polymerization even under solvating circumstances, due to the high crosslinking and entanglement of polymer chains. Therefore, the network structure and polymer density of these highly crosslinked regions does not change much between a dry and a solvating environment. On the contrary, due to the weak elastic free energy⁶⁴ the structure of the gel regions is more flexible. In the dry state, with no sorbed organic solvent, the gel regions of the matrix collapse completely into a structure having the smallest possible spaces between the chains. While

in the solvent-swollen condition, the gel regions are extensively swollen and have larger inter-chain pore spaces than do the micropore regions that do not swell much.

2.3 Sorption Isotherms and Capillary Condensation

Sorption isotherms are a well-studied topic which has been included in many papers and books.^{65,66,67,68} A sorption isotherm describes the distribution of a sample between the adsorbed phase and the unadsorbed phase at a given temperature. In the case of liquid-solid adsorption, the sorption isotherm is usually plotted using the equilibrium concentration of the sample adsorbed on a solid sorbent versus the concentration of the sample in the liquid solution. The study of sorption isotherms may provide information about sample/sorbent interaction and maximum sample capacity of the sorbent, and the shape of the isotherm is of importance in diagnosing the process responsible for sample sorption.

In sorption of a sample solute from solution, the simultaneous sorption of the solvent from the same solution must have an influence on the sorption of the sample. Therefore, while the interest is normally focused on the sample sorption isotherm, attention also has to be drawn to the solvent sorption isotherm. In this work, the sorption isotherms of THF and MeOH, two commonly used HPLC solvents, were studied.

The liquid-solid isotherms have been classified in terms of their shape by Giles, *et al.*⁶⁹ The main classification has four types of isotherm: S-type (S shaped, with a concave curve at low concentration region), L-type (Langmuir, with a convex curve at low concentration region), H-type (high affinity between the adsorbate and adsorbent) and C-type (constant partition of the adsorbate between the solution and adsorbent, with a linear line at the low concentration region), which were classified based on the initial slope of the isotherm. The sub-classification of each type, based on the isotherm shape at higher concentrations, has also been made by the same authors.⁶⁹ The Langmuir type isotherm is most common by far in liquid-solid adsorption systems of chromatographic interest. Giles's sub-classification of Langmuir type isotherm is shown in Figure 2.3.

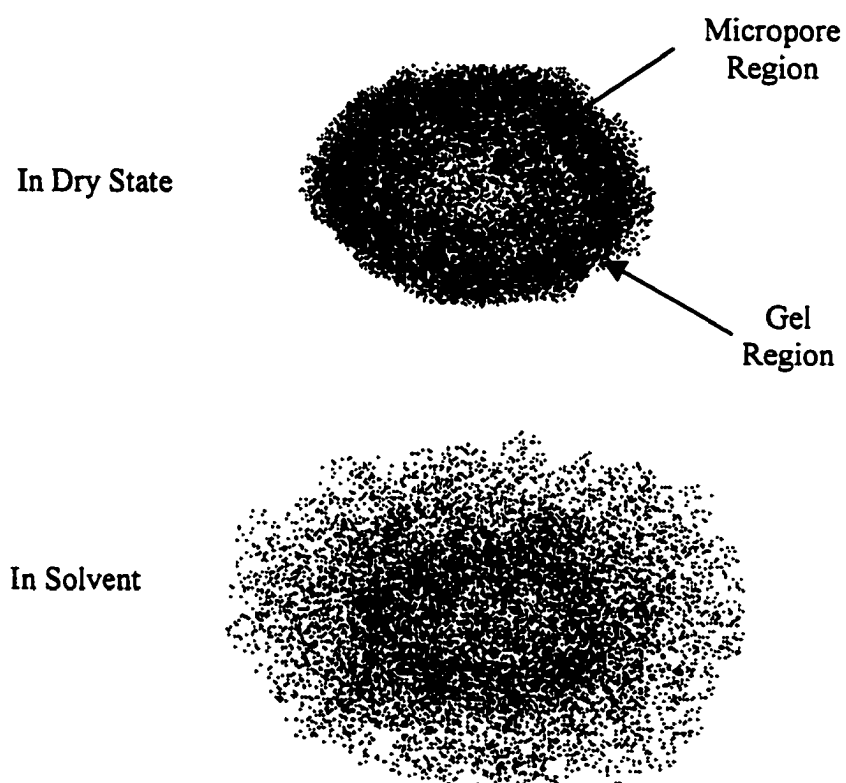


Figure 2.2 Polymer structure change in solvent

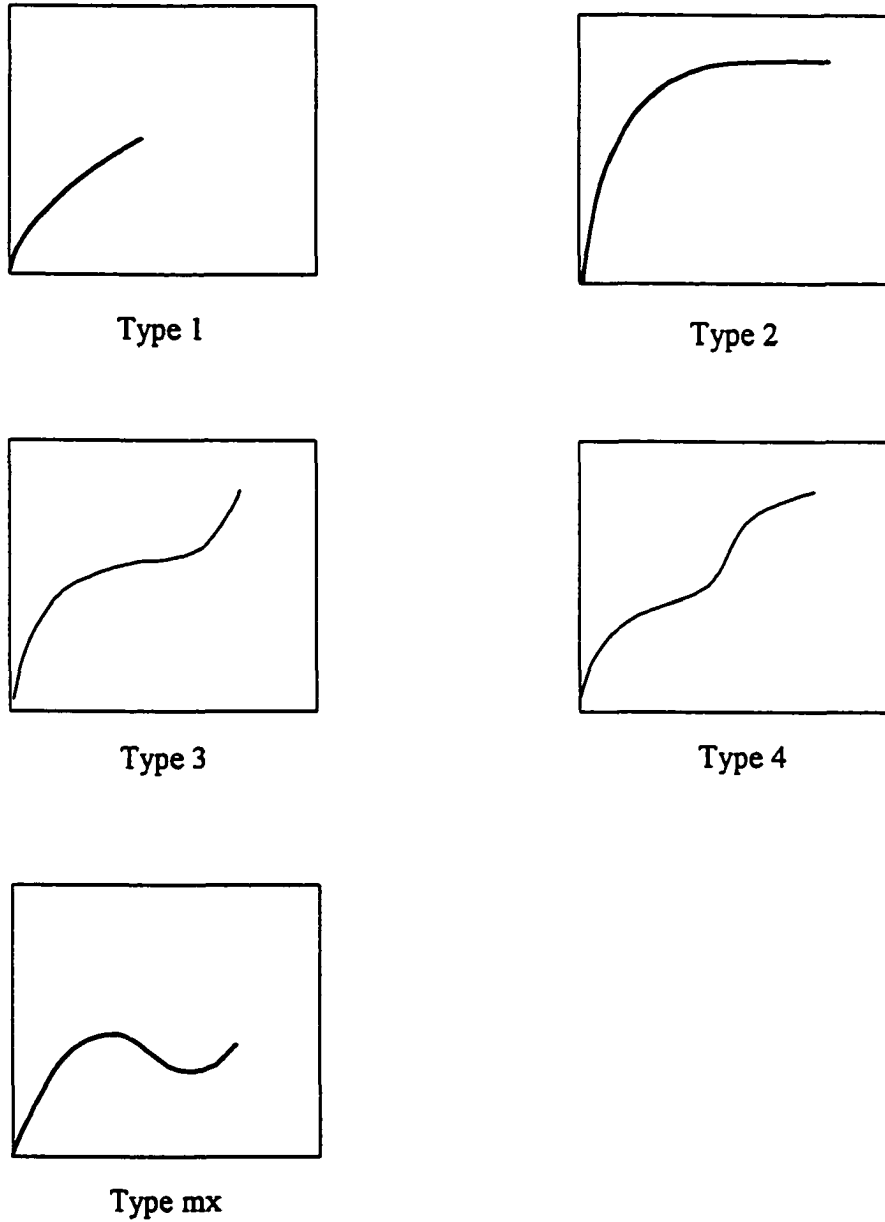


Figure 2.3 Giles's sub-classification of L-type isotherm
(The x-axes are the concentrations of the solute in liquid phase; y-axes are the concentrations of the adsorbed solute in solid phase.)

For adsorption in gas-solid systems, Brunauer, *et al.*, have described five basic isotherm types (type I to V).⁶⁵ In this classification, type III and V have a concave curve in low concentration region as in Giles's S-type isotherm, and type I, II and IV have a similar shape and may be compared to type 2, type 3 and type 4 in Giles's L-type isotherm, respectively.

In Figure 2.3, type 1 and type mx are very uncommon types of isotherms, and thus will not be discussed here. Type 2 isotherms occur when monolayer adsorption is distinctly favored over multilayer adsorption, in which case, the sample can be adsorbed onto the sorbent surface in amounts up to a monolayer. After the monolayer is completely uptaken by the sample, the sorption reaches its equilibrium as indicated by the leveling off of the isotherm. In other cases, when the monolayer becomes more and more crowded, the adsorbed sample molecules may not only interact with the sorbent, but also interact significantly with their neighbor molecules within the layer. A densely occupied monolayer will act in some degree as an extension of the sorbent, and will be able to attract more sample molecules. As a consequence, an adsorbed layer may become several molecules thick, which is the so-called multilayer. As shown in Type 3 isotherms (Figure 2.3) the strong concave upward turning after the leveling off is due to the formation of a second layer of the adsorbed molecules. Type 4 isotherms are extensions of type 3 isotherms. Multilayer adsorption could result in capillary condensation in which the pores of a porous sorbent are gradually filled by condensed liquid, which will be discussed below.

The sorption of a sample on a sorbent could be the outcome of two main kinds of forces acting between the sorbent and the sample molecules: physical and chemical forces, which give rise to physical ("van der Waals") adsorption and chemisorption, respectively. The physical forces, which are the same in nature as the van der Waals forces, are those that bring about the condensation of a vapor to the liquid state.⁶⁸

In a porous sorbent there is a continuous adsorption progress in which the smaller pores become completely filled by condensed liquid, which is the process of capillary condensation. When it happens, it can be understood as filling. It has been found^{70,71} that the pressure difference cross a curved interface increases as the radius of the curvature decreases by the effect of surface tension. Thus, the vapor will condense in small capillary pores due to the reduction of saturation vapor pressure. The criteria for capillary condensation are embodied in the Kelvin equation.^{68,70,71}

$$\ln \frac{p}{p_0} = -\frac{2\gamma V \cos\theta}{r_p R_g T} \quad (2.2)$$

where p is the saturation vapor pressure within the pore, p_0 is the saturation vapor pressure of the solvent on a flat surface, γ is surface tension, V is the molar volume of the liquid, θ is the contact angle (Figure 2.4), r_p is the radius of a straight capillary pore (Figure 2.4), R_g is the gas constant, and T is temperature. The condition for capillary condensation to occur requires a low saturation vapor pressure within the pore. Accordingly, a solvent with larger surface tension and molar volume has a better chance for capillary condensation.

The capillary condensation will occur first in the finest pores, and then, as the pressure is progressively increased, wider and wider pores are filled until saturation is reached at which all pores are full.

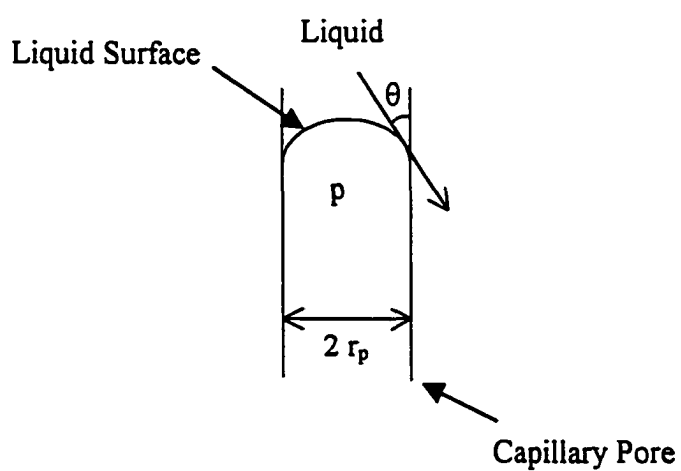


Figure 2.4 Illustration of the contact angle between the liquid and the wall of the pore (θ) and the saturation vapor pressure within the pore (p).

Sorption isotherms can be measured by equilibrium and non-equilibrium methods. The non-equilibrium methods can be accomplished by making use of the peak maxima or the breakthrough profiles of a chromatogram.^{72,73,74} The equilibrium methods include batch equilibrium and column equilibrium.^{51,75,76} In a batch equilibrium technique, typically, several mixtures with fixed quantities of the sorbent and water are placed in bottles along with various amounts of the sorbate compound, for a predetermined equilibration time in an agitated and thermostated environment. A portion of the aqueous phase is then withdrawn from each bottle and analyzed for the sorbate concentration, and the amount sorbed is calculated by material balance. In a column equilibrium technique, a sorbate solution is passed through the column until the sorbent packed in the column reaches equilibrium with the loading solution. Then, eluant without sample is used to elute the sorbed amount from the column for quantitation. In the present work a column equilibrium method was used (section 3.3.3).

2.4 Polymer Swelling

The degree of polymer swelling is determined by the balance between polymer rigidity and the overall affinity of the polymer for the solvent. Low cross-linking degree of the polymer and extensive solvating ability of the solvent favor swelling.⁶⁴ The solvation force, which is brought about by the difference of chemical potential of the solvent inside and outside the polymer matrix, is the driving force of swelling. On the other hand, as the swelling proceeds with more sorption, each segment between cross-linked junctions of the polymer is completely associated with solvent molecules so that the segments are forced to form elongated configurations to enlarge their volume space.⁷⁷ During this process, the elastic retraction in the polymer network increases until the balance between the solvation force and the elastic force is reached.

A variety of experimental techniques has been described in the literature to measure the dependence of swelling of polymeric sorbent particles on mobile phase solvent composition.^{42,46,57,78,79,80,81,82,83} The classic and most commonly used techniques involve the gravimetric measurement⁷⁹ of the solvent uptake after centrifugation or the

measurement⁴² of the volume of a bed polymer beads before and after swelling. These techniques normally involve time-consuming procedures and often provide information of limited reliability owing to the human errors and low accuracy inherent in the procedures. The modern techniques for swelling measurement of polymer beads include the utilization of the microscope⁸² and more sophisticated electronic and/or photographic equipment⁸¹ to determine the volume of the individual polymer bead before and after swelling in the test solvent. Among all these techniques, only microscopy gives a direct measurement of physical change of a polymer particle size. And also, the microscopic measurement of individual particles may reveal behavior normally hidden in the averaged ensembles studied by conventional techniques. Therefore, microscopy is the technique employed in the present work.

2.5 Sample Diffusion in Polymer Matrix

If the spherical PRP- ∞ particle behaves as a homogeneous medium, then the rate of sample sorption can be described by the expression:^{41,84}

$$F = \frac{n_t}{n_\infty} = 1 - \frac{6}{\pi^2} \sum_{m=1}^{\infty} \frac{1}{m^2} \cdot \exp\left(-m^2 \cdot \pi \cdot \frac{D}{r^2} \cdot t\right) \quad (2.3)$$

in which F is the fraction of the equilibrium amount of sample sorbed at time t ; n_t and n_∞ are the moles of sample sorbed per dry gram of PRP- ∞ at time t and at equilibrium, respectively; m is an integer; r is the radius of the particle; and D is the diffusion coefficient of the sample within the particle. Although PRP- ∞ is actually heterogeneous, as indicated in section 2.1, the distances between the centers of the polymer nuclei are so small that an average value of D is adequate to describe diffusion.

The diffusion coefficient of a solute in the polymer matrix in the presence of solvent (D) can be related to that in the dry polymer matrix (D_p) by the equation:⁸⁵

$$D = \frac{D_p \lambda}{\theta} \quad (2.4)$$

where λ is the ratio of the hindrance parameters and θ is the ratio of tortuosities, in the presence and absence of solvent. Hindrance depends on the ratio of solute radius to pore radius.⁸⁶ Under swelling conditions this ratio decreases due to the enlargement of pores, so does the hindrance, which is reflected in equation 2.4 as an increase in λ . Swelling also reduces tortuosity, causing θ to get smaller, though only marginally so.⁸⁷

If, for simplicity, the continuum of crosslinking densities in the matrix is approximated by only two degrees of crosslinking, one representing all gel and one representing all permanent micropores, then the relative contributions to the hindrance and tortuosity can be defined by:

$$\lambda^{-1} \approx \frac{n_{gel} \lambda_{gel}^{-1} + n_{\mu} \lambda_{\mu}^{-1}}{n_{gel} + n_{\mu}} \quad (2.5)$$

and

$$\theta \approx \frac{n_{gel} \theta_{gel} + n_{\mu} \theta_{\mu}}{n_{gel} + n_{\mu}} \quad (2.6)$$

where n_{gel} and n_{μ} are the sorption capacities of the gel and micropore regions, respectively.

2.6 Activity Considerations

When a binary aqueous/organic solvent mixture is employed as a mobile phase, the organic modifier is selectively sorbed by the polymer. A plot of concentration sorbed against concentration in solution at a fixed temperature is the sorption isotherm of the modifier. Sorption occurs because of free energy and spatial changes which occur upon transfer of an organic modifier molecule from one phase into the other.⁸⁸ If it is desired to know how the contribution to sorption by the polymer phase alone differs at different points along the isotherm, it is necessary to plot activity of the modifier in the solution phase, rather than its concentration.⁸⁹

The activity coefficients (pure-solute state) for MeOH in MeOH/H₂O were calculated using Margules Equation.⁹⁰

$$\ln \gamma_1 = [A_{12} + 2(A_{21} - A_{12})\chi_1] \chi_2^2 \quad (2.7)$$

Where, γ_1 is the activity coefficient of the organic modifier; χ_1 is its mole fraction; χ_2 is the mole fraction of water; and A_{12} , A_{21} are constants from the literature.⁹¹ Activity coefficients for tetrahydrofuran (THF) in THF/H₂O were calculated using the NRTL Equation.⁹²

$$\ln \gamma_1 = \chi_2^2 \left[\tau_{21} G_{21}^2 / (\chi_1 + \chi_2 G_{21})^2 + \tau_{12} G_{12} / (\chi_2 + \chi_1 G_{12})^2 \right] \quad (2.8)$$

where the parameters G_{12} , G_{21} , τ_{12} and τ_{21} are constants obtained from the literature.⁹³ Among these constants, A_{12} , A_{21} , τ_{12} and τ_{21} are related to the difference between the interaction energy between the same molecules and that between the difference molecules;⁹⁴ and G_{12} and G_{21} are related to both the interaction energy and the nonrandomness parameters.^{92, 94}

Plots of γ_1 vs. weight-volume concentration in aqueous solution, C_1 , are shown in Figure 2.5 for both MeOH and THF. Activity coefficients express the deviation of the behavior of solution of mixed components from the behavior that would be expected of an ideal solution. The ideal solution is defined as one that follows Raoult's Law over the entire range of concentration.⁹⁵ In an ideal solution, the interactions among the molecules in the solution are all the same, and the activity coefficients are equal to 1. In real solution with more than one component, the various molecular interactions of different components usually cause deviation of the solution behavior from an ideal solution behavior. From Figure 2.5 we can see that in aqueous solution both MeOH and THF aqueous solutions exhibit positive deviation from ideal behaviors (activity coefficients are larger than 1). The positive deviation indicates repulsion of the organic solvent molecules exerted by solvent-water interaction.

Activities, a_1 , are obtained as the product:

$$a_1 = \gamma_1 \cdot \chi_1 \quad (2.9)$$

in which γ_1 are obtained from Figure 2.5 and χ_1 have to be calculated as shown in the following:

In binary solutions used in the present work, the weight-volume concentrations of organic modifier in aqueous solution, C_1 (g/mL), were obtained experimentally by diluting organic modifier of known weight, W_1 , to a known volume, V_{mix} , with water. The initial volume, V_1 , of the organic modifier having W_1 can be calculated using the density of the pure modifier, ρ_1 :

$$V_1 = \frac{W_1}{\rho_1} \quad (2.10)$$

while the volume, V_2 , and weight, W_2 , of water added for the dilution are unknown, because

$$V_1 + V_2 \neq V_{\text{mix}}$$

due to the volume change after mixing two liquids.

Since

$$x_1 = \frac{\frac{V_1 \rho_1}{m_1}}{\frac{V_1 \rho_1}{m_1} + \frac{V_2 \rho_2}{m_2}} \quad (2.11)$$

where ρ_2 is the density of pure water, and m_1 and m_2 are molar masses of organic modifier and water, respectively, then

$$x_1^{-1} = 1 + \frac{m_1 V_2 \rho_2}{m_2 V_1 \rho_1} = 1 + \frac{m_1}{m_2} \left(\frac{\frac{V_1 \rho_1 + V_2 \rho_2}{V_{\text{mix}}} - \frac{V_1 \rho_1}{V_{\text{mix}}}}{\frac{V_1 \rho_1}{V_{\text{mix}}}} \right) \quad (2.12)$$

Since the density of the solution, ρ_{mix} , is

$$\rho_{\text{mix}} = \frac{V_1 \rho_1 + V_2 \rho_2}{V_{\text{mix}}} \quad (2.13)$$

and

$$C_1 = \frac{V_1 \rho_1}{V_{\text{mix}}} \quad (2.14)$$

then, insertion of equation 2.13 and 2.14 into equation 2.12 yields:

$$\chi_1^{-1} = 1 + \frac{m_1}{m_2} \left(\frac{\rho_{\text{mix}} - C_1}{C_1} \right) \quad (2.15)$$

Reorganizing equation 2.15, we get

$$\chi_1 = \left[1 - \frac{m_1}{m_2} \left(1 - \frac{\rho_{\text{mix}}}{C_1} \right) \right]^{-1} \quad (2.16)$$

According to equations 2.13 and 2.14, in order to calculate ρ_{mix} , we need to know the relationship between V_{mix} and (V_1+V_2) , which can be figured out from information provided in the literature⁹⁶ on the volume change on mixing for MeOH-water and THF-water mixtures. As a consequence, the plots of χ_1 as a function of C_1 for both MeOH and THF aqueous solutions were generated as shown in Figure 2.6. The densities of pure organic solvents employed in the calculation for MeOH and THF are 0.7864 g/mL (25 °C) and 0.8811 g/mL (25 °C), respectively.⁹⁷

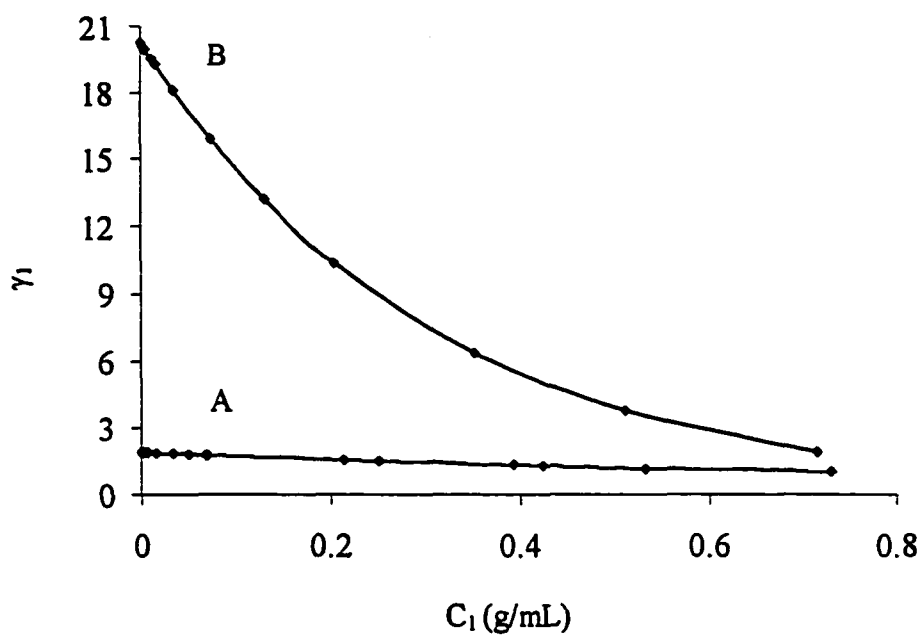


Figure 2.5 Change in activity coefficients with change in weight-volume concentrations in aqueous solution for MeOH (A) and THF (B)

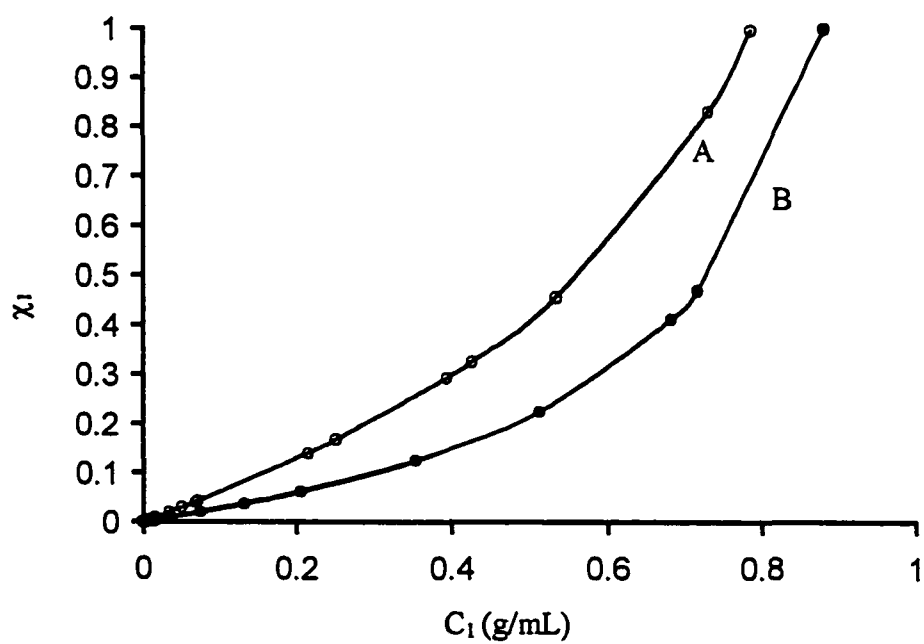


Figure 2.6 Change in mole fraction with change in weight-volume concentrations in aqueous solution for MeOH (A) and THF (B)

Chapter 3

Experimental Section for Part I

3.1 Sorbent and Chemicals

PRP- ∞ (Batch No:EE2, Hamilton, Reno, NV), a nominally nonporous PS-DVB copolymer having a spherical particle diameter of $19 \pm 1 \mu\text{m}$, was used. Water was distilled and deionized (Barnstead NANO pure system, Boston, MA). Blue Dextran (Sigma) as received, was dissolved in water. Tetrahydrofuran (THF) (Caledon Laboratories Ltd, Georgetown, Ont., Canada) and methanol (Fisher Scientific Co.) were both reagent grade. THF, methanol and water were filtered through a $0.45 \mu\text{m}$ pore size Nylon 66 filter (Mandel Scientific Co. Ltd., Guelph, Ont.) before use.

3.2 Apparatus

3.2.1 Isotherm and Polymer Density Measurement

Figure 3.1 is a schematic diagram of the set-up for the isotherm and polymer density measurements. The center of the set-up is the column as shown in Figure 3.2, which was made of glass, with stainless steel frits ($2 \mu\text{m}$ pore size, Chromatronix, Incorporated, Berkeley, California), Teflon sealing discs and polypropylene end fittings (Chromatronix, Incorporated). The PRP- ∞ particles of an accurately measured weight of about 0.08 gram were packed in the glass column by the "tap-fill" dry packing technique.

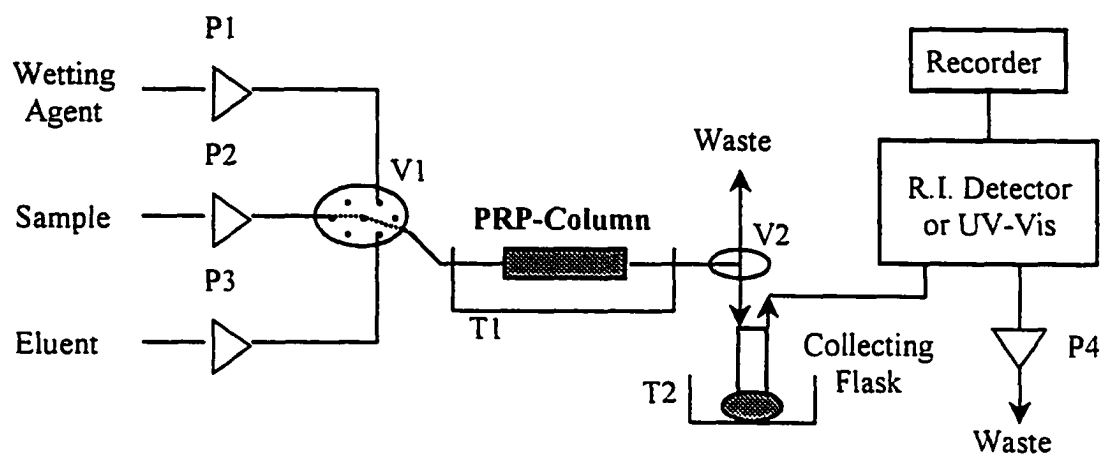


Figure 3.1 Column equilibration set-up

(P1, P2 and P3 are constant pressure pumps; P4 is a peristaltic pump;
 V1 is a six-port rotary valve; V2 is a three-port slider valve;
 T1 is a thermostated water bath was thermostated at 25°C;
 T2 is a water jacket circulated with the cold water circulating through
 the refractometer.)

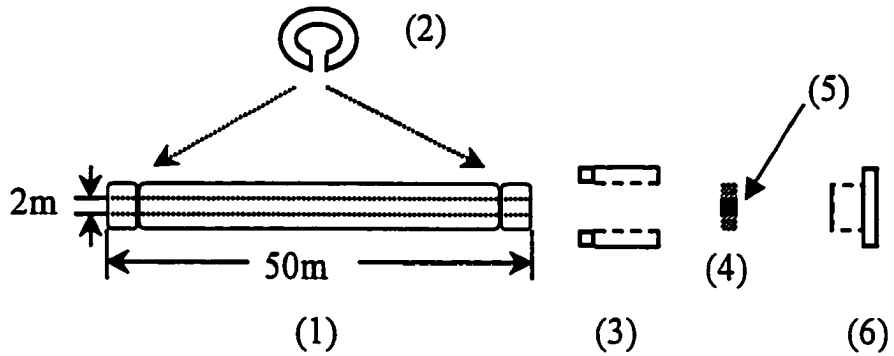


Figure 3.2 Column

Note: not to scale

- (1) Glass tube;
- (2) Plastic split-ring;
- (3) Plastic fitting with female thread;
- (4) Teflon sealing disc;
- (5) Stainless steel frit;
- (6) Plastic fitting with male thread

As shown in Figure 3.1, Teflon tubing was used to connect three constant pressure pumps with the inlet of the glass column, and to connect the outlet of the glass column with the detection system. The constant pressure pumps⁹⁸ functioned by placing the liquid containing bottles inside the aluminum cylinders, which were pressurized by Helium. The three pumps contained, respectively, the following: methanol, for initially wetting the dry PRP- ∞ ; the aqueous/organic solvent mixture of interest for equilibration with the PRP- ∞ ; and water, for eluting the sorbed organic modifier from PRP- ∞ .

After being degassed as shown in Figure 3.3 in fume hood, the solutions were placed in the aluminum cylinders of the pumps and then were pumped through the six-port rotary valve (Cheminert, R603LV3P) to reach the PRP- ∞ packed in the column, which is located in a thermostat (Lauda K4R, Brinkmann Instruments, Canada). The outlet of the column was connected to a three-port slider valve (Cheminert), which permitted the effluent from the column to be directed to waste, during the wetting and equilibration steps, or to a volumetric flask, during the elution step. The volume of the collecting flask was commensurate with the concentration of the eluting solutions, in order to meet the linear range of detection. The eluate in the collecting volumetric flask was mixed and then it was pumped through either a differential refractometric chromatographic detector (Series R-400, Water Associates, Inc.) for organic solvent component determination by a peristaltic pump (minipuls 2, Gilson) or a UV-VIS (HP8452) spectrophotometer for blue dextran.

The Teflon tubing between the rotary valve and the column and that between the column and the slider valve was 1/16 inch OD \times 0.3mm ID (Chromatographic Specialist Inc.), totally 23.5 cm long. The rest of the connection tubing in the system was 1/16 inch OD \times 0.5mm ID.

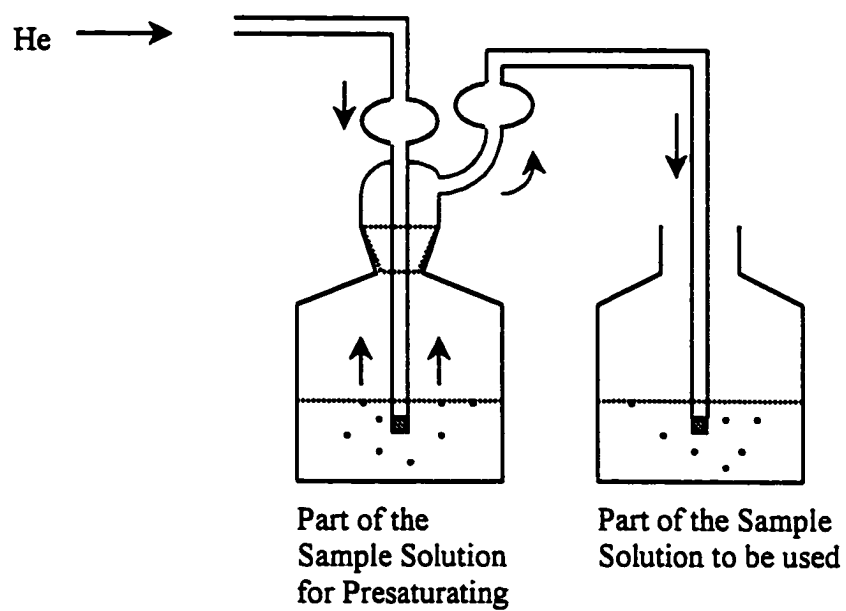
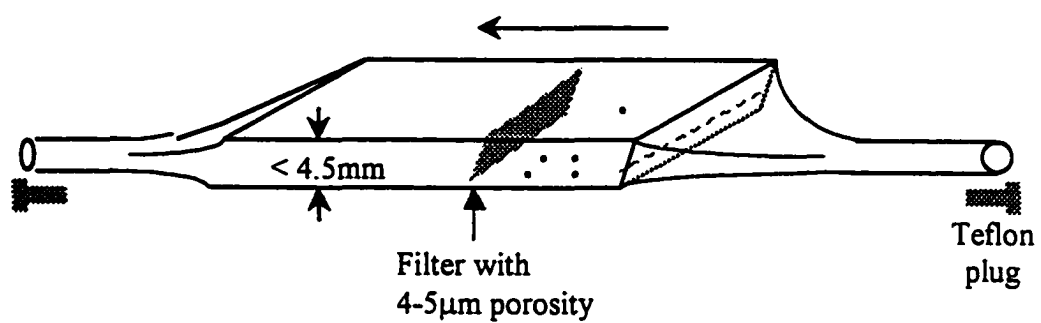


Figure 3.3 Degassing equipment

3.2.2 Polymer Swelling Measurement

Swelling of individual particles of PRP- ∞ was measured microscopically at room temperature in a flat flow-through cell (Figure 3.4), which was placed on the stage of a Leitz/Wetzlar Ortholux-Pol Microscope. The microscope was fitted with a 125 X reflective, long working distance (4mm) objective (Leitz, $\infty/0$, plan, L125 \times /0.80) and a 10 X eyepiece which contained a scale (Bausch & Lomb Opt. Co., USA). The smallest scale division corresponded to 0.7 μm so that the length could be estimated to $\pm 0.1 \mu\text{m}$. Transmitted light from an incandescent source was passed through a sub-stage condenser (Polarizing No.50f, NA0.85 and 1.40 swing-out top, five lens and two diaphragm).

As shown in Figure 3.4 the heart of the sample cell was made of two pieces of 2 mm thick boro-silica glass plates (Corning), fused together at the sides, leaving a 0.5 mm high space in between. A boro-silica glass filter of 4-5.5 μm pore size (Corning) was built into the cell. Two glass tubes (Corning) of 3 mm ID with removable Teflon plugs were fused to the ends of the cell. The distance from the inside bottom of the cell to the outside top of the cell was 2.5 mm, which met the need of a working distance of 4 mm, required by the objective.



- Represents particle

Figure 3.4 Flow-through cell for polymer swelling measurement

3.3 Measurement Procedures

3.3.1 Measurement of Hold-up Volume

In the measurement of both polymer density and sorption isotherm, a knowledge of the hold-up volume of the system is required. Hold-up volume is the volume between two valves (six-port rotary valve and three-port slider valve in Figure 3.1), which includes the volume in the connecting tubing between the column and the two valves and the inter-particle space within the column. Blue dextran, which has a M.W. of 2×10^6 g/mol and a smallest molecular dimension of approximately 18 nm (Appendix 1), was used in this work as the unretained component in the aqueous solution to measure hold-up volume.

It is required to measure hold-up volume for each different aqueous/organic solution. When the concentration of the organic solvent was low, hold-up volume was measured by a binary aqueous solution with a low concentration of blue dextran. The concentration of blue dextran, $C_{b,o}$, and the concentration of organic modifier, C_m , which is the same as in the loading solution of a given experiment, are known. This solution was pumped through the column until equilibrium was reached. By switching both the rotary valve and the slider valve (in Figure 3.1) pure water replaces the binary solution to elute the trapped solution in between the two valves to a collecting volumetric flask with volume V_b . The concentration of blue dextran in the eluate, $C_{b,f}$, was determined by a UV-VIS spectrometer. Thus, the hold-up volume of the system loaded with organic solution with concentration C_m , $V_{o,m}$, was calculated as:

$$V_{o,m} = \frac{C_{b,f} \cdot V_b}{C_{b,o}} \quad (3.1)$$

Blue dextran can not be dissolved in highly concentrated organic solutions. However, the swelling of PRP- ∞ in high concentrated organic solutions does change the

hold-up volume. In this case, the hold-up volume was measured by using blue dextran aqueous solution (without organic modifier) and corrected for microscopically measured polymer swelling. The following correction was made to obtain the hold-up volume, $V_{o,m}$, of the system loaded with organic solution of certain high concentration C_m , from the measured hold-up volume, $V_{o,w}$, of the system loaded with water alone:

$$V_{o,m} = V_{o,w} - \Delta V_{p,m} \cdot W_p \quad (3.2)$$

where ΔV_p is the unit volume change per gram of PRP- ∞ in organic solution of concentration C_m , and W_p is the weight of PRP- ∞ in the column.

3.3.2 Polymer Density Measurement

The density of dry PRP- ∞ was measured from the volume of aqueous blue dextran solution displaced by a known weight of PRP- ∞ . The measurement involved the following steps:

- Step 1. Determine the hold-up volume of the system with an empty column, $V_{o,e}$;
- Step 2. Weigh PRP- ∞ before it was packed in the column to get W_p ;
- Step 3. Determine the hold-up volume of the system with a packed column, $V_{o,p}$;
- Step 4. Calculate the volume of PRP- ∞ in the column, $V_p = V_{o,p} - V_{o,e}$;
- Step 5. Calculate the density of PRP- ∞ as,

$$\rho_{\text{PRP-}\infty} = W_p / V_p$$

The resultant density, which was used in the calculations throughout the present work, $\rho_{\text{PRP-}\infty} = 1.050 \pm 0.032$ g/mL, is the average of eight measurements, with a relative error of 3.1%.

3.3.3 Sorption Isotherm Measurement

The sorption isotherm measurements were accomplished by a “column equilibration” method, using apparatus shown in Figure 3.1, which require the following steps:

Step 1. *Column Packing Step* A mass, W_p (about 0.8 g, accurately measured to 0.1 mg), of dry PRP- ∞ was loosely packed into the glass column. The column was thermostatted at 25.0 ± 0.5 °C in a water bath.

Step 2. *Wetting Step* When a low concentrated organic solution was used, the dry polymer needed first to be wetted by methanol before the loading (equilibration) step took place.

Step 3. *Loading (Equilibration) Step* The loading solution of a known concentration of organic modifier C_m in water was pumped through the column of PRP- ∞ to reach sorption equilibrium.

Step 4. *Elution Step* By switching the rotary valve and the slider valve (in Figure 3.1), water as the eluent then replaced the loading solution and passed through the column to elute the organic modifier into a collecting volumetric flask of volume, V_E . The eluate was collected to volume.

Step 5. *Detection Step* The eluate in the volumetric flask was mixed and then pumped by a peristaltic pump through a differential refractometric chromatographic detector in order to measure the concentration, $C_{m,E}$ (g/mL), of organic modifier in the eluate. In the measurement of $C_{m,E}$, calibration curves of organic modifiers were generated by plotting the signal from the differential refractometric chromatographic detector vs the concentrations of the standard solutions. The linear calibration curve of MeOH had a slope of $(1.28 \pm 0.01) \times 10^4$ mL/g and an intercept of -2.49 ± 1.14 g/mL; the

linear calibration curve of THF had a slope of $(7.40 \pm 0.11) \times 10^4$ mL/g and an intercept of 1.19 ± 0.96 g/mL.

Conversion of $C_{m,E}$ (g/mL) into the concentration of organic modifier that had been sorbed per gram of PRP- ∞ , $C_{m,S}$ (g/g), can be calculated by the following equation with the aid of hold-up volume, $V_{o,m}$:

$$C_{m,S} = \frac{C_{m,E} \cdot V_E - C_m \cdot V_{o,m}}{W_p} \quad (3.3)$$

To facilitate later comparison with polymer swelling, $C_{m,S}$, was converted to the volume sorbed, $V_{m,S}$, by the equation:

$$V_{m,S} = \frac{C_{m,S} \cdot \bar{v}_m \cdot N_{av}}{\bar{M}_m} \quad (3.4)$$

in which \bar{M}_m is the gram molecular weight of the organic modifier, N_{av} is Avogadro's number, and \bar{v}_m is the volume of one molecule of organic modifier, as obtained from the software program Molecular Modeling (Windowchem Software Inc.).

3.3.4 Polymer Swelling Measurement

A suspension of PRP- ∞ particles in 10% methanol/water was prepared to a concentration of about 5 particles per droplet (approximate 0.05mL). Three droplets were transferred to the flow-through sample cell (Figure 3.4) by means of a Pasteur pipette at one end-tube of the cell with vacuum sucking at the other end. A similar technique was used to change solvents throughout the experiment, i.e., by connecting the front end-tube of the sample cell to the vacuum with the rear end-tube connected to the solvent reservoir. Because the particles tended to adhere to the inner surface of the glass cell

without being dislodged by the gentle flowing solvent, it was easy to keep track of the individual particles through many changes of solvent and microscopic measurements.

During the equilibration step, the solvent of interest was pumped slowly through the sample cell for an hour to guarantee that the particles had come to equilibrium with the solvent. The cell was then disconnected from the pump, the inlet and outlet tubes were plugged with Teflon stoppers, and it was placed on the stage of a microscope. The magnification was 125×10 . A condenser providing a focused beam of light was used for illumination. The image of a spherical object, reflected by oblique focused light, does not represent the very middle cross section of the object in size. It was however proved in Appendix 2 that the radius of the image circle was only 0.0045 % less than the real radius of the spherical object, so the difference is negligible. Therefore, the measurements of particle diameters were made directly from the observed images.

The image of a spherical object seen under microscope of high power is not a solid one, because of diffraction effects. Owing to the diffraction bands, difficulty was experienced in determining where the best focus is situated. When the operator moved the objective further and further away from the particle, the following changes in the image were observed (Figure 3.5): (1) Before the best focus: the foggy image became clearer and clearer, the center of the image became brighter and brighter, the edge of the image became sharper and sharper, and no fringes could be seen; (2) At the best focus: the edge of the image is the sharpest, and fringes still could not be seen; (3) After the best focus: a bright fringe first appeared by the edge of the image, and then more and more fringes became visible. Moreover, the fringes did not stay at the same positions, but moved towards the center of the image. In this work, the measured images were at step (2).



Figure 3.5 Images of a particle under high magnification (125×10)

The diameter of each particle in the horizontal plane was measured in four orientations as shown below, which were averaged in order to compensate for any slight deviations from perfect sphericity. The relative standard deviation of measurement in a given orientation was found to be 0.5% by a multiple focus/defocus technique⁸¹, i.e., when a sphere is focused on, the operator upsets the focus and then refocuses a total of three times, acquiring an image at each repetition.



Solvent composition was changed successively from low to high concentration for each organic modifier, MeOH and THF, in water. The diameter of the particle, d_m , observed in a given aqueous/organic solvent was converted to a fractional volume swelling, Q , by the equation:

$$Q = \left(\frac{d_m}{d_w} \right)^3 - 1 \quad (3.5)$$

where d_w is the diameter in pure water. The volume increment per unit dry mass of particles, ΔV_p , is given by:

$$\Delta V_p = \frac{Q \cdot \frac{4}{3} \cdot \pi \cdot \left(\frac{d_w}{2} \right)^3}{\rho_{PRP-\infty}} \quad (3.6)$$

in which $\rho_{PRP-\infty}$ is the density of dry PRP- ∞ as measured in section 3.3.2.

3.4 Optimum Experimental Conditions

Loading and elution times for the isotherm measurements were chosen to be 40 min. and 60 min., respectively, according to loading (Figure 3.6) and elution (Figure 3.7) curves, which were generated by using pure THF as the loading solution and 0.15 mL/min. flowing rate for both loading and elution. The time used to reach swelling equilibrium was chosen to be 60 min. according to the swelling equilibration curve (Figure 3.8), which was obtained by immersing polymer particles in pure THF for various time and then measuring their diameters.

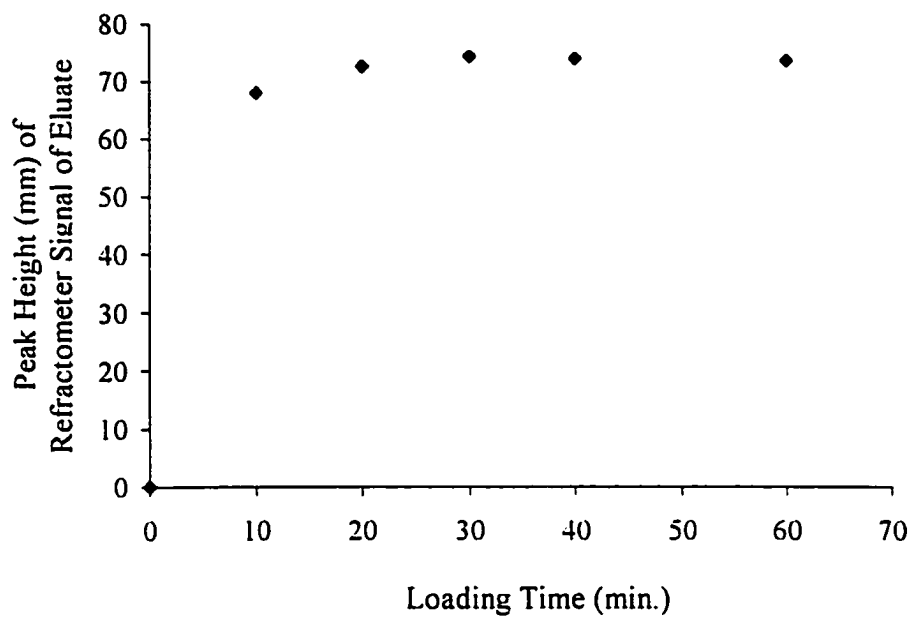


Figure 3.6 Loading curve of THF on PRP- ∞ column plotted as heights of eluted peak (see text) vs. loading time. Both loading and elution are at flow rate of 15 mL/min. Water both is thermostated at 25 C°.

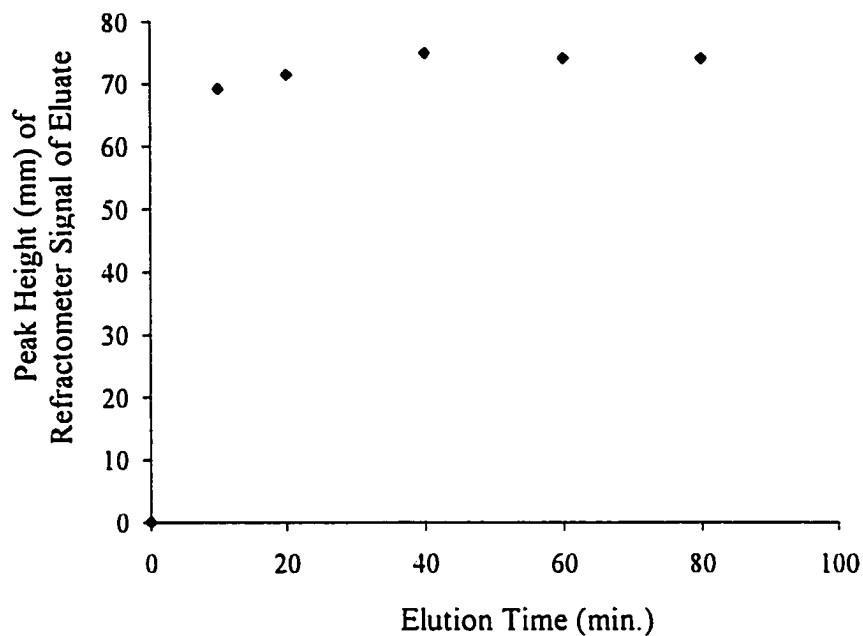


Figure 3.7 Elution curve of THF from PRP- ∞ column plotted as heights of eluted peak (see text) vs. eluting time. Both loading and elution are at flow rate of 15 mL/min. Water both is thermostated at 25 C°.

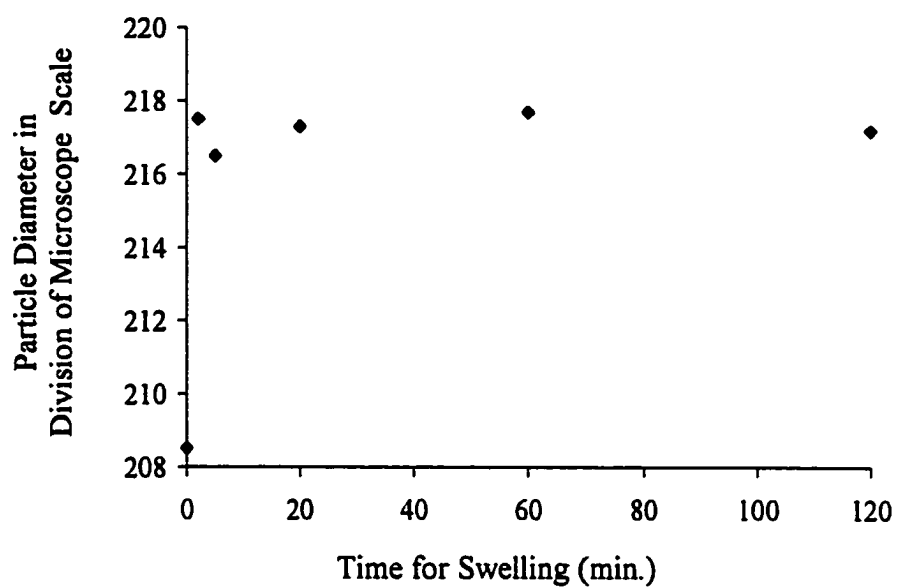


Figure 3.8 Swelling curve of PRP- ∞ in pure THF at room temperature

Chapter 4

Results and Discussion for Part I

4.1 Solvent Sorption Isotherms

Shown in Figure 4.1 are sorption isotherms for both organic modifiers, MeOH and THF, plotted as volume of organic modifier sorbed per gram of PRP- ∞ ($V_{m,S}$, mL/g) *versus* activity in solution ($a_{m,M}$). $V_{m,S}$ is calculated *via* equation (3.4), in which the values employed for the volume of one molecule of organic modifier, \bar{v}_m , were 3.26×10^{-23} mL/molecule for MeOH and 7.46×10^{-23} mL/molecule for THF. Although sorption isotherms are conventionally plotted *versus* solution concentration,^{42,99} the solution phase activities ($a_{m,M}$) have been used in order for the isotherm to reflect only processes occurring in the sorbent phase, because high solution concentrations of organic modifier sorbate are involved in the present work.

If MeOH and THF were adsorbed only on the outside of the 19 μm diameter particles, then on 1.00 g (i.e. 2.6×10^8 particles) of PRP- ∞ , a close-packed monolayer of these sorbates would contain only 5.6×10^{-5} mL/g for MeOH or 6.4×10^{-5} mL/g for THF. Since all of the experimental points in Figure 4.1 have values of $V_{m,S}$ that are far above these values, it is clear that most of the sorbed MeOH and THF are in the polymer particle rather than on the particle surface.

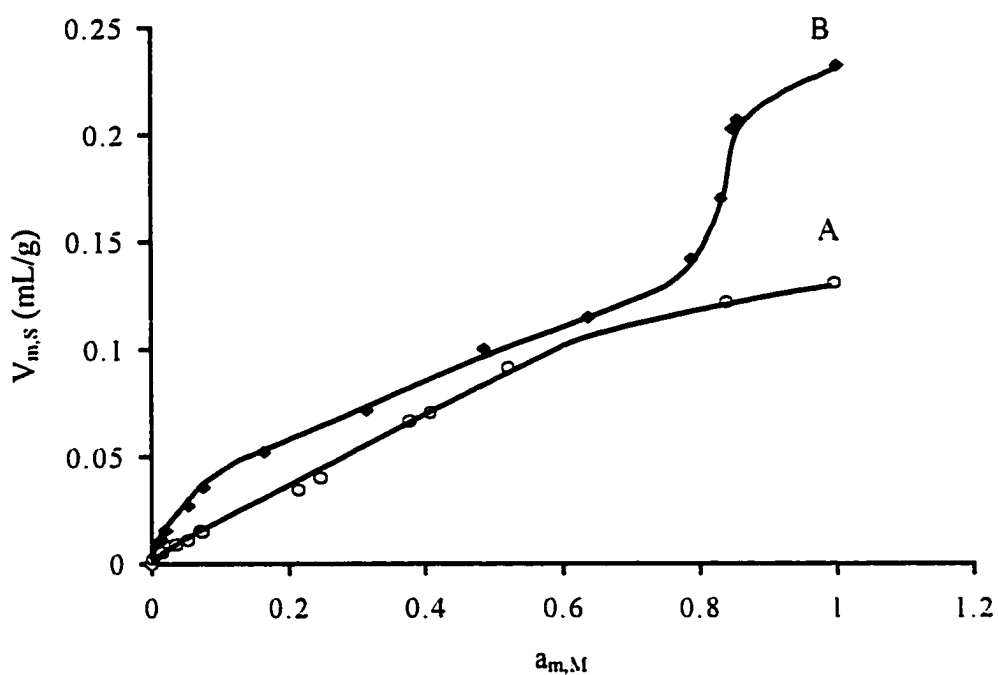


Figure 4.1 Sorption Isotherms for Methanol (A) and THF (B) on PRP- ∞ , using solution phase activities. Solid lines are empirical fits, by eye, to the data.

The isotherm of MeOH sorption, as shown in Figure 4.1 (curve A), is nearly linear up to a point with co-ordinates $V_{\text{MeOH,S}} \approx 0.1$ mL/g and $a_{\text{MeOH,M}} \approx 0.6$, above which it becomes convex and levels off at a limiting value of $V_{\text{MeOH,S}} = 0.13$ mL/g at $a_{\text{MeOH,M}} = 1.00$ (i.e. in pure MeOH). The isotherm of THF sorption, as shown in Figure 4.1 (curve B), is convex up to $a_{\text{MeOH,M}} \approx 0.8$ where $V_{\text{MeOH,S}} \approx 0.13$ mL/g. Above this point, the THF isotherm exhibits a strong upward concavity which persists to about $V_{\text{MeOH,S}} \approx 0.21$ mL/g, at which it again becomes convex and reaches its limiting value of $V_{\text{MeOH,S}} = 0.23$ mL/g at $a_{\text{MeOH,M}} = 1.00$ (i.e. in pure THF).

The overall shape of the THF sorption isotherm in Figure 4.1 (curve B) is similar in shape to the Type 4 isotherm of the Langmuir-Type in Giles's classification of liquid-solid isotherms, representing multilayer sorption, or to the Brunauer Type IV gas-solid isotherm that has been reported in the literature for adsorption of nitrogen gas on macroporous PS-DVB polymers.¹⁰⁰ In gas-solid adsorption from a single-component gas, the upward concavity followed by a leveling off is the result of multilayer adsorption in micropores and complete filling of these pores by capillary condensation.^{70,101} In the present work of liquid-solid sorption, capillary condensation of THF is possible because only one of the two components of the binary solvent/water mixture enters the polymer matrix.^{66,101,102}

The fact that a concave upturn is completely absent from the MeOH isotherm (Figure 4.1 (curve A)) implies a lack of multilayer sorption and capillary condensation of MeOH in the permanent micropores of PRP- ∞ . The different sorption behavior between MeOH and THF lies in the difference of their surface tensions and molar volumes, which determine whether capillary condensation can occur. During the sorption process, the permanent micropores are in equilibrium with the bulk solution and with the headspace above the bulk solution. The vapor pressure of the organic modifier above the bulk solution is directly proportional to its activity in the bulk solution. Taking into account this fact and the Kelvin equation (section 2.3), in which the criteria for capillary condensation are embodied, we have the expression:

$$\ln(\text{activity}) \propto \ln \frac{p}{p_0} = -\frac{2\gamma V \cos\theta}{r_p R_g T} \quad (4.1)$$

The molar volumes obtained from Molecular Modeling Program (Windowchem Software Inc.) for THF and MeOH are 81.1 cm³/mol and 40.7 cm³/mol, respectively. The surface tensions at 25°C are 26.40 dynes/cm for THF and 21.85 dynes/cm for MeOH.⁹⁷ According to equation (4.1), for a particular size pore, the higher surface tension and larger molar volume of THF mean that the activity in solution that is required for the onset of capillary condensation is lower for THF than for MeOH.

Therefore, in the THF sorption isotherm (Figure 4.1B), the convex nature at low THF activity implies that condensation of THF in permanent micropores takes place even when THF activity is low. The more linear region that follows the initial convex region indicates the solvent sorption into the gel region of the polymer matrix. And then, at high activity, the strong upward concavity clearly shows THF condenses in larger micropores after most of the gel region is full. The leveling off at the end of the isotherm represents the completion of capillary filling by the condensed THF. While in the MeOH sorption isotherm, the almost linear region followed by a leveling off indicates swelling of the gel and monolayer sorption in its micropores. There is no capillary condensation of MeOH in the micropores of PRP-∞.

4.2 Polymer Swelling

Shown in Figure 4.2 are swelling curves for both MeOH and THF, plotted as volume increase per gram of PRP-∞ (ΔV_p , mL/g) versus activity of the organic modifier in the solution ($a_{m,M}$). Both of the swelling curves are convex in nature, and the THF curve is twice as high as the MeOH curve except at $a_{m,M} \leq 0.05$ where the two curves are superimposed. At high activity ($a_{m,M} \approx 0.8$), swelling is seen to increase sharply and then level off as sorption of THF experiences capillary condensation. The swelling seen in this

region of capillary condensation indicates that here condensation is occurring in permanent micropores that are not the most highly crosslinked ones.

This research group has done a number of investigations of bandbroadening on the polymeric HPLC packings.^{15,41,51} A mathematical model has been developed to predict the plate heights and peak shapes of sample peaks by using the empirical tri-exponential curve fit to the sample sorption rate curve.⁵¹ The sample sorption rate curves that has been established most recently used naphthalene as the sample and 7/3 methanol/water, 0.2/6.8/3 THF/methanol/water and 1/6/3 THF/methanol/water as the mobile phases.⁸⁶ In order to investigate the effect of swelling of the packing materials on sample sorption rate, the swelling of PRP- ∞ particles in 7/3 methanol/water, 0.2/6.8/3 THF/methanol/water and 1/6/3 THF/methanol/water were measured in this work. As can be seen in the results shown in Table 4.1, comparing with the swelling in 7/3 methanol/water, the presence of 2 % THF only caused a slight change in swelling, while the presence of 10 % THF caused a large increase in swelling.

As indicated in section 2.4, the degree of swelling experienced by a PS-DVB polymer at equilibrium represents a balance between the interaction energy for solvation of the polymer chains by the organic solvent and the elastic forces of the polymer network. The solvation energy is greater for a smaller difference between the solubility parameters of the polymer^{57,60,80} and the organic modifier and for a higher activity of the organic modifier in the aqueous solution, while the elastic force is greater for a higher cross-linking density in the polymer.^{57,60, 64, 80, 83, 103} A more detailed understanding of the changes occurring in the polymer with solvent sorption requires a comparison of the swelling curves with the sorption isotherms.

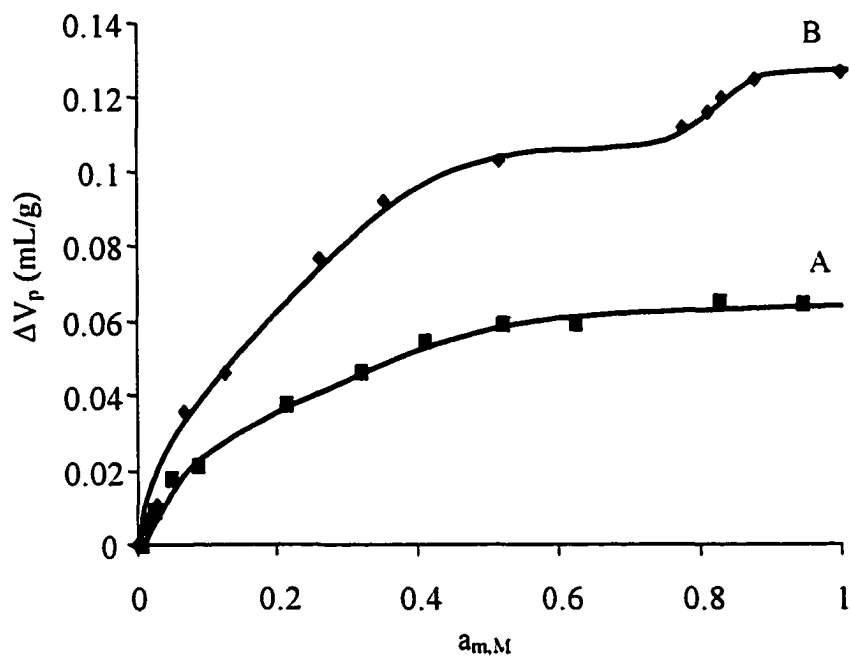


Figure 4.2 Swelling of PRP- ∞ produced by the sorption of methanol (A) and THF (B) at different solution phase activities. Solid lines are empirical fits, by eye, to the data.

Table 4.1 The effect of THF on swelling

THF/methanol/water	ΔV_p (mL/g)	ΔV_p (v/v %)
0/7/3	0.0613	6.43 ± 0.10
0.2/6.8/3	0.0645	6.77 ± 0.01
1/6/3	0.1114	11.7 ± 0.80

4.3 Swelling *versus* Solvent Sorption

Shown in Figures 4.3 and 4.4 are plots of volume change of PRP- ∞ , ΔV_p , vs. volume of modifier sorbed by PRP- ∞ , $V_{m,S}$, for MeOH/H₂O and THF/H₂O, respectively. The points on these plots are from the corresponding vertical axis in Figure 4.1 and 4.2. Thus, $a_{m,M}$ cancels out and the plots in Figure 4.3 and 4.4 show the volume swelling produced by the volume sorbed. All swelling is due to MeOH or THF since water is not sorbed by the polymer matrix.¹⁰⁴ When the sorbed organic modifier causes only “external” or “isotropic” swelling,^{42,105} in which the polymer gel expands without loss of any of the permanent porosity that was present in the dry matrix, the points will fall on a straight line.

The swelling vs. sorption curve for MeOH can be divided into two regions as shown in Figure 4.3. The initial linear region labeled SW indicates the “external” swelling. At sorbed volumes above $V_{MeOH,S} \approx 0.02$ mL/g, region AD in Figure 4.3, the negative deviation from linearity implies that the predominant process is sorption of methanol into permanent micropores.⁴²

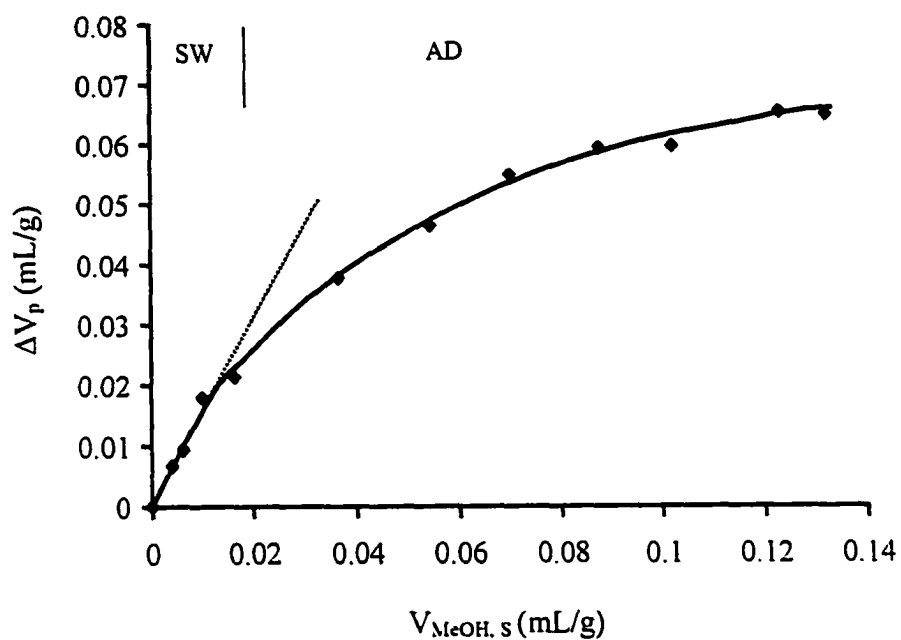


Figure 4.3 Swelling produced by sorbed volume of methanol on PRP- ∞ . Solid line is empirical fit, by eye, to the data. The dashed straight line identifies the linear “external” swelling region. “SW” indicates the “external” swelling; and “AD” indicates the sorption into the permanent micropores.

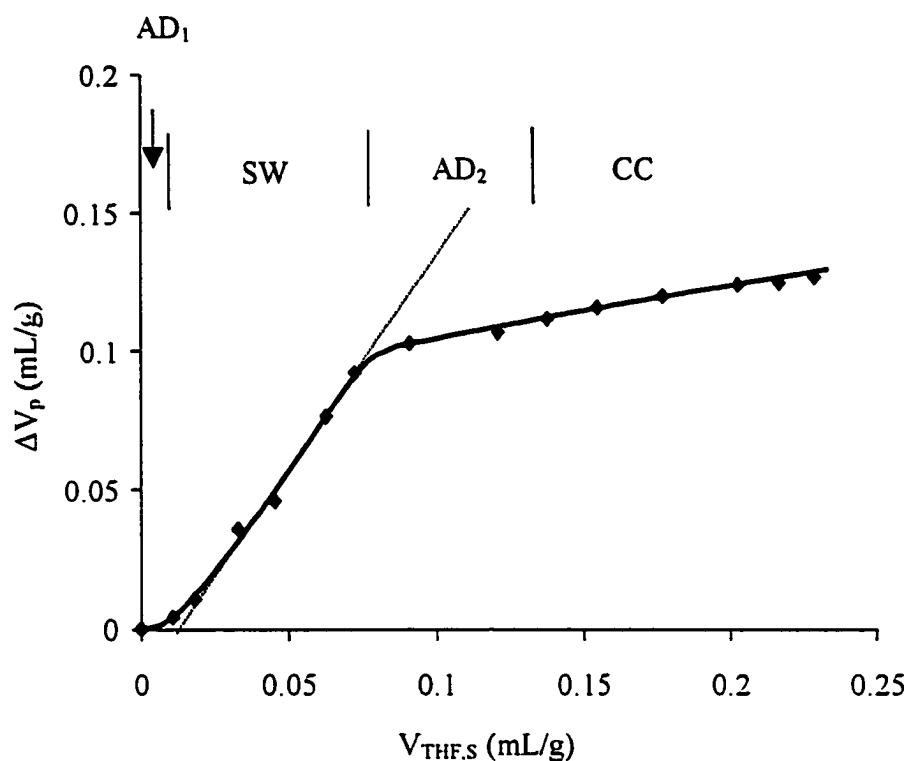


Figure 4.4 Swelling produced by sorbed volume of THF on PRP- ∞ . Solid line is empirical fit, by eye, to the data. The dashed straight line identifies the linear “external” swelling region. “SW” indicates the “external” swelling; “AD₁” and “AD₂” indicate the sorption into the permanent micropores; and “CC” indicates capillary condensation.

The swelling vs. sorption curve for THF can be divided into four regions as shown in Figure 4.4. At sorbed volumes of THF, $V_{\text{THF,S}} \leq 0.01$ mL/g, little or no measurable swelling of the polymer occurs with sorption. This is indicated by region AD₁ in Figure 4.4, where THF is experiencing multilayer sorption and capillary condensation. The fact that this occurs at a very low $a_{\text{THF,M}}$ and is not accompanied by swelling implies that this condensation is occurring in the smallest, most highly crosslinked micropores. The next region in Figure 4.4 labeled SW is fit with a dashed straight line, indicating sorbed THF causes external swelling of the gel. Above a sorbed volume of 0.08 mL/g, region AD₂ in Figure 4.4, the predominant process is again THF entering the micropores. From the THF isotherm in Figure 4.1B, it is seen that multilayer sorption and capillary condensation occur within the micropores at sorbed volumes above 0.13 mL/g. CC indicates this region in Figure 4.4.

4.4 Effect of THF on Sample Sorption Isotherms and Sample Sorption Kinetics

In order to investigate the effect of THF, as an organic modifier present in the mobile phase, on sample sorption in liquid chromatography, the sorption isotherms and sorption rate curves of naphthalene sorption were measured from a 0.2/6.8/3 THF/MeOH/H₂O solution and a 1/6/3 THF/MeOH/H₂O solution, and compared with that from a 0/7/3 THF/MeOH/H₂O solution. This work was done by Barbara Ells⁸⁶ of this research group and is presented here as an aid to further understand the effect of THF on the polymer matrix.

Shown in Figure 4.5 are the isotherms for the sorption of the sample compound naphthalene (NA) on PRP- ∞ from 7/3 MeOH/H₂O (A), 0.2/6.8/3 THF/MeOH/H₂O (B), and 1/6/3 THF/MeOH/H₂O (C). The vertical axis units are mL NA per gram of PRP- ∞ and the horizontal axis units are mL NA per mL of solution. The solid line presents the non-linear least squares fit to the data by the “solubility-limited Langmuir” equation.⁹⁹ The parameters obtained from the fitting include the sorption capacity of PRP- ∞ , $V_{i,S,\text{max}}$, which is proportional to the total number of sorption sites. For a solubility-limited isotherm, $V_{i,S,\text{max}}$ is measured using a saturated solution of NA, in which $a_{\text{NA,M}} = 1.00$.

Since PRP- ∞ is at equilibrium with a saturated solution of NA, it is necessarily at equilibrium with pure NA. Differences in the values of $V_{i,S,max}$ that are observed among the three solvents can arise only from a difference in the number of sorption sites in PRP- ∞ . As indicated by the values of $V_{i,S,max}$ presented in column 3 of Table 4.2, this number decreases by 11 % and by 17 % upon going from 0 % THF to 2 % THF and 10 % THF, respectively.

Shown in Figure 4.6 are the sample sorption rate curves for NA on PRP- ∞ from 0%, 2% and 10% THF in MeOH/H₂O. The sorption rate curves were measured within the linear regions of the respective isotherms, at a concentration of NA of 9.7×10^{-5} M. The curves have been plotted as the fractional attainment of the equilibrium amount sorbed vs. time. The solid lines are the non-linear least square fits to the data by equation (2.1), representing diffusion through a homogeneous sphere. The resultant fitting parameters include the diffusion coefficient of NA through the polymer, D , for each case. As presented in the fourth column of Table 4.2, D increased by 90% upon changing from 0% THF to 2% THF, and by additional 20% upon increasing to 10% THF. As pointed out by Ellis,⁸⁶ the increase in D upon the addition of THF to the mobile phase is not accompanied by a corresponding change in the free-solution diffusion coefficient.

4.5 Summary of the Effect of THF on Polymer Matrix

The results of the sorption of THF by PRP- ∞ are summarized in Table 4.2, in which column 2 clearly shows that the addition of THF in the solvent increased swelling of PRP- ∞ , and column 3 shows that the sorption of THF decreased sorption capacity for the solute naphthalene. These two effects are in some way the cause of the increase of the diffusion coefficient of the solute in the polymer shown in column 4 of Table 4.2.

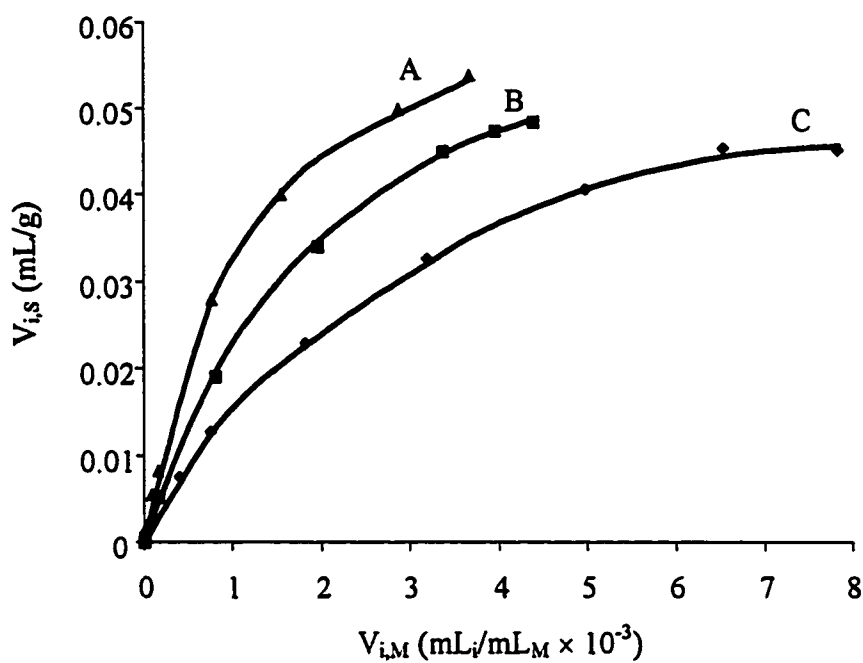


Figure 4.5 Sample sorption isotherm of naphthalene on PRP-∞ from different composition solvents: 0/7/3 THF/MeOH/H₂O (A); 0.2/6.8/3 THF/MeOH/H₂O (B); 1/6/3 THF/MeOH/H₂O (C). The data have been fit by the solubility limited Langmuir isotherm equation. Adopted from Ells.⁸⁶

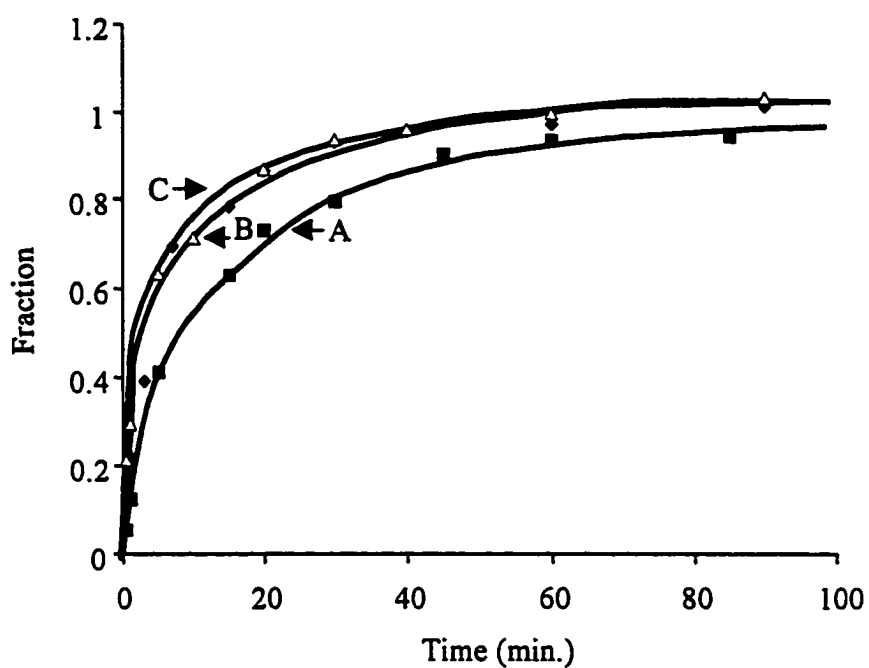


Figure 4.6 Sample sorption rate curves of naphthalene on PRP- ∞ from different composition solvents: 0/7/3 THF/MeOH/H₂O (A); 0.2/6.8/3 THF/MeOH/H₂O (B); 1/6/3 THF/MeOH/H₂O (C). The data have been fit by equation (2.1). Concentration of NA in solution was 9.7×10^{-5} M, within the linear region of the isotherm. Adopted from Ells.⁸⁶

Table 4.2 The results of the sorption of THF by PRP- ∞

THF/MeOH/water	ΔV_p (v/v %)	$V_{i,S,max}$ (mL/g)	D (cm ² /s)
0/7/3	6.43 ± 0.10	0.0542±0.0003	(7 ± 1) × 10 ⁻¹¹
0.2/6.8/3	6.77 ± 0.01	0.0484±0.0006	(13 ± 2) × 10 ⁻¹¹
1/6/3	11.7 ± 0.80	0.0450±0.0010	(15 ± 1) × 10 ⁻¹¹

The possible influence of swelling and sorption capacity on solute diffusion coefficient can be expressed in terms of equations (2.2), (2.3) and (2.4) that have been described in chapter 2:

$$D = \frac{D_p \lambda}{\theta} \quad (2.4)$$

$$\lambda^{-1} \approx \frac{n_{gel} \lambda_{gel}^{-1} + n_{\mu} \lambda_{\mu}^{-1}}{n_{gel} + n_{\mu}} \quad (2.5)$$

$$\theta \approx \frac{n_{gel} \theta_{gel} + n_{\mu} \theta_{\mu}}{n_{gel} + n_{\mu}} \quad (2.6)$$

where λ are parameters related to hindrance and increase with less hindrance, θ are parameters related to tortuosity, and n are the sorption capacities. As described earlier,

the polymer matrix can be simplified to consist of only the gel region (represented by subscript “gel”) and the micropore region (represented by subscript “ μ ”).

Increased swelling will have little effect on θ , neither will it on θ_{gel} and θ_{μ} , because tortuosity typically has a narrow range of values (between 1 and 5).^{87,106} As far as λ are concerned, a different region of polymer matrix experiences a different effect of swelling on hindrance effect. Within the gel region, in a swollen state caused by the sorption of solvent λ_{gel} should become significantly larger than that in a dry state, since a small change in pore size with swelling has a large effect on hindrance.¹⁰⁷ While in the permanent micropore region, because there is essentially no swelling, λ_{μ} should remain unchanged. On the other hand, decreased sorption capacity would mean a smaller value of n_{gel} , n_{μ} or both.

The increased sample diffusion coefficient, which improves the chromatographic peak shape, has been suggested in the literature to be due to increased polymer swelling as pointed out in chapter 1. However, a comparison of the polymer swelling results and the change of sample diffusion coefficient in Table 4.2 leads to a discrepancy with the above suggestion. As can be seen in Table 4.2, an increase in particle volume of 0.4%, upon adding 2% THF, corresponds to the 90% increase in the value of D , while a further increase of over 4% in particle volume upon changing to 10% THF corresponds to the additional 20% increase in D . Hence, the increase in D , which is observed upon adding THF, does not correlate with the swelling. Besides, the 0/7/3 THF/MeOH/H₂O solvent, with no THF and an activity of MeOH of 0.61, falls on the plateau in the methanol swelling curve in Figure 4.2 (A). This implies that the 0/7/3 THF/MeOH/H₂O solvent has already caused the gel regions of the polymer matrix to swell sufficiently so that the hindrance for sample diffusion in the gel is small, i.e. λ_{gel} is large. Therefore, there is the relationship: $(n_{\text{gel}} \cdot \lambda_{\text{gel}}^{-1}) \ll (n_{\mu} \cdot \lambda_{\mu}^{-1})$.

According to equation (2.4), the significant increase of D is most likely due to the increase of λ , since D_p , which is based on diffusion within the solvent-free polymer, is a constant, and θ can only make a slight difference. In equation (2.5), when $(n_{\text{gel}} \cdot \lambda_{\text{gel}}^{-1}) \ll$

$(n_{\mu} \cdot \lambda_{\mu}^{-1})$, the increase of λ will be due to the increase of $(n_{\mu} \cdot \lambda_{\mu}^{-1})$. Since permanent micropores do not swell, λ_{μ} does not change upon solvent sorption, so the decrease in n_{μ} , the sorption capacity in the micropores, is identified as being primarily responsible for the increase of λ and thus the increase in D . This inference is supported by the sorption capacity change presented in column 3 of Table 4.2. The 11% decrease in sorption capacity ($V_{i,s,max}$) that is produced upon changing from 0% THF to 2% THF and the further 6% decrease in capacity produced by changing to 10% THF correlate with the 90% and 20% increase in D that are observed.

Therefore, it is clear that the significant effect of THF on sample sorption occurs when the concentration of sorbed THF is small and has not yet brought about significant swelling of the polymer. This is the process labeled as region AD_1 in Figure 4.4, where THF is experiencing self-association and capillary condensation in the smallest, most highly crosslinked permanent micropores. From Figure 4.4, it is seen the volume associated with these small, permanent micropores is about 0.01 mL/g, which corresponds to 10% of the 0.10 mL/g of MeOH sorbed from 0/7/3 THF/MeOH/H₂O (in Figure 4.2, at $a_{m,M} \approx 0.6$). This correlates well with the 11% reduction in sorption capacity for NA on going from 0% THF to 2% THF in MeOH/H₂O (column 3 in Table 4.2). The filling of these micropores by THF effectively blocks them to the entrance of sample solutes.

4.6 Conclusions and Future Work

In this work, the experimental set-up for the “column equilibration” technique was established, on the basis of which the methods for measuring solvent sorption isotherms on polymer packings and density of dry polymer particles were developed. Furthermore, the swelling of PRP- ∞ particles in organic modifier/water solutions was accurately measured in terms of the swelling of individual particles. The results of solvent uptake and swelling of PRP- ∞ were combined, resulting in the further understanding of poor chromatographic performance in PS-DVB HPLC packing materials.

It was found there are a number of permanent micropores, which are significantly smaller than the majority of the micropores in PS-DVB polymer matrix, and therefore, in which, in the absence of THF, sample solute diffusion is most highly hindered, and causes poor chromatographic performance. As indicated in equation (4.1), the smaller the pore size the less the vapor pressure needed for the condensation, and the easier for the condensation to occur. Therefore, THF can condense in those smallest micropores even when THF is in low concentrations. The interaction between THF and these permanent micropores gives rise to the increase of sample diffusion and thereby good chromatographic performance. However, this effect of THF on polymer matrix is not due to the swelling of these permanent micropores as the literature suggested, but rather due to the blocking of these micropores by self-association and capillary condensation of THF.

Therefore, the addition of a small amount of THF in MeOH/H₂O solvent, as a mobile phase used in performing liquid chromatography on PS-DVB columns, will block the most highly hindered sorption sites in the polymer matrix. This blocking prevents the diffusion of sample solute molecules into those sites so as to quicken the sample diffusion and thus eliminate the poor chromatographic performance caused by slow sample diffusion into polymer micropores.

Instead of the *in situ* reversible filling of the permanent micropores by using trace amount of suitable organic modifiers, such as THF, in mobile phase, as described in the present work, investigation into permanently blocking these micropores through polymerization may open up an alternative and more efficient way to improve PS-DVB packings. This may be explored by using a monomer molecule with solubility parameter close to that of PS-DVB, such as vinyltoluene ($\delta = 18.6 \text{ (MPa)}^{1/2}$) or vinylacetate ($\delta = 18.4 \text{ (MPa)}^{1/2}$). After a suitable amount of monomer is adsorbed into the permanent micropores, polymerization can be initiated by radical initiation, heat ($\geq 200^\circ\text{C}$) or light. This additional “polymerization” reaction may occur among the absorbed monomers or between the absorbed monomers and the unreacted double bonds that are always present in PS-DVB porous polymers.

Chapter 5

Introduction to Part II

In part II of this work, a novel metal ion speciation technique, which couples a micro-drop solvent extraction technique with inductively coupled plasma mass spectrometry (ICP/MS) through a direct sample insertion device (DSID), is investigated. Since this method involves the application of several techniques, Chapter 5 will introduce the relevant concepts and techniques such as metal speciation, common metal speciation methods, metal solvent extraction techniques, micro-extraction techniques and DSID-ICP/MS. The last section outlines the objective of the present work.

5.1 Metal Speciation

Metal speciation is a broad term, which may be defined as the determination of the concentrations of the various physico-chemical forms of a metal element which together make up its total concentration in the sample.¹⁰⁸ The individual physico-chemical forms may include particulate matter, dissolved forms and the adsorbed forms on inorganic particles and organic colloids. With respect to solution samples, the chemical forms of an element can be characterized with parameters such as the oxidation state and associated ligands in the inner and outer coordination spheres of the element.¹⁰⁹ An important distinction is that between the free (hydrated) metal ion form and the complexed forms with various organic and inorganic ligands. The term, “speciation”, is often used somewhat loosely as defined by the purposes of particular work using operational classifications. For instance, it has been used¹¹⁰ to refer to the speciation of trace heavy metals in water particulates using the following categories: weakly adsorbed, bound to carbonates, iron and manganese oxides, organic and residual matter. In this work the emphasis is on measuring the concentration of the free (hydrated) metal ion.

5.1.1 Role of Metal Speciation

As predicted by Florence and Batley ¹⁰⁸ in 1980, there has been increasing interest in metal speciation during the past decade due to the growing awareness of its impact on environmental chemistry, toxicology, biomedical science, etc. It is necessary to understand that knowledge of only the total concentration of a metal in a sample is not sufficient to determine the possible effects and significance of the metal in the sample.

Each metal species carries a message which is vital for the evaluation of the mobility, bio-availability, accumulation and toxicological properties of the metal. ¹¹¹ An accurate assessment of metal elements will require knowledge of both their concentrations and speciation. The toxic and beneficial effects of a metallic element in a system should not be attributed to the element itself but to particular species with specific biological, physical and chemical properties. For example, many essential metals are known to exist in a variety of chemical forms, the assimilability of which varies greatly. The most assimilable form of iron for man is heme iron from meat. ¹¹² Inorganic iron salts and simple organic complexes are far less available. Therefore, analysis of a diet for total iron with no information about its chemical forms is not very useful. Another example can be given in metal toxicity. It is generally accepted that the free (hydrated) metal ion is the most toxic form to aquatic life, and metal complexes, or metal associated with colloids is much less toxic. ^{112, 113, 114} Consequently, a water sample with a higher total metal concentration may not necessarily be more toxic. In the case of environmental systems, adsorption to sediments can be either reduced or enhanced depending on the metal complexes present. It has been reported ¹¹⁵ that PbCO_3 is much more strongly bound to silica than is Pb^{2+} . On the other hand, the release of mercury from sediment may be due to the formation of soluble chloro complexes. ¹¹⁶ As a consequence, measurement of total concentration of a metal alone not only provides very little information but may also be misleading. Since the removal of metal pollutants is highly species dependent, speciation analysis can also be applied to aid in methods development for decontamination. In addition, knowledge of the metal species associated with protein

may assist in understanding the biological significance of the metal elements in the structures and functions of the macromolecules. Furthermore, knowledge of the metal species present has been sought for a better control of industrial processes.¹¹¹

5.1.2 Methods for Metal Speciation

As mentioned earlier, a metal element in a sample may exist in a variety of different forms: soluble free (hydrated), soluble complexed with various organic and inorganic ligands, colloidal, particulate and incorporated in living organisms. To determine the concentrations of all of the different species is obviously much more difficult than to measure the total concentration of the metal. There are two basically different broad approaches that have been applied to determine the soluble metal speciation. One involves calculation of the equilibrium concentrations of the species using known values of concentrations of total metal and ligands and published values of stability constants of the relevant metal complexes. Another broad approach for soluble metal speciation involves experimental measurements. This approach involves identifying the metal species of interest and measuring them by analytical techniques that are selective for the various species, either with or without prior separation.¹¹⁷ In the absence of a pre-separation step a direct determination is made on the sample by using an analytical technique which is highly selective for one species or one group of species in the presence of many other metal species. Among the few "species-specific" analytical techniques that respond to only one specific chemical form of an element in the sample, ion-selective electrode (ISE) potentiometry is perhaps the best example.¹⁰⁸ It responds only to the activity of the free (hydrated) metal ion. Other electrochemical techniques also show some degree of species specificity, for example, anodic stripping voltammetry (ASV)¹¹⁸. More examples in this category are some classical techniques, such as indicator dye methods, biological techniques, UV/VIS spectrophotometry, titrimetry and coprecipitation methods.¹¹⁸ Recently, electrospray mass spectrometry (ES-MS) has also been applied to direct determination of solution species.^{109,119}

A combination of a preceding separation procedure to isolate the species of interest and a following analytical technique to determine the metal concentration in the separated component is also frequently employed. A variety of analytical techniques which themselves are not species-specific can be made specific by coupling with proper separation techniques. Dialysis, ultrafiltration,^{120, 121} electrophoresis¹²¹ and centrifugation¹²² are separation techniques that have all been used to separate metal associated with colloidal particles from ionic metal species, while ion exchange equilibrium (IEE), extraction methods including liquid-liquid extraction and liquid-solid extraction,^{108, 117} and selective hydride generation¹²³ are some commonly used separation techniques for soluble metal species. Due to the advantages, such as the time-saving, the minimization of trace contamination and losses of analytes, the direct on-line coupling of a high-resolution separation technique with an element-specific determination method has become popular. Chromatographic methods are the most widely applied separation methods in these coupled techniques. In many instances of speciation studies the chromatographic separations achieved are difficult to obtain by conventional methods, because they often require complexation of the metal ion in the samples.^{124, 125} However, since chromatography of complexes can be performed in all areas of chromatography including gas chromatography (GC), thin-layer chromatography (TLC), high performance liquid chromatography (HPLC) and supercritical fluid chromatography (SFC), the chromatographic methods used in metal speciation are diverse. Recently, capillary electrophoresis (CE) with a separation mechanism complementary to chromatographic methods and with its high resolution has also developed to be a powerful separation method for on-line coupling techniques.^{126, 127} Cryotrapping/thermal desorption-based techniques represent another type of separation for speciation, which is particularly attractive for volatile (b.p. below 200°C) species and for those that can readily be converted to such by means of a suitable derivatization procedure.

With respect to detection techniques that follow the separation procedures, plasma spectrometric techniques are favored over atomic absorption spectrometry (AAS) because of their much higher sensitivity. Microwave-induced plasma (MIP) atomic emission spectrometry (AES) is the choice for GC,¹²⁸ whereas a more energetic

inductively coupled plasma (ICP)-AES is the choice for LC and CE.¹²⁹ The very sensitive technique of ICP-MS has also been used.¹³⁰ However, for many applications conventional detection based on conductivity, UV/VIS, electrochemical or fluorescence detectors is adequate.

5.1.3 Lability of Metal Species

The term “speciation” has often been used to refer only to kinetically inert species, which are the species defined as being kinetically stable, or not being capable of rapid inter-conversion with one another as a result of any physical or chemical changes to the system under investigation in the time required for the speciation measurement. However, some chemical species are readily affected by any change to the system during the time of measurement, in which case, the species are called kinetically labile species. In many cases “speciation” has been used in a broader sense to also differentiate between these labile species.

As a matter of fact, the term “kinetically labile species” is ambiguous and often operationally defined by the measurement itself, which means, the total amount of labile metal species in a sample solution may not be the same when measured by electrochemical, ion-exchange or other techniques. There is no standard definition or measurement of “lability”. Figura and McDuffie¹³¹ have divided soluble metal species into “labile” and “nonlabile” categories based on their anodic stripping voltammetry (ASV) characteristics. The labile species are free metal ions and complexed metal which can dissociate very rapidly to the free electroreducible form and yield an ASV signal. The nonlabile species are metal complexes with a rate of dissociation to the free metal that is slow compared to the time scale of the ASV measuring technique. Not surprisingly, the results depend on the electrochemical deposition time employed.

Although all of the separation-based methods discussed in section 5.1.2 work well for kinetically inert species, most of them will not work for labile species because of the redistribution of the labile species of the metal of interest. As a consequence, techniques

such as conventional solvent extraction, chromatography and some ion exchange methods can only be applied to the speciation of kinetically inert species. In the next section, a detailed introduction of speciation methods will focus on those techniques that can be applied to kinetically labile species.

5.1.4 Non-Perturbing Speciation Techniques

As indicated earlier, to measure kinetically labile species is more difficult than to measure kinetically inert chemical forms, because the separation and analysis techniques involved in the measurement can bring about disruption of the chemical equilibria in a labile system. Nevertheless, in order to achieve accurate speciation information, many techniques or experimental conditions employed have been carefully designed so that the perturbation from the measurement device could be made negligible.

5.1.4.1 Computational Methods

Rather than using experimental measurements of species, metal speciation information can be obtained by calculations. Since metals and ligands in a dynamic system are involved in a complicated interrelated network of chemical interaction among all chemical species,¹³² the calculation of concentrations of each species requires simultaneous solution of equations representing all the thermodynamic equilibria in the system using total metal concentrations, concentrations of complexing ligands and pertinent constants involved in the equilibria. Due to the complexity of the system in question, such as in natural water, the assistance of computer modeling has been widely sought for the determination of metal species distribution. A number of computer models for equilibrium calculations in aqueous systems have been compared in the report of Nordstrom.¹³³ Some more recent examples of popular computer models for trace metal speciation are: MINTEQA2,¹³⁴ GEOCHEM,¹³⁵ WATEQ4F,¹³⁶ and EQ3NR.¹³⁷ An attempt to delineate the useful range and limitations of different experimental measurements of species and computational approaches for speciation has been made by Nordstrom.¹³⁸

In spite of the wide application of the computational methods for speciation, the computer modeling results normally lack credibility when obtained for a complicated system, especially for practical samples. For many metals in real samples, for example, in sea water or river waters, the predominant physico-chemical forms are unknown. Any natural water contains many metals capable of reacting with each ligand, and many ligands which can react with each metal. Meaningful computational results can be obtained only when all significant complexing species are accounted for, and the thermodynamic data and analytical data input are reliable. However, in many cases, neither the nature nor the concentrations of the dominant ligands in the system of interest are known. In addition, the required equilibrium constants and corrections for ionic strength are frequently not available, or have considerable variations in published data indicating significant uncertainty. Furthermore, for practical reasons, the system of interest may not be tested under equilibrium condition.

Nevertheless, computational methods can be a powerful tool for well-defined experimental samples, or for metal species at high concentrations. It is also a very useful tool for validation of new experimental methods for metal speciation.

5.1.4.2 Electroanalytical Methods

This section will focus on the two most commonly applied electroanalytical metal speciation methods: ion selective electrode potentiometry (ISE) and anodic stripping voltammetry (ASV).

The use of an ISE for the determination of M^{n+} allows the fundamental distinction between free (hydrated) metal ions and complexed metal forms. ISE is the most non-ambiguous “species-specific” technique due to its response only to the activity of the free metal ion.¹¹⁷ ISE has been popular also because of its relatively low cost. Moreover, one advantage of ISE over many other methods is that it may be used directly

on samples containing suspended solids. However, this apparently ideal method suffers the following problems¹³⁹:

1. Though ISE is generally believed to respond only to the free metal ion activity, which is almost equal to its concentration at low concentrations, it has been found that the copper electrode also responds to hydroxide and bicarbonate copper species in basic solutions.¹⁴⁰

2. ISE can only provide detection for a limited number of heavy metals such as cadmium, copper, lead, silver, mercury and zinc. Moreover, even for these metals, ISE is usually insufficiently sensitive for use in natural waters, which contain trace metal with concentration below 10^{-6} M.¹⁴¹ In situations of low concentrations, either non-Nernstian behavior or the difficulty of achieving the steady state potential responses have frequently been reported.

3. Copper ISE determinations have generally not been used in marine environmental samples because of the interference caused by high levels of chloride in the sample matrix.¹⁴²

4. A practical difficulty involved when dealing with unknown samples is the requirement that the standard solutions have the same constituents and ionic strength as in the samples.

Anodic stripping voltammetry (ASV) methods are composed of two steps. The first step is a deposition step, in which the metals are concentrated by cathodic deposition at a thin mercury-film electrode (TFE) or on a single, hanging mercury drop electrode (HMDE). The second step is a stripping step, in which the reversed voltage is applied so that the metals can be determined by an anodic polarographic analysis.¹⁴³ The TFE is generally more sensitive than the HMDE, whereas the HMDE is believed to be the most reliable for routine analysis, because it suffers less interference and can be applied over a

large potential range with high reproducibility and sensitivity.¹⁴⁴ The application of differential pulse ASV can enhance the detection limit of metals to about 10^{-10} M.^{144,145}

ASV differentiates metal species on the basis of electrochemical lability.^{108, 117, 146} It thus can only discriminate “unbound” and “bound” metal species. The so-called “unbound” metal species refers to the sum of the free metal ions, which are reducible at the mercury electrode, and the kinetically labile metal complexes, which may rapidly dissociate during the deposition step. The “bound” metal species refers to the kinetically inert metal complexes. The signal due to the metal depends on the rate of dissociation rather than stability constants of its complex. Therefore, in general, ASV suffers the inability to differentiate between labile complexes and free metal. Nevertheless, this differentiation can theoretically be made from shifts in peak positions towards more cathodic potentials provided that the rate of stripping in the second step is slower than the rate of complex formation.¹⁴⁷ Recently, chemically modified electrodes (CMEs) have been used in ASV for metal speciation.^{148,149} The CME method is considered to be more selective than conventional ASV, because the sensitivity and selectivity of CMEs are based on the chemical reactivity of the modifier rather than the redox potential of the analytes.

Despite its advantages, including relatively low cost, no preliminary separation required, no blanks involved and small sample volume requirements, the ASV method has its limitations.^{117,139} For one thing, as mentioned above, ASV can only differentiate the non-labile metal complexes from the labile metal species group, which include free metal ions and labile metal complexes. For example, metal carbonate and hydroxide complexes are electrochemically indistinguishable from the free metal by ASV.¹⁵⁰ And also, Cu-nitilotriacetate and Cu-EDTA complexes have been found to be reducible under certain conditions.¹⁵¹ The results of metal measurement are likely to be higher than true values when measuring free metal ions, due to the perturbation of metal-ligand equilibria as a result of lowering the free metal ion concentration in the vicinity of the electrode.¹⁵² Furthermore, overlapping peaks have been observed for zinc and nickel, and copper, nickel and vanadium,¹⁵³ which may produce erroneous results. Moreover, adsorption of

organic matter on the electrode surface may result in changes in the reversibility of electrode reactions so as to cause anomalous anodic stripping signals.¹³²

5.1.4.3 Ion Exchange Methods

Conventional cation and anion exchange resins have been widely applied to the study of trace metal speciation.^{108,117} Ion exchange resins sort dissolved metal into anionic, cationic or neutral species.¹⁵⁴ In common cases, metal combined in inert complexes having a different sign of charge will not be retained by the resins, which may therefore be used to separate stable complexes from dissociable complexes and free metal.¹⁴⁶ Cation exchange techniques have been applied to measure the concentration of free metal ion in the presence of its complexes.^{155,156,157,158,159} Reliable results can only be obtained when the following conditions are met: 1. free metal ions are the only species in the sample system that are sorbed onto the resins; 2. the ionic strength of sample solution remains constant, which has usually been met by an addition of “swamping” electrolyte so that the effect of other cations on the ionic strength is insignificant; 3. the free ligand concentration in the sample system must remain constant; 4. measurement must be undertaken after the system has reached equilibrium; 5. a trace loading condition is required, meaning that the number of exchange sites occupied by the cations of the swamping electrolyte greatly exceeds that occupied by the trace metal cations so that the change of metal concentration during the ion exchange process will not significantly alter the bulk composition of the resin phase; 6. non-perturbing condition is maintained by taking up only a small fraction of free metal onto the resins so that the equilibria in the sample solution are not perturbed.

Cantwell, *et. al.*¹⁵⁷ have employed a strong acid cation exchange resin (Dowex 50W-X8) for the determination of free nickel ion (Ni^{2+}). The measurement was undertaken by both batch and column methods. In the batch method, the non-perturbing condition is met by conducting multiple equilibrations with fresh portions of sample solution, if the sample is not well-buffered with respect to free metal ion. The column equilibration method was more preferred because of its greater convenience in meeting

the non-perturbing condition by continuously pumping the sample through the resin bed until the resin has reached equilibrium with the sample solution and no further free metal ions are sorbed.

Similar techniques have been used in other work.^{155,156,160} Interferences in the ion exchange technique have also been investigated.¹⁶¹ Semi-automation of an ion exchange/atomic absorption system has been established by Treit, *et. al.*¹⁶² Various sorbents have been modified by immobilized ligands and investigated as cation exchangers in terms of selectivity and less interference.^{163, 164, 165}

The advantages of the cation exchange methods and the use of immobilized ligands include: wide application range to a large number of metals, low detection limits (e.g. 10^{-7} to 10^{-8} M), less interference from other metals and organic matter in the sample solution, and minimal sample pretreatment. Its disadvantages include: interference from positively charged and, sometimes, neutral complexes, addition of inert electrolyte salt is required to maintain trace ion exchange and complexation conditions, and a time-consuming elution procedure is involved.

5.1.4.4 Extraction Methods

Extraction techniques are primarily used in two main applications. One is to separate the analyte of interest from the sample matrix before detection so as to eliminate or reduce the interference from the other components. Another is to preconcentrate the analyte in the case of trace analysis. Recently, the application of extraction techniques in speciation analysis of environmental samples has been reviewed by Morabito.¹⁶⁶

Two of the most used extraction techniques are liquid liquid extraction (LLE) and solid phase extraction (SPE). Traditional LLE is a long-standing, widely used technique, though it has some problems, including the use of a large volume of organic solvent, which may cause laborious handling, potential health hazard and high cost. More discussion of LLE in metal speciation analysis will be given in section 5.2. In contrast

with LLE, SPE, which has been used extensively in the last 15 years as an alternative to LLE, can avoid the use of organic solvents and is consequently characterized by easy handling, low potential health hazard and portability.

SPE involves sorbing the analyte onto a modified solid support and then desorbing it either by thermal means or by using a solvent. In metal speciation analysis, the selectivity of SPE is controlled by the specific functional groups immobilized on the SPE substrate.¹⁴⁴ For example, the C₁₈ material has been found to be suitable for the extraction of neutral metal complexes, whereas the LC-NH₂ material is applicable to the direct extraction of free metal species.¹⁶⁷ In spite of the advantages, SPE has some drawbacks.¹⁶⁶ For example, the SPE carried out by batch methods is more laborious with extra procedures. In addition, the elution step from the solid phase may be non-quantitative.

As mentioned earlier, in speciation analysis, one requirement of the measurement method is not to perturb the original species distribution. However, the removal of analyte species of concern from the sample system through conventional extraction techniques may be a severe disturbance of the original speciation when the system consists of kinetically labile species. Micro-scale extraction techniques such as solid phase micro-extraction (SPME), which considerably reduce the amount of extractant may extract analyte without significantly changing its concentration, and thus reduce the perturbation problem.¹⁶⁸

SPME is a novel technique first introduced by Pawliszyn, *et. al.*,¹⁶⁹ in which a fused silica fiber coated with liquid organic polymer or solid sorbent is exposed to the sample matrix wherein a distribution equilibrium of the analyte is established between the matrix and the coating. Once sampling is completed, the coated fiber is directly transferred to the detection system. SPME has been extensively applied to analysis of organic compounds^{170,171} from various matrices, such as air, water and soil. Since the amount of analyte extracted by SPME is very small, this technique has been applied to the measurement of the free concentration (unbound) of a target organic compound,

based on the assumption that no significant speciation perturbation is caused by extraction.^{168,172}

The first application of SPME to metal speciation was reported by Pawliszyn *et al.*¹⁷³ In order to achieve the extraction of metal ions, the liquid organic polymer coated on the fiber probe has to be modified to contain ion exchanging functionalities. In this report, the liquid ion exchanger, di-(2-ethylhexyl)phosphoric acid (HDEHP), was used for the modification. Bismuth(III) in aqueous nitric acid solution was extracted and latter desorbed into an acidic potassium iodide solution to form the yellow colored BiI_4^- complex which was determined by spectrophotometry. In a more recent report of Pawliszyn *et al.*,¹⁷⁴ the fiber doped with dibenzo-18-crown-6 (DBC), which could form a stable complex with mercury, was used to extract mercury ions from aqueous solution. The procedure includes dipping a fiber into a solution of DBC and then dipping the coated fiber into HgCl_2 aqueous solution for extraction. The fiber with extracted mercury complex was then directly inserted into a specially designed interface for an HPLC injector.

In addition to the advantages that have been mentioned earlier for SPE, SPME possesses the following additional advantages.^{168,173} 1. SPME can sample matrices directly in their natural environment; 2. it can be coupled to various conventional instruments and can be applied to any matrix; 3. in the case of metal speciation analysis, the ion exchange capacity of the fiber can be changed readily by varying the coating size, which depends on the volume of the fiber, the type of fiber, and so on; 4. the selectivity can be readily controlled by using different already existing selective liquid ion exchangers, or choosing proper extraction/desorption or complexation solution so that only sought-for-species can be extracted or form detectable complexes, and also, new specific ion exchanging ligands can always be developed; 5. for speciation study, the most important feature of SPME is that it takes up only a small amount of analyte from the sample, and has a fast response time. The disturbance of natural speciation can therefore be minimized.

In spite of the wide application of SPME, it has flaws. For example, when SPME is coupled to other commonly used detection methods than GC, such as HPLC, CE, UV/VIS and so on, it often requires a solvent desorption step, which involves the use of a sophisticated setup and also sometimes is a tedious process.^{175,176} In addition, when the same fiber sorbent in SPME is used more than once, there is a potential carry over problem. Moreover, the selectivity of SPME solid phase depends on its coatings, not many types of which are commercially available.¹⁷⁷

5.1.4.5 Electrospray Mass Spectrometry

Ever since the pioneering work of coupling the electrospray process and mass spectrometry (ES-MS) in the mid-1980s, the application of ES-MS has been growing explosively and primarily focusing on biological studies and total element analysis. Nevertheless, its potential as a powerful tool in the elemental speciation work has recently drawn considerable attention.^{109,178,179}

ES is an electrostatic process established by applying a high potential to a capillary through which a solution is flowing, resulting in a spray of charged droplets at the end of the capillary from which ultimately come gas phase ions.^{109,180} It has been realized that ES is not an ionization source in the classical sense.^{179,181} Instead, it is a very gentle technique, causing minimal fragmentation, which facilitates the transfer of pre-existing ions in solution to the gas phase rather than creating ions. In this way, instead of destroying the chemical form of the solution ion, the solution information is preserved since the ion remains solvated while being transferred from solution to the gas phase. This approach therefore offers an alternative way of doing speciation, which could prevent perturbation of the system caused by invasion of measurement devices, through isolating the species of interest physically, rather than chemically.¹⁰⁹

As pointed out by Horlick, *et. al.*¹⁰⁹ ES-MS has a unique feature among kinetically labile speciation techniques, that is, ES-MS is able to directly and selectively measure all ionic species of an element present in solution. Elemental speciation by ES-

MS includes both the oxidation states¹⁷⁹ and the form of the ion in solution, existing either as a solvated metal ion^{182,183,184} or a complex molecular ion species.^{178,185,186}

Several problems associated with ES-MS as a speciation tool have been summarized.¹⁰⁹ Firstly, the requirement in ES-MS measurement of addition of an inert electrolyte as an electrospray stabilizer to solution being electrosprayed may affect species distribution in solution. Secondly, to date, almost all ions measured by ES-MS are from methanol solutions due to the low efficiency of ion transfer by aqueous solutions. Thirdly, there is a matrix effect on the sensitivity of analyte ion species. Finally, the ionization process that involves solvent evaporation and Rayleigh fissions may affect the solution-state species distribution. In other research,¹⁸⁷ evidence has been presented where species may undergo electrochemical reactions at the solution capillary interface, showing the possibility of creating new ions during the electrospray process.

5.2 Metal Solvent Extraction with Chelating Extractant Lix63

Solvent extraction (liquid – liquid extraction) of metals, which is a subject of wide technological, analytical and fundamental interest, has been recognized as an excellent separation method for decades. LLE, with the assistance of organic solvents such as n-octanol, chloroform and hexanol, is usually used to separate chemical forms that are lipid soluble from the inorganic metal fraction.¹⁴⁶ This is the case in the application of the extraction technique to organometallic speciation, which is normally based on the simultaneous extraction of all the species of interest. The organic solvents used in this case may or may not contain complexing agents.^{188,189} In the case of inorganic speciation to determine the metal ions, the extraction separation is usually performed with the assistance of a complexing agent.¹⁹⁰ The approach is based on selective complex formation between the metal ion of interest and the complexing agent used.

In the metal solvent extraction process the key role is played by the chelating extractant in the organic phase, which is capable of reacting with the aqueous metal species, and transferring them into the organic phase. One requirement of a chelating

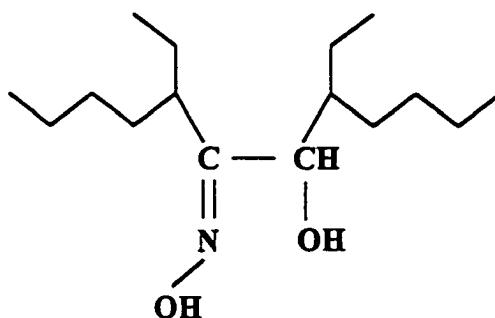
extractant is that it must have at least two atoms such as oxygen, nitrogen, sulfur and sometimes selenium, tellurium and possibly certain other elements as well, which can be simultaneously coordinated by the metal ion. Another requirement for a chelating extractant in metal solvent extraction is that the molecule of the extractant must have a nonpolar part to ensure that the substance remains in the organic phase.¹⁹¹

Danesi, *e. al*¹⁹² have classified chelating extractant into three groups: acidic extractants, basic extractants and neutral extractants. The acidic extractants have the largest extractant family, which is composed of the chelating agents characterized by the presence of a donor group having a dissociating proton. Examples of such extractants are β -diketones, hydroxy-oximes, 8-hydroxyquinolines, hydroxamic acids, thiocarbazonates, etc.

The first commercial chelating extractant, which is an aliphatic α -hydroxyoxime, was introduced in 1963-64 by the Henkel Corporation, (formerly General Mills Chemicals, Inc.), under the trade name Lix63¹⁹³ for the hydrometallurgical refining of copper. Since then the chelating extractant family has grown to contain more new chemical forms and modified forms of their original products to improve their extraction performance, in terms of their pH functionality, selectivity for specific metals and extraction kinetics. The chelating extractant family is marketed by several companies under different trade names, such as the Lix series products by Henkel Corporation, the Kelex series products by Ashland Chemicals, SME529 by Shell Chemicals, P series products by Acorga, etc. There are mainly two types¹⁹⁴: substituted aliphatic and aromatic α -hydroxyoximes, and a substituted 8-hydroxyquinoline. The active component in a commercial product of these extractants is normally a mixture of two or even more than two chemical compounds. Almost all of these extractants are primarily produced for use as copper-specific extractants, however, many developments^{195, 196, 197, 198, 199} have been made later to extend the application of them to a wide variety of metal elements.

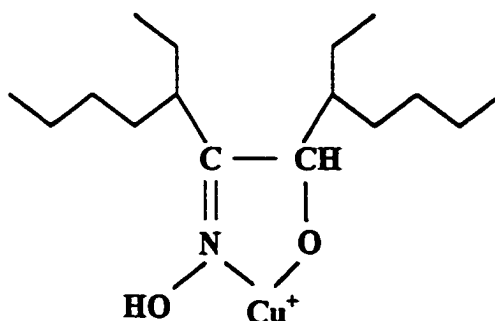
Lix63, which is one of the commercialized chelating extractants mentioned above, was chosen for the present work because it consists of only one active component, the

aliphatic α -hydroxyoxime²⁰⁰: 5, 8-diethyl-7-hydroxyl-6-dodecanone oxime, the structure of which is shown below¹⁹⁴:



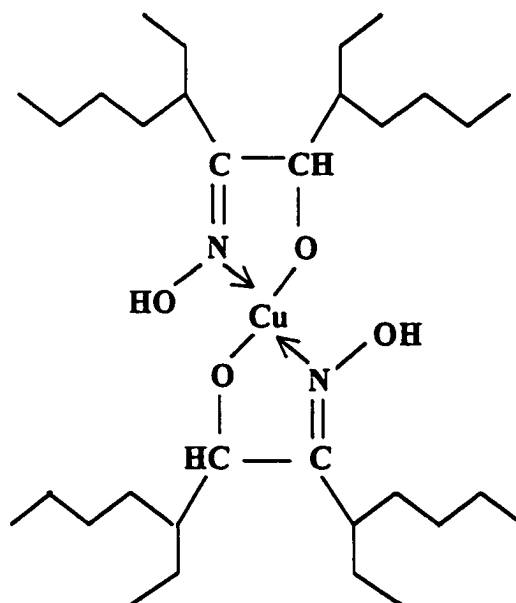
5, 8-diethyl-7-hydroxyl-6-dodecanone oxime

Lix63 is normally added into commercial metal extractants as a catalyst. Hudson has clearly described the complex formation mechanism between metal and Lix63.²⁰¹ It was found Lix63 was able to rapidly form a complex with the metal in the aqueous phase. The complex is charged and contains a five-membered ring (as shown below, if copper was the metal.). Here, Lix63 is a monoprotic acid (HL).



CuL^+ complex

This charged complex then further reacted with Lix63 (L) at the phase interface (there is higher concentration of Lix63 in the organic phase.) to form a 1:2 Cu-Lix63 neutral complex, which was then extracted into organic phase. This 1:2 Cu-Lix63 complex, as shown below, agrees with the composition of Cu-Lix63 complex in organic solvent described in most of the literature.^{195, 202, 203}



CuL_2 complex

5.3 Solvent Micro-extraction Techniques

As described earlier, solvent extraction (liquid/liquid extraction) (LLE) is one of the most classical and effective sample preparation techniques in analytical chemistry. In its conventional applications LLE collects extracted sample components of interest into a large volume of organic solvent, which is often hazardous, and examines only a small fraction of it. For analysis of trace amounts of sample in this way, either sensitivity is lost

or preconcentration of the analyte by somehow removing the solvent has to be done, which is often a tedious and time-consuming process and can result in substantial material losses. To overcome these problems, it is necessary to develop complementary micro-extraction techniques by applying solvent extraction principles to very small solvent volumes.

The attempt to achieve lower solvent consumption, high speed and low cost in LLE has been made successfully by Karlberg *et al.*,²⁰⁴ and Bergamin *et al.*²⁰⁵, who first introduced the flow injection extraction (FIE) technique. In the FIE procedures, a flowing system is used, in which the sample is injected into an aqueous flowing stream. Solvent extraction is carried out by continuously inserting organic segments into this stream and passing the segmented stream through a coil. Phase separation is then made and the organic phase with the extracted sample is led through a flow cell for measurement. In addition to the advantages over traditional LLE as mentioned above, FIE also offers the possibility of automation of a LLE process, minimization of sample zone dispersion due to the segmented type of flow, and so on. Consequently, FIE is a LLE technique that has practically been widely applied²⁰⁶ and theoretically been well characterized^{207, 208}. However, FIE generally can not achieve preconcentration, due to the approximately equal amounts of aqueous phase and organic phase normally utilized, and also it is generally less sensitive than batch extraction methods and requires more sophisticated hardware.

Other efforts have been made to reduce solvent consumption in LLE by modifying the conventional solvent extraction device. Several ideas^{209,210,211} have been based on the application of a narrow capillary neck, into which the organic phase was drawn after extraction and sampled with a syringe needle. Murray's²⁰⁹ device is a modification of a conventional extraction flask with a capillary tube replacing the conventional neck of a flask. Van Rensburg *et al.*²¹⁰ have modified the tip of a glass syringe into an extraction syringe so that it is able to connect with a glass tubing, one end of which is drawn out to a small capillary. While all these above mentioned micro-extraction techniques can reduce the consumption of organic solvent to the level of several hundred microliters per analysis, the micro-extractor devised by Attygalle *et al.*²¹¹

has reduced the solvent volume to no more than 10 μL . However, their design and operation of the device are complex.

The recently developed application of one single drop of solvent as organic phase in LLE has brought solvent micro-extraction to a greater level of reproducibility, simplicity, speed and low cost. Liu and Dasgupta²¹² have developed an automated extraction and detection system by performing LLE in a drop-in-drop arrangement, in which a 1.3 μL drop of chloroform was enclosed in a 25 - 45 μL flowing aqueous drop. The performance of the system has been demonstrated with extraction of an anionic surfactant by methylene blue (MB) through ion pair formation and the windowless optical detection offered by the organic drop itself as an optical cell.

Independent of the above work, Jeannot and Cantwell²¹³ have studied, both theoretically and experimentally, a micro-extraction system with an 8 μL organic drop located at the end of a Teflon rod which is immersed in an agitated aqueous sample solution. To achieve further convenience and simplicity for routine practice with GC analysis as sample detection method, this system has been modified by the same authors²¹⁴ to use a 1 μL drop, formed at the tip of a microsyringe needle suspended in a stirred aqueous solution. In addition to the advantages mentioned earlier for micro-extraction techniques, the single drop micro-extraction system also offers some other features. First, there is no dispersion of either phase in the course of extraction so no phase coalescence is required after the extraction step. Second, the interfacial area is known with accuracy and the phase ratio is readily adjusted by varying the volume of aqueous phase.

Since the phase ratio in the micro-drop system could be adjusted to be extremely small, the removal of sample by extraction can be made negligible so as to avoid perturbation of the aqueous phase equilibrium. This point enabled the application of this single drop system as a speciation tool to the determination of unbound progesterone in an aqueous medium containing protein.²¹⁵

The coupling of solvent micro-extraction and GC detection, by using a microdrop formed at the tip of a syringe needle, has also been reported by others. He and Lee¹⁷⁷ have developed two modes of the application: static mode with a static drop suspended in the aqueous phase during the extraction process; and dynamic mode with repeated withdrawing and pushing out of the 3 μL sample solution with the syringe plunger, always keeping 1 μL of organic solvent inside the needle.

If the analyte is an ionizable or charged species, a back extraction of the extracted species from the organic phase into a second aqueous phase is often desirable. Simultaneous forward and backward extractions are made possible by a technique called the "supported liquid membrane (SLM) technique".²¹⁶ The SLM technique involves an organic solvent immobilized in a porous membrane, which serves as a barrier between two aqueous phases in a flow system. The transport of analyte from one aqueous phase to another through the organic solvent is controlled by adjusting the different pHs in the two aqueous phases. Since the volume of the supported organic solvent is in the range of 10-15 μL in flat membranes, or 1-2 μL in a porous fiber²¹⁷, the technique can be considered to be a micro-extraction technique. It has been widely applied in sample preparation and enrichment.^{218,219}

Very recently a solvent micro-extraction technique has been developed²²⁰ to perform forward and backward extraction simultaneously and quantitatively with the aid of an unsupported micro liquid membrane. Owing to the elimination of supporting materials for the solvent membrane, there are no memory effects and no long-term instability problems normally encountered in SLM. This technique has subsequently been modified by combining the micro-drop and membrane techniques.²²¹ A single microdrop from the tip of a syringe needle is suspended in the organic membrane located above another bulk aqueous phase. As a result of the increase in source-to-receiving aqueous phase ratio, the microdrop technique has achieved a large preconcentration enrichment factor in a short time.

5.4 Direct Sample Insertion Device (DSID) for ICP/MS

The ICP/MS is generally recognized as the most powerful technique for the ultra-trace detection of metals.²²²

The sample introduction system is an essential link between the sample and the ICP. There is a variety of sample introduction devices. Some provide continuous sampling that requires a relatively large sample volume (greater than 1 mL),²²³ whereas some provide discrete sampling that offers the potential to deal with micro-samples.^{224, 225, 226} The discrete samples can be introduced into the ICP in numerous ways²²⁷, such as electrothermal vaporization,^{228, 229} direct insertion or probe techniques,^{230, 231, 232} flow injection,²³³ vapor introduction (e.g. hydride techniques),²³⁴ chromatographic introduction,^{235, 236} arc and spark determinations²³⁷ and so on. The signals produced in these discrete sampling techniques are transient because the fixed amount of sample is completely consumed during the measurement period.

Among the techniques mentioned above, the direct sample insertion technique has its unique merits over other techniques. Included in these are: the ideal desire to analyze original sample without complex pre-treatments becomes possible; dilution errors and sample transfer losses arising from extra sample handling steps are avoided; contamination from reagents and the time delay between sample collection and analysis is minimized.²²² Other than these, perhaps the major advantage of direct sample insertion is the significant improvement of sample transport efficiency over conventional pneumatic nebulization techniques. This improvement in transport efficiency results in at least an order of magnitude increase in sensitivity, with a corresponding improvement of detection limits and ability to analyze small sample volumes.

The term, Direct Sample Insertion, was first introduced by Salin and Horlick²³⁸ in 1979 to describe the use of a conventional undercut d. c. arc electrode as the means to introduce mg quantities of powders/solids and μL volumes of liquid samples into a medium power ICP. Since then, numerous papers related to the DSI technique have been

published. Among them Karanassios and Horlick²³⁹ have provided a comprehensive review on DSI, which is defined as a system, device or technique, in which a sample is placed into or onto a probe, with subsequent introduction of the sample-carrying probe into the plasma.

The DSI technique allows the analysis of sample at or below the ppm and ppb levels for ICP/AES and ICP/MS, respectively. A diagram illustrating the basic components of a DSI-ICP/MS set up is shown in Figure 5.1. The process of sample probe insertion can be accomplished manually or automatically. The data collected are time-dependent intensities.

DSI devices can be classified in terms of the type of sample insertion probe utilized.²³⁹ These probes can be made of a material such as graphite, tantalum, or tungsten in the shape of a cup, rod or wire loop. Energy transfer results in rapid heating of the sample probe and vaporization of the analyte into the ICP. DSI devices can also be classified in terms of the operation mode as vertical or horizontal.

The DSI device employed in this work was devised by Karanassios and Horlick²⁴⁰ for ICP/MS (SCIEX Elan 250). The design is composed of four functional component parts: a torch support assembly, a translation platform with probe assembly, a base plate and a drive mechanism. Figure 5.2 illustrates how the sample is inserted into the ICP by the DSI. The device features the capability of swinging the probe from the vertical plane, for sample loading, to the horizontal plane for insertion into the ICP. The stops that the sample probe makes during the process of insertion into and withdrawal from the ICP, at positions for sample ashing, atomization and probe cooling are all controlled by computer.

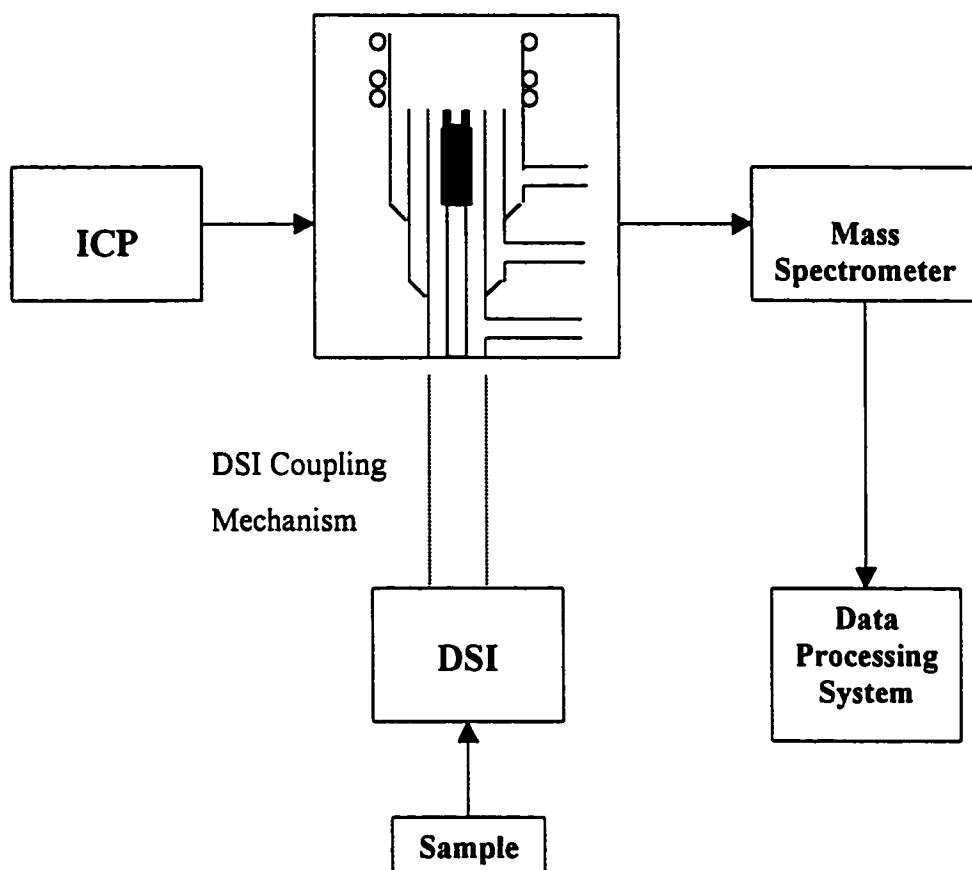


Figure 5.1 Diagram of basic component of set-up for DSI-ICP/MS

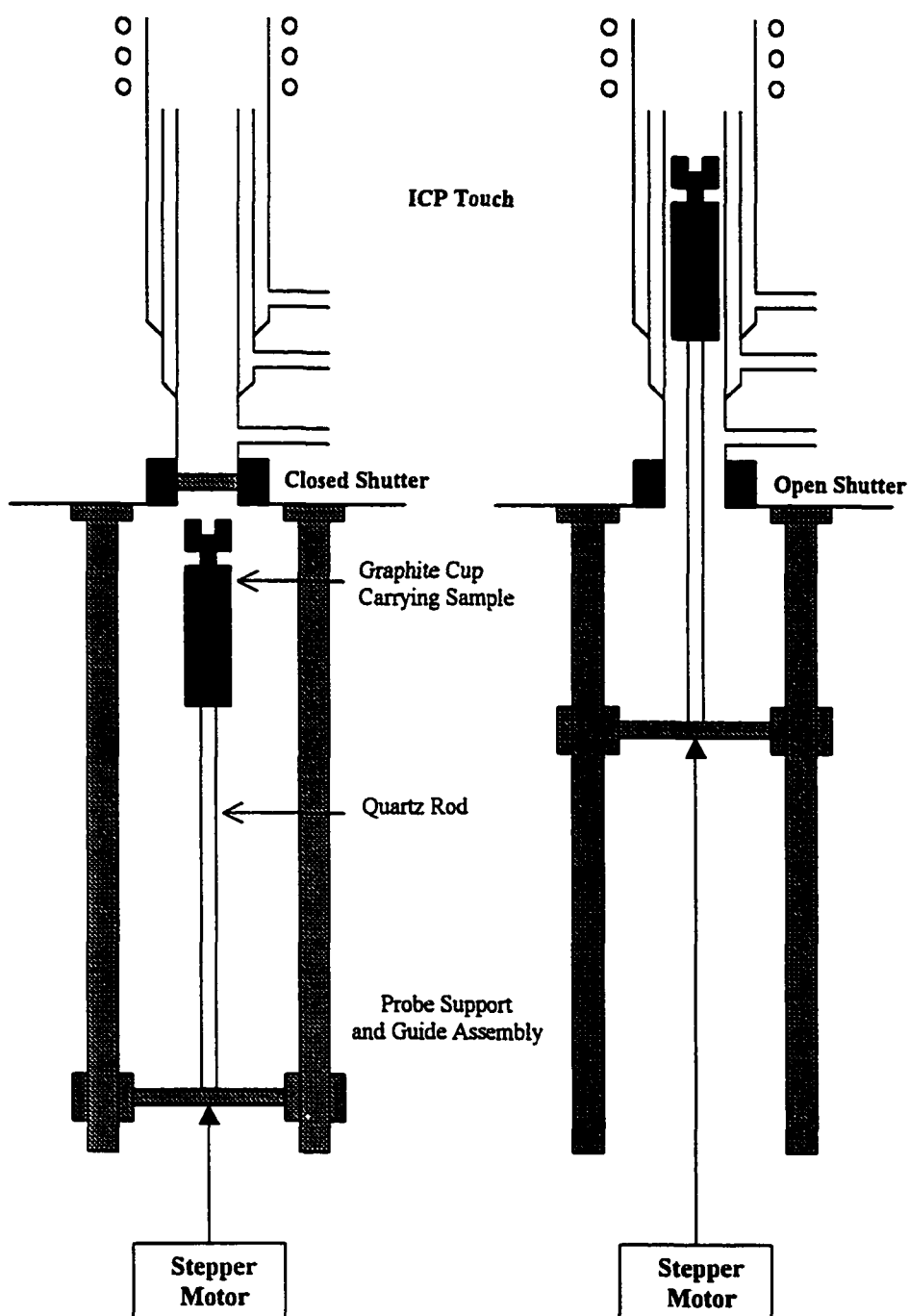


Figure 5.2 Schematic diagram of DSI (drawn based on the figure of a DSI system given by Karanassios and Horlick.²⁴⁰)

5.5 Objective of the Present Work

The previously developed technique²¹⁴ of solvent extraction into a 1- μ L drop of n-octane suspended at the tip of a microsyringe needle in a stirred aqueous solution, as introduced in section 5.3, has been shown to be a simple, inexpensive, and reproducible quantitative technique. This technique has been applied²¹⁵ to extract the steroid hormone progesterone from an aqueous medium containing the protein bovine serum albumin, with which this steroid forms a non-extractable complex. The volume of the aqueous medium in the system, in which the 1 μ L n-octane drop is suspended, is 500 mL, resulting in a very small phase ratio. Therefore, the removal of progesterone from the aqueous phase due to the extraction was too small to significantly perturb the equilibria in the aqueous phase, so the unbound (i.e. free) progesterone species could be successfully determined directly. This work suggested the feasibility of a novel speciation technique to determine the concentration of free metal ion in an aqueous medium which contains non-extractable metal complexes.

Extraction of metal ions directly into a water-immiscible organic phase is energetically unfavorable, and this process can only be accomplished by arranging that the metal ion be transferred to the organic phase as a neutral species. Such species can be produced by metal complexation or by the association of metal cations with anions whereby, by careful choice of ligand, a neutral species extractable by an organic solvent can be produced. Such extraction can be assisted by addition of solvating chelating agents to the organic phase.

In the present work a 1 μ L solution of a metal-chelating extractant in n-octane is employed as the organic phase. Therefore, free-metal species that can complex with the metal-chelating agent in n-octane are extracted into the organic drop. The analysis of this organic drop by ICP/MS then provides a measure of the free metal ion species. The coupling of micro-drop solvent extraction with ICP/MS is accomplished through a direct sample insertion device (DSID) (section 5.4).

Of the various metal species present in a sample, the free (hydrated) ion is often the most important species determining the behavior of metals in industrial, biological, clinical, and natural aqueous system.⁵⁰ Copper is an important metal pollutant because of its wide-spread application and subsequent distribution into the environment. It is evident that the free cupric ion (Cu^{2+}) is the most toxic copper species,⁵ and therefore, the determination of free Cu^{2+} is extremely important. In addition, copper is a well-studied element, and accordingly there is plentiful information from both the chemical and environmental points of view. Thus, copper is often the choice of element for evaluation of metal speciation methods. As a consequence, Cu^{2+} is the chosen species for investigation of the speciation technique developed in this work. And a copper complexing agent, Lix63, is used in organic phase as the desired chelating extractant.

The fundamental objectives of the present work are to explore the feasibility of the coupling technique of micro-drop solvent extraction-DSID-ICP/MS as a metal speciation tool, and to delineate the conditions required by this technique for determination of free Cu^{2+} ion in an aqueous sample in the presence of a soluble, labile copper(II) complex. In Chapter 6 of this work the theoretical basis of the extraction system under investigation is elucidated. The characterization of this technique is described in Chapter 7; its application for the determination of free Cu^{2+} in the presence of ligands is examined in Chapter 8; and some comments on the present work and the future work are given in Chapter 9.

Chapter 6

Theory for Part II

6.1 Introduction

In this chapter, some important equations describing the equilibrium aspects of metal solvent extraction are given. Among them, a derived expression gives the relationship between the concentration of the extracted metal chelate, $[ML_2]_o$, and the reported concentration of the free-metal ion, $[M^{2+}]$, in aqueous phase, where the ligand L⁻ is added as HL (i.e. Lix63) in the organic solvent. The conditions under which the extraction of ML_2 yields information of original $[M^{2+}]$ without being perturbed in an aqueous sample solution, which contains soluble, kinetically labile complex, MX^+ , are discussed. A perturbation model is also established to quantitatively describe the degree of perturbation.

Discussion of the equilibrium and perturbation consideration is then followed by a discussion of the kinetic mechanism of solvent extraction of ML_2 , with emphasis on the classification of extraction regime and the strategies to identify each individual regime. The kinetic consideration for the present work is then presented.

The computed metal distribution in aqueous phase will be used as a reference to compare with the experimental data. The last section of this chapter demonstrates the calculation of metal distribution used in this work.

6.2 Equilibrium Consideration

6.2.1 Equilibria in Metal Solvent Extraction Systems and Criteria for Speciation Measurement

The major components in the metal solvent extraction system discussed in this work are an organic phase containing metal chelating extractant and an aqueous phase containing various metal species, which include the free (hydrated) metal ions and soluble, kinetically labile metal complexes.

The following equation²⁴¹ describes the percentage of extraction, %E, in a solvent extraction system

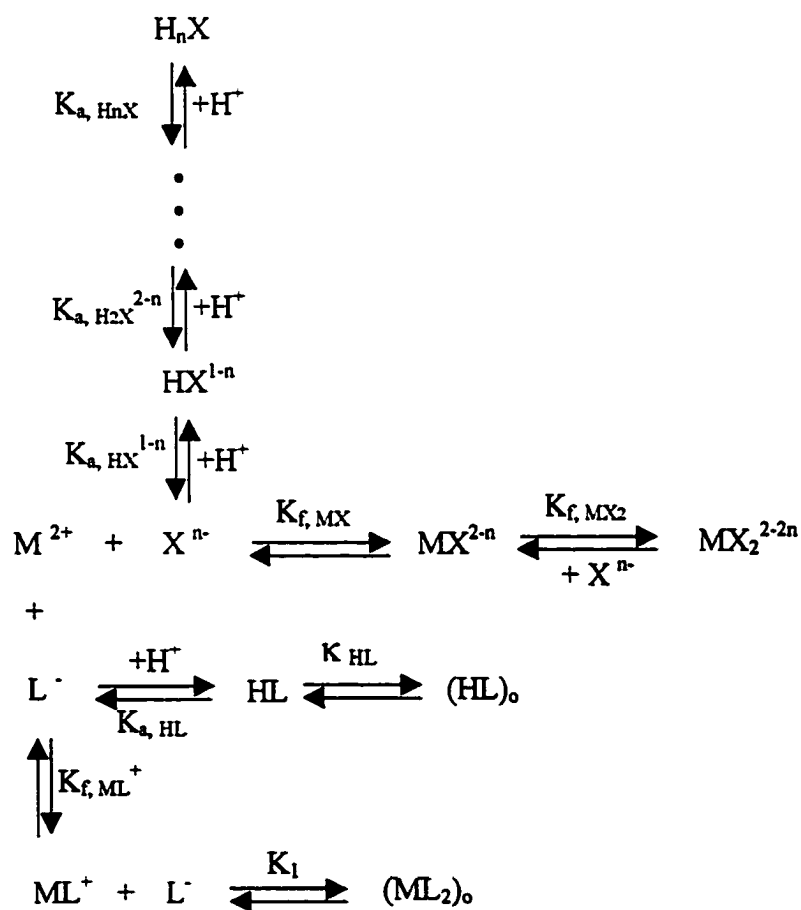
$$\%E = \frac{100\kappa}{\kappa + \frac{V_{\text{aq}}}{V_{\text{o}}}}$$

where κ is the distribution coefficient, and V_{aq} and V_{o} are the volumes of aqueous phase and organic phase, respectively. In order for a component to remain largely in the organic phase, both κ and the phase ratio of the system, $V_{\text{o}}/V_{\text{aq}}$, need to be relatively large.

In conventional metal solvent extraction, the phase ratio is usually near 1 and rarely as low as 0.01. As a consequence, it is not necessary for a chelating extractant to have a very large distribution coefficient to be able to remain in the organic phase with negligible dissolution of chelating extractant in the aqueous phase. However, in solvent micro-extraction systems the phase ratio is so small (for example, 2×10^{-6} in this work) that the dissolution of chelating extractant can not be neglected.

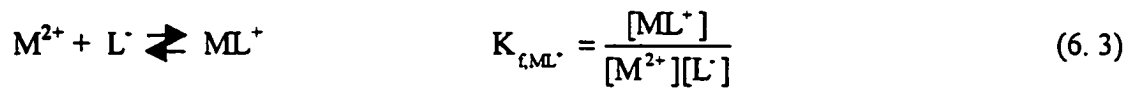
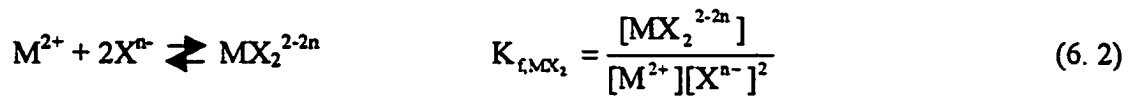
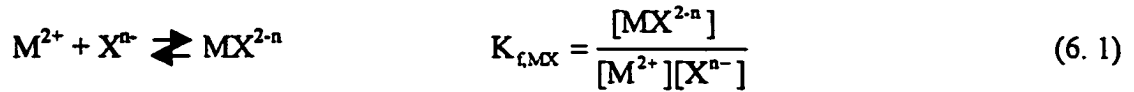
The equilibria present in the metal solvent extraction system are illustrated in Scheme 6.1, in which “M” stands for metal, “HL” represents the conjugate acid of the chelating extractant and “ H_nX ” represents the neutral acid form of a ligand X^{n-} which is present in the aqueous phase. For simplicity, it is assumed that: (a) free metal ion is doubly charged; (b) X^{n-} is the only complexing ligand present in the aqueous sample; and (c) MX^{2-n} , MX_2^{2-2n} , ML^+ and ML_2 are the only M-X complexes and M-L complexes formed in the system. The aqueous system also contains hydroxo-complexes of Cu(II), such as $Cu(OH)_2$. However, since all solutions (test and standard) will be buffered at the

same pH, they will contain the same concentrations of OH⁻. Therefore, the Cu(II) concentration of the test solution obtained with the aid of calibration curve established by the standard solutions will be correct even though the existence of copper-hydroxo species is not explicitly taken into account in the following discussion. The subscripts “f” and “a” indicate formation constant and acidic dissociation constant, respectively. The subscript “o” indicates “in organic phase”. In the equations below the additional symbol K_f' stands for conditional formation constant, and “C” represents the initial total concentration. All species without subscripts are in the aqueous phase.

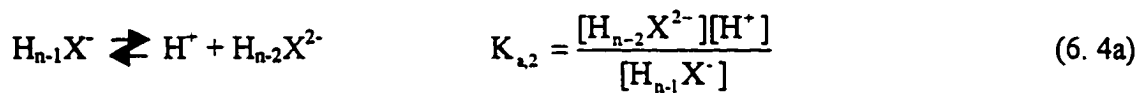
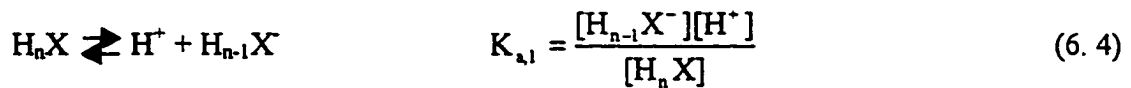


Scheme 6.1 Equilibria in Metal Solvent Extraction Systems

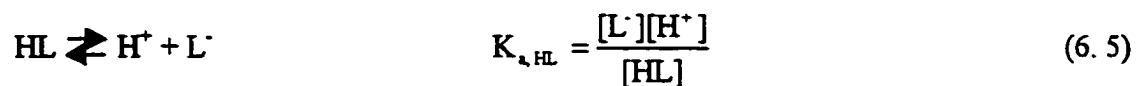
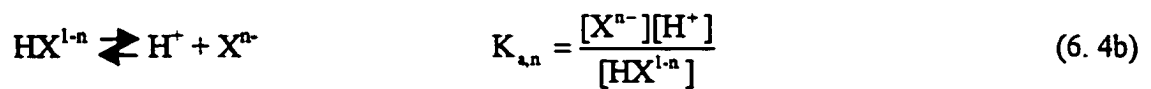
Equilibria in complexation:



Equilibria in dissociation reactions:



...



Distribution Equilibrium:



If $[L^-]$ is constant, we can get

$$\frac{[ML_2]_o}{[ML^+]} = K_1[L^-] = K_2 \quad (6.6a)$$

Since MX^{2-n} and MX_2^{2-2n} are assumed to be the only M-X complexes, a further simplification in later discussions will be to use the symbol "MX" and "MX₂" instead of "MX²⁻ⁿ" and "MX₂²⁻²ⁿ".

Mass balances that are involved in the system are presented below:

$$C_{M, aq} = [M^{2+}] + [MX] + [MX_2] + [ML^+] + [ML_2]_o \frac{V_o}{V_{aq}} \quad (6.7)$$

$$C_{X, aq} = [H_n X] + [H_{n-1} X^-] + \dots + [X^{n-}] + [MX] + 2[MX_2] \quad (6.8)$$

$$C_{L, o} \frac{V_o}{V_{aq}} = [L^-] + [HL] + [HL]_o \frac{V_o}{V_{aq}} + [ML^+] + 2[ML_2]_o \frac{V_o}{V_{aq}} \quad (6.9)$$

The following conditions need to be maintained in the system in order to obtain speciation information:

- (1) ML_2 is the only extractable species among all M(II)-complexes in the aqueous phase.
- (2) The amount of complexed chelating extractant is much less than the total amount of

extractant present in the system, i.e., $[ML^+] + 2[ML_2]_o \frac{V_o}{V_{aq}} \ll C_{L,o} \frac{V_o}{V_{aq}}$. In

other words, the extraction system is under the condition of trace loading of reagent.

- (3) The original equilibria in the aqueous phase must not be perturbed. This requirement can be met by keeping the amount of metal that is complexed by the chelating extractant much less than that of the total metal in the system, i.e., $[ML^+] + [ML_2]_o$

$$\frac{V_o}{V_{aq}} \ll C_{M, aq}.$$

- (4) The rate of extraction must not be controlled by the rate of diffusion in aqueous phase.

In order to achieve the second and third conditions, both the concentration of species (ML^+) and the concentration of species $(ML_2)_o$ should be kept small.

Consequently, any factors that will cause the increase of either $[ML^+]$ or $[ML_2]_o$ should be avoided. This point will be further discussed in section 6.3. Condition (4) will be discussed in section 6.4.2.

When condition (2) is maintained, i.e., $[ML^+] + 2[ML_2]_o \frac{V_o}{V_{aq}} \ll C_{L,o} \frac{V_o}{V_{aq}}$, we

can assume that the change of $[L^-]$ due to its complexation with metal is negligible. Alternatively speaking, $[L^-]$ is constant during the extraction process. In simplification, $[L^-]$ will be treated as a constant throughout the derivation in the following section.

6.2.2 Relationship between $[ML_2]_o$ and $C_{M, aq}$

6.2.2.1 EDTA, Glycine and Citrate Systems

In those systems studied in this work in which EDTA, glycine and citrate are present as the complexing ligand in the aqueous sample, the principal copper complex with the ligand is a 1:1 copper to ligand complex, and other copper complexes are negligible. Therefore, in these cases, MX is the only $M-X$ complex considered and

species MX_2 (which appears in earlier sections) will be ignored from the following derivation.

Rearrangement of equation 6.1 and 6.3 yields

$$[\text{MX}] = K_{f,\text{MX}}[\text{M}^{2+}][\text{X}^{n-}] \quad (6.10)$$

$$[\text{M}^{2+}] = \frac{[\text{ML}^+]}{[\text{L}^-]K_{f,\text{ML}^+}} \quad (6.11)$$

Inserting equation 6.6a, 6.10 and 6.11 into equation 6.7 and rearranging, gives

$$[\text{ML}_2]_o = \frac{C_{\text{M,eq}}}{\frac{V_o}{V_{\text{eq}}} + \frac{1}{K_2} + \frac{1}{K_2[\text{L}^-]K_{f,\text{ML}^+}} + \frac{[\text{X}^{n-}]K_{f,\text{MX}}}{K_2[\text{L}^-]K_{f,\text{ML}^+}}} \quad (6.12)$$

Rearranging equation 6.1 and the equations 6.4, 6.4a, and 6.4b and then inserting them into equation 6.8, gives

$$C_{\text{X,eq}} = \frac{[\text{X}^{n-}][\text{H}^+]^n}{K_{a,1}K_{a,2} \dots K_{a,n}} + \frac{[\text{X}^{n-}][\text{H}^+]^{n-1}}{K_{a,2}K_{a,3} \dots K_{a,n}} + \dots + [\text{X}^{n-}] + [\text{X}^{n-}][\text{M}^{2+}]K_{f,\text{MX}} \quad (6.13)$$

Recognizing that $[\text{X}^{n-}]$ is common to all terms:

$$C_{X,aq} = [X^{n-}] \left(\frac{[H^+]^n}{K_{a,1} K_{a,2} \dots K_{a,n}} + \frac{[H^+]^{n-1}}{K_{a,2} K_{a,3} \dots K_{a,n}} + \dots + 1 + [M^{2+}] K_{f,MX} \right) \quad (6.14)$$

The fraction of component X which is present as the species X^{n-} when no metal present, α_X , is

$$\alpha_X = \frac{1}{1 + \frac{[H^+]}{K_{a,n}} + \frac{[H^+]^2}{K_{a,n} K_{a,(n-1)}} + \dots + \frac{[H^+]^n}{K_{a,n} K_{a,(n-1)} \dots K_{a,1}}} \quad (6.15)$$

Inserting equation 6.15 into 6.14 yields

$$[X^{n-}] = \frac{\alpha_X C_{X,aq}}{1 + [M^{2+}] K_{f,MX} \alpha_X} \quad (6.16)$$

and then applying equation 6.6a and 6.11 to equation 6.16 gives

$$[X^{n-}] = \frac{\alpha_X C_{X,aq}}{1 + \frac{[ML_2]_o K_{f,MX} \alpha_X}{K_2 [L^-] K_{f,ML^+}}} \quad (6.17)$$

The conditional formation constant of MX is

$$K_{f,MX}' = K_{f,MX} \alpha_X \quad (6.18)$$

Inserting equations 6.17 and 6.18 into equation 6.12 yields

$$\begin{aligned}
 & [\text{ML}_2]_o \\
 & = \frac{C_{\text{M,aq}}}{\frac{V_o}{V_{\text{aq}}} + \frac{1}{K_2} + \frac{1}{K_2[\text{L}^-]K_{\text{f,ML}^*}} + \frac{C_{\text{X,aq}}K_{\text{f,MX}}}{K_2[\text{L}^-]K_{\text{f,ML}^*} + K_{\text{f,MX}} [\text{ML}_2]_o}}
 \end{aligned} \tag{6.19}$$

Equation 6.19, which is a quadratic equation in $[\text{ML}_2]_o$, gives the relationship between the concentration of extracted ML_2 in the organic phase, $[\text{ML}_2]_o$, and the concentration of original total metal in the aqueous phase, $C_{\text{M,aq}}$, for the system in the presence of EDTA, glycine or citrate.

6.2.2.2 Phthalate System

In the above discussion, MX is the only M-X species significantly present in the system as assumed earlier. However, in the system studied in which phthalate is present as the complexing ligand H_nX , both MX and MX_2 are the principle M-X species. In this case, equation 6.12 becomes

$$\begin{aligned}
 & [\text{ML}_2]_o \\
 & = \frac{C_{\text{M,aq}}}{\frac{V_o}{V_{\text{aq}}} + \frac{1}{K_2} + \frac{1}{K_2[\text{L}^-]K_{\text{f,ML}^*}} \left(1 + [\text{X}^{n-}]K_{\text{f,MX}} + [\text{X}^{n-}]^2K_{\text{f,MX}_2} \right)}
 \end{aligned} \tag{6.12a}$$

In the phthalate system of the present work, $C_{\text{X,aq}} \gg C_{\text{M,aq}}$, (i.e. $C_{\text{X,aq}}/C_{\text{M,aq}} \geq 200$), so the

fraction of X^{n-} that complexes with metal is negligible, then

$$[X^{n-}] \approx C_{X, \text{aq}} \alpha_X \quad (6.16a)$$

Inserting equation 6.16a into equation 6.12a yields

$$[ML_2]_o = \frac{C_{M, \text{aq}}}{\frac{V_o}{V_{\text{aq}}} + \frac{1}{K_2} + \frac{1}{K_2[L^-]K_{f, ML^+}} \left(1 + C_{X, \text{aq}} \alpha_X K_{f, MX} + C_{X, \text{aq}}^2 \alpha_X^2 K_{f, MX_2} \right)} \quad (6.19a)$$

Instead of a quadratic equation, as equation 6.19, equation 6.19a gives a simpler expression of $[ML_2]_o$ for the phthalate case.

6.2.3 Calibration Curve

For an X - containing aqueous sample before solvent extraction

$$C_{M, \text{aq}} = [M^{2+}]_{L=0} + [MX]_{L=0} + [MX_2]_{L=0} \quad (6.20)$$

where the subscript "L=0" refers to the sample solution prior to adding reagent HL.

Comparing equation 6.20 with equation 6.7 we can see that the addition of HL to the sample solution produces the two more species, which are present in the right hand side of equation 6.7. Here, we can rewrite equation 6.7 as following, which emphasizes the presence of HL.

$$C_{M, \text{aq}} = [M^{2+}]_{L \neq 0} + [MX]_{L \neq 0} + [MX_2]_{L \neq 0} + [ML^+] + [ML_2]_o \frac{V_o}{V_{\text{aq}}} \quad (6.7a)$$

In quantitative analysis, calibration curves are required and they are often generated by adding reagent (e.g. HL) to standard metal solutions which do not contain complexing ligands (e.g. X) and hence only have free metal species, M^{2+} . It is noteworthy that even in the measurement of a standard metal solution, if the chelating extractant dissolves from the organic phase into the aqueous phase, the original aqueous phase containing only free metal species ($[M^{2+}]_{L=0}$) will be changed to have both free metal M^{2+} and M-L complex. In this case the mass balance of metal is obtained by omitting $[MX]$ and $[MX_2]$ from equation 6.7 to get:

$$C_{M, aq} = [M^{2+}]_{L=0} = [M^{2+}]_{L \neq 0} + [ML^+] + [ML_2]_o \frac{V_o}{V_{aq}} \quad (6.21)$$

When establishing a calibration curve by using standard solutions, since there are no M-X species, equation 6.19 and 6.19a can be simplified to be

$$[ML_2]_o = \frac{C_{M, aq}}{\frac{V_o}{V_{aq}} + \frac{1}{K_2} + \frac{1}{K_2[L^-]K_{fML^+}}} \quad (6.22)$$

Inserting equation 6.21 into equation 6.22 yields

$$[ML_2]_o = \frac{[M^{2+}]_{L=0}}{\frac{V_o}{V_{aq}} + \frac{1}{K_2} + \frac{1}{K_2[L^-]K_{fML^+}}} \quad (6.23)$$

Equation 6.23 describes the calibration curve, which is the plot of $[ML_2]_o$ vs. $[M^{2+}]_{L=0}$, where $[ML_2]_o$ is measured directly from experiment and $[M^{2+}]_{L=0}$ is equal to the concentration of free metal in the standard solution before having added HL to the system.

In the X – containing sample system, there are M-X species in addition to the free metal species. If M-X species are kinetically inert, the sample solution can be simply considered as a solution containing only free metal ions. Then, the free metal concentration ($[M^{2+}]_{L=0}$ in equation 6.20) in the sample can be obtained through applying calibration curve (equation 6.23) by using the measured value of $[ML_2]_o$ as in the following equation:

$$\text{Reported } [M^{2+}] = [ML_2]_o \left(\frac{V_o}{V_{aq}} + \frac{1}{K_2} + \frac{1}{K_2[L^-]K_{f,ML^+}} \right) \quad (6.24)$$

However, if M-X species are kinetically labile, “reported $[M^{2+}]$ ” is equal to $[M^{2+}]_{L=0}$ only when the system is non-perturbed. When the system is perturbed, the “reported $[M^{2+}]$ ” will be a false value of the free metal ion concentration. This will be further discussed in section 6.3.

From equation 6.23 we can see that the slope of the calibration curve is

$$\text{Slope} = \left(\frac{V_o}{V_{aq}} + \frac{1}{K_2} + \frac{1}{K_2[L^-]K_{f,ML^+}} \right)^{-1} \quad (6.25)$$

It is obvious that the slope is constant and the calibration curve is linear, as long as the value of $[L]$ is kept constant by having $C_{L,o} \gg C_{M,aq} \times \frac{V_{aq}}{V_o}$.

6.3 Discussion of Perturbation at Equilibrium

In a speciation study, it is essential that the original species distribution of the system be non-perturbed during measurement. In a sample containing kinetically labile M-X species, the presence of the reagent HL can cause two types of perturbation as a result of complexation of M^{2+} by L^- . They may be understood from the fourth and fifth terms on the right hand side of equation 6.7, $[ML^+]$ and $[ML_2]_o \frac{V_o}{V_{aq}}$. The first type of perturbation arises from the formation and presence of ML^+ in the aqueous phase and the second arises from the extraction of ML_2 into the organic phase.

Criteria used for indicating the presence and degree of perturbation would be very helpful to know when choosing experimental conditions. For this purpose, the ratio of the reported concentration of free metal ion calculated from the experimentally measured values of $[ML_2]_o$ in the presence of HL, "Reported $[M^{2+}]$ ", to the true value in the original unperturbed sample solution in the absence of HL, $[M^{2+}]_{L=0}$, is chosen to be the criterion for perturbation. This ratio is called Perturbation Factor. Its value is predicted through following steps:

a. Calculation of "Reported $[M^{2+}]_{t=\infty}$ " at equilibrium

"Reported $[M^{2+}]_{t=\infty}$ " is obtained by inserting $[ML_2]_o$ obtained from solving the quadratic equation 6.19 (for EDTA, glycine and citrate systems) or equation 6.19a (for phthalate system), into equation 6.24.

b. Calculation of $[M^{2+}]_{L=0}$ at equilibrium

(1) For EDTA, glycine and citrate systems (MX is the only M-X species):

When there is no HL present in the system ($L=0$), the mass balance of metal is given by equation 6.20. Inserting equation 6.10 along with equation 6.16 into equation 6.20 and omitting all the MX_2 terms gives

$$C_{M,eq} = [M^{2+}]_{L=0} \left(1 + \frac{C_{X,eq} K_{f,MX}'}{1 + [M^{2+}]_{L=0} K_{f,MX}} \right) \quad (6.26)$$

The solution of this quadratic equation for $[M^{2+}]_{L=0}$ is:

$$[M^{2+}]_{L=0} = \frac{(C_{M,eq} - C_{X,eq}) K_{f,MX}' - 1 + \sqrt{[(C_{M,eq} - C_{X,eq}) K_{f,MX}' - 1]^2 + 4 K_{f,MX}' C_{M,eq}}}{2 K_{f,MX}'} \quad (6.27)$$

(2) For phthalate system (with both MX and MX_2):

Inserting equation 6.1, 6.2 and equation 6.16a into equation 6.20 gives

$$[M^{2+}]_{L=0} = \frac{C_{M,eq}}{1 + K_{f,MX} C_{X,eq} \alpha_X + K_{f,MX_2} C_{X,eq}^2 \alpha_X^2} \quad (6.27a)$$

c. Calculation of Perturbation Factor at equilibrium:

$$\text{Perturbation Factor (PF)} \equiv \frac{\text{Reported } [M^{2+}]_{t=\infty}}{[M^{2+}]_{L=0}} \quad (\text{at equilibrium}) \quad (6.28)$$

If there is no perturbation during extraction, “Reported $[M^{2+}]$ ” should be equal to $[M^{2+}]_{L=0}$, so the Perturbation Factor is one. Otherwise, when perturbed, the Perturbation Factor is greater than one because the ligand L^- has removed some M^{2+} from the $M-X$ complex to produce more ML^+ which raises $[ML_2]_o$ and thereby leads to a falsely greater value of “Reported $[M^{2+}]$ ” (equation 6.24). In this case, the falsely high values of the “reported $[M^{2+}]$ ” would have to be *divided by the Perturbation Factor* in order to obtain the true value of $[M^{2+}]$. The reason why “Reported $[M^{2+}]$ ” for an X^- - containing sample is larger than $[M^{2+}]_{L=0}$ for that sample is because L^- competes with X^- for M^{2+} in the sample giving a larger value of $[ML_2]_o$ than is obtained in a calibration standard (free of X^-) which contains the same $[M^{2+}]_{L=0}$. In short, if added HL reduces the concentration of MX , then perturbation occurs and “reported $[M^{2+}]$ ” $>$ $[M^{2+}]_{L=0}$.

Shown in figure 6.1, 6.2 and 6.3 are plots of the Perturbation Factor versus $\log K_{f,MX'}$ as function of $C_{X, aq} / C_{M, aq}$, $K_{f, ML^+} [L^-]$ and $\log K_2$, respectively. These plots reveal the important features of perturbation caused by the presence of the ligand-producing reagent HL.

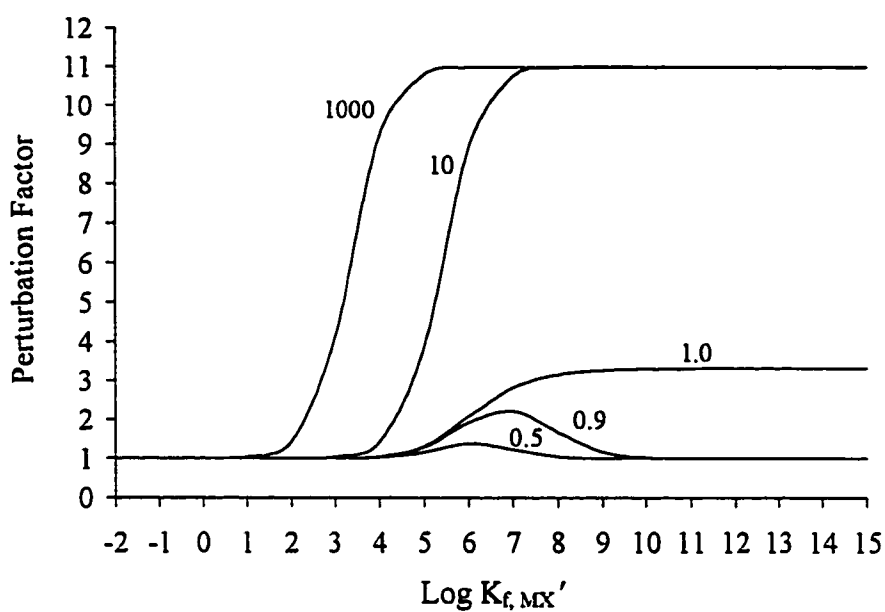


Figure 6.1 Equilibrium Perturbation Factor versus $\text{Log } K_{f, \text{MX}'}$ at the various values of $C_{X, \text{aq}} / C_{M, \text{aq}}$ shown by the numbers next to the curves, at constant values of $V_o / V_{\text{aq}} = 2.00 \times 10^{-6}$, $C_{M, \text{aq}} = 5.00 \times 10^{-6} \text{M}$, $K_2 = 367$ (calculated according to equation 8.4) and $K_{f, \text{ML}^+}[\text{L}] = 10.0$. The horizontal line at $\text{PF} = 1.00$ indicates no perturbation caused by the presence of reagent HL.

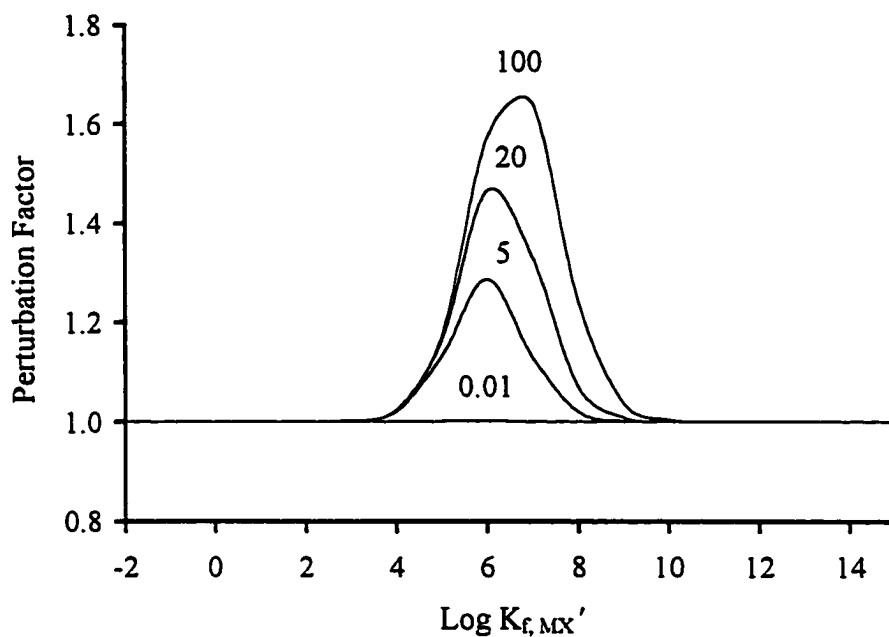


Figure 6.2 Equilibrium Perturbation Factor versus $\text{Log } K_{f, MX}'$ at the various values of $K_{f, ML}^+[L]$ shown by the numbers next to the curves, at constant values of $V_o / V_{aq} = 2.00 \times 10^{-6}$, $C_{M, aq} = 5.00 \times 10^{-6} M$, $C_{X, aq} / C_{M, aq} = 0.50$, and $K_2 = 186, 193, 220$ and 1860 (calculated according to equation 8.4) for the case of $K_{f, ML}^+[L] = 100, 20, 5$ and 0.01 , respectively. The horizontal line at $PF = 1.00$ indicates no perturbation caused by the presence of reagent HL.

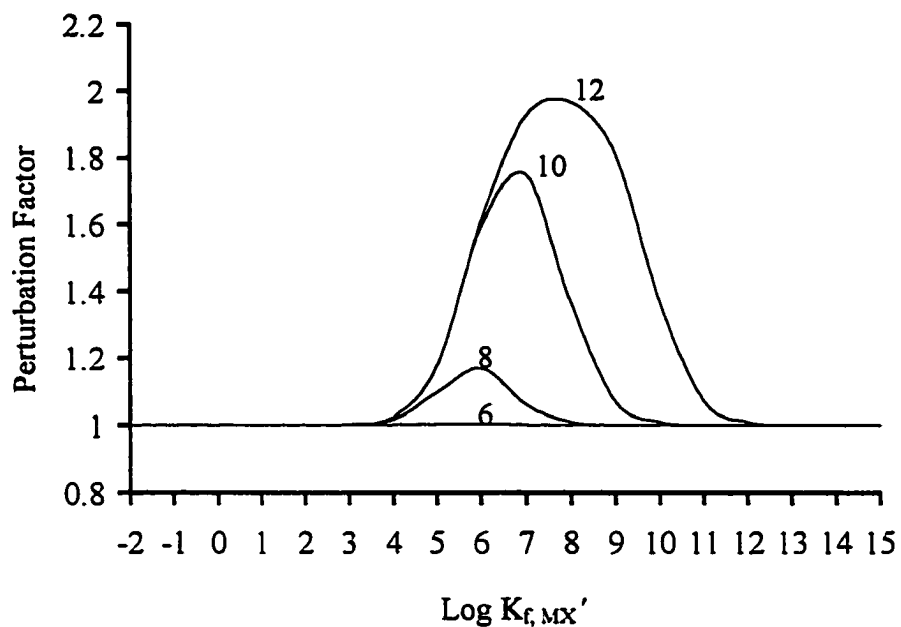


Figure 6.3 Equilibrium Perturbation Factor versus $\text{Log } K_{f, \text{MX}'}$ at the various values of $\log K_2$ shown by the numbers next to the curves, at constant values of $V_o/V_{\text{aq}} = 2.00 \times 10^{-6}$, $C_{\text{M, aq}} = 5.00 \times 10^{-6} \text{M}$, $K_{f, \text{ML}^+[\text{L}]} = 0.01$ and $C_{\text{X, aq}} / C_{\text{M, aq}} = 0.50$. The horizontal line at $\text{PF} = 1.00$ indicates no perturbation caused by the presence of reagent HL.

In all these figures it can be seen that for a small value of $\log K_{f,MX}$, which means that the $[M^{2+}]_{L=0} \gg [MX]_{L=0} + [MX_2]_{L=0}$ in the original sample, there is no perturbation (i.e. Perturbation Factor = 1.00). The trivial case, in which there is no X^{n-} present in the sample, will obviously also yield a perturbation factor of 1.00, since sample and standard are perturbed equally and equation 6.24 describes both.

In Figure 6.1 it can be seen that when $C_{X, aq} / C_{M, aq} < 1$ there is no perturbation for a sufficiently large value of $\log K_{f,MX}$. However, when $C_{X, aq} / C_{M, aq} > 1$ there is always a perturbing effect of added reagent HL for high values of $\log K_{f,MX}$. This is because in the sample solution, which contains X^{n-} , when the value of $\log K_{f,MX}$ is large and $C_{X, aq} / C_{M, aq} > 1$, most of the metal is in the MX form so that the solution is well buffered in M^{2+} . Thus, the sample is not perturbed by HL but the standard is.

It is seen in Figure 6.2, that a lower value of $K_{f, ML^+} [L^-]$ reduces the perturbation. As already pointed out in the beginning of this section, the perturbation is caused by the presence of $[ML^+]$ in the aqueous phase and the presence of $[ML_2]_o$ in the organic phase. On one hand, since the amount of $[ML^+]$ depends on the value of K_{f, ML^+} and $[L^-]$, the condition for $[ML^+]$ to be negligible is to have a small value of $K_{f, ML^+} [L^-]$. On the other hand, since $[ML_2]_o$ is associated with $[ML^+]$ via the constant K_2 (as defined in equation 6.6a), then the condition for $[ML_2]_o$ to be negligible is a small value of $K_2 K_{f, ML^+} [L^-]$. The value of K_2 used in Figure 6.2 was calculated using the experimental result obtained in Cu-Lix63 system, as described in section 8.3 below.

Figure 6.3 demonstrates how the value of K_2 effects perturbation when $K_{f, ML^+} [L^-]$ (=0.01) is small enough to make $[ML^+]$ negligible. In this case K_2 can be as large as 1×10^6 and still $[ML_2]_o$ is negligible (no perturbation, i.e. Perturbation Factor = 1.00). However, these limiting values of $K_{f, ML^+} [L^-]$ and K_2 for the unperturbed condition vary with other experimental conditions, such as V_o / V_{aq} and $C_{X, aq} / C_{M, aq}$.

Although it is desirable to have a small value of K_2 , this constant must not be made too small because $[ML_2]_o$ will become too small to measure, and the technique

depends on measuring $[ML_2]_o$. With this in mind, if the values of $K_{f,ML^+} [L^-]$ and $K_2 K_{f,ML^+} [L^-]$ are small enough, the unperturbed condition is achieved and equation 6.21 for the standard then becomes:

$$C_{M,aq} = [M^{2+}]_{L=0} = [M^{2+}]_{L \neq 0} \quad (\text{for the unperturbed case at equilibrium})$$

and equation 6.23 for the calibration curve becomes:

$$[ML_2]_o = [M^{2+}]_{L=0} \cdot [K_2 [L^-] K_{f,ML^+}] \quad (\text{for the unperturbed case at equilibrium}) \quad (6.29)$$

The calibration curve has the slope $(K_2 [L^-] K_{f,ML^+})$.

For the sample, equation 6.7 becomes identical to equation 6.20:

$$C_{M,aq} = [M^{2+}]_{L=0} + [MX]_{L=0} + [MX_2]_{L=0} \quad (\text{for the unperturbed case at equilibrium})$$

and equations 6.19 and 6.19a lose their first two denominator terms as a result of the derivation using equation 6.20 instead of equation 6.7. Combining equation 6.19 with equation 6.29 and 6.26 (for EDTA, glycine and citrate) yields:

$$[ML_2]_o = \frac{[M^{2+}]_{L=0} \cdot \left(1 + \frac{C_{X,aq} K_{f,MX} K_2 [L^-] K_{f,ML^+}}{K_2 [L^-] K_{f,ML^+} + K_{f,MX} [ML_2]_o} \right)}{\frac{1}{K_2 [L^-] K_{f,ML^+}} \cdot \left(1 + \frac{C_{X,aq} K_{f,MX} K_2 [L^-] K_{f,ML^+}}{K_2 [L^-] K_{f,ML^+} + K_{f,MX} [ML_2]_o} \right)} \quad (\text{for the unperturbed case at equilibrium}) \quad (6.30)$$

for EDTA, glycine and citrate. Combining equation 6.19a with equation 6.27a (for phthalate) yields:

$$[\text{ML}_2]_0 = \frac{[\text{M}^{2+}]_{\text{L}=0} \cdot \left(1 + K_{\text{f, MX}} C_{\text{X, aq}} \alpha_X + K_{\text{f, MX}_2} C_{\text{X, aq}}^2 \alpha_X^2\right)}{\frac{1}{K_2 [\text{L}^-] K_{\text{f, ML}^-}} \cdot \left(1 + K_{\text{f, MX}} C_{\text{X, aq}} \alpha_X + K_{\text{f, MX}_2} C_{\text{X, aq}}^2 \alpha_X^2\right)}$$

(for the unperturbed case at equilibrium) (6.30a)

for phthalate. Canceling the parenthetic terms in numerator and denominator in either equation 6.30 or equation 6.30a yields

$$[\text{ML}_2]_0 = [\text{M}^{2+}]_{\text{L}=0} \cdot \left[K_2 [\text{L}^-] K_{\text{f, ML}^-} \right] \quad (\text{for the unperturbed case at equilibrium}) \quad (6.31)$$

Equation 6.31 is the same as equation 6.29 showing that under the unperturbed conditions the calibration curve gives the correct relationship between the measured value of $[\text{ML}_2]_0$ and the desired value of $[\text{M}^{2+}]_{\text{L}=0}$ for a sample which contain the kinetically labile M-X complex.

Naturally, if the complex MX^{n-2} is kinetically inert then no perturbation is possible and, even under the conditions of equation 6.21, the calibration curve will yield the correct relationship between $[\text{ML}_2]_0$ and $[\text{M}^{2+}]_{\text{L}=0}$ for the sample.

6.4 Extraction Kinetics

Although the general topic of solvent extraction of metals is well treated in many textbooks and reviews, there are only limited studies on the kinetic mechanism of the metal extraction due to the relatively small amount of literature available and the inconsistent concepts used on this subject by different research groups. Nevertheless,

there are a number of publications,^{192,242,243,244,245,246,247,248,249,250} among which Danesi and Chiarizia¹⁹² have presented a comprehensive review, on the issue of metal extraction kinetics, based on which the theoretical discussion in this section is given.

6.4.1 Extraction Regime and Its Identification

In the course of the extraction of metal cations from an aqueous phase by a chelating extractant located in the organic phase, extractant molecules react with metal ions after removing their surrounding water molecules, to form a new coordination compound, soluble in the organic phase. In the meantime, the chemical species are transferred from the bulk of each phase to the interface and from one phase to another. All the mass transfer and chemical reaction steps can, in principle, be slow enough to determine the rate of metal solvent extraction. Since, in most practical solvent extraction processes, agitation is provided in one or both of the phases, the diffusion processes are limited to a so-called interfacial zone composed of diffusion films on both sides of the interface, located in the immediate proximity of the interface.

If all the chemical reaction steps that characterize the overall reaction mechanism are sufficiently fast and the agitation in the system is moderate, the mass transfer in the two diffusional films is the rate-determining step in the extraction process. In this case the chemical reactions can be considered to be instantaneous, the system is said to be in a “diffusional regime” and the kinetics of solvent extraction can be treated in terms of mass transfer theories. On the other hand, if the agitation in the system is sufficient or the diffusion coefficients of the chemical species are very large, the thickness of the interfacial diffusional zone can be negligibly thin. In this case the mass transfer process can be considered to be instantaneous with respect to the chemical reaction, which becomes the rate-determining step. Since the extraction process is chemically controlled and the kinetics of solvent extraction can be treated in terms of chemical kinetics, the system is said to be in a “chemical kinetic regime”.

The two cases described above are limiting cases. Sometimes metal solvent extraction is controlled by both mass transfer and chemical reaction, and the system is said to be in a “mixed regime”. This situation can occur when the rates of diffusion and the chemical reactions can not be neglected with respect to each other.

A number of works have been reported to identify the metal solvent extraction regime and to set the criteria for the identification of the regimes.²⁵¹ Whether or not there is an effect of agitation, temperature, phase ratio and phase inversion of the system on the extraction speed can all be applied as criteria to identify the regime. The influence of extraction regime on both the heat and mass transfer coefficients has also been reported as criteria.^{252, 253, 254} In addition, the determination of activation energy is suggested by Nemtsov to enable the distinguishing of extraction regimes.²⁵⁵ However, the uncertainty of the measurement of activation energy makes the suggestion of little practical application. Furthermore, a technique, called “the reference substance method”, has been suggested by Russian workers to identify the kinetic regimes.^{254, 256} This method is based on the addition to the solution to be studied of an inert component whose rate of extraction is known to be controlled only by diffusion.

Among all the above methods for identification of extraction regimes, the most convenient and commonly used methods are based on the influence of stirring speed and phase ratio on the rate of extraction. In these investigations, the initial rate of metal extraction, which is defined as $V_{\text{init}} = -dC/dt$, where C is the molar concentration of the extracted metal and t is time, has played an important role. When the system is in a diffusional regime, since the progressive increase of the stirring rate reduces the thickness of the diffusional stagnant films so as to speed up the extraction, this will result in that the initial rate of metal extraction, V_{init} , will increase with the stirring speed.¹⁹² As the stirring speed is increased and the diffusion processes become faster, a slow chemical reaction starts to become competitive with the diffusional processes in controlling the rate of extraction. The chemical reaction itself would finally become rate determining when a further decrease of thickness of the stagnant films has no further influence on the overall rate of the extraction process. In this circumstance, the initial rate of the extraction should

be independent of the degree of agitation in the system and the plot of V_{init} vs. stirring rate reaches a plateau.

Sometimes the independence of the extraction rate on stirring speed may not really mean the chemical reaction is the controlling step in a solvent extraction process. Since the agitation in a common extraction system produces one phase dispersed as droplets in the other (continuous) phase, any increase in interfacial area caused by increased agitation will be accompanied by a decrease in size of the dispersed drop. This can decrease the disperse phase mass transfer coefficient by reducing the extent of internal circulation in the drops and the extent of drop coalescence.¹⁹² These factors can compensate for the increased interfacial area and hence make an extraction process in the diffusional regime appear insensitive to agitation. However, this problem is eliminated in the present work, because the organic phase in the solvent extraction system in this work is a suspended drop, which is very stable and approximately keeps a constant surface area regardless of the agitation applied in the aqueous phase. In consequence, the agitation will be expected to increase the mass transfer rate by increasing the circulation in both the organic drop and the aqueous bulk solution, without other side effects.

An effect of changes in phase ratio on solvent extraction rate is expected in a diffusional regime.¹⁹² In contrast, if an extraction process is controlled by chemical reaction in one phase, then the reaction rate should depend only on the conditions in the phase in which the reaction takes place and have nothing to do with the other phase and hence the phase ratio.

6.4.2 Kinetic Consideration in the Present Work

In the present work, it is desired to determine $[M^{2+}]_{t=0}$ from measurements of $[ML_2]_0$ made at times $t > 0$. In section 6.3 it was shown that at equilibrium (i.e. $t = \infty$), in the absence of perturbation, it is possible to calculate the desired value of $[M^{2+}]_{t=0}$ (i.e. $[M^{2+}]_{L=0}$) from a measurement of $[ML_2]_0$ using equation 6.29 and 6.31 with a calibration curve; and that at equilibrium, in the presence of perturbation, it is possible to calculate a

Perturbation Factor which can be used to predict the error in the process of calculating $[M^{2+}]_{t=0}$ from $[ML_2]_0$.

However, making measurements at equilibrium may not be practical if the extraction rate is slow. Whether $[M^{2+}]_{t=0}$ can accurately be calculated from values of $[ML_2]_0$ measured prior to equilibration depends on the mechanism of the extraction kinetics, i.e. chemical reaction rate control or mass transfer rate control, and, for the latter, whether the slow mass transfer step occurs in the aqueous or the organic (microdrop) phase. These cases are examined below.

6.4.2.1 Chemical Kinetic Control

Since the reaction between M^{2+} and L^- to form ML^+ is reported to be fast and the reaction between ML^+ and L^- to produce $(ML_2)_0$ is slow for Cu^{2+} ,²⁰¹ the case of chemical reaction rate control will be modeled as a pseudo-first order reaction between ML^+ and L^- , either in the bulk aqueous phase or at the interface, with a large excess of HL. The relationship between the equilibrium concentration $[ML_2]_0$ and the concentration $[ML_2]_{0,t<\infty}$ at a time less than infinity is given by:

$$[ML_2]_{0,t<\infty} = [ML_2]_0 \cdot (1 - \exp(-k_s t)) \quad (6.32)$$

where k_s is the chemical reaction rate constant and its expression is derived below. The following derivation is performed for both the case of the sample (with X^{n-} present) and the case of the standard (with no X^{n-} present).

(1) For the standard (with no X^{n-} present)

Experimentally, it is shown in section 7.4.2 below that the rate of reaction is first order. Although reaction 6.6 is reversible, the reaction is studied for only 5 min. and, therefore, can be approximated as irreversible (i.e. initial rate). Furthermore, since $[L^-]$ is present in large excess it is constant, so that:

$$\frac{d[\text{ML}_2]_o}{dt} = k[\text{ML}^+] \quad (6.33)$$

where k is the rate constant. Combining equation 6.3, 6.21, 6.33, rearranging and multiplying and dividing the right hand side by $\frac{V_0}{V_{\text{aq}}}$ yields

$$\frac{d[\text{ML}_2]_o}{dt} = \frac{k \left(\frac{V_0}{V_{\text{aq}}} \right)}{\left(1 + \frac{1}{K_{\text{fML}^+} [\text{L}^+]} \right)} \left(\frac{C_{\text{M,aq,STD}}}{\frac{V_0}{V_{\text{aq}}}} - [\text{ML}_2]_o \right) \quad (6.34)$$

At equilibrium ($t = \infty$)

$$[\text{ML}_2]_{o,t=\infty,\text{STD}} = \frac{C_{\text{M,aq,STD}}}{\frac{V_0}{V_{\text{aq}}}} \quad (6.35)$$

Substituting from 6.35 into 6.34 and identifying

$$k_{\text{STD}} \equiv k \left(\frac{K_{\text{fML}^+} [\text{L}^+] \frac{V_0}{V_{\text{aq}}}}{1 + K_{\text{fML}^+} [\text{L}^+]} \right) \quad (6.36)$$

gives the rate law:

$$\frac{d[\text{ML}_2]_o}{dt} = k_{\text{STD}} \left([\text{ML}_2]_{o,t=\infty,\text{STD}} - [\text{ML}_2]_o \right) \quad (6.37)$$

Integrating gives the rate equation for the standard:

$$[\text{ML}_2]_{o,t<\infty,\text{STD}} = [\text{ML}_2]_{o,t=\infty,\text{STD}} (1 - \exp(-k_{\text{STD}} t)) \quad (6.38)$$

The value of k_{STD} can be obtained experimentally by non-linear curve fitting of equation 6.38 to the first order reaction curve in Figure 7.8.

(2) For the sample (with X^{n-} present)

Combining equations 6.1, 6.2, 6.3 and 6.7, rearranging and multiplying and dividing the right-hand side by $\frac{V_0}{V_{\text{aq}}}$ yields

$$\frac{d[\text{ML}_2]_o}{dt} = \frac{k \left(\frac{V_0}{V_{\text{aq}}} \right)}{1 + \frac{1}{K_{\text{f,ML}^+} [\text{L}]} + \frac{K_{\text{f,MX}} [\text{X}^{n-}]}{K_{\text{f,ML}^+} [\text{L}]} + \frac{K_{\text{f,MX}_2} [\text{X}^{n-}]^2}{K_{\text{f,ML}^+} [\text{L}]}} \left(\frac{C_{\text{M,eq,SAMP}}}{\frac{V_0}{V_{\text{aq}}}} - [\text{ML}_2]_o \right) \quad (6.39)$$

At equilibrium ($t = \infty$)

$$[\text{ML}_2]_{o,t=\infty,\text{SAMP}} = \frac{C_{\text{M,eq,SAMP}}}{\frac{V_0}{V_{\text{aq}}}} \quad (6.40)$$

Substituting from 6.40 into 6.39 and identifying:

$$k_{\text{SAMP}} \equiv \frac{k \left(\frac{V_u}{V_{\text{aq}}} \right)}{1 + \frac{1}{K_{\text{f,ML}^{\cdot}}[\text{L}^{\cdot}]} + \frac{K_{\text{f,MX}}[\text{X}^{n-}]}{K_{\text{f,ML}^{\cdot}}[\text{L}^{\cdot}]} + \frac{K_{\text{f,MX}_2}[\text{X}^{n-}]^2}{K_{\text{f,ML}^{\cdot}}[\text{L}^{\cdot}]}} \quad (6.41)$$

gives the rate law:

$$\frac{d[\text{ML}_2]_0}{dt} = k_{\text{SAMP}} \left([\text{ML}_2]_{0,t=\infty,\text{SAMP}} - [\text{ML}_2]_0 \right) \quad (6.42)$$

Integrating gives the rate equation for the sample:

$$[\text{ML}_2]_{0,t<\infty,\text{SAMP}} = [\text{ML}_2]_{0,t=\infty,\text{SAMP}} (1 - \exp(-k_{\text{SAMP}} t)) \quad (6.43)$$

The relationship between k_{SAMP} and k_{STD} can be seen by comparing equation 6.36 and 6.41:

$$k_{\text{SAMP}} = \frac{k_{\text{STD}} (1 + K_{\text{f,ML}^{\cdot}}[\text{L}^{\cdot}])}{1 + K_{\text{f,ML}^{\cdot}}[\text{L}^{\cdot}] + K_{\text{f,MX}}[\text{X}^{n-}] + K_{\text{f,MX}_2}[\text{X}^{n-}]^2} \quad (6.44)$$

Unlike k_{STD} , the values of k_{SAMP} may change over time during the sample extraction because, although $[\text{L}^{\cdot}]$ is constant, the value of $[\text{X}^{\cdot}]$ may increase with time due to perturbation resulting from the competition of L^{\cdot} . However, as shown in (2a) and (2b) immediately below, under the experimental conditions employed, $[\text{X}^{\cdot}]$ is constant for the sample and, thus, k_{SAMP} is constant.

(2a) Rate constants for samples containing EDTA, glycine or citrate

The term $K_{\text{f,MX}_2}[\text{X}^{n-}]^2$ is deleted from equation 6.7 and 6.44. In addition, when the extraction is allowed to proceed for only a short time (i.e. 5 min in the present case) it

may be approximated as an initial-rate measurement during which the amount of $(ML_2)_0$ formed is small so that the term $[ML_2]_0 \frac{V_0}{V_{aq}}$ can also be deleted from equation 6.7.

Equation 6.7 then has the form:

$$C_{M,aq} = [M^{2+}] + [MX] + [ML^+] \quad (6.45)$$

Combining equation 6.10 and 6.11 with 6.45 and rearranging gives:

$$[ML^+] = \frac{C_{M,aq}}{1 + \frac{1}{K_{f,ML^+}[L^-]} + \frac{K_{f,MX}[X^{n-}]}{K_{f,ML^+}[L^-]}} \quad (6.46)$$

The relation between $[ML^+]$ and $[X^{n-}]$ may also be expressed by combining equations 6.11 and 6.16 to give:

$$[X^{n-}] = \frac{\alpha_X C_{X,aq}}{1 + \frac{[ML^+]K_{f,MX}\alpha_X}{[L^-]K_{f,ML^+}}} \quad (6.47)$$

Substituting from 6.47 into 6.46 and rearranging gives an expression for $[ML^+]$:

$$[ML^+] = \frac{C_{M,aq}}{1 + \frac{1}{[L^-]K_{f,ML^+}} + \frac{C_{X,aq}\alpha_X K_{f,MX}}{[L^-]K_{f,ML^+} + \alpha_X K_{f,MX} [ML^+]}} \quad (6.48)$$

This is a quadratic equation in $[ML^+]$ which can be solved for the value of $[ML^+]$ at the start of the slow reaction between ML^+ and L^- , as well as during the short initial-rate period. This value of $[ML^+]$ can then be put into equation 6.47 to solve for $[X^{n-}]$ which, in turn, can be used in equation 6.44 in order to obtain k_{SAMP} .

(2b) Rate constant for sample containing phthalate

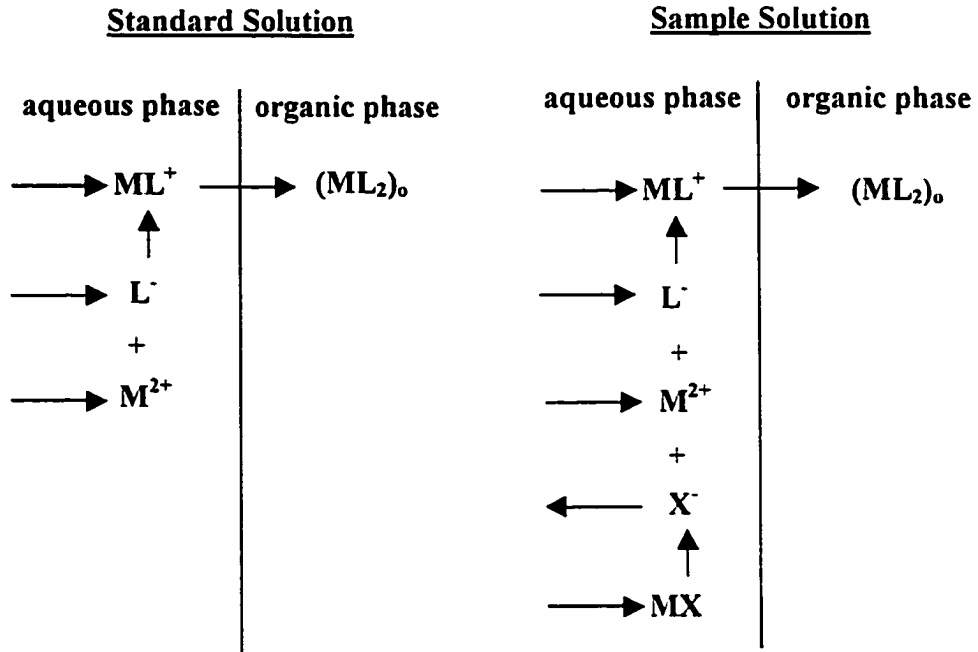
There is a large excess of X^{n-} in this case. The value of $[X^{n-}]$ from equation 6.16a can be substituted into equation 6.44 to give:

$$k_{\text{SAMP}} = \frac{k_{\text{STD}} (1 + [L^-] K_{f,ML^*})}{1 + [L^-] K_{f,ML^*} + K_{f,MX} C_{X,aq} \alpha_X + K_{f,MX_2} C_{X,aq}^2 \alpha_X^2} \quad (6.49)$$

6.4.2.2 Diffusional Control

Since the concentration of free-metal ion in the original sample solution is calculated with the aid of a calibration curve which is generated using standard solutions, it is desired that the conditions in the sample and standard are the same.

In the case of diffusional control, the diffusion mechanism in standard solutions and in sample solutions may be different due to the different composition present in the two solutions. Following is a diagram illustrating the diffusion of the species in both of the solutions. Horizontal arrows in the diagram indicate the diffusion direction of each species. To simplify the discussion, it is assumed that there are only free metal ions, M^{2+} , in the original standard solutions and that there are both M^{2+} and metal complex MX in the original sample solutions.



Scheme 6.2 Diffusion Across Nernst Diffusion Film

As shown in the diagram, there is only the extracted $(ML_2)_o$ in the organic phase in both standard and sample solutions. If diffusion in the organic phase is the rate-controlling step, then the diffusion mechanisms involved in both sample and standard solutions are the same. There is no inaccuracy that will be brought about by applying the calibration curve.

In contrast, if diffusion in the aqueous phase is the rate-controlling step, the different composition in standard and sample solutions could cause measurement error. This is because the diffusion of MX , in addition to the diffusion of M^{2+} and ML^+ , in the

sample solution will result in a rate enhancement compared with what would be observed with only M^{2+} and ML^+ as in the standard solution. Consequently, at a certain time t before extraction equilibrium has been reached, the amount of extracted $(ML_2)_o$ from sample solution may not be greater than that from the standard solution originally containing the same amount of free metal. Therefore, the use of a calibration curve to deduce the results may lead to wrong information. An analogous phenomenon was reported for the measurement of free progesterone in the presence of protein-bound progesterone.²¹⁵

To summarize, measurements made before equilibrium, with extraction rate controlled by diffusion in the organic phase, gives the same results as measurements made at equilibrium.

6.5 Discussion of Perturbation Before Equilibrium

In section 6.3 above, perturbation was described for the case when $t = \infty$. When $t < \infty$ and the extraction kinetic is controlled by the chemical reaction, the Perturbation Factor is calculated through the following steps:

a. Calculation of "Reported $[M^{2+}]$ " before equilibrium

"Reported $[M^{2+}]$ " is obtained by substituting $[ML_2]_{o, t < \infty}$ from equation 6.43 into equation 6.24:

$$\text{Reported } [M^{2+}]_{t < \infty} = [ML_2]_{o, t = \infty} (1 - \exp(-k_{SAMP} t)) \left(\frac{V_o}{V_{aq}} + \frac{1}{K_2} + \frac{1}{K_2[L^-]K_{f,ML^+}} \right) \quad (6.50)$$

where $[ML_2]_{o, t = \infty}$ can be obtained by solving equation 6.19 or 6.19a.

- b. Calculation of $[M^{2+}]_{L=0}$ before equilibrium is the same as that at equilibrium, as described in section 6.3.
- c. Calculation of Perturbation Factor before equilibrium:

$$\text{Perturbation Factor (PF)} = \frac{\text{Reported } [M^{2+}]_{t \rightarrow \infty} \text{ (before equilibrium)}}{[M^{2+}]_{L=0}} \quad (6.51)$$

As shown above, the Perturbation Factors (PF) before equilibrium depend on the chemical reaction rate constant k_{SAMP} and time t . In Figure 6.4, 6.5, 6.6 and 6.7, the effect of k and t on the PF is demonstrated by a series of plots for each of the complexing ligands studied in the present work, with various ligand to copper concentration ratio (C_X/C_M). If the chemical reaction rate constant k_{SAMP} is known, the Perturbation Factor of any specific system for any given time can be obtained by using these figures.

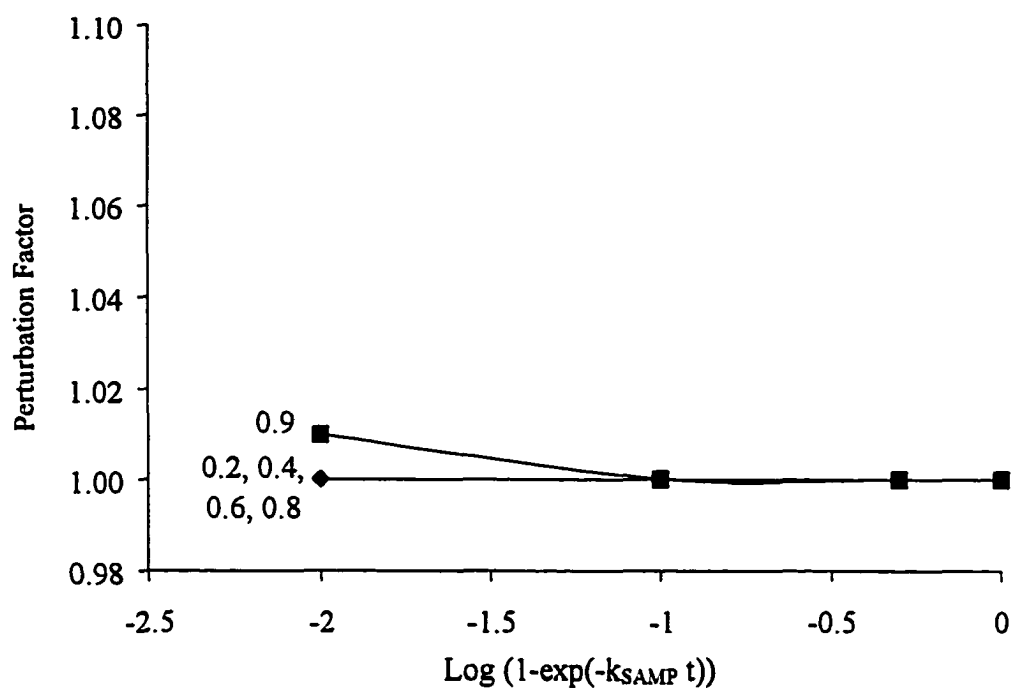


Figure 6.4 Perturbation Factor versus $\text{Log}(1-\exp(-k_{\text{SAMP}} t))$ for EDTA system at the various values of C_X/C_{Cu} shown by the numbers next to the curves, at constant values of $V_o/V_{\text{aq}} = 2.00 \times 10^{-6}$, $\text{pH} = 7.00$, $K_2 = 205.6$ (The calculation of K_2 is given in section 8.3), $K_{\text{f, CuL}^+}[\text{L}] = 10$ (assumed), $K_{\text{f, CuEDTA}'} = 2.51 \times 10^{13}$.

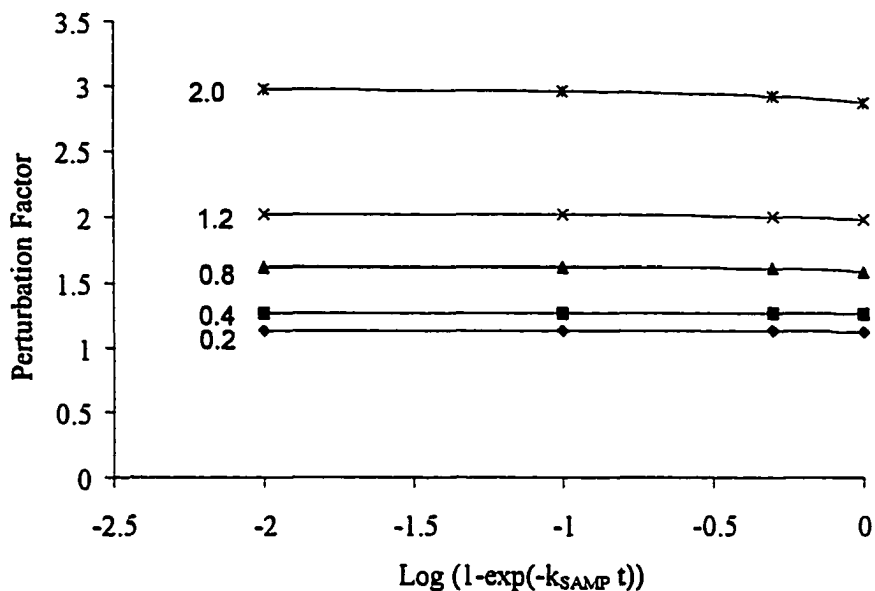


Figure 6.5 Perturbation Factor versus $\text{Log}(1-\exp(-k_{\text{SAMP}} t))$ for glycine system at the various values of C_X/C_{Cu} shown by the numbers next to the curves, at constant values of $V_o/V_{\text{aq}} = 2.00 \times 10^{-6}$, $\text{pH} = 7.00$, $K_2 = 205.6$ (The calculation of K_2 is given in section 8.3), $K_{\text{f,CuL}^+}[\text{L}^-] = 10$ (assumed), $K_{\text{f,CuGly}'} = 2.94 \times 10^5$.

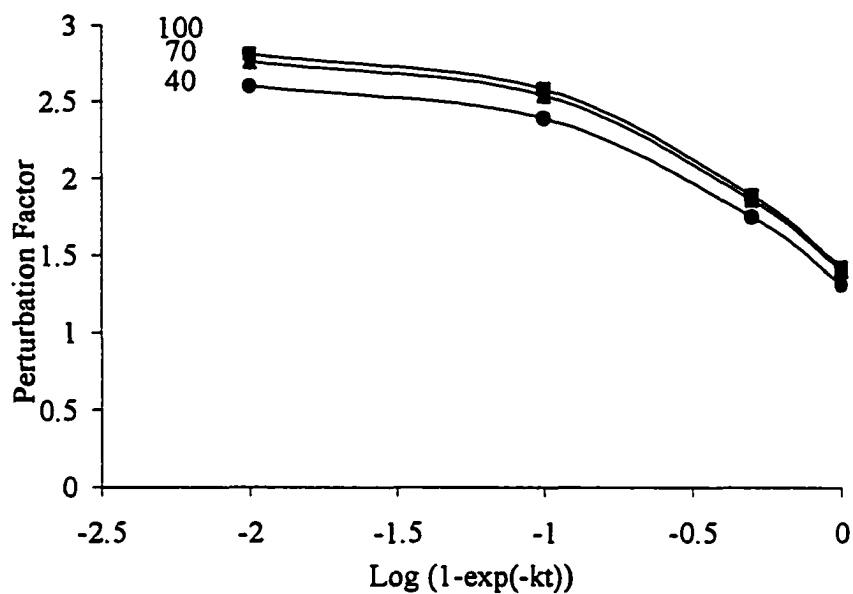


Figure 6.6 Perturbation Factor versus $\text{Log}(1-\exp(-k_{\text{SAMP}}t))$ for citrate system at the various values of C_X/C_{Cu} shown by the numbers next to the curves, at constant values of $V_o/V_{\text{aq}} = 2.00 \times 10^{-6}$, $\text{pH} = 6.00$, $K_2 = 403.8$ (The calculation of K_2 is given in section 8.3), $K_{f,CuL^+} [L^-] = 1$ (assumed), $K_{f,CuCit'} = 6.02 \times 10^5$.

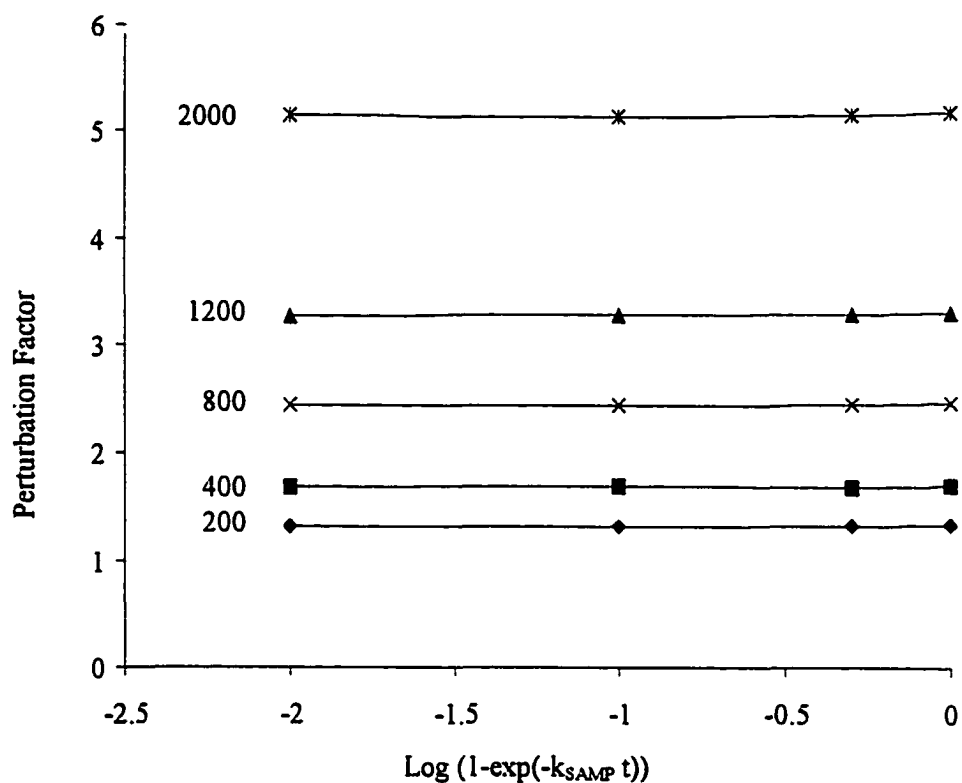


Figure 6.7 Perturbation Factor versus $\text{Log}(1-\exp(-k_{\text{SAMP}} t))$ for phthalate system at the various values of C_X/C_{Cu} shown by the numbers next to the curves, at constant values of $V_o/V_{\text{aq}} = 2.00 \times 10^{-6}$, $\text{pH} = 7.00$, $K_2 = 205.6$ (The calculation of K_2 is given in section 8.3), $K_{f, \text{CuL}^+}[\text{L}] = 10$ (assumed), $K_{f, \text{CuPh}}' = 1.66 \times 10^3$, $K_{f, \text{Cu(Ph)}_2}' = 2.88 \times 10^5$.

6.6 Calculation of Metal Species Distribution

In metal speciation studies it is usually desired to calculate the species distribution in the test solution to allow the comparison of the experimental values with the predicted species concentrations.

Consider that a known concentration of dibasic weakly acidic ligand, H_2X , is added to a test solution containing a trace amount of metal, M^{2+} , and a high concentration of a non-complexing electrolyte. If the metal forms only mononuclear complexes with the ligand, then the metal-containing species distribution as a function of the concentration of ligand can be calculated as shown below.

$$C_{M, aq} = [M^{2+}] + [MX] + [MHX^+] + [MX_2^{2-}] \quad (6.52)$$

Where, $C_{M, aq}$ is the total concentration of metal. Substituting for each species concentration in terms of its cumulative formation constant (β) and individual ligand concentration, then we get

$$C_{M, aq} = [M^{2+}] + \beta_{MX} \cdot [M^{2+}] \cdot [X^{2-}] + \beta_{MHX^+} \cdot [M^{2+}] \cdot [HX^-] + \beta_{MX_2} \cdot [M^{2+}] \cdot [X^{2-}]^2 \quad (6.53)$$

where the formation constants (β) are defined in the following equations:

$$\beta_{MX} = \frac{[MX]}{[M^{2+}][X^{2-}]} \quad (6.54a)$$

$$\beta_{MHX^+} = \frac{[MHX^+]}{[M^{2+}][XH^-]} \quad (6.54b)$$

$$\beta_{MX_2} = \frac{[MX_2^{2-}]}{[M^{2+}][X^{2-}]^2} \quad (6.54c)$$

Substituting for $[HX^-]$ in terms of $[H^+]$ and $[X^{2-}]$ according to the dissociation equilibrium of H_2X , and recognizing that $[M^{2+}]$ is common to all terms, we then get

$$C_{M,aq} = [M^{2+}] \left\{ 1 + \beta_{MX} \cdot [X^{2-}] + \beta_{MHX^+} \cdot \frac{[H^+] \cdot [X^{2-}]}{K_{a2,H_2X}} + \beta_{MX_2} \cdot [X^{2-}]^2 \right\} \quad (6.55)$$

Then, the fraction of the free metal species is:

$$\alpha_{M^{2+}} = [M^{2+}] / C_{M,aq} = 1 / \left\{ 1 + \beta_{MX} \cdot [X^{2-}] + \beta_{MHX^+} \cdot \frac{[H^+] \cdot [X^{2-}]}{K_{a2,H_2X}} + \beta_{MX_2} \cdot [X^{2-}]^2 \right\} \quad (6.56)$$

From the above equation, we can see that $\alpha_{M^{2+}}$ is dependent only on the complexing ligand concentration, $[X^{2-}]$, at a given pH. To figure out $[X^{2-}]$, we need the mass balance of X-containing species as shown below, where, $C_{X,aq}$ is the total concentration of the X-containing species.

$$C_{X,aq} = [X^{2-}] + [HX^-] + [H_2X] + [MX] + [MHX^+] + 2[MX_2] \quad (6.57)$$

Substituting for each species concentration in terms of its formation constant and the acid dissociation constant, we get

$$C_{X,aq} = [X^{2-}] + \frac{[H^+] \cdot [X^{2-}]}{K_{a2,H_2X}} + \frac{[H^+]^2 \cdot [X^{2-}]}{K_{a2,H_2X} \cdot K_{a1,H_2X}} + \beta_{MX} \cdot [M^{2+}] \cdot [X^{2-}] + \beta_{MHX^+} \cdot [M^{2+}] \cdot \frac{[H^+] \cdot [X^{2-}]}{K_{a2,H_2X}} + 2\beta_{MX_2} \cdot [M^{2+}] \cdot [X^{2-}]^2 \quad (6.58)$$

An iterative procedure is required to determine $[X^{2-}]$ from eq. 6.58 and thereby to figure out $\alpha_{M^{2+}}$ using eq. 6.56.

A computer program in C language, as presented in Appendix 3, has been written in this work to calculate the copper species distribution as a function of ligand concentration. The constants employed are listed in Table 6.1.

Table 6.1 Constants Used in the Calculation of Copper Species Distribution ^a

Ligand	pK _a values	logβ values
EDTA	pK _{a1} = 6.15	CuY ²⁻ , 18.8
	pK _{a2} = 10.22	CuHY ⁻ , 3.0
Phthalate	pK _{a1} = 2.76±0.03	CuPth, 3.22±0.22
	pK _{a2} = 4.92±0.05	CuHPth ⁺ , 1.3
		Cu(Pth) ₂ ²⁻ , 5.5
Glycine	pK _{a1} = 2.34±0.02	CuGly ⁺ , 8.15±0.09
	pK _{a2} = 9.58±0.04	Cu(Gly) ₂ , 15.03±0.1
Citrate	pK _{a1} = 2.87±0.08	CuCit ⁻ , 5.9±0.1
	pK _{a2} = 4.35±0.05	CuHCit, 3.42
	pK _{a3} = 5.69±0.05	CuH ₂ Cit ⁺ , 2.26

- a. All of the constants were obtained from "Critically Selected Stability Constants of Metal Complexes Database", Version 2.0, developed by Arthur E. Martell and Robert M. Smith at Texas A&M University, with ionic strength $\mu = 0.1$.

Chapter 7

Characterization of Microdrop Solvent Extraction-Direct Sample Insertion (DSI)-ICP/MS

7.1 Introduction

In this chapter, the coupling of microdrop solvent extraction with direct sample insertion (DSI) – ICP/MS is detailed. The characterization of this technique is presented.

The time required to reach the equilibrium in the system under investigation turned out to be fairly long (about 3 hours). Minimizing the measurement time is desired from a practical point of view. A kinetic study that provides rate information on the system has therefore become necessary. An analytical methodology which allows the extraction to be performed for a time that is much shorter than the time required for the attainment of equilibrium is proposed on the basis of the kinetic study results.

The extraction calibration curve is also established, which provides the direct correlation between the measured quantity of the extracted copper and the quantity of initial free copper in sample solutions.

7.2 Experimental Section

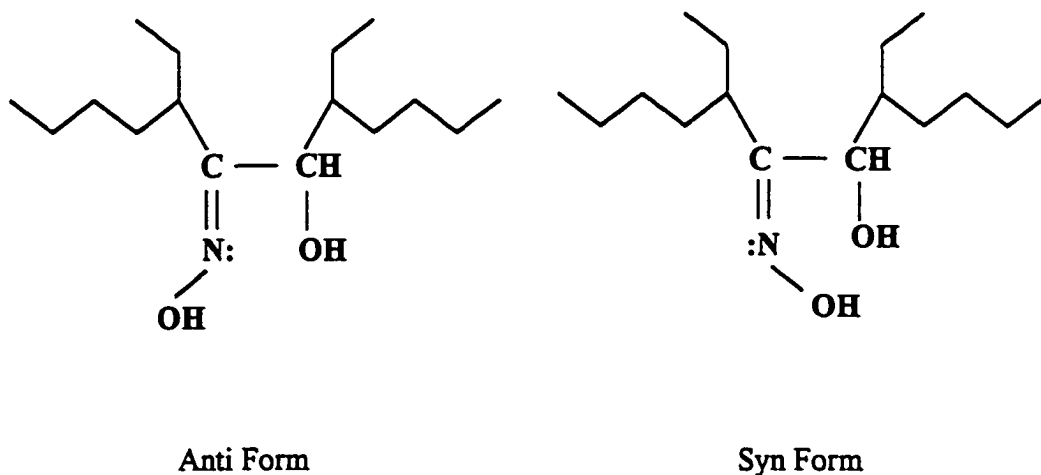
7.2.1 Chemicals

Lix63 was kindly supplied by Henkel Corporation, Tucson, Arizona in its diluted form. However, only the anti isomer of 5,8-diethyl-7-hydroxy-dodecan-6-one oxime, purified from the as-supplied Lix63, was used throughout this work. (See section 7.2.2) Moreover, the term, Lix63, which appears later refers to the purified anti isomer.

Cupric nitrate, $\text{Cu}(\text{NO}_3)_2$ (standards for plasma emission spectroscopy, SPEX Industries, Inc., Edison, NJ) of 9980 ppm copper, was serially diluted with water to make $\text{Cu}(\text{NO}_3)_2$ solution. Sodium nitrate, NaNO_3 (BDH), nickelous sulfate, $\text{NiSO}_4 \cdot \text{H}_2\text{O}$ (Anachemia Science, Lot: 390104, Montreal, Canada), sodium hydroxide, NaOH (BDH), nitric acid, HNO_3 (Fisher, Ottawa, Canada), sulfuric acid, H_2SO_4 (Fisher), and 2, 6-Dimethylpyridine (2, 6-Lutidine) (Lancaster, Windham, NH, USA) were all used as received. Water was purified by the Nanopure system (Barnstead, Dubuque, IA, USA).

7.2.2 Purification of Lix63

The manufacturer of commercial Lix products has not made the pure active component available, nor indicated their actual composition. Commercial Lix63 is a light yellow liquid containing up to 70% inert solvent. Lix63 itself is insoluble in water ($<1 \times 10^{-5}$ M).²⁵⁷ Not only does the inert diluent in the commercial reagent constitute an impurity, but also all the Lix extractants have two isomeric forms: a syn form and an anti form, as shown below:^{258, 259}



In the anti isomer, the orientation of the oxime group is such that complexation with a metal ion is expected to be more rapid than with the syn isomer where isomerisation is necessary prior to complexation. This difference accounts for the observation that the anti isomers of α -hydroxyoximes have a reactive nature towards copper ion, while the syn isomers of α -hydroxyoximes have a relatively unreactive nature. It is, therefore, only the anti isomers of the α -hydroxyoxime which is the active component in the Lix products. Thus, it is necessary to purify the commercial product and isolate the isomers in order to know the concentration of the real active component of the extractant.

Ashbrook has reported¹⁹⁴ a procedure for purification of Lix63 based on chromatography on alumina and elution with acetone, but did not report any attempt to isolate the isomers of this reagent. Tammi has reported²⁶⁰ two ways of purifying Lix63 and isolating syn and anti isomers. In one method, the petroleum spirit is first removed by distillation from the commercial product. Then the residue is dissolved in ether and the ethereal solution is shaken with an aqueous solution of Cu (II). The anti isomer is then converted to a copper complex. Upon adding acetone to the organic phase, the complex between copper and the anti isomer is precipitated. The complex precipitate is then filtered from the ether/acetone solution which contains the syn isomer. In another method, the as-received sample of Lix63 was contacted with nickel sulfate solution to obtain a blue precipitate of Ni-SO₄-anti isomer complex. The anti isomer in the precipitate is thus separated from the syn isomer that still stays in the organic solution.

Both of Tammi's methods to isolate these two types of isomers make use of the difference between the two isomers in their ability to extract metal. Only the anti isomers are active in extracting copper or nickel. In the Cu complexation method the Lix63 as-supplied has to be distilled to remove the solvent contained in the sample to eventually precipitate the Cu-Lix complex. In the nickel complexation method, on the other hand, the Ni- SO₄ -Lix complex is so insoluble in the organic solvent that it can be precipitated easily in the presence of organic diluent. The nickel complexation method is chosen in the present work.

Following are the experimental procedures for isolating anti isomer of Lix63 employed in this work (All the chemicals and reagents used are described in section 7.2.1 and 7.2.3.):

Step 1. Quantities of 200 mL Lix63 as-received and 200 mL of 1.00 M Ni SO₄ solution were mixed in a 600 mL beaker, which was located on a magnetic stirrer (Fisher, Thermix Stirrer, Model 120MR) with the stirring speed set at 8.

Step 2. NaOH (16 mL of 30%) was added to the above mixture dropwise in the course of 4 hr. mixing under stirring. In this step, while NaOH is added, large pieces of white precipitate were initially formed in the aqueous layer and eventually dissolved in the organic layer.

Step 3. After 4 hr. mixing (step 2) phase separation was achieved by using a 1000 mL separatory funnel, and the organic phase was left in the funnel. Then, 200 mL of 0.5 M Ni SO₄/1.5 M H₂SO₄ aqueous solution was added to the separatory funnel. Upon stirring for 0.5 hr. (stirring speed set at 8), dark green precipitates were produced in the aqueous phase.

Step 4. Again, phase separation was made. The aqueous phase left in the separatory funnel, containing the dark green precipitate, was then washed with 50 mL of acetone four times (by mixing it well with acetone and then discarding the acetone layer four times). After these washing procedures the precipitate in the aqueous phase became light blue in color.

Step 5. After discarding the supernatant the light blue precipitate was left in a 1000 mL beaker with addition of 200 mL of 1.0 M HNO₃ and 270 mL of ether (Anachemia, Montreal, Canada). The mixture was stirred for 1.5 hr with stirring speed set at 8. While stirring, the blue precipitate was gradually dissolved, and the lower aqueous layer became

dark green and the upper organic layer became clear (without precipitate) and light yellow colored.

Step 6. The two layers were then separated. Thereafter, the light yellow colored organic layer was left in the fume hood for several days to let ether evaporate away. The final product, which was the desired anti isomer of 5,8-diethyl-7-hydroxy-dodecan-6-one oxime, was a waxy, off-white powder weighing 37.83 g.

Purity of the final product was checked by TLC following the procedures reported by Mumallah, *et al.*²⁶¹: Commercial silica gel plates 60 F₂₅₄ were placed in the developing jar containing the developing solvent of 96:4 toluene/ethyl acetate until the solvent front reached the end of the plate. The plate was then taken out and left to dry for a few minutes and then examined under a UV lamp. The distances traveled by the purified anti isomer of Lix63 and by the solvent front were measured. The R_f value was 0.48, which was exactly the same as given in the literature for purified anti isomer of Lix63.²⁶¹

7.2.3 Reagents and Test Solution Preparation

Solution of anti-isomer of Lix63 (0.500 M) was prepared by dissolving 3.380 g purified anti-isomer solid in 25 mL of n-octane. Sodium nitrate stock solution in water (0.500 M) was prepared by dissolving 84.99 g of the salt in 2 L of solution. 2, 6-Lutidine stock solution (0.100 M) was prepared by dissolving the neat liquid (21.43 g) in water and diluting to 2L.

The Cu (II) test solution was generally prepared by dispensing 100.0 mL of sodium nitrate solution (0.500 M) and 5.00 mL of 2,6-Lutidine stock solution (0.100 M) into a 500 mL beaker. Lutidine is used as a pH buffer. About 200 mL of water was added and the pH was adjusted to the desired value with dilute HNO₃. Then the appropriate volume of daily-prepared dilute copper solution was added slowly to the magnetically stirred mixture. A final adjustment of pH was necessary in some cases. The beaker

contents were then quantitatively transferred to a 500 mL volumetric flask, diluted to volume with water, and shaken well. The pH of the test solution was then rechecked and readjusted when necessary using very small volumes of HNO₃ or NaOH solution so as to cause negligible further dilution of the metal ion.

The following reagents were prepared for the purification of Lix63: Nickelous sulfate solution (1.00 M) was prepared by dissolving 131.63 g NiSO₄•H₂O in 500 mL water; 30 wt% NaOH solution was prepared by dissolving 15.14 g NaOH in 50 mL water; HNO₃ solution (1.00 M) was obtained by diluting 31.84 mL concentrated HNO₃ (70%) to 500 mL; the solution of 0.50 M NiSO₄ and 1.50 M H₂SO₄ was prepared by dissolving 65.20 g NiSO₄ in about 200 mL water and then dispensing 41.52 mL of concentrated H₂SO₄, as received, to the above contents, and then quantitatively transferred to a 500 mL volumetric flask and diluting to index line.

7.2.4 Apparatus for Microdrop Solvent Extraction

The microdrop solvent extraction apparatus is shown in Figure 7.1. The aqueous solution was contained in a 500 mL beaker, which is located in a flat-bottom water-jacketted glass vessel with thermostated water ($25.00 \pm 0.02\text{C}^\circ$) circulated by a thermostat (MGW Lauda, Germany). The aqueous solution was stirred at a constant speed during extraction by a one-inch glass-covered magnetic stir bar placed at the bottom of the beaker and controlled by a stirrer motor controller (G. K. Heller Corp., Floral Park, NY), which is located under the water jacketted vessel. A feedback mechanism in the motor controller maintains the stirring rate at better than $\pm 1\%$ rsd, in spite of changes in line voltage and stirring load. The motor has been modified as follows: the motor chuck used to hold the stirring blades is inverted and modified to hold a 1.75 inch rotating magnet assembly from a conventional plate-type magnetic stirrer.

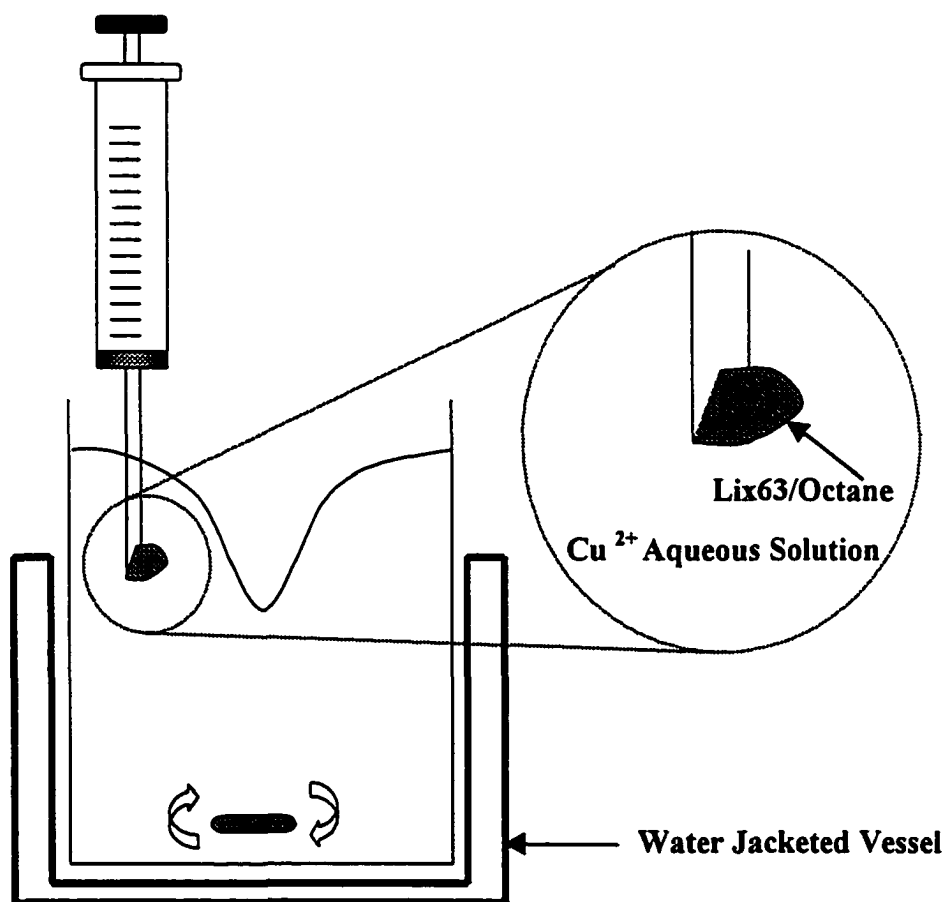


Figure 7.1 Microdrop solvent extraction apparatus

The 5 μL microsyringe (Model 7105 KH, Hamilton Co., Reno, NV) holding the 1 μL Lix63/n-octane drop is clamped above the aqueous solution beaker. The microsyringe employed here is a so-called plunger-in-needle type of syringe, meaning that the plunger wire is inside the needle itself. The detailed description of the microsyringe can be obtained elsewhere.²⁶² In this type of syringe, the liquid in the syringe is contained entirely within the needle.

3.2.5 Direct Sample Insertion Device for ICP

The Direct Sample Insertion device (DSID) employed in this work to introduce extracted sample into the ICP/MS was developed and characterized by Dr. Gary Holick's group.^{263, 264} The schematic diagram of the DSID is shown in Figure 5.2.

The sample probes are standard d.c. arc graphite electrodes (Gay Carbon, Inc., Bay City, Michigan, USA) modified by drilling a hole in the bottom of the electrode (as shown in Figure 7.2) prior to mounting it on one end of a quartz rod of the DSI assembly. The other end of the quartz rod is held by a cylindrical Teflon adapter, which is mounted inside the probe assembly support and locked into place with the aid of a nut-and-bolt clamp. The graphite electrode cup containing the test sample and mounted on the quartz rod will be inserted into a SCIEX Elan Model 250 (Perkin-Elmer/SCIEX Instruments, Thornhill, Ontario, Canada) ICP/MS when the appropriate data and instructions have been sent to the stepper motor (Oriental motor, type PH 299-01 supplied by Rogers Labs) via IBM.



Figure 7.2 Modified graphite electrode

7.2.6 Experimental Procedures

Followings are the experimental steps used in this work:

Step 1. *Set-up of the Organic Drop* After thoroughly flushing the microsyringe, 1.00 μL of 0.500 M Lix63/n-octane solution was taken up, and the syringe was quickly transferred to the aqueous test solution and held in place with a clamp. The needle tip was located about 1cm under the surface of the aqueous solution and about 2cm from the side

of the 10.2 cm diameter, 500 mL beaker. A volume of 0.90 μL of the organic solution was then dispensed out as a drop suspended in the aqueous solution from the needle tip and 0.10 μL remained inside the needle.

Step 2. *Extraction* After setting up the organic drop, the stirrer and the timer were initiated at the same time and stopped at the same time after a desired extraction period.

Step 3. *Transfer of the Sample* After extraction, the 0.90 μL suspended drop was withdrawn into the syringe needle, which was then quickly brought to a graphite electrode cup. All of the 1.00 μL solution in the needle was then immediately injected into the graphite cup, and then an appropriate volume of aqueous solution containing internal standard was also transferred into the cup by a 25 $\mu\text{L} \pm 0.1 \mu\text{L}$ syringe (Hamilton).

Step 4. *Detection by ICP/MS* The graphite electrode cup containing the sample and internal standard was mounted on the probe assembly of the DSI. After sending insertion instructions to the stepper motor through the microcomputer the graphite electrode cup was delivered to the ICP torch. The data acquired by the Elan microcomputer were serially transferred to the Macintosh at 1200 baud for further processing and presentation.

7.3 Measurement on DSI-ICP/MS

7.3.1 Operating Conditions of DSI-ICP/MS

Operating conditions of DSI-ICP/MS system are listed in Table 7.1.

Table 7.1 Parameters used for DSI-ICP/MS**ICP Operating Conditions:**

Forward Power: 1.5 kW

Reflected Power: < 5 W

Outer (Coolant) Gas (Ar): 14.5 L/min.

Intermediate (Auxiliary) Gas (Ar): 0.2 L/min.

Central (Nebulizer) Gas (Ar) : 1.75 L/min.

Ion Lens Voltage Settings:	Setting	Voltage (V)
Bassel Box Barrel (B)	99	10
Bassel Box Plates (P)	40	-24
Einzel Lens (E1)	99	-20
Photon Stop (S2)	40	-8

Parameter Set of Data Acquisition

Resolution		L
Ion Multiplier	HV	4000
Rod Offset	V	0.0
Nebulizer Pressure	psi	30.0
Sample Flow		1000
Measurement/Peak		1
Scanning Mode		E
Measurement Mode		S
Measurement Time	sec	0.4
Repeats/Integration		0
Threshold Ions/sec		1
Counting Precision	%	0.100

DSI Setting

Position of Graphite Electrode		Level off to the Front of Load Coil
Preheating Time	sec	0
Ashing Time	sec	10
Atomization Time	sec	30
Cooling Time	sec	10

7.3.2 Choice of Internal Standard

The stability of the gas flow rates and the applied power in ICP, and the reproducibility of the sample insertion position of the DSI are major non-spectroscopic factors that affect the precision of the measurement in the DSI-ICP/MS. The consequent drift of analyte sensitivities and calibration curves is a common problem that limits accuracy. In order to achieve maximum precision and accuracy for quantitative analysis the use of internal standards is highly recommended. If the internal standard is chosen to have chemical and spectroscopic properties similar to those of the analyte, then the analytical signals from both the analyte and the internal standard change proportionally when analyte interferences or fluctuations in experimental conditions occur. Therefore, the internal standard method is commonly applied to partially compensate for drifts or random nonfundamental fluctuations in experimental conditions which cause systematic error or random error, respectively.

Several studies^{265, 266, 267} of the application of the internal standard method for non-spectroscopic interference have shown that internal standardization is most effective when the analytes and internal standards are closely matched on the basis of mass and first stage ionization potential. It is also preferable for a suitable internal standard to have low natural abundance in the sample, freedom from significant spectral interference and negligible memory effects in the spectrometer system. Based on the above considerations gallium (Ga^{69}) was selected as the internal standard element for the measurement of copper (Cu^{63}). The typical signals of copper and gallium obtained on DSI-ICP/MS are shown in Figure 7.3.

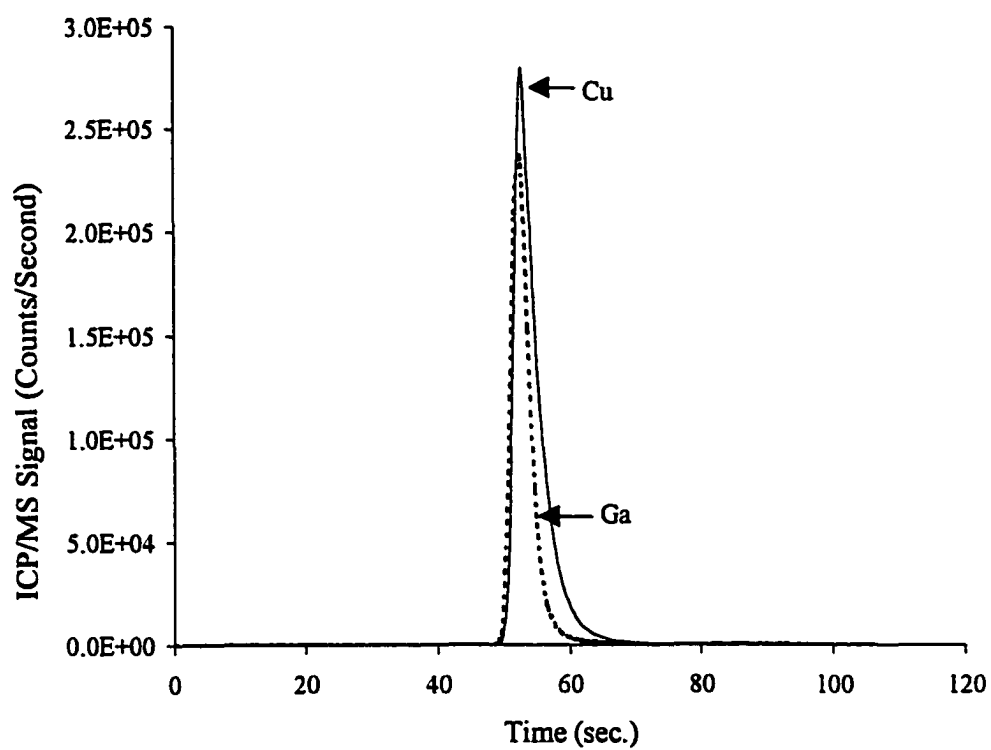


Figure 7.3 Typical ICP/MS signals of Cu^{63} and internal standard Ga^{69}

7.3.3 Data Treatment and Calibration Curve

With the DSI sample introduction method, the sample residue is completely vaporized from the graphite electrode cup within the predetermined atomization time (30 seconds for copper in the present work), which is determined by the operating condition of the ICP and the physical and chemical characteristics of the sample. This generates a discrete quantity of material reaching the plasma and resulting in a peak-like, transient signal, as shown in Figure 7.3.

In this work, peak areas of the transient signal have been used to quantitate the analyte. Each individual signal peak is integrated for a period of time, starting from the point where ion intensity exceeds the preset intensity threshold, and ending up at the point where ion intensity returns back below the threshold. The threshold is set to be three times the standard deviation of the ion intensities of blank insertion. To customize the daily routine data treatment, a macro program in Microsoft Excel (Appendix 4) has been made in this work to calculate peak areas directly from the intensity data. A calibration curve is generated daily, in which the ratio of peak areas of copper standard solution to that of gallium standard solution, both added to the graphite cup in appropriate microvolume, is plotted vs. the copper concentration of the copper standard solution.

A typical calibration curve is shown in Figure 7.4. According to the study done on the same DSI-ICP/MS²⁶⁸, the measurement of copper on this apparatus offers: detection limit: 7.74 pg; linear range: 3 orders of magnitude; precision: 2-3%.

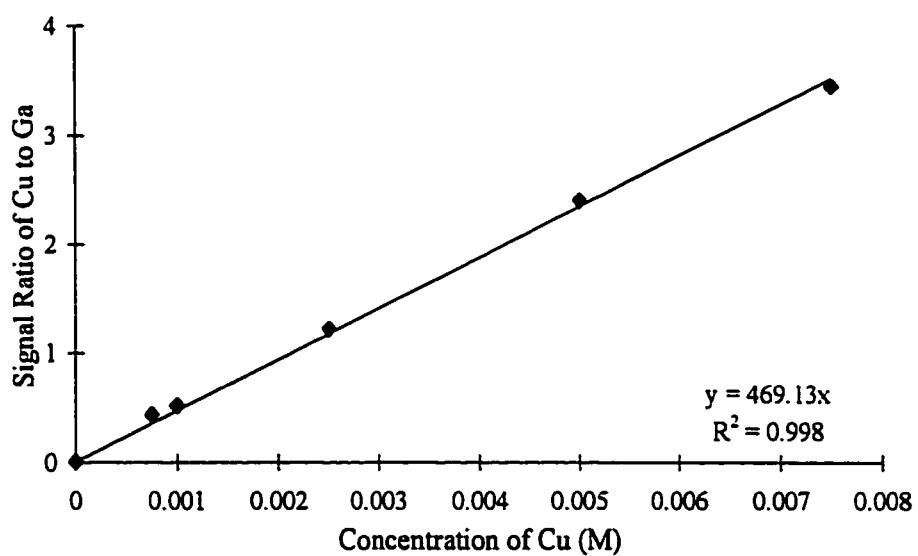


Figure 7.4 Typical calibration curve on ICP/MS

7.4 Investigation of Kinetic Mechanism

In attempting to analyze the kinetic mechanism in the metal solvent extraction system in this work, measurements were made of the influences of stirring speed and organic drop size on initial velocity of copper extraction, V_{init} , which is defined as

$$V_{\text{init}} = d[\text{CuL}_2]_o/dt \text{ when } t \approx 0 \text{ sec}$$

where $[\text{CuL}_2]_o$ is the extracted Cu-lix63 complex, and V_{init} is the initial slope of the rate curve.

7.4.1 Effect of Stirring Speed and Organic Drop Size on Initial Rate

Figure 7.5 and Figure 7.6 give the observed initial rate curves for extraction performed with varying stirring speed in the aqueous phase and with varying organic drop volume, respectively. The initial rate of each extraction process is shown by the straight line, through zero, which has the initial slope of the rate curve. To give a clearer picture of these effects, Figure 7.7 is made by directly plotting the initial rate vs. the change of stirring speed and organic drop size.

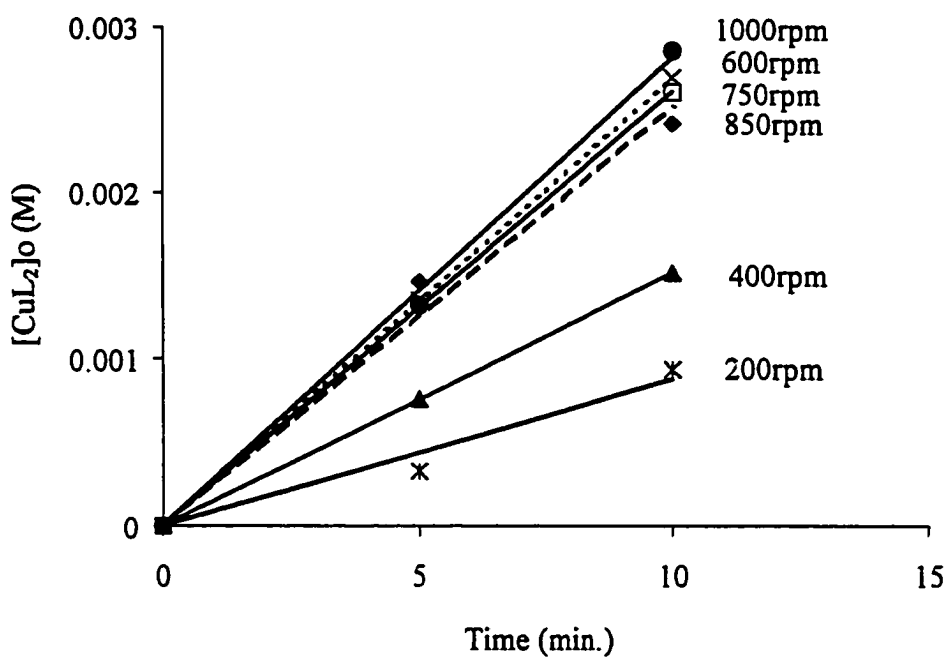


Figure 7.5 Initial rate curves with varying stirring speeds. The straight lines have the initial slopes of the rate curves. Experimental Conditions: volume of organic drop $V_o = 0.60 \mu\text{L}$, concentration of copper nitrate aqueous solution $[\text{Cu}^{2+}] = 5.0 \times 10^{-6} \text{ M}$, concentration of Lix63 octane solution $C_{L,o} = 0.50 \text{ M}$.

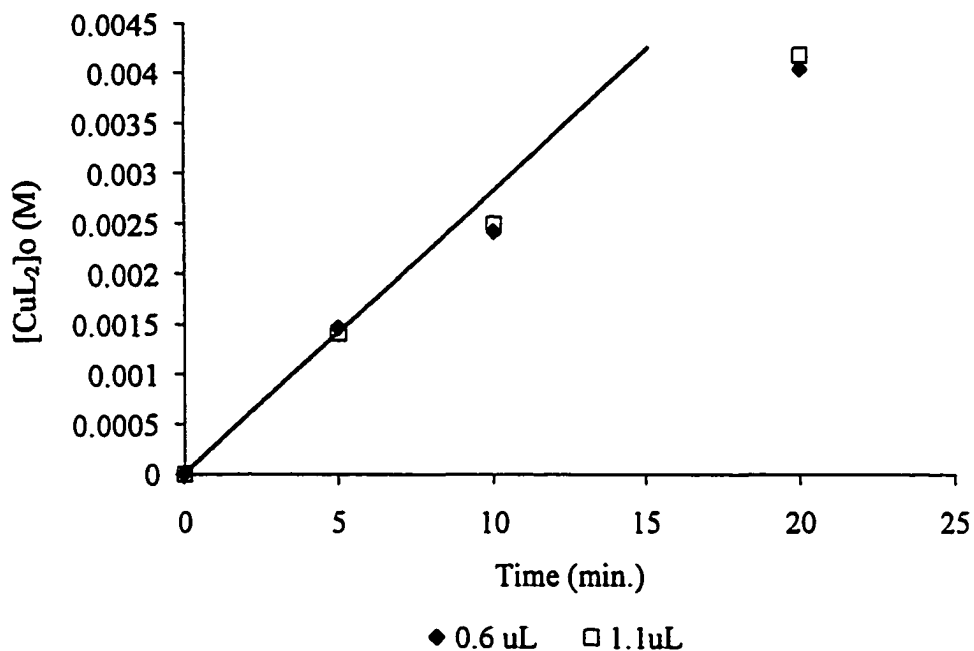


Figure 7.6 Initial rate curves with varying organic drop size. The straight line has the initial slope of the rate curves. Experimental Conditions: stirring speed = 850 rpm, concentration of copper nitrate aqueous solution $[\text{Cu}^{2+}] = 5.0 \times 10^{-6} \text{ M}$, concentration of Lix63 octane solution $C_{L,o} = 0.50 \text{ M}$.

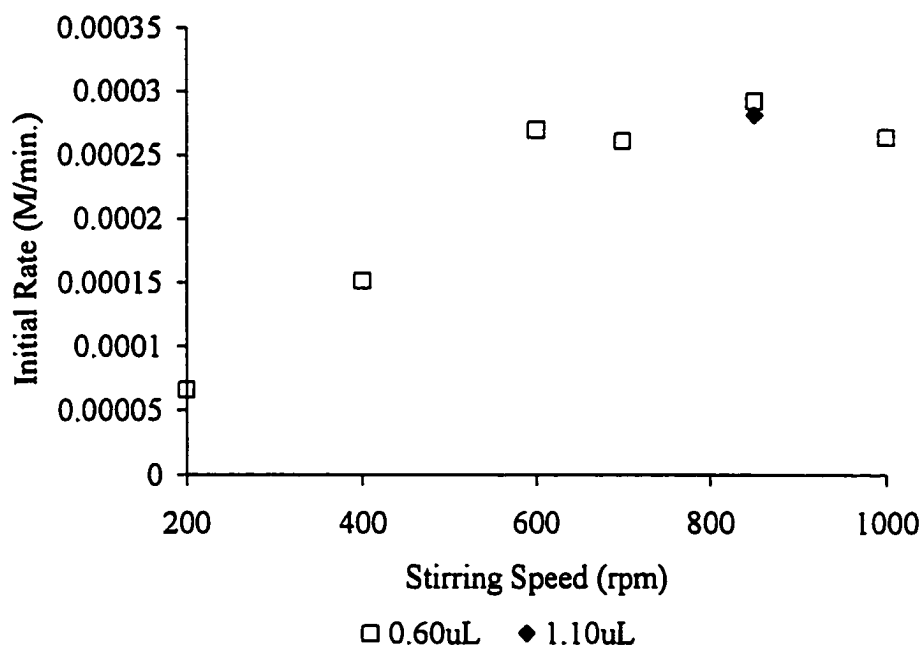


Figure 7.7 Plot of initial rate vs. stirring speed and organic drop size. Experimental Conditions are the same as in Figure 7.5 and 7.6.

As can be seen in Figure 7.7, the initial rates are increasing with stirring speed up to about 600 rpm, where a plateau region is reached. As discussed in section 6.4.1, a plateau region indicates that at these stirring rates the diffusion processes in both the aqueous and the organic diffusional films have become so fast compared to the chemical reaction that they no longer influence the rate of extraction, and hence the extraction rate is kinetically controlled. Therefore, in the test system extraction at stirring rates larger than 600rpm will be in the chemical kinetic regime.

Furthermore, the initial rates of both points at 850 rpm (Figure 7.7), do not significantly differ from each other, though the organic phase volume and therefore the phase ratio have been almost doubled. According to the discussion in section 6.4.1, this independence of extraction rate on phase ratio also indicates a chemical kinetic regime of the extraction process.

7.4.2 First Order Rate Curve Fit with Respect to Copper

In the literature about copper extraction by hydroxyoximes, the conclusions on the kinetic mechanism of the extraction are controversial. The disagreement concerns the chemical reaction mechanism and whether or not the extraction process is in a kinetic regime. However, while there is disagreement over detail, there is general agreement that when extraction is in the chemical kinetic regime the rate is first order with respect to copper.

The rate curve, i.e., the plot of concentration of extracted copper vs. time, obtained in this work, is fitted with a first order rate equation:

$$C_{o,t} = C_{o,e} (1 - e^{-kt}) \quad (7.1)$$

where $C_{o,t}$ and $C_{o,e}$ are the concentrations of extracted copper at time t and at equilibrium, respectively; k is the reaction rate constant. As shown in Figure 7.8, the experimental data fit a first order equation well.

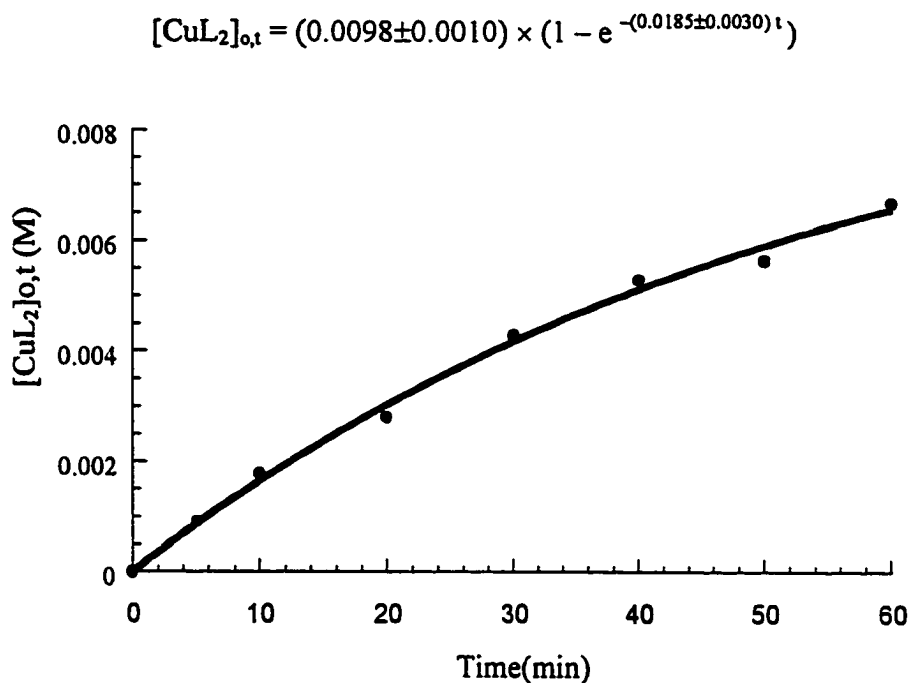


Figure 7.8 First Order Rate Curve Fitting. Experimental conditions: $[\text{Cu}^{2+}]_{t=0} = 5.00 \times 10^{-6} \text{ M}$, $C_{L,o} = 0.500 \text{ M}$, volume of organic drop = $1.00 \mu\text{L}$, Volume of aqueous solution = 500 mL , Stirring speed = 750 rpm .

7.4.3 Conclusions Regarding Extraction Kinetics

As demonstrated in section 7.4.1, the initial rate of extraction is independent of the stirring rate and volume of organic drop or phase ratio. These are strong evidences of the extraction process being in the chemical kinetic regime. In addition, the good fitting of the extraction rate curve to the first order rate equation shows that the extraction rate is first order with respect to copper.

7.5 Extraction Calibration Curve

Since the extraction system in this work is kinetically controlled by a chemical reaction, the extraction of $[\text{CuL}_2]_0$ from a sample solution for the purpose of determining $[\text{Cu}^{2+}]_{t=0}$ can be performed for any predetermined time t , no matter whether it has reached equilibrium or not. For practical reasons, the extraction time chosen for the present work is 5 min. An extraction calibration curve for extraction of 5 min. is shown in Figure 7.9. It is linear below about 7.5×10^{-6} M copper (dashed line). Concentrations employed in the speciation studies described below were in this linear region. The curvature in the upper part of the plot is due to the over-consumption of chelating extractant Lix63 which leads to a non-constant value of $[\text{L}^-]$.

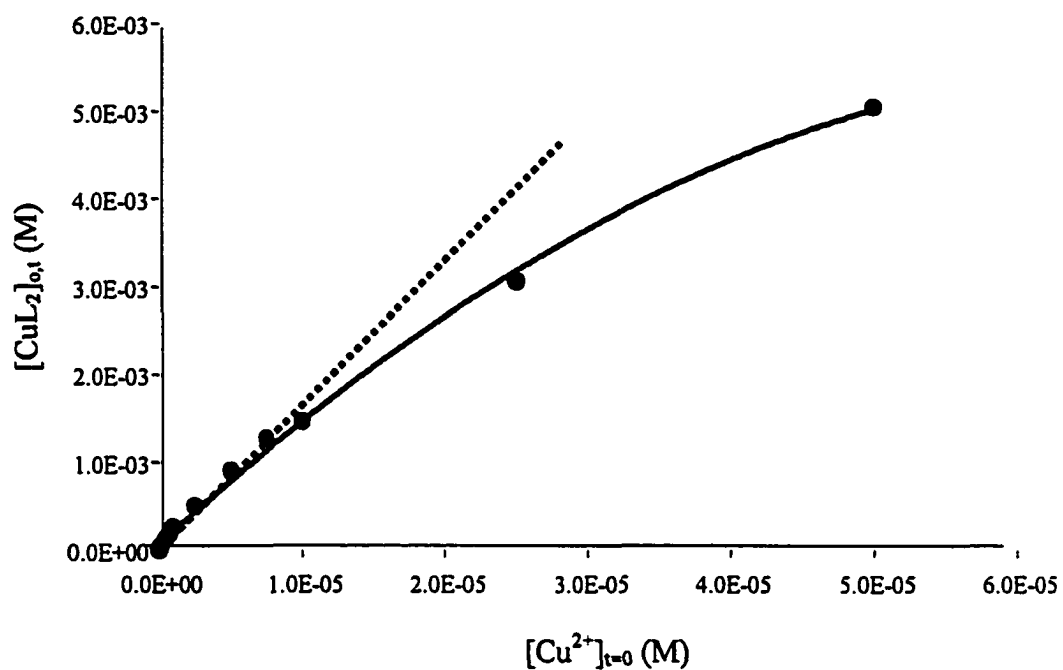


Figure 7.9 Extraction Calibration Curve. Experimental conditions: cupric nitrate standard aqueous solution, 1.00 μL of Lix63/Octane ($C_{L,o} = 0.500 \text{ M}$), 5 min. extraction time. The solid line is the empirical fit by applying a Stineman function to the data using KaleidaGraph.

Chapter 8

Free Copper Ion Determination by Microdrop Solvent Extraction – DSI – ICP/MS in the Presence of Complexing Ligands

8.1 Introduction

In this chapter the application of microdrop solvent extraction-DSI-ICP/MS to sample solutions in the presence of complexing ligands is demonstrated. Section 8.2 gives the experimental details. The experimental results for sample solutions containing EDTA, glycine, citrate and phthalate are presented in section 8.3. As will be seen, the results for copper solutions in the presence of all four ligands are in accordance with theoretical prediction, and, furthermore, the Cu-EDTA system is unperturbed by the presence of Lix63, but the Cu-Glycine, Cu-Citrate and Cu-Phthalate systems are perturbed.

8.2 Experimental Section

Except for the chemicals and reagents stated in this section, all the others have been described in section 7.2.1 and 7.2.3. The experimental set-ups, equipment, procedures and operating conditions for ICP/MS (SCIEX 250) were all the same as described in section 7.2.4, 7.2.5, 7.2.6 and 7.3.1.

8.2.1 Chemicals

The disodium salt of ethylenediaminetetraacetic acid (EDTA), $C_{10}H_{14}N_2O_8Na_2 \cdot 2H_2O$ (Fisher), glycine, $NH_2 \cdot CH_2 \cdot COOH$ (BDH Chemicals Ltd., Poole, England), citric acid, $HOCOCH_2C(OH)-(COOH)CH_2COOH \cdot H_2O$ (Caledon Laboratories Ltd.) and phthalic acid, $C_6H_6O_4$ (Caledon Laboratories Ltd.) were reagent grade. All of the above were used as received, without further purification.

8.2.2 Reagents

EDTA stock solution (0.025 M) was prepared by weighing 4.6530 g of the salt and dissolving in a 500 mL volumetric flask and diluting to volume with water. Glycine stock solution (0.010 M) was prepared by dissolving 0.3753 g of glycine in water in a 500 mL volumetric flask and the volume was brought to index line with water. Citric acid stock solution (0.005 M) was prepared by dissolving 0.9606 g of citric acid in water in a 1 L volumetric flask and diluting to volume. The crystals of phthalic acid as received have to be crushed down to small powder-like pieces to be dissolved in water. Phthalic acid stock solution (0.020M) was prepared by dissolving 1.6613 g of the crushed crystals in a 500mL volumetric flask and diluting to volume with water.

8.2.3 Preparation of Test Solutions

A series of test solutions were prepared with varying ligand concentrations but keeping constant the total sodium concentration (0.100 M) and lutidine buffer concentration (0.001 M) in the following way:

100 mL of 0.500 M NaNO_3 , 5.00 mL of 0.100 M lutidine buffer and the appropriate volume of the ligand solution were delivered into a 500 mL beaker, and then water was added to give a solution of total volume of approximately 450 mL. The pH was adjusted to 7.00 ± 0.05 by addition of HNO_3 and NaOH , if necessary. Then, a suitable volume of $\text{Cu}(\text{NO}_3)_2$ was dropwise added to the solution with stirring on a magnetic stirrer. This was followed by a final pH adjustment, if necessary. The contents of the beaker were then quantitatively transferred to a 500 mL volumetric flask, and the volume was brought to 500 mL with water. After shaking well the contents were put in a dry, clean 500 mL beaker for the extraction experiment.

8.3 Results and Discussion

The results of the determination of free copper concentration in sample solutions containing EDTA, glycine, citrate and phthalate, respectively, are presented and discussed in this section. The determined free copper is represented by the ratio $([\text{Cu}^{2+}]_{\text{X}\neq 0, \text{t}=0} / [\text{Cu}^{2+}]_{\text{X}=0, \text{t}=0})$, where $[\text{Cu}^{2+}]_{\text{X}=0, \text{t}=0}$ is the concentration of free copper in the original solution before any ligand X has been added, and $[\text{Cu}^{2+}]_{\text{X}\neq 0, \text{t}=0}$ is the concentration of free copper after a certain amount of ligand, X, has been added to the original solution. This ratio should be 1 when $[\text{X}] = 0$ (no addition of ligand) and less than 1 when $[\text{X}] \neq 0$ (with addition of ligand), and decrease when the added $[\text{X}]$ increases. (Note: this ratio is different from “Reported $[\text{Cu}^{2+}]$ ”/ $[\text{Cu}^{2+}]_{\text{L}=0}$, the Perturbation Factor, which relates to the reagent ligand L.) In Figure 8.1, 8.3, 8.5 and 8.7, the experimental data for 5.00 min. of stirring are presented as solid points along with the theoretically predicted equilibrium lines, which were calculated as described in section 6.6.

In Figure 8.2, 8.4, 8.6 and 8.8 are presented families of plots of Perturbation Factor versus $\log K_{\text{f}, \text{CuX}'}$, which are similar as the plots in Figure 6.1-6.3 in Chapter 6. The difference between these figures is that the Perturbation Factors in Figure 6.1-6.3 are calculated at equilibrium, while those in Figure 8.2, 8.4, 8.6 and 8.8 are calculated at 5.00 min. of stirring. In these 4.x figures, the Perturbation Factors are calculated as the ratio of “Reported $[\text{Cu}^{2+}]$ ”, from equation 6.50, to $[\text{Cu}^{2+}]_{\text{L}=0}$, from equation 6.27 (in Figure 8.2, 8.4, 8.8) or from equation 6.27a (in Figure 8.6). The vertical arrows in Figure 8.2, 8.4, 8.6 and 8.8 identify the value of $\log K_{\text{f}, \text{CuX}'}$ at the pH in question. Values for the constants shown in the captions of Figure 8.2, 8.4, 8.6 and 8.8 are the ones that are appropriate for the conditions employed. In the calculation of the Perturbation Factor, the rate constant, k_{SAMP} , the constant K_2 (defined in equation 6.6a), and $[\text{L}^-]$ are needed. k_{SAMP} is obtained from combining equation 6.44, 6.47 and 6.48 (for glycine and citrate) or from equation 6.49 (for phthalate). The following shows how K_2 and $[\text{L}^-]$ are obtained for the specific pH.

The value of $[L^-]$ can be calculated for any given value of pH by first of all solving equation 8.1 below.

$$\kappa_{HL} = \frac{[HL]_o}{[HL]_{aq}} \approx \frac{C_{L,o} - [HL]_{aq} \frac{V_{aq}}{V_o} - [L^-] \frac{V_{aq}}{V_o}}{[HL]_{aq}} \quad (8.1)$$

where, $C_{L,o}$ is the known total concentration of Lix63, V_{aq}/V_o is the known phase ratio, $[HL]_{aq}$ and $[HL]_o$ are the concentration of Lix63 in aqueous and organic phase,

respectively. In equation 8.1, the assumption, $[CuL^+] + 2[CuL_2]_o \frac{V_o}{V_{aq}} \ll [HL] +$

$[HL]_o \frac{V_o}{V_{aq}} + [L^-]$, is used. This assumption is based on the second criterion of speciation

measurement (described in section 6.2.1), i.e. $[CuL^+] + 2[CuL_2]_o \frac{V_o}{V_{aq}} \ll C_{L,o} \frac{V_o}{V_{aq}}$.

According to this assumption, we have

$$C_{L,o} \frac{V_o}{V_{aq}} = [L^-] + [HL] + [HL]_o \frac{V_o}{V_{aq}} \quad (6.9a)$$

in place of equation 6.9 in which the terms $[CuL^+]$ and $2[CuL_2]_o \frac{V_o}{V_{aq}}$ are neglected. The

relationship between $[L^-]$ and $[HL]_{aq}$ is given by equation 6.5, which is rearranged as in equation 8.2 below:

$$[\text{HL}]_{\text{aq}} = \frac{[\text{L}^-][\text{H}^+]}{K_{\text{a,HL}}} \quad (8.2)$$

$[\text{HL}]_{\text{aq}}$ from equation 8.2 is substituted in equation 8.1 which is then rearranged and solved for $[\text{L}^-]$ as in the equation below:

$$[\text{L}^-] = \frac{C_{\text{L},\text{o}}}{\frac{\kappa_{\text{HL}}[\text{H}^+]}{K_{\text{a,HL}}} + \frac{[\text{H}^+]}{K_{\text{a,HL}}} \frac{V_{\text{aq}}}{V_{\text{o}}} + \frac{V_{\text{aq}}}{V_{\text{o}}}} \quad (8.3)$$

Upon knowing $[\text{L}^-]$, K_2 can be calculated through equation 6.22. The following is the rearranged equation 6.22.

$$K_2 = \frac{1 + K_{\text{f,CuL}^+}[\text{L}^-]}{K_{\text{f,CuL}^+}[\text{L}^-] \left(\frac{C_{\text{Cu, aq}}}{[\text{CuL}_2]_{\text{o}}} - \frac{V_{\text{o}}}{V_{\text{aq}}} \right)} \quad (8.4)$$

In equation 8.4, the term on the right hand side, $\frac{C_{\text{Cu, aq}}}{[\text{CuL}_2]_{\text{o}}}$, is the reciprocal of the slope of the linear part of the extraction calibration curve in Figure 7.9 ($<7.5 \times 10^{-6}$ M copper), which is 183.6. Therefore, with known values of $\frac{V_{\text{o}}}{V_{\text{aq}}}$, $[\text{L}^-]$, $K_{\text{f,CuL}^+}$ and $\frac{C_{\text{Cu, aq}}}{[\text{CuL}_2]_{\text{o}}}$, K_2 can be easily solved out through equation 8.4.

In the entire calculation of the Perturbation Factor, there are three constants which need to be estimated. They are the formation constant, $K_{\text{f,CuL}^+}$, the acid dissociation constant of Lix63, $K_{\text{a,HL}}$, and the distribution coefficient of HL between octane and aqueous phase, κ_{HL} . Among them, $K_{\text{a,HL}}$ and κ_{HL} are used to calculate the value of $[\text{L}^-]$ (equation 8.3), and $K_{\text{f,CuL}^+}$, along with the value of $[\text{L}^-]$, i.e. $K_{\text{f,CuL}^+}[\text{L}^-]$, is used to calculate K_2 (equation 8.4). Hence, the value of $K_{\text{f,CuL}^+}[\text{L}^-]$ can be used to represent the estimated constants. Therefore, $K_{\text{f,CuL}^+}[\text{L}^-]$ is treated as an empirical fitting parameter in

each of the systems, and then, the average of the best fit from the systems of glycine, citrate and phthalate is used in every system. The details are shown below.

For simplicity, we let

$$K_{f,CuL^+}[L^-] = f \quad (8.5)$$

A series of values of f have been tried in each of the three systems to find out the best ones, which give the right Perturbation Factors to make experimental data and the theoretical data the closest in Figure 8.3, 8.5 and 8.7. These best values of f for each of the systems are listed in Table 8.1. Since pH is 7 in the systems of EDTA, phthalate and glycine, but 6 in the system of citrate, the f value in citrate system is in a different order of magnitude than that in the other three systems. When $[H^+] \gg K_{a,HL}$, which is true in our case, i.e. $[H^+]$ is either 10^{-6} or 10^{-7} and $K_{a,HL}$ is estimated to be 10^{-9} based on the known formation constants for copper with other oxime ligands²⁶⁹, equation 8.3 could be simplified to be

$$[L^-] = \frac{C_{L,o}}{\frac{[H^+]}{K_{a,HL}} \left(\kappa_{HL} + \frac{V_{sq}}{V_o} \right)} = \frac{C_{L,o} K_{a,HL}}{[H^+] \left(\kappa_{HL} + \frac{V_{sq}}{V_o} \right)} \quad (8.6)$$

On the right hand side of equation 8.6, all the terms other than $[H^+]$ are constants, so $[L^-] \propto 1/[H^+] \propto 10^{\text{pH}}$. Hence, when pH=6 the value of $K_{f,CuL^+}[L^-]$ should be about 10 times smaller than that when pH=7. Keeping this in mind, the values of f in the three systems of interest are averaged in the way that are shown in Table 8.1. The values of f in the fourth column in Table 8.1 are used to calculate Figure 8.2, 8.4, 8.6 and 8.8. The Perturbation Factors used in these figures are listed in Table 8.2, 8.3 and 8.4.

Table 8.1 Average f Values

SYSTEM	BEST f	AVERAGE f (f_{AVG})	f USED
Glycine	$f_{Gly} = 15.0$	$f_{AVG} = \frac{f_{Gly} + f_{Phth} + 10 \times f_{Cit}}{3} = 30.0$	$f_{Gly, Avg} = f_{AVG} = 30.0$
Phthalate	$f_{Phth} = 50.0$		$f_{Phth, Avg} = f_{AVG} = 30.0$
Citrate	$f_{Cit} = 2.5$		$f_{Cit, Avg} = f_{AVG} / 10 = 3.0$
EDTA			$f_{EDTA, Avg} = f_{AVG} = 30.0$

8.3.1 Free Copper Ion Determination in the Presence of EDTA

The result of free copper determination in the presence of EDTA is shown in Figure 8.1. As can be seen, the experimental data points match the theoretical prediction line very well. The K_f' of Cu-EDTA is $10^{13.4}$ at pH 7,²⁷⁰ which indicates that EDTA is a strong ligand, the Cu-EDTA complexes in the sample experience hardly any competition from Lix63 during measurement. As shown in Figure 8.2, for this case there is no perturbation, as discussed in section 6.3. This explains the good agreement between theoretical and experimental data in Figure 8.1.

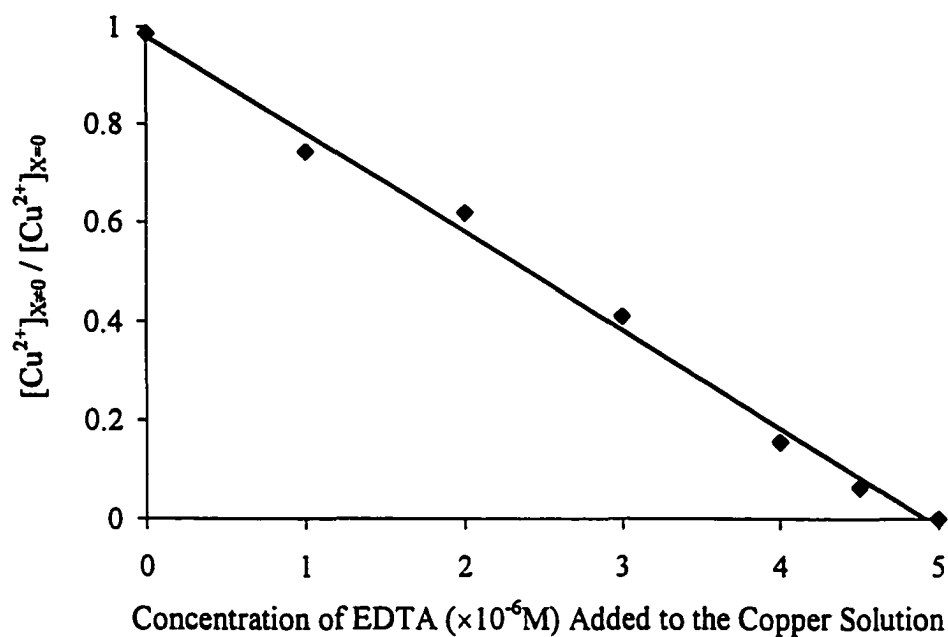


Figure 8.1 Effect of EDTA on Free Copper Determination.

$[Cu^{2+}]_{X=0} = 5.00 \times 10^{-6} M$, $X=EDTA$, $pH=7.00$. Points are experimental data for 5.00 min. stirring, line is the theoretical prediction calculated *via* equation 6.56 in Section 6.6. There is negligible perturbation due to the presence of Lix63.

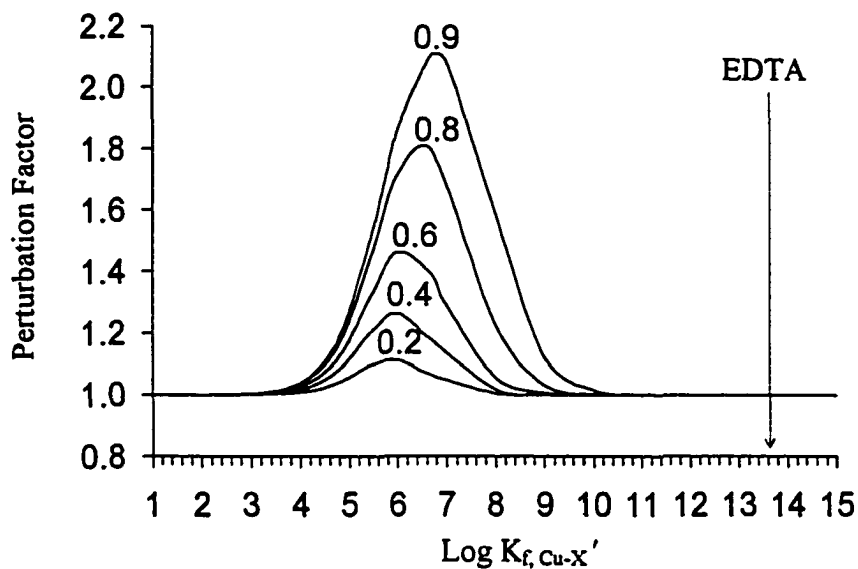


Figure 8.2 Perturbation Factor versus $\log K_{f, Cu-X'}$ at the various values of $C_{EDTA, aq} / C_{Cu, aq}$ shown by the numbers next to the curves, at constant values of $V_o / V_{aq} = 2.00 \times 10^{-6}$, $K_2 = 205.6$, $pH = 7.00$, $K_{f, CuL^+}[L] = 30.0$, extraction time $t = 5.00$ min. and extraction rate constant $k_{STD} = 0.0185$. The vertical arrow identifies the value of $\log K_{f, Cu-EDTA'} (= 13.4)$ at $pH 7.00$.

8.3.2 Free Copper Ion Determination in the Presence of Glycine, Phthalate, or Citrate

The result of free copper determination in the presence of glycine, phthalate and citrate is shown in Figures 8.3, 8.5 and 8.7, respectively. The solid points are the measured concentrations of free copper in solutions with increasing addition of the ligand, the open points are the corrected experimental data obtained by dividing the experimentally observed data by the Perturbation Factor, and the lines are the theoretically predicted free copper concentration calculated in section 6.6.

It will be observed in Figures 8.3, 8.5 and 8.7, below, that for glycine, phthalate and citrate, there are disagreements between experimental results (solid points) and theoretical prediction (lines). This divergence can be explained by the perturbation curves shown in Figures 8.4, 8.6, and 8.8 for the glycine, phthalate and citrate systems, respectively. Glycine with $\text{Log}K_{f,\text{Cu-Gly}}' = 5.47$ (in Figure 8.4), phthalate with $\text{Log}K_{f,\text{Cu-phthalate}}' = 3.22$ (in Figure 8.6), and citrate with $\text{Log}K_{f,\text{Cu-citrate}}' = 5.78$ (in Figure 8.8) all fall in the perturbation region (with Perturbation Factor larger than 1) as shown in each of the figures. As discussed earlier in section 6.3, the perturbation is caused by the dissolution of extractant Lix63 (HL) from the organic phase into the aqueous phase. This unwanted dissolution results in the removal of Cu-X complexes to form CuL_2 , so as to raise the value of $[\text{CuL}_2]_o$. Consequently, the reported $[\text{Cu}^{2+}]$ obtained by using the calibration curve (i.e. plot of $[\text{CuL}_2]_o$ versus $[\text{Cu}^{2+}]$) would be falsely high. In Figure 8.4 and 8.6 (glycine and phthalate), the degree of perturbation (Perturbation Factor) increases with increasing amount of ligand added to the solutions, and this compensates for the decrease of free copper concentration as expected when more and more ligand X is present in the systems. This results in the almost constant values of the experimentally observed data (solid points in Figure 8.3 and 8.5). In the case of citrate, seen in Figure 8.8, the Perturbation Factors are more or less the same regardless of the change of the ligand amount present. Therefore, although the perturbed experimental data are falsely larger than the theoretical data the declining trend of the data points due to the increasing addition of ligand X is not greatly changed (Figure 8.7).

Division of the observed experimental points by the appropriate Perturbation Factor yields the open-circle points in Figures 8.3, 8.5 and 8.7. The data in these figures shows that the perturbation due to the presence of L^- in the aqueous phase is so great that the observed values of $[Cu^{2+}]_{X \neq 0} / [Cu^{2+}]_{X=0}$ in all of the three systems are larger than the theoretical values. The results are also shown in Table 8.2-8.4. In each of these tables, the experimental data in the second column are divided by the Perturbation Factors to yield the corrected data listed in column 4. As can be seen by comparison of column 4 with column 5 in these tables and also by comparison of the open points with the lines in Figures 8.3, 8.5 and 8.7, the experimental data corrected by the perturbation factors are in good agreement with the theoretical predicted data. This indicates that the derived perturbation model, including the kinetic contribution resulting from not waiting until equilibrium is reached, could considerably compensate for the perturbation.

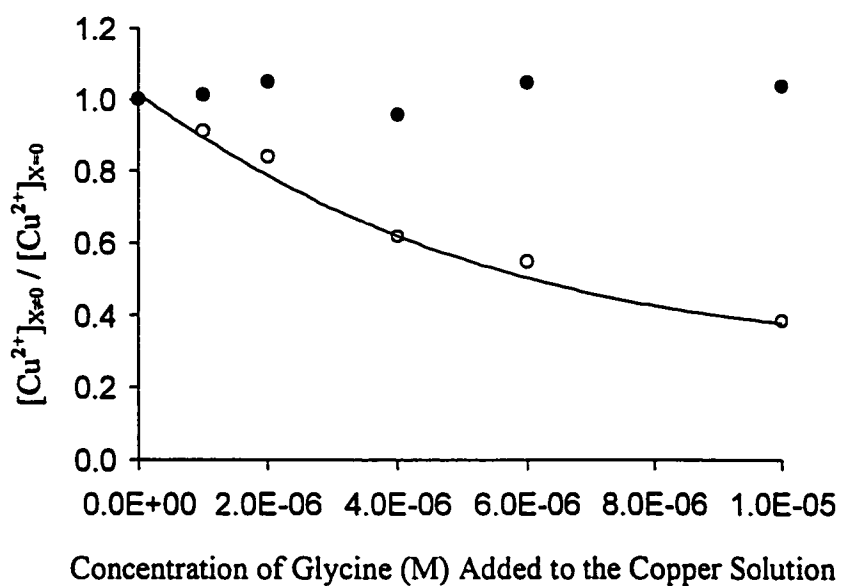


Figure 8.3 Effect of glycine on Free Copper Determination.

$[\text{Cu}^{2+}]_{\text{X}=0} = 5.00 \times 10^{-6} \text{M}$, X = glycine, pH=7.00. The solid circles are experimental data for 5.00 min. stirring, open circles are obtained by dividing the experimental values (solid circles) by the Perturbation Factor from Figure 8.4 and Table 8.2, and line is the theoretical prediction calculated *via* equation 6.56 in Section 6.6.

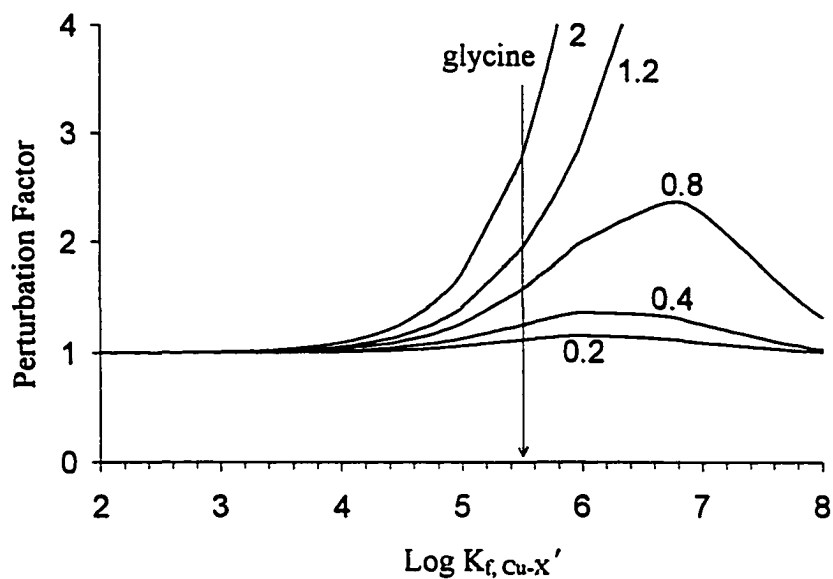


Figure 8.4 Perturbation Factor versus $\log K_{f, Cu-X'}$ at the various values of $C_{glycine, aq} / C_{Cu, aq}$ shown by the numbers next to the curves, at constant values of $V_o / V_{aq} = 2.00 \times 10^{-6}$, $K_2 = 205.6$, $pH = 7.00$, $K_{f, CuL^+} [L] = 30.0$, extraction time $t = 5.00$ min. and extraction rate constant $k_{STD} = 0.0185$. The vertical arrow identifies the value of $\log K_{f, Cu-glycine}' (= 5.47)$ at $pH 7.00$.

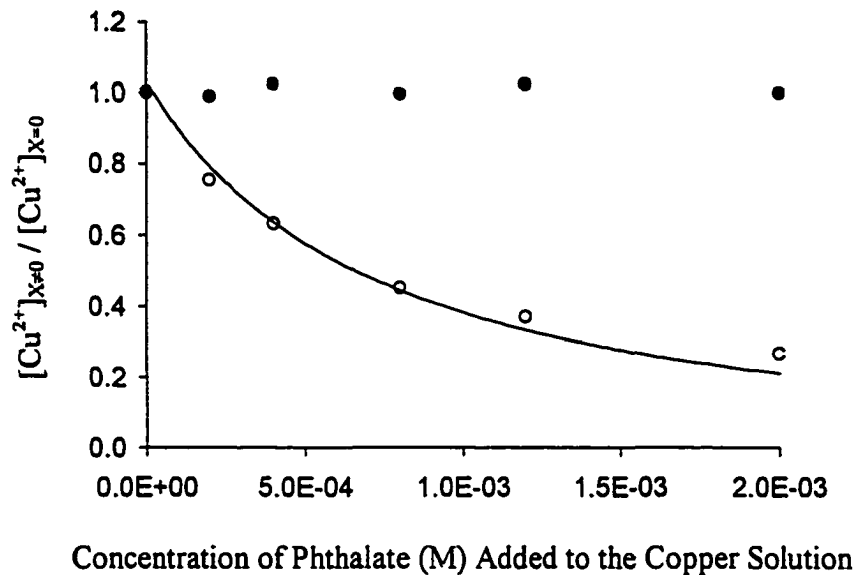


Figure 8.5 Effect of phthalate on Free Copper Determination.

$[\text{Cu}^{2+}]_{x=0} = 1.00 \times 10^{-6} \text{M}$, X = phthalate, pH = 7.00. The solid circles are experimental data for 5.00 min. stirring, open circles are obtained by dividing the experimental values (solid circles) by the Perturbation Factor from Figure 8.6 and Table 8.3, and line is the theoretical prediction calculated *via* equation 6.56 in Section 6.6.

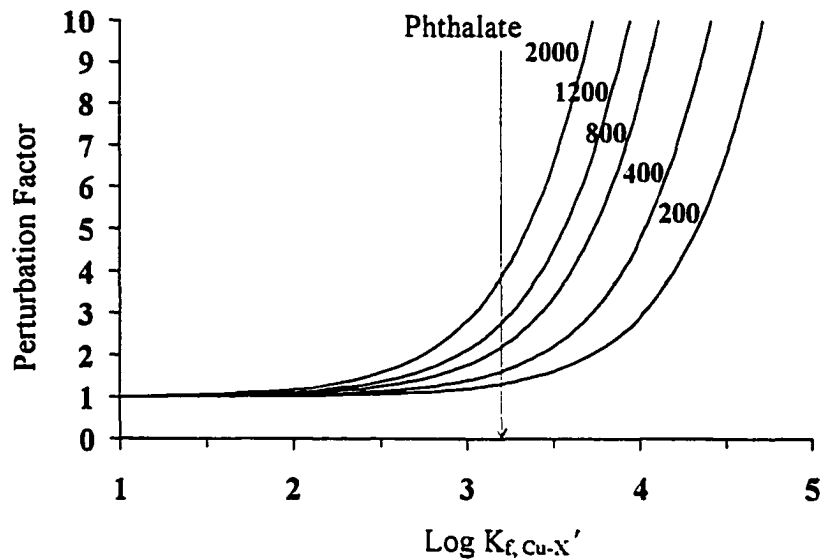


Figure 8.6 Perturbation Factor versus $\log K_{f, Cu-X'}$ at the various values of $C_{phthalate, aq} / C_{Cu, aq}$ shown by the numbers next to the curves, at constant values of $V_o / V_{aq} = 2.00 \times 10^{-6}$, $K_2 = 205.6$, $pH = 7.00$, $K_{f, CuL^+}[L] = 30.0$, extraction time $t = 5.00$ min. and extraction rate constant $k_{STD} = 0.0185$. The vertical arrow identifies the value of $\log K_{f, Cu-phthalate}' (= 3.22)$ at $pH 7.00$.

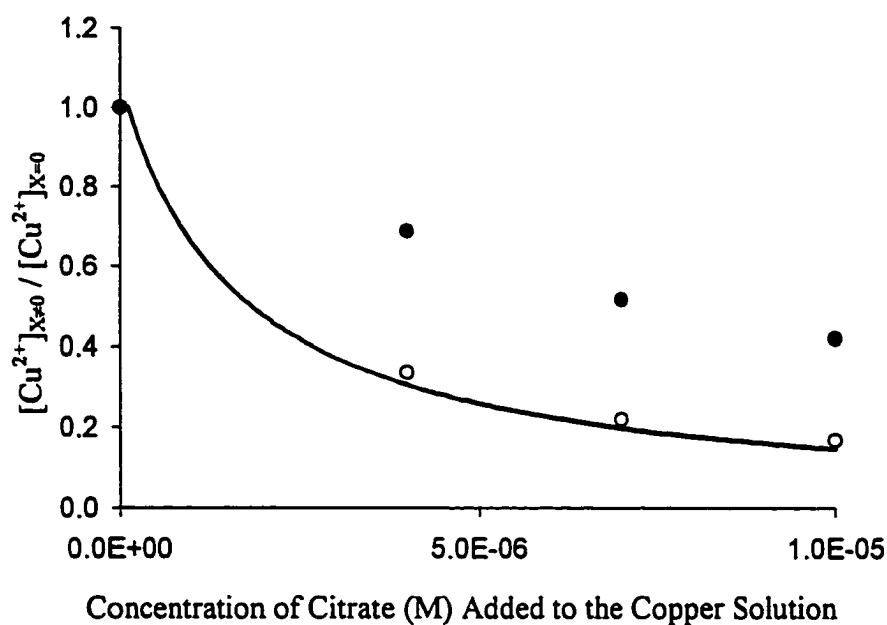


Figure 8.7 Effect of citrate on Free Copper Determination.

$[\text{Cu}^{2+}]_{x=0} = 10^{-7}\text{M}$, $X = \text{citrate}$, $\text{pH} = 6.00$. The solid circles are experimental data for 5.00 min. stirring, open circles are obtained by dividing the experimental values (solid circles) by the Perturbation Factor from Table 8.4, and line is the theoretical prediction calculated *via* equation 6.56 in Section 6.6.

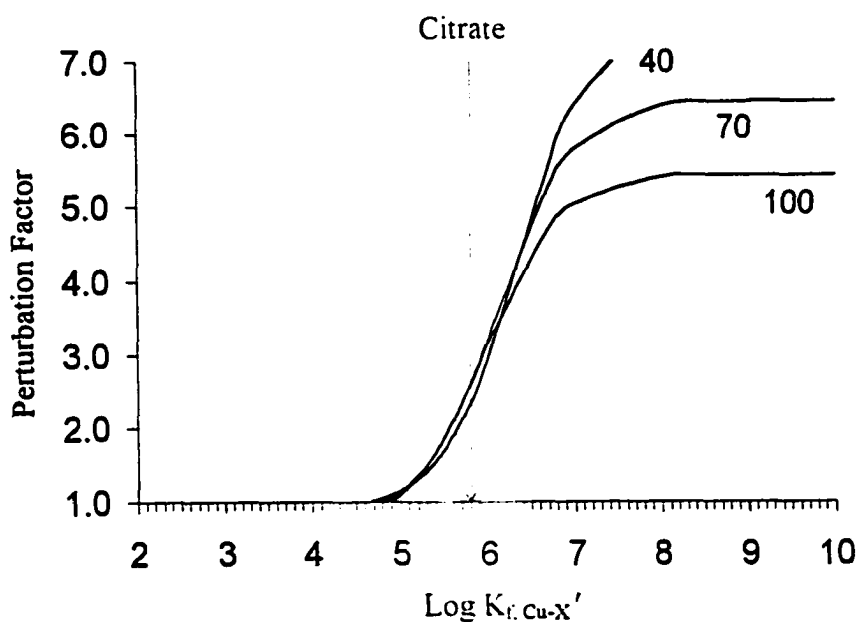


Figure 8.8 Perturbation Factor versus $\log K_{f, Cu-X'}$ at the various values of $C_{citrate, aq} / C_{Cu, aq}$ shown by the numbers next to the curves, at constant values of $V_o / V_{aq} = 2.00 \times 10^{-6}$, $K_2 = 403.8$, $pH = 6.00$, $K_{f, CuL^+}[L] = 3.0$, extraction time $t = 5.00$ min. and extraction rate constant $k_{STD} = 0.0185$. The vertical arrow identifies the value of $\log K_{f, Cu-citrate'} (= 5.78)$ at $pH 6.00$.

**Table 8.2 Comparison of Theoretical Data and Experimental Data
Corrected by Perturbation Factor (X=Glycine)**

$\frac{C_{X,aq}}{C_{Cu,aq}}$	$\frac{[Cu^{2+}]_{X \neq 0}^{(a)}}{[Cu^{2+}]_{X=0}}$		Perturbation Factor ^(b)		$\frac{[Cu^{2+}]_{X \neq 0}^{(c)}}{[Cu^{2+}]_{X=0}}$	$\frac{[Cu^{2+}]_{X \neq 0}^{(d)}}{[Cu^{2+}]_{X=0}}$
0	1.00±0.05	÷	1.00	=	1.00±0.05	1.00±0.05
0.2	1.01±0.05	÷	1.11	=	0.91±0.04	0.89±0.04
0.4	1.05±0.05	÷	1.25	=	0.84±0.04	0.79±0.04
0.8	0.96±0.05	÷	1.55	=	0.62±0.03	0.62±0.03
1.2	1.05±0.05	÷	1.91	=	0.55±0.02	0.50±0.02
2.0	1.04±0.05	÷	2.70	=	0.38±0.02	0.38±0.02

(a) Experimentally observed data.

(b) Calculated by using $f = 30.0$.

(c) Data corrected by Perturbation Factors.

(d) Data predicted by the theoretical line in Figure 8.3.

Table 8.3 Comparison of Theoretical Data and Experimental Data
Corrected by Perturbation Factor (X=Phthalate)

$\frac{C_{X,aq}}{C_{Cu,aq}}$	$\frac{[Cu^{2+}]_{X \neq 0}^{(a)}}{[Cu^{2+}]_{X=0}}$		Perturbation Factor ^(b)		$\frac{[Cu^{2+}]_{X \neq 0}^{(c)}}{[Cu^{2+}]_{X=0}}$	$\frac{[Cu^{2+}]_{X \neq 0}^{(d)}}{[Cu^{2+}]_{X=0}}$
0	1.00±0.05	÷	1.00	=	1.00±0.05	1.00±0.05
200	0.99±0.05	÷	1.31	=	0.75±0.04	0.79±0.04
400	1.02±0.05	÷	1.62	=	0.63±0.03	0.64±0.03
800	1.00±0.05	÷	2.21	=	0.45±0.02	0.44±0.02
1200	1.02±0.05	÷	2.76	=	0.37±0.02	0.33±0.02
2000	1.00±0.01	÷	3.74	=	0.27±0.01	0.21±0.02

(a) Experimentally observed data.

(b) Calculated by using $f = 30.0$.

(c) Data corrected by Perturbation Factors.

(d) Data predicted by the theoretical line in Figure 8.5.

Table 8.4 Comparison of Theoretical Data and Experimental Data
Corrected by Perturbation Factor (X=Citrate)

$\frac{C_{X,aq}}{C_{Cu,aq}}$	$\frac{[Cu^{2+}]_{X \neq 0}^{(a)}}{[Cu^{2+}]_{X=0}}$		Perturbation Factor ^(b)		$\frac{[Cu^{2+}]_{X \neq 0}^{(c)}}{[Cu^{2+}]_{X=0}}$	$\frac{[Cu^{2+}]_{X \neq 0}^{(d)}}{[Cu^{2+}]_{X=0}}$
0	1.00±0.05	÷	1.00	=	1.00±0.05	1.00±0.05
40	0.69±0.04	÷	2.05	=	0.34±0.02	0.31±0.02
70	0.53±0.03	÷	2.36	=	0.22±0.02	0.20±0.04
100	0.42±0.02	÷	2.49	=	0.17±0.01	0.15±0.01

(a) Experimentally observed data.

(b) Calculated by using $f = 3.0$.

(c) Data corrected by Perturbation Factors.

(d) Data predicted by the theoretical line in Figure 8.7.

8.4 Conclusions

The purpose of the present work is to develop a new metal speciation technique, which can be applied to speciation studies in the presence of kinetically labile species. It employs micro-extraction with the intention to limit the perturbation of the original equilibrium in the system of interest. The technique is a combination of a one-drop (1 μL) solvent micro-extraction (SME) technique and the Direct Sample Insertion (DSI) – ICP/MS technique. The use of the DSI-ICP/MS has further improved the system by providing an easy way of sample introduction and an accurate and specific elemental analysis.

The present work has covered a complete characterization of the developed SME-DSI-ICP/MS system, which includes the characterization of the operation of the SME and DSI-ICP/MS systems, the investigation of the kinetic mechanism of the solvent micro-extraction process, the comparison of the experimental data and the theoretically calculated data, and the discussion of the perturbation observed in this speciation system.

The simple and easily operated SME process turns out to be kinetically controlled by chemical reaction. This conclusion allows the solvent extraction to be stopped at any time before equilibrium is reached (5 min. stirring time is chosen in this work, though the equilibrium will be reached after about one hour stirring.) and hence brings this technique to a higher level of convenience.

For the systems in the presence of a strong complexing ligand (i.e. with a larger formation constant of the copper complex than that of Cu-Lix63), such as EDTA, there is a good agreement between the experimental and the theoretical data. However, for the systems in the presence of a weak ligand (i.e. with a smaller formation constant of the copper complex than that of Cu-Lix63), such as glycine, phthalate or citrate, there are divergences between the experimental results and the theoretical predications. These disagreements evidence the perturbation present in the systems of interest.

Perturbation is an inherent problem in speciation studies in the presence of kinetically labile species, which requires that the analysis procedure should not disturb the original equilibrium in the system. In a conventional solvent extraction system, the perturbation is mainly brought about by the removal of analyte from the aqueous phase due to the extraction. That is essentially eliminated in micro-drop extraction as used in this work. However, the extraction of the Lix63 into aqueous phase introduces an additional source of perturbation. The unwanted dissolution of Lix63 in aqueous phase is due to the small organic/aqueous phase ratio required by the micro-extraction system, and/or to inadequate hydrophobicity of the extractant. The presence of Lix63 in aqueous sample solution results in the competition between Lix63 and the complexing ligand originally present in the sample system towards copper. Only if the complexing ligand in the sample is a stronger ligand towards copper than Lix63 is, could the sample system be tested without perturbation.

In this work, a perturbation model was established, which embodies criteria for perturbation conditions. The so-called Perturbation Factor, which is the ratio of the reported concentration of free copper ions in the presence of the chelating extractant to that in the absence of the chelating extractant, i.e. "Reported $[Cu^{2+}]^*$ "/ $[Cu^{2+}]_{L=0}$, is shown to be a function of the phase ratio (V_o/V_a), the formation constant of metal-chelating agents originally present in the aqueous phase ($K_{f,MIX}$), the formation constant of metal-chelating extractant originally present in organic phase ($K_{f,ML}^*$), the constant K_2 , which relates to the distribution of M-L complexes between aqueous and organic phase, the distribution coefficient of HL (κ_{HL}), pH, the extraction time (t) and the rate constant (k) of the first order reaction with respect to copper. This perturbation model permits a quantitative prediction of the extent of perturbation for a given combination of these experimental parameters. As shown in section 8.3, the experimental data corrected by Perturbation Factor have good agreements with the theoretical data.

Chapter 9

Comments and Future Work for Part II

9.1 Comments

In the present work, a metal speciation technique has been developed by coupling the microdrop solvent extraction technique with ICP/MS, with the aid of a direct sample insertion device (DSID). This technique has the following features:

(1) Since the 1 μL organic solvent drop is very small with respect to the 500 mL aqueous solution, i.e. the phase ratio (V_o/V_a) is 2×10^{-6} , the system can eliminate the perturbation caused by the extraction of metal from aqueous phase into organic phase, which is often a problem for speciation studies using solvent extraction techniques. Under this circumstance, the extraction system behaves like a sampling probe, which is similar to the very classically and commonly used pH electrode that measures concentration of H^+ without perturbing the solution composition significantly. This aspect of the system is the origin of the whole idea of developing the technique described in this work.

(2) Metal ion solvent extraction is a commonly applied technique for metal analysis. However, the use of a large amount of organic solvent that is associated with the conventional solvent extraction technique is undesirable. Since the microdrop of organic solvent used in this work is only 1 μL , the consumption of the solvent is negligible. Moreover, during the experimental procedures in this work, the entire drop of octane, after the extraction, was transferred into the graphite cup of the sample insertion device, and then was completely delivered into ICP and burned out.

(3) Desorption of metal from the microdrop is not required in this work. This is in contrast to what is required with solid phase microextraction (SPME)¹⁷³ and ion

exchange^{157,158,159} for metal speciation. Both of the aforementioned techniques, which involve the use of solid sorbents, require desorption of the analyte that is often time-consuming and tedious.

(4) Another advantage of the present micro-drop technique over SPME is that the drop used in each experiment is always fresh. This eliminates the possibility of carry-over caused by repeatedly using the same solid phase probe.

(5) Since the chelating extractant in the organic drop can always be replaced by other chelates for other element selectivity without changing the whole system, there is a great potential for this technique to be adopted to the analysis of many other metal elements. Furthermore, the use of mass spectrometry as the detector makes the technique more tolerant to the presence of other metals in the same system, provided the extraction of interference does not cause significant perturbation. Hence, the same chelating extractant (if it is a “universal” chelating agent) could possibly be used simultaneously for other metal elements that are prominent in the system of interest.

(6) The analysis can be done even under non-equilibrium conditions and the analysis time can be as conveniently short as the operator chooses.

(7) The drawback of the present system is the dissolution of the chelating extractant Lix63 from organic phase into aqueous phase. This has caused the undesired perturbation problem and limited the application of this technique. A perturbation model has been successfully established in this work to understand the data obtained from the perturbed systems and to confirm the cause of the perturbation. This perturbation problem leaves room for improvement of this technique in future work.

9.2 Future Work

The chelating extractant used in this work is Lix63, which is a liquid ion exchanger with a complexing functional group (oxime group) and alkyl chains (with 16

carbon atoms per molecule). The solubility of Lix 63 in aqueous phase in low pH (= 4.8) is 2.14×10^{-5} M.²⁵⁷ However, since the phase ratio in the micro-extraction system is so small (2×10^{-6}), a significant fraction of the Lix63 (even with 16 carbon alkyl chain) enters the aqueous phase and causes perturbation. This limits the application of this technique only to systems that contain stronger metal complexing ligand than Lix63.

To find a system in which a slight or negligible amount of chelating extractant dissolves in aqueous phase would be the challenge of future work. This may be accomplished in two ways. One way is to use a different solvent than octane. A chelating extractant requires a polar group for metal complexation. It is this polar group that enhances the dissolution ability of the chelating extractant in aqueous phase. If the organic solvent is very hydrophobic as octane is, the chelating extractant with the polar group would have a relatively larger affinity for the aqueous phase. On the other hand, if the organic solvent is hydrophobic as required by the extraction procedure and also has hydrophilic features, such as in the case of some long-chain alcohols, which have long alkyl chains ensuring that they stay as the organic phase and also have an hydroxyl group, then it might keep the chelating extractant more extensively in the organic phase and decrease the dissolution of it into the aqueous phase.

Another way to reduce the dissolution of chelating extractant in aqueous phase is to choose or synthesize chelating extractants that are more hydrophobic. Polymer-supported chelating reagents are commonly used in the ion exchange technique for metal analysis or speciation.^{271, 272, 273, 274} Non-crosslinked polymers with low molecular weight, which can dissolve in suitable organic solvent, can also be modified to have complexing functionality.²⁷⁵ The modified soluble polymers could be one choice as a chelating extractant. A similar idea involves using dendrimers,^{276, 277} which have hydrophobic exteriors in a heavy density and chelating functional interior, can also be investigated.

Bibliography

1. Melander, W. R.; Horvath, Cs. In *High-Performance Liquid Chromatography Advances and Perspectives*, Horvath, Cs., Eds., Vol 2, Academic Press Inc.: London, 1980, Chapter 1.
2. Tanaka, N.; Kimata, K.; Hosoya, K.; Miyanishi, H.; Araki, T. *J. Chromatogr. A* **1993**, 656, 265.
3. Moore, S.; Stein, W. H. *J. Biol. Chem.* **1954**, 211, 907.
4. Snyder, L. R., Kirkland, J. J., Glatch, J. L. In *Practical HPLC Method Development*, 2nd ed, John Wiley & Sons, Inc.: Toronto, 1997, Chapter 5.
5. Benson, J. R.; Woo, D. J. *J. Chromatogr. Sci.* **1984**, 22, 386.
6. Tanaka, N.; Araki, M. In *Advances in Chromatography*, Vol.30, Selectivity and Retention in Chromatography, Giddings, J. C.; Grushka, E.; Brown, P. R., Eds., Marcel Dekker, Inc.: New York, 1989, pp.81.
7. Lloyd, L. L. *J. Chromatogr.* **1991**, 544, 201.
8. Rolls, W. A.; Jagodzinski, J. J. *J. Chromatogr.* **1992**, 59, 89.
9. Hosoya, K.; Maruya, S.; Kimata, K.; Kinoshita, H.; Araki, T.; Tanaka, N. *J. Chromatogr.* **1992**, 625, 121.
10. Gustafson, R. L.; Albright, R. L.; Heisler, J.; Lirio, J. A.; Reid Jr., O.T. *Ind. Eng. Chem., Prod. Res. and Dev.* **1968**, 7, 107.
11. Kunin, R.; Meitzner, E. F.; Oline, J. A.; Fisher, S. A.; Frisch, N. *Ind. Eng. Chem., Prod. Res. and Dev.* **1962**, 1, 140.
12. Millar, J. R.; Smith, D. G.; Marr, W. E.; Kressman, T. R. E. *J. Chem. Soc.* **1963**, 218.
13. Millar, J. R.; Smith, D. G.; Marr, W. E.; Kressman, T. R. E. *J. Chem. Soc.* **1963**, 2779.
14. Millar, J. R.; Smith, D. G.; Marr, W. E.; Kressman, T. R. E. *J. Chem. Soc.* **1964**, 2740.
15. Gowanlock, D.; Bailey, R.; Cantwell, F. F. *J. Chromatogr. A* **1996**, 726, 1.
16. Nevejans, F.; Verzele, M. *J. Chromatogr.* **1987**, 406, 325.

16. Nevejans, F.; Verzele, M. *J. Chromatogr.* **1987**, 406, 325.
17. Jacobelli, H.; Bartholin, M.; Guyot, A. *J. Appl. Polym. Sci.* **1979**, 23, 927.
18. Nevejans, F.; Verzele, M. *Chromatographia* **1985**, 20, 173.
19. Moore, J. C. *J. Polym. Sci.* **1964**, Part A, 2, 835.
20. Dawkins, J. V.; Stone, T.; Yeadon, G.; Warner, F. P. *Polymer* **1979**, 20, 1164.
21. Dawkins, J. V.; Lloyd, L. L.; Warner, F. P. *J. chromatogr.* **1986**, 352, 157.
22. Lee, Dan P. *J. Chromatogr.* **1988**, 443, 143.
23. Smith, R. L.; Pietrzyk, D. J. *J. Chromatogr. Sci.* **1983**, 21, 283.
24. Uchida, M.; Tanimura, T. *J. Chromatogr.* **1977**, 138, 17.
25. Iskandarani, Z.; Pietrzyk, D. J. *Anal. Chem.* **1982**, 54, 1065.
26. Grobe-Rhode, C.; Kicinski, H. G.; Kettrup, A. *J. Chromatogr.* **1988**, 26, 209.
27. Yang, Y. B.; Verzele, M. *J. Chromatogr.* **1987**, 387, 197.
28. Tweeten, K. A.; Tweeten, T. N. *J. Chromatogr.* **1990**, 522, 95.
29. Yuan, D.; Pietrzyk, D. J. *J. Chromatogr.* **1990**, 509, 357.
30. Moats, W. A. *J. Chromatogr.* **1986**, 366, 69.
31. Hoogmartens, J. *J. Pharm. Biomed. Anal.* **1992**, 10, 845.
32. Gawdzok, B. *J. Chromatogr.* **1992**, 600, 115.
33. Weiner, M. P.; Thannhauser, T. W.; Laity, J. H.; Bennis, M. E.; Lee, D. P.; Scheraga, H. A. *Nucleic Acids Res.* **1988**, 16, 8185.
34. Reh, E.; Kapfer, U. *Chromatographia* **1990**, 30, 663.
35. Huber, C. G.; Oefner, P. J.; Bonn, G. K. *Anal. Biochem.* **1993**, 212, 351.
36. Huber, C. G.; Oefner, P. J.; Bonn, G. K. *Anal. Biochem.* **1993**, 37, 653.
37. Hirukawa, M.; Arai, Y.; Hanai, T. *J. Chromatogr.* **1987**, 395, 481.
38. Tanaka, N.; Hashizume, K.; Araki, M. *J. Chromatogr.* **1987**, 400, 33.
39. Tanaka, N.; Ebata, t.; Hashizume, K.; Hosoya, K.; Araki, M. *J. Chromatogr.* **1989**, 475, 195.
40. Lloyd, L. L.; Dryzek, Z.; Harrison, D. B.; Warner, F. P. *10th Int. Symp. Column Liquid Chromatography*, San Francisco, may 1986.
41. Li, J.; Cantwell, F. F. *J. Chromatogr. A* **1996**, 726, 37.
42. Cornel, P.; Sontheimer, H. *Chem. Eng. Sci.* **1986**, 41, 1791.

43. Bowers, L. D.; Pedigo, S. *J. Chromatogr.* 1986, 371, 243.
44. Brandrup, B. A.; Immergut, E. H. *Polymer Handbook*, Wiley: New York, 1975.
45. Smith, R. M.; Garside, D. R. *J. Chromatogr.* 1987, 406, 19.
46. Coppi, S.; Betti, A.; Bigli, C.; Cartoni, G. P.; Coccioli, F. *J. Chromatogr.* 1988, 442, 97.
47. Stuurman, H. W.; Kohler, J.; Jansson, S. O.; Litzen, A. *Chromatographia* 1987, 23, 341.
48. Barton, A. F. M. *Handbook of Solubility Parameters and Other Cohesion Parameters*, CRC Press, 1991
49. Gardon, J. L. In *Encyclopedia of Polymer Science and Technology*; Mark, H. F.; Gaylord, N. G.; Bikales, N. M., Eds.; Interscience: New York, 1965, pp.833.
50. D. Liru; H. Xizhang; W. Qihui; M. Qingcheng; L. Yuliang; Z. Youliang *Scinetia Sinica (Series B)* 1982, 25, 905.
51. Li, J.; Litwinson, L.M.; Cantwell, F. F. *J. Chromatogr. A* 1996, 726, 25.
52. Sederel, W. L.; Jong, G. J. De *J. of Appl. Polym. Sci.* 1973, 17, 2835.
53. Kun, K. A.; Kunin, R. *Journal of Polymer Science* 1968, Part A-1, 6, 2889.
54. Howard, G. J.; Midgley, C. A. *J. of Appl. Polym. Sci.* 1981, .26, 3845.
55. Heitz, W. In *Advances in Polymer Science*, 23 Reactivities, 1977.
56. Shea, K. J.; Stoddard, G. J. *Macromolecules* 1991, 24, 1207.
57. Shea, K. J.; Sasaki, D. Y.; Stoddard, G. J. *Macromolecules* 1989, 22, 1722.
58. Galina, H.; Kolarz, B. N. *J. of Appl. Polym. Sci.* 1979, 24, 891.
59. Wiley, R. H.; Sale, E. E. *J. Polymer Sci.* 1960, 42, 291.
60. Poinescu, I. C.; Beldie, C.; Vlad, C. *J. Appl. Polym. Sci.* 1984, 29, 23.
61. Karger, B. L.; Snyder, L. R.; Eon, C. *J. Chromatogr.* 1976, 125, 71.
62. Tijssen, R.; Billiet, H. A. H.; Schoenmakers, P. J. *J. Chromatogr.* 1976, 122, 185.
63. Sun, Z. L.; Liu, M. C.; Hu, Z.D. *Chromatographia* 1994, 38 (9/10), 599.
64. Yan, J.; Xu, R.; Yan, J. *J. of Appl. Polym. Sci.* 1989, 38, 45.
65. Brunauer, S.; Deming, L. S.; Deming, W. E.; Teller, E. *J. Amer. Chem. Soc.* 1940, 62, 1723.

66. Kipling, J. J. In *Adsorption from Solutions of Non-Electrolytes*, Academic Press: London-New York, 1965.
67. Snyder, R. L. In *Principles of Adsorption Chromatography*, Marcel Dedder, Inc.: New York, 1968.
68. Gregg, S. J.; Sing, K. S. W. In *Adsorption, Surface Area and Porosity*, Academic Press: London-New York, 1982.
69. Giles, H. C.; MacEwan, T. H.; Nakhwa, S. N.; Smith, D. *J. Chem. Soc.* **1960**, 3973.
70. Hiemenz, P. C. In *Principles of Colloid and Surface Chemistry*, Marcel Dekker: New York, 1986, Chapter 9.
71. Ruthven, D. M. In *Principles of Adsorption and Adsorption Processes*, Wiley: New York, 1984, Chapter 5 and 6.
72. Dondi, F.; Betti, A.; Blo, G.; Bigli, C.; Versino, B. *J. Chromatogr.* **1979**, 68, 293.
73. Slaats, E. H.; Makarovski, W.; Fekete, J.; Poppe, H. *J. Chromatogr.* **1981**, 207, 299.
74. Huber, J. F. K.; Alderlieste, E. T.; Harren, H.; Poppe, H. *Anal. Chem.* **1973**, 45, 1337.
75. Cantwell, F. F.; Puon, S. *Anal. Chem.* **1979**, 51, 623.
76. Deelder, R. S.; Linssen, H. A. J.; Konignendijk, A. P.; Venne, J. L. M. v.d. *J. Chromatogr.* **1979**, 185, 241.
77. Errede, L. A., *J. Appl. Polymer Sci.* **1986**, 31, 1750.
78. Nevejans, F.; Verzele, M. *J. Chromatogr.* **1985**, 350, 145.
79. O'Kane, J. M.; Sherrington, D. N. *Macromolecules* **1990**, 23, 5286.
80. Arshady, R. *Makromol. Chrom.* **1988**, 189, 1295.
81. Wironen, J.; Shen, C.; Yan, J.; Batich, C. *Journal of Applied Polymer Science* **1996**, 59, 825.
82. Wilks, D.; Pietrzyk, D. J. *Anal. Chem.* **1972**, 44, 676.
83. Errede, L. A.; Stoesz, J. D.; Sirvio, L. M. *J. Appl. Polymer Sci.* **1986**, 31, 1749.
84. Crank, J. In *The Mathematics of Diffusion*, Oxford University Press: London, 1975, Chapter 6 and 14.
85. Fujita, H. In *Diffusion in Polymers*, Crank, J.; Park, G. S., Eds., Academic Press: New York, 1968, pp.98.

86. Ells, B. In *Role of the Matrix in Bandbroadening on Polymeric HPLC Packings*, Ph.D. thesis, University of Alberta, Edmonton, 1998.
87. Meares, P. In *Diffusion in Polymers*, Crank, J.; Park, G. S., Eds., Academic Press: New York, 1968, pp.373.
88. Chen, J. G.; Weber, S. G.; Glavina, L. L.; Cantwell, F. F. *J. Chromatogr. A.* **1993**, 656, 549.
89. Hammers, W. E.; Meurs, G. J.; Lignz, C. L. D. *J. Chromatogr.* **1982**, 246, 169.
90. Margules, M. S.-B.; Wien, A. W. *Math.-Naturwiss. Kl. II* **1895**, 104, 1234.
91. As cited in: Gmehling, J.; Onken, U.; Arlt, W. In *Vapor-Liquid Equilibrium Data Collection*, Aqueous-Organic Systems (Supplement 1), Chemistry Data Series, Vol. 1, Part 1a, DECHEMA, Germany 1981, pp. 49.
92. Renon, H.; Prausnitz, J. M. *AIChE J.* **1968**, 14, 135.
93. As cited in: Gmehling, J.; Onken, U.; Arlt, W. In *Vapor-Liquid Equilibrium Data Collection*, Aqueous-Organic Systems (Supplement 1), Chemistry Data Series, Vol. 1, Part 1a, DECHEMA, Germany 1981, pp. 285.
94. Gmehling, J.; Onken, U.; Arlt, W. In *Vapor-Liquid Equilibrium Data Collection*, Aqueous-Organic Systems (Supplement 1), Chemistry Data Series, Vol. 1, Part 1a, DECHEMA, Germany 1981, page xxvii.
95. Castellan, Gilbert W. In *Physical Chemistry*, 3rd edition, Addison-Wesley Publishing Company: Reading, Massachusetts, 1983
96. Katz, E. D.; Ogan, K.; Scott, R. P. W. *J. Chromatogr.* **1986**, 352, 67-90.
97. Riddick, J. A.; Bunger, W. B.; Sakano, T. K. In *Organic Solvents: Physical Properties and Methods of Purification*, 4th Edition, John Wiley & Sons: New York, 1986.
98. Fossey, L.; Cantwell, F. F. *Anal. Chem.* **1982**, 54, 1693.
99. P. Jandera; G. Guiochon *J. Chromatogr.* **1992**, 605, 1.
100. Nevejans, F.; Verzele, M. *Chromatographia* **1985**, 20, 173.
101. Boyd, G. E.; Adamson, A. W.; Myers, J. L. S. *J. Amer. Chem. Soc.* **1947**, 69, 2836.
102. Simpson, E. J.; Abukhadra, R. K.; Koros, W. J.; Schechter, R. S. *Ind. Eng. Chem. Res.* **1993**, 32, 2269.

103. Errede, L. A. *Polymer Preprints* 1985, Japan, 26, 77.
104. Errede, L. A.; Stoesz, J. D.; Sirvio, L. M. *J. Appl. Polym. Sci.* 1986, 31, 2721.
105. Oday, O.; Gurun, C. *J. Appl. Polym. Sci.* 1992, 46, 421.
106. Giddings, J. C. In *Dynamics of Chromatography*, Part I, Principles and Theory, Marcel Dekker, Inc.: New York, 1965, Chapter 6.
107. Paine, P. L.; Scherr, P. *Biophysical Journal*, 1975, 15, 1087.
108. Florence, T. M.; Batley, G. E. *CRC Critical Reviews in Analytical Chemistry* 1980, August, 219.
109. Agnes, George R.; Stewart, Ian I.; Horlick, Gary *Applied Spectroscopy* 1994, 48(11), 1347.
110. Tessier, A.; Campbell, P. G. C.; Bisson, M. *Anal. Chem.* 1979, 51, 844.
111. Dabek-Zlotorzynska, E.; Lai, E. P. C.; Timerbaev, A. R. *Analytica Chimica Acta* 1998, 359, 1-26.
112. Florence, T. M.; Batley, G. E. *Talanta* 1977, 24, 151.
113. Merlini, M.; Pozzi, G. *Environ. Pollut.* 1977, 13, 119.
114. Giesy, J. P.; Leversee, G. J.; Williams, D. R. *Water Res.* 1977, 11, 1013.
115. Stumm, W.; Bilinski, H. *Advances in Water Pollution Research*, Proceeding of the 6th International Conference; Jenkins, S. H., Eds; Pergamon, 1972, 39.
116. Feick, G.; Horne, R. A.; Yeaple, D. *Science* 1972, 175, 1142.
117. Sterritt, R. M.; Lester, J. N. *The Science of the Total Environment* 1984, 34, 117.
118. Nordstrom, D. Kirk *Water, Air, Soil Pollut.* 1996, 90, 257-267.
119. Stewart, Ian I.; Horlick, Gary *Journal of Analytical Atomic Spectrometry* 1996, 11, 1203.
120. Benes, P.; Steinnes, E. *Water Res.* 1974, 8, 947.
121. Benes, P.; Steinnes, E. *Water Res.* 1975, 9, 741.
122. Hart, B. T.; Davies, S. H.; Aust, J. Mar. *Freshwater Res.* 1977, 28, 105.
123. Braman, R.S.; Justen, L. L.; Foreback, C. C. *Anal. Chem.* 1972, 44, 2195.
124. Alexander, J. F. *CRC Crit. Rev. Anal. Chem.* 1987, 18, 1
125. Szczepaniak, W.; Nawrocki, J.; Wasiak, W. *Chromatographia* 1979, 12, 539.
126. Timerbaev, A. R. *Electrophoresis* 1997, 18, 185.

127. Jandik, P.; Bonn, G. In *Capillary Electrophoresis Principles and Practice*, VCH Publishers: Berlin, Heidelberg, 1993.
128. Lobinski, R. ; Adams, F. C. *Trends Anal. Chem.* 1993, 12, 41.
129. Vela, N. P.; Olson, L. K; J. A. Caruso *Anal. Chem.* 1993, 65, 585A.
130. Kim, A. W.; Hill, S. J.; Ebdon, L.; Rowland, S. J. *J. High Resolut. Chromatogr.* 1992, 15, 965.
131. Figura, P.; McDuffie, B. *Anal. Chem.* 1980, 52, 1433.
132. Stumm, W.; Brauner, P. A. *Chem. Oceanogr.* 1975, 1; Riley, J. P. and Skirrow, G., Eds.; 173.
133. Nordstrom, D. K. "A Comparison of Computerized Chemical Models for Equilibrium Calculations in Aqueous Systems", in *Chemical Modeling in Aqueous Systems*; Jenne, E. A., Eds.; ASC Symposium Series No. 93, Washington, D.C, 1979.
134. Allison, J. D.; Brown, D. S.; "MINTEQA2/PRODEFA2 – A Geochemical Speciation Model and Interactive Preprocessor", in *Chemical Equilibrium and Reaction Models*; Loeppert, R. H.; Schwab, A. P.; Goldberg, S., Eds.; Soil Science Society of American Special Publication Number 42, 1995, 253.
135. Parker, D. R.; Norvell, W. A.; Chaney, R. L., "GEOCHEM-PC – A Chemical Speciation Program for IBM and Compatible Personal Computers", in *Chemical Equilibrium and Reaction Models*, Loeppert, R. H.; Schwab, A. P., Goldberg, S., Eds.; Soil Science Society of America Special Publication Number 42, 1995, 253.
136. Ball, J. W.; Nordstrom, D. K., "User's Manual for WATEQ4F, with Revised Thermodynamic Data Base and Test Cases for Calculating Speciation of Major, Trace and Redox Elements in Natural Waters", In *U. S. Geological Survey Open-File Report*, 1992, 91, revised and reprinted.
137. Wolery, T. J., "EQ3NR, A Computer Program for Geochemical Aqueous Speciation-solubility Calculations: Theoretical Manual, User's Guide, and Related Documentation (Version 7.0)", Lawrence Livermore National Laboratory, UCRL-MA-110662 PTIII.

138. Nordstrom, D. Kirk, *Water, Air, Soil Pollut.* 1996, 90, 257.
139. Sweileh, J. A., Ph.D. thesis, University of Alberta, 1986.
140. Wagemann, R. *J. Phys. Chem.* 1980, 84, 3433.
141. Blaedel W. J.; Dinwiddie, D. E. *Anal. Chem.* 1974, 46, 873.
142. Belli, Stuart L.; Zirino, Alberto *Anal. Chem.* 1993, 65, 2583.
143. Pecsok, R. L.; Shields, L. D.; Cairns, T.; Mcwilliam, I. G., In *Modern Methods of Chemical Analysis*, second edition, John Wiley & Sons: New York / Santa Barbara / London / Sydney / Toronto, 1976.
144. Smichowski, P.; Madrid, Y.; Camara, C. *Fresenius J. Anal. Chem.* 1998, 360, 623.
145. Hurnburg, H.W. *Sci. Total Environ.* 1979, 12, 35.
146. Florence, T. M.; Morrison, G. M.; Stauber, J. L. *The Science of the Total Environment* 1992, 125, 1.
147. Wang, J. *Environ. Sci. Technol.* 1982, 16, 104A.
148. Gao, Z.; Wang, G.; Li, P.; Zhao, Z. *Anal. Chem.* 1991, 63, 953-957.
149. Zen, J.; Lee, M. *Anal. Chem.* 1993, 65, 3238.
150. Aen, H. E.; Crosser, M. L.; Brisbin, T. D. In *Proc. Workshop on Toxicity to Biota of Metal Forms in Natural Water*, Duluth, Minnesota, October 1975, pp.33.
151. Tuschall, J. R.; Brezonik, P. L. *Anal. Chem.* 1981, 53, 1986.
152. Hanck, K. W.; Dillard, J. W. *Anal. Chim. Acta* 1977, 89, 329.
153. Smith, D. J.; Redmond, J. D. *J. Electroanal. Chem.* 1971, 33, 169.
154. Filby, R. H.; Shah, K. R.; Funk, W. H. In *Proc. 2nd Int. Conf. Nuclear Methods in Environ. Res.*, Meyer, W., Eds., NITS, Springfield, VA., 1974, 10.
155. Christianson, G.; Jeness, R.; Coulter, S.T. *Anal. Chem.* 1954, 26, 1923.
156. Pearce, K. N.; Creamer, L. K. *Anal. Chem.* 1974, 46, 457.
157. Cantwell, F. F.; Nielsen, J. S.; Hrudey, S. E. *Anal. Chem.* 1982, 54, 1498.
158. Treit, J.; Nielsen, J. S.; Kratochvil, B.; Cantwell, F. F. *Anal. Chem.* 1983, 55, 1650.
159. Nielsen, J. S.; Hrudey, S. E.; Cantwell, F. F. *Environ. Sci. Technol.* 1984, 18, 883.
160. Zorkin, N. G.; Grill E. V.; Lewis, A. G. *Analytica Chimica Acta* 1986, 183, 163.

161. Sweileh, J. A.; Lucyk, D.; Kratochvil, B.; Cantwell, F. F. *Anal. Chem.* **1987**, *59*, 586.
162. Treit, J.; Nielsen, J. S.; Kratochvil, B.; Cantwell, F. F. *Anal. Chem.* **1983**, *55*, 1650.
163. van den Berg, C. M. G.; Kramer, J. R. *Analytica Chimica Acta* **1979**, *106*, 113.
164. Chow, Patrick Y. T.; Cantwell, F. F. *Anal. Chem.* **1988**, *60*, 1569.
165. Persaud, G.; Cantwell, F. F. *Anal. Chem.* **1992**, *64*, 89.
166. Morabito, R. *Fresenius J. Anal. Chem.* **1995**, *351*, 378.
167. Urasa, I. T.; Macha, S. F.; II-Maaty, W. *J. Chromatogr. Sci.* **1997**, *35*, 519.
168. Poerschmann, J.; Zhang, Z.; Kopinke, F.; Pawliszyn, J. *Anal. Chem.* **1997**, *69*, 597.
169. Belardi, R. P.; Pawliszyn, J. *Water Pollut. Res. J. Can.* **1989**, *24*, 179.
170. Arthur, C. L.; Pawliszyn, J. *Anal. Chem.* **1990**, *62*, 2145.
171. Louch, D.; Motlagh, S.; Pawliszyn, J. *Anal. Chem.* **1992**, *64*, 1187.
172. Vaes, W. H. J.; Ramos, E. U.; Verhaar, H. J. M.; Seinen, W.; Hermens, J. L. M. *Anal. Chem.* **1996**, *68*, 4463.
173. Out, E. O.; Pawliszyn, J. *Mikrochim. Acta* **1993**, *122*, 41.
174. Jia, C.; Luo, Y.; Pawliszyn, J. *J. Microcolumn Separation* **1998**, *10(2)*, 167.
175. Daimon, H.; Pawliszyn, J. *Anal. Commun.* **1997**, *34*, 365.
176. Li, S.; Weber, S. G. *Anal. Chem.* **1997**, *69*, 1217.
177. He, Y.; Lee, H. K. *Anal. Chem.* **1997**, *69*, 4634.
178. Colton, R.; Dakternieks, D. *Inorganica Chimica Acta* **1993**, *208*, 173.
179. Stewart, I. I.; Horlick, G. *J. of Analytical Atomic Spectrometry* **1996**, *11*, 1203.
180. Anges, G.R.; Horlick, G. *Applied Spectroscopy* **1994**, *48(6)*, 649.
181. Barnett, David A.; Horlick, G. *J. of Analytical Atomic Spectrometry* **1997**, *12*, 497.
182. Blades, A. T.; Jayaweera, P.; Ikonou, M. G.; Kebarle, P. *Int. J. Mass Spectrom. Ion Processes* **1990**, *102*, 251.
183. Blades, A. T.; Jayaweera, P.; Ikonou, M. G.; Kebarle, P. *Int. J. Mass Spectrom. Ion Processes* **1990**, *101*, 325.
184. Cheng, Z. L.; Siu, K. W. M.; Guevremont, R.; Berman, S. S. *Org. Mass Spectrom.* **1992**, *27*, 1370.

185. Cardwell, T. J.; Colton, R.; Mitchell, S. M.; Traeger, J. C. *Inorg. Chim. Acta* **1994**, 216, 75.
186. Colton, R.; Klaui, W. *Inorg. Chim. Acta* **1993**, 211, 235.
187. Berkel, V.; McLuckey, S. A., and Glish, G. L., *Anal. Chem.*, **1992**, 64, 1586.
188. Chiavarini, S.; Cremisini, C.; Ferri, T.; Morabito, R.; Perini, A. *Sci. Tot. Environ.* **1991**, 101, 217.
189. Harino, H.; Fukushima, M.; Tanaka, M. *Anal. Chim. Acta* **1992**, 264, 91.
190. Beceiro-Gonzales, E.; Barciela-Garcia, J.; Bermejo-Barrera, P.; Bermejo-Barrera, A. *Fresenius J. Anal. Chem.* **1992**, 344, 301.
191. Stary, J. In *The Solvent Extraction of Metal Chelates*, the Macmillan Company, New York, **1964**; and Zolotov, Yu. A. In *Extraction of Chelate Compounds*, Ann Arbor-humphrey Science Publishers, Ann Arbor-London, **1970**.
192. Danesi, P.R.; Chiarizia, R. *CRC Critical Reviews in Anal. Chem.* **1980**, 10.
193. Dyrssen, D.; Liljenzin, J.-O.; Rydberg, J. In *Solvent Extraction Chemistry*, Proceeding of the International Conference held at Gothenburg, Sweden, 27 August – 1 September 1966, North-Holland Publishing Company: Amsterdam, John Wiley & Sons, Inc.: New York.
194. Ashbrook, A.W. *Hydrometallurgy* **1975**, 1, 5.
195. Preston, J. S. *J. Inorg. Nucl. Chem.* **1975**, 37, 1235.
196. Siladitya, B.; Sen, K.; Bag, S. P. *Indian Journal of Chemistry* **1992**, February, 31A, 116.
197. Fritz, J. S.; Beuerman, B. R. *Anal. Chem.* **1972**, 44(4), 692.
198. Chen, F.; Ma, H.; Freiser, H.; Muralidharan, S. *Langmuir* **1995**, 11, 3235.
199. Flett, D. S., Cox, M.; Heels, D. *J. Inorg. Nucl. Chem.* **1975**, 37, 2533.
200. Habashi, F. In *Principles of Extractive Metallurgy*, Vol.II, Gordon and Breach: New York, **1970**.
201. Hudson, M.J. *Hydrometallurgy*, **1982**, 9, 149.
202. Paatero, E.Y.O.; Sjoblom, J. *Hydrometallurgy* **1986**, 17, 39.
203. Fritz, J.S.; Beuerman, D. R.; Richard, J. J. *Talanta*, **1971**, 18, 1095.
204. Karlberg, B.; Thelander, S. *Anal. Chim. Acta* **1978**, 98, 1.

205. Bergamin, H.; Medeiros, J. X.; Reis, B.F.; Zagatto, E. A. G. *Anal. Chim. Acta* **1978**, 101, 9
206. Valcarcel, M.; Luque de Castro, M. D. *J. Chromatogr.* **1987**, 393, 3.
207. Lucy, C. A.; Cantwell, F. F. *Anal. Chem.* **1989**, 61, 101.
208. Lucy, C. A.; Cantwell, F. F. *Anal. Chem.* **1989**, 61, 107.
209. Murray, D. A. J. *J. Chromatogr.* **1979**, 177, 135.
210. van Rensburg, J. F. J.; Hassett, A. J. *J. of HRL & CC* **1982**, October, 5, 574.
211. Attygalle, A. B.; Morgass, E. D. *Anal. Chem.* **1986**, 58, 3054.
212. Liu, H.; Dasgupta, P. K. *Anal. Chem.* **1996**, 68, 1817.
213. Jeannot, M. A.; Cantwell, F. F. *Anal. Chem.* **1996**, 68, 2236.
214. Jeannot, M. A.; Cantwell, F. F. *Anal. Chem.* **1997**, 69, 235.
215. Jeannot, M. A.; Cantwell, F. F. *Anal. Chem.* **1997**, 69, 2935.
216. Audunsson, G. *Anal. Chem.* **1992**, 11, 106.
217. Thordarson, E.; Palmarsdottir, S.; Mathiasson L.; Jonsson, J. A. *Anal. Chem.* **1996**, 68, 2559.
218. Knutsson, M.; Nilve, G.; Mathiasson, L.; Jonsson, J. A. *J. Chromatogr. A* **1996**, 754, 197.
219. Megersa, N.; Jonsson, J. A. *Analyst* **1998**, 123, 225.
220. Ma, M.; Cantwell, F. F. *Anal. Chem.* **1998**, 70(18), 3912.
221. Ma, M.; Cantwell, F. F. *Anal. Chem.* **1999**, 71(2), 388.
222. Montaser, A. In *Inductively Coupled Plasma Mass Spectrometry*, Wiley-Vch: New York, 1997
223. Sharp, B. L. *J. Anal. At. Spectrom.* **1988**, 3, 613-652; Sharp, B. L. *J. Anal. At. Spectrom.* **1988**, 3, 939.
224. Matusiewicz, H.; Sturgeon, R. E. *Spectrochim. Acta* **1996**, 51B, 377.
225. Huang, M-F.; Jiang, S-J.; Huang, C-J. *J. Anal. At. Spectrom.* **1995**, 10, 31.
226. Wylie, P. L.; Quimby, B. D. *J. High Resolut. Chromatogr.* **1989**, 12, 813.
227. Ingle, J. D. Jr.; Crouch, S. R. In *Spectrochemical Analysis*, Prentice Hall: Upper Saddle River, New Jersey, 1988.
228. Alves, L. C.; Allen, L. A.; Houk, R. S. *Anal. Chem.* **1993**, 65, 2468.

229. Akatsuka, K.; McLaren, J. W.; Lam, J. W.; Berman, S. S. *J. Anal. At. Spectrom.* **1992**, *7*, 889.
230. Shao, Y.; Horlick, G. *Applied Spectroscopy* **1986**, *40*(3).
231. Chan, W. T.; Horlick, G. *Applied Spectroscopy* **1990**, *44*(3).
232. Liu, X. R.; Horlick, G. *Journal of Analytical Atomic Spectrometry* **1994**, *9*, 833.
233. Ruzicka, J.; Hansen, E. H. In *Flow Injection Analysis*, 2nd Eds., Wiley-Interscience: New York, 1988, pp.498.
234. Thompson, M.; Pahlavanpour, B.; Walton, S. J.; Kirkbright, G. F. *Analyst* **1978**, *103*, 568.
235. Olson, L. K.; Vela, N. P.; Caruso, J.A. *Spectrochim. Acta* **1995**, *50B*, 355.
236. Uden, P. C. *J. Chromatogr. A* **1995**, *703*, 393.
237. Jiang, S-J.; Houk, R. S. *Anal. Chem.* **1986**, *58*, 1739.
238. Salin E. D.; Horlick, G., Paper #564, *Pittsburgh Conference on Analytical Chemistry and Applied Spectroscopy*, Cleveland, OH, March 5-9, 1979
239. Karanassios, V.; Horlick, G. *Spectrochimica Acta Rev.* **1990**, *13*(2), 89.
240. Karanassios, V.; Horlick, G. *Spectrochimic. Acta* **1989**, *44B*(12), 1345.
241. Morrison, G. H.; Freiser, H. In *Solvent Extraction in Analytical Chemistry*, John Wiley & Sons Inc.: New York, 1966.
242. Flett, D. S.; Okuhara, D. N.; Spink, D. R. *J. Inorg. Nucl. Chem.* **1973**, *35*, 2471.
243. Carter, S. P.; Freiser, Henry *Anal. Chem.* **1979**, *51*(7), 1100.
244. Carter, S. P.; Freiser, Henry *Anal. Chem.* **1980**, *52*, 511.
245. Van der Zeeuw, A. J.; Kok, R. *Abstracts Proc. Int. Solv. Extr. Conf. ISEC 77*, Toronto, paper 4e, **1977**.
246. Atwood, R. L.; Thatcher, D. N.; Miller, J. D. *Metall. Trans.*, **1975**, *6B*, 465.
247. Hanson, C.; Hughes, M. A.; Whewell, R. J. *J. Appl. Chem. Biotechnol.*, **1978**, *28*, 426.
248. Fleming, C. A.; Nicol, R. D. H.; Finkelstein, N. P. *J. Appl. Chem. Biotechnol.*, **1978**, *28*, 443.
249. Hughes, M. A.; Preston, J. S.; Whewell, R. J. *J. Inorg. Nucl. Chem.* **1976**, *38*, 2067.
250. Whewell, R. J.; Hughes, M. A.; Hanson, C. *J. Inorg. Nucl. Chem.* **1976**, *38*, 2071.

251. Hanson, C. In *Recent Advances in Liquid-Liquid Extraction*, Hanson, C., Eds., Pergamon Press: Oxford, 1971, chapter 12.
252. Nitsch, W.; Kruis, B. *J. Inorg. Nucl. Chem.* **1978**, *40*, 857.
253. Nitsch, W.; Raab, M.; Wiedholz, R. *Chem. Ing. Tech.* **1973**, *45*, 1035.
254. Tarasov, V. V.; Yagodin, G. A.; Yurtov, E. V. *Chimii i Chimiceskaia Tech.* **1976**, *19*(2), 245.
255. Nemtsov, M. S. *Zh. Prikl. Khim.* (Moscow) **1960**, *33*, 1075.
256. Yagodin, G. A.; Tarasov, V. V.; Fomin, V. V. *Dokl. Akad. Nauk SSSR*, **1974**, *218*(3), 647.
257. Ashbrook, A.W. *Anal. Chim. Acta* **1972**, *115*, 58.
258. Taylor, T. W. J.; Ewbank, E. K. *J. Chem. Soc.* **1926**, 2818.
259. Blatt, A. H. *J. Amer. Chem. Soc.* **1938**, *61*, 214.
260. Tammi, T. T. *Hydrometallurgy*, **1976/1977**, *2*, 371.
261. Mumallah, N.; Wilson, D. J. *Separation Science and Technology* **1980**, *15*(10), 1753.
262. Jeannot, M. A., In *Single Drop Microextraction: Principles and Application*, Ph. D. thesis, University of Alberta, Edmonton, Canada, 1997.
263. Karanassios, V.; Horlick, G. *Spectrochimica Acta* **1989**, *44B*(12), 1345.
264. Chan, W. T.; Horlick, G. *Applied Spectroscopy* **1990**, *44*(3), 525.
265. Beauchemin, D.; McLaren, J. W.; Bermon, S. S. *Spectrochim. Acta* **1987**, *42B*, 467.
266. Gregoire, D. C. *Spectrochim. Acta* **1987**, *42B*, 895
267. Thompson, J. J.; Hauk, R. S. *Appl. Spectrosc.* **1987**, *41*, 801.
268. Sheng, S., In *Measurement of Trace Elements by DSI-ICP-MS in Biological Samples*, M. Sc. Dissertation, University of Alberta, Edmonton, Canada, 1999.
269. Sillen, L. G.; Martell, A. E. In *Stability Constants of Metal-ion Complexes*, IUPAC, London:Chemical Society, 1971.
270. Ringbom, A. In *Complexation in Analytical Chemistry*, Interscience Publishers: New York/London, 1963.
271. Helfferich, F. G., *Ion Exchange*, McGraw-Hill, New York, 1962.
272. Alexandratos, S. D.; Crick, D. W. *Ind. Eng. Chem. Res.* **1996**, *35*, 635.

273. Thamizharasi, S.; Reddy, A.; Venkata R.; Balasubramanian, A. *J. of Appl. Polymer Sci.*, 1998, Vol. 67, 177.
274. Kennedy, J.; Ficken, G. E. *J. Appl. Chem.*, 1958, July 8, 459.
275. Billmeyer, F. W., *Textbook of Polymer Science*, Interscience Publishers, New York, 1962.
276. Zeng, F.; Zimmerman, S. C. *Chem. Rev.*, 1997, 97, 1681.
277. Cooper, A. I.; Londono, J. D.; Wignall, G.; McClain, J. B.; Samuiski, E. T.; Lin, J. S.; Dobrynin, A.; Rubinstein, M.; Burke, A. L. C.; Frechets, J. M. J.; DeSimone, J. M. *Nature*, 1997, Sept. 25, Vol. 389, 368.

Appendix 1

Size of the Blue Dextran Molecule

All dextrans are composed exclusively of α -D-glucopyranosyl units, differing only in degree of branching and chain length.¹ Blue dextran has a formula of $(C_6H_{10}O_5)_n$ ¹ and it is a type of dextran from *Leuconostoc mesenteroides* NRRL- β -512(F).²

The dimensions of one $(C_6H_{10}O_5)$ unit from the Molecular Modeling Program (Windowchem Software Inc.) are $x = 7.2001 \text{ \AA}$, $y = 6.5879 \text{ \AA}$, $z = 9.0660 \text{ \AA}$. If we take the space occupied by one unit as a cube, then the approximate volume of this space, V_i , is 430.033 \AA^3 ($V_i = xyz$).

The molar mass of one unit $(C_6H_{10}O_5)$ is 162.142 g/mol , and the average molar mass of blue dextran $(C_6H_{10}O_5)_n$ is $2 \times 10^6 \text{ g/mol}$. So the average $n = 12334.87$. Therefore, the approximate volume of one $(C_6H_{10}O_5)_n$ is $5.3 \times 10^6 \text{ \AA}^3$ ($= nV_i$). If we also assume that the space occupied by $(C_6H_{10}O_5)_n$ is a cube, the one dimension of it would be about 180 \AA or 18 nm . However, this is the smallest possible size, and in the more likely cases the size would be larger than this.

¹ In *The Merck Index*, Budavari, S., Eds., Merck & Co., Inc.: Whitehouse Station, NJ, 1996, 25th edition, 2989, Dextran.

² Jeanes, A. *Polyelectrolytes* 1976, 207-25.

Appendix 2

Comparison of the Real Particle Size and the Particle Image Size

The microscope is used in this work for quantitative measurement of spherical particles. As shown in Figure A2.1, the two-dimensional image of a spherical object does not correlate with the very middle cross section of the object but with a smaller cross section. Therefore, the measured diameter of the image is not equal to the diameter of the particle. The following is a calculation to compare these two diameters.

The values of the angular aperture and the numerical aperture associated with the microscope are required for the calculation. The angular aperture, α , is the angle of the light source as shown in Figure A2.2.³ The numerical aperture, N.A., is expressed as the product of the refractive index, n , of the medium through which the light passes and the sine of one half the angular aperture of the light ($\alpha/2$):³

$$\text{N.A.} = n \sin (\alpha/2)$$

The height from the light source to the object, h , is also required for the calculation. In order to obtain this value, a $\times 3.5$ objective is used to allow the whole light spot from the condenser to fall in the field of view, as shown in Figure A2.2, so that the width of this light spot, $2R$, can be measured to be 1.75 mm.

Following are the calculations. The symbols used are illustrated in Figure A2.3.

(1) Calculation of h

$$\text{N.A. of the condenser} = n \sin (\alpha/2) = 0.85$$

³ Born, M.; Wolf, E. In *Principles of Optics*, 4th Edition, Pergamon Press: New York, 1970.

If we assume the medium surrounding the particle is pure water, then $n = 1.33^3$

So, $\sin(\alpha/2) = 0.6391$, and $\alpha/2 = 39.72^\circ\text{C}$

And also, $R = 1.75 \text{ mm}/2 = 0.875 \text{ mm} = 875 \mu\text{m}$

Then, $h = R/\text{tg}(\alpha/2) = 875 \mu\text{m} / \text{tg}(39.72^\circ\text{C}) = 1.053 \times 10^3 \mu\text{m}$

(2) *Calculation of r_i and r_r*

$$\text{Since } \text{tg}(\beta/2) = r_i/h = \frac{\sqrt{(r_r)^2 - (r_i)^2}}{r_i}$$

Where r_i is the radius of the image, and r_r is the radius of the real object sphere.

If $r_i = 10 \mu\text{m}$, and inserting r_i into the above equation, then, $r_r = 10.00045 \mu\text{m}$.

Therefore, the radius of the image is only 0.0045 % less than the radius of the object, so the difference is negligible.

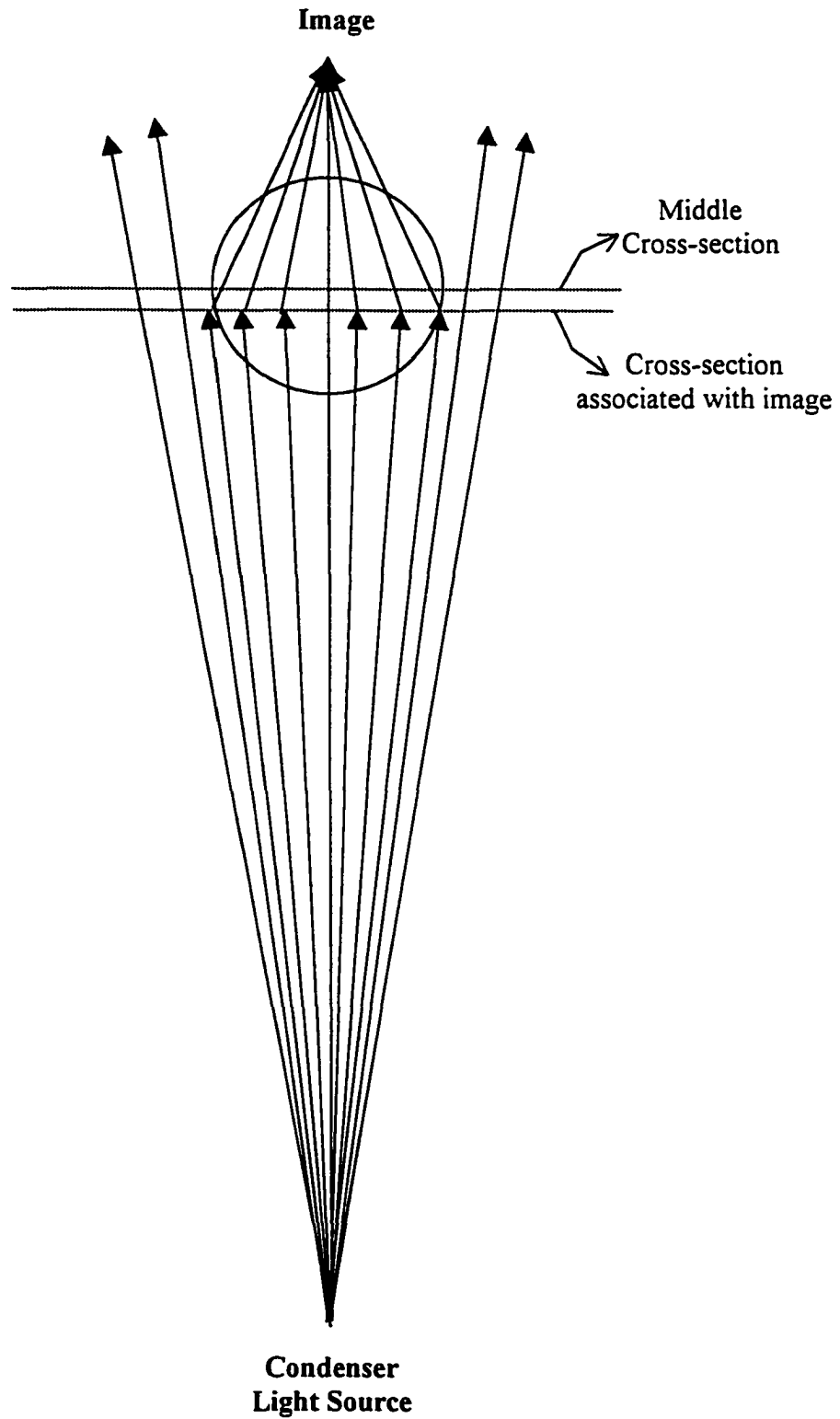


Figure A2.1 Schematic diagram of image formation in a microscope

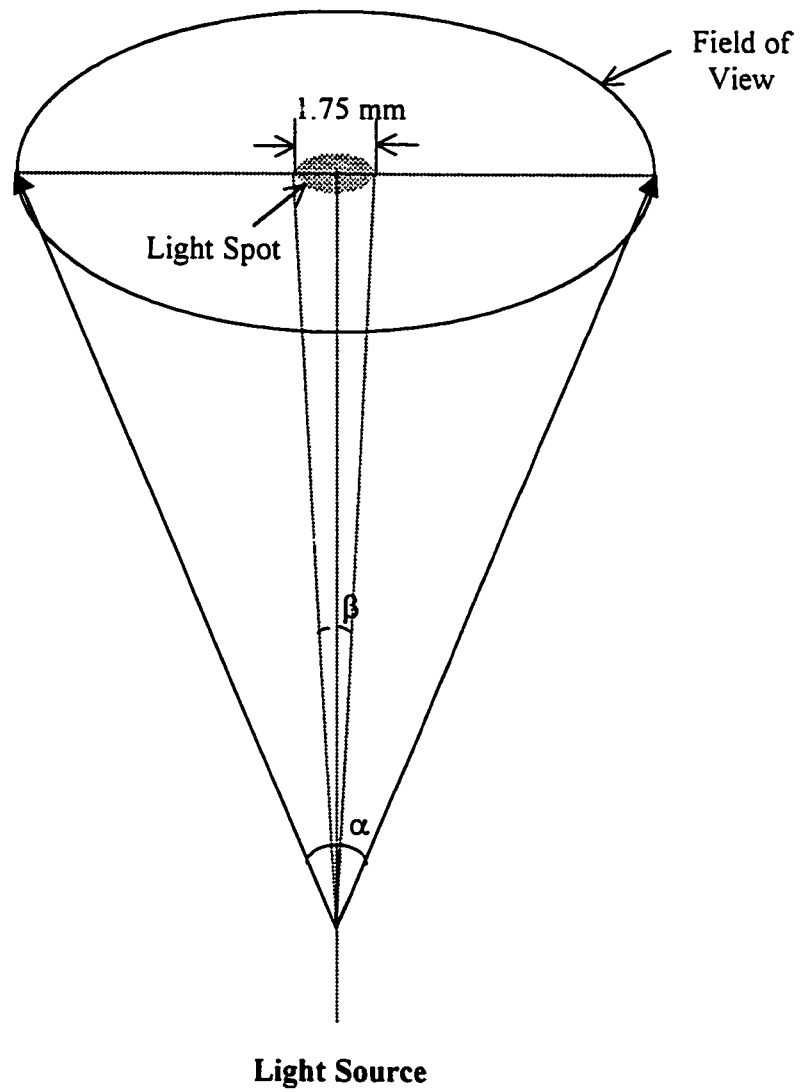


Figure A2.2 Light spot in microscope fitted with $\times 3.5$ objective

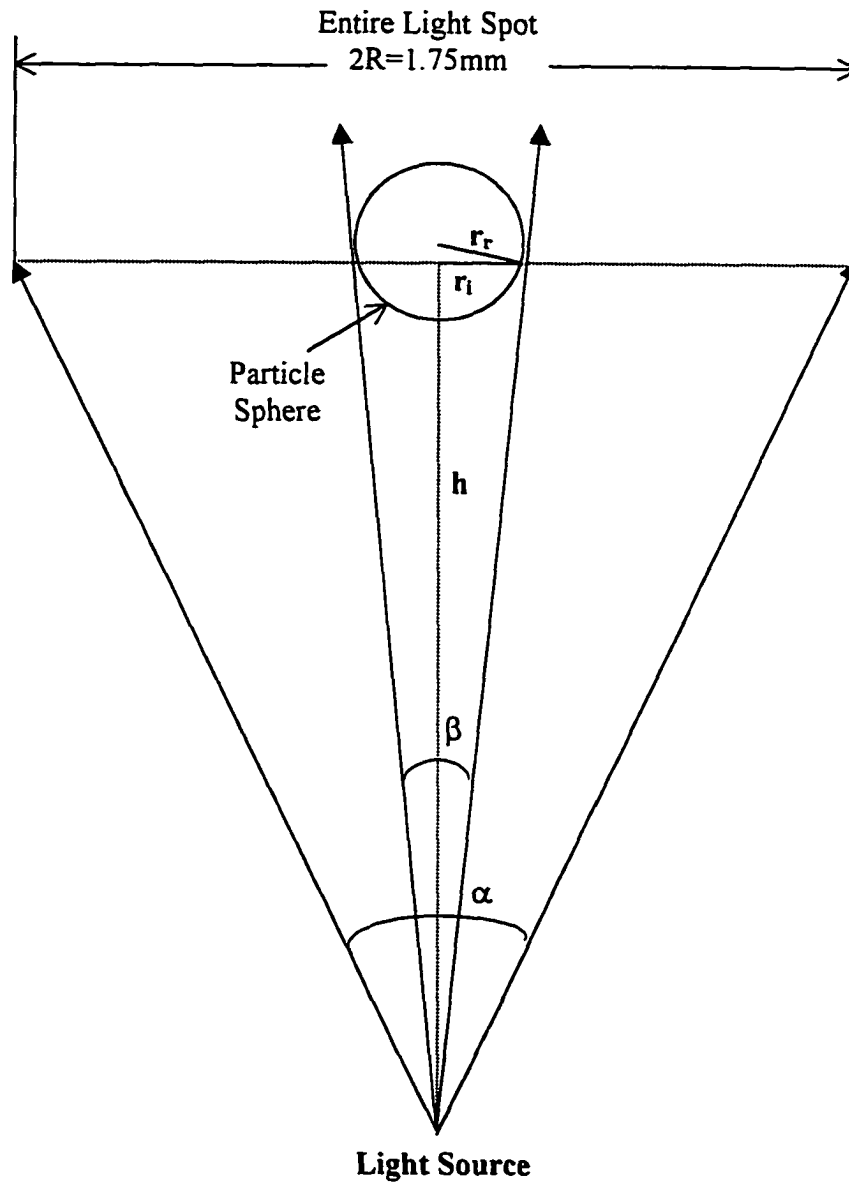


Figure A2.3 Schematic diagram for calculation of the real particle size and the particle image size

Appendix 3

C Program for Calculation of Metal Species Distribution

In the course of writing this program, my husband, Jeff Lu, has given me a lot of sound technical advice and devoted his time to the revision and refinement of the program. Therefore, I would like to thank him for his support and love.

This program can be run under C, C++, or MS VC++ compiler.

```
#include <stdio.h>
#include <stdlib.h>
#include <math.h>

FILE *infile;

#define B_MOH      1.258925e6 //Cumulative formation constant of CuOH
#define B_MOH2     3.9810717e11 //Cumulative formation constant of (CuOH)2
#define KW         1e-14      //kw

#define KA1_E      7e-7       //ka1 of EDTA
#define KA2_E      6e-11      //ka2 of EDTA
#define B_MA_E     6.309573e18 //Cumulative formation constant of CuY2-
#define B_MHA_E   1e3        //Cumulative formation constant of CuHY-
#define B_MA2_E    0         //Cumulative formation constant of CuY2

#define KA1_G      4.365158e-3 //ka1 of glycine
#define KA2_G      2.754229e-10 //ka2 of glycine
#define B_MA_G     1.412538e8  //Cumulative formation constant of CuGly+
#define B_MHA_G    0         //Cumulative formation constant of CuHGly
#define B_MA2_G    1e15      //Cumulative formation constant of Cu(Gly)2

#define KA1_P      1.7783e-3   //ka1 of phthalate
#define KA2_P      1.2023e-5   //ka2 of phthalate
#define B_MA_P     1.6596e3    //Cumulative formation constant of CuPth
#define B_MHA_P    21.38      //Cumulative formation constant of CuHPth-
#define B_MA2_P    2.88403e5  //Cumulative formation constant of Cu(Pth)2
```

```

#define KA1_S      1.5488e-3    //ka1 of salicylate
#define KA2_S      3.9811e-14   //ka2 of salicylate
#define B_MA_S     3.9811e10    //Cumulative formation constant of CuSal
#define B_MHA_S    0           //Cumulative formation constant of CuHSal-
#define B_MA2_S    2.5511886e18 //Cumulative formation constant of Cu(Sal)2

#define KA1_C      1.348963e-3  //ka1 of citrate
#define KA2_C      4.466836e-5  //ka2 of citrate
#define KA3_C      2.041738e-6  //ka2 of citrate
#define B_MA_C     7.94328e5    //Cumulative formation constant of CuCit-
#define B_MHA_C    2.81838e3    //Cumulative formation constant of CuHCit
#define B_MH2A_C   181.97      //Cumulative formation constant of CuH2Cit

```

```
void main()
```

```
{
//Followings define variables.
```

```
    int code, i, j;
```

```
    float bba, delt, low, high, c_moh, c_moh2, c_mha, c_ha, c_h2a;
```

```
    float ka1, ka2, ka3, b_ma, b_mha, b_ma2, b_mh2a, m_t, m_t2,
          a_t, a_t_max, h, m, a;
```

```
    float f_moh, f_moh2, f_ma, f_mha, f_ma2, f_m;
```

*/*c_moh, c_moh2, c_mha, c_ha, c_h2a are the concentration of CuOH⁺, Cu(OH)₂, CuHX, HX, H₂X, respectively. ka1, ka2 and ka3 are dissociation constants of the ligand. b_ma, b_mha, b_ma2 and b_mh2a are the cumulative formation constants of CuX, CuHX, CuX₂ and CuH₂X, respectively. f_moh, f_moh2, f_ma, f_mha, f_ma2 and f_m are fractions of species CuOH⁺, Cu(OH)₂, CuX, CuHX and CuX₂, respectively. X represents any of the ligand which is chosen at very beginning by the input code. m_t is the total concentration of copper; a_t_max is the total concentration of the ligand. All the others are intermediate variables. */*

```
//Give each ligand of interest a code
```

```
    printf("choose a ligand:\n");
    printf("\t1 ----- E\n");
    printf("\t2 ----- G\n");
    printf("\t3 ----- P\n");
    printf("\t4 ----- S\n");
    printf("\t5 ----- C\n");
    printf("\t6 ----- exit.\n");
    printf("Enter your choice: ");
```

```

scanf("%d",&code); //Input code

if (code == 6)
    exit(0);

printf("enter total Cu:");
scanf("%f", &m_t); //Keyboard input total concentration of the copper.

printf("enter total ligend:");
scanf("%f", &a_t_max); // Keyboard input total concentration of the ligand.

printf("enter total H:");
scanf("%f", &h); // Keyboard input total concentration of H+.

printf("ligend=%d, m_t=%0.2e, 2e, a_t_max=%0.2e, h=%0.2e\n",
       code, m_t, a_t_max, h); //Display

infile = fopen("species", "w"); //Open data file "species"

fprintf(infile,"Ligend is %d, m_t=%0.2e, a_t_max=%0.2e, h=%0.2e\n",
        code, m_t, a_t_max, h); //Output the results into file "species"

//Select calculation method depends on the code

switch (code)
{
case 1: //EDTA
    ka1 = float(KA1_E);
    ka2 = float(KA2_E);
    b_ma = float(B_MA_E);
    b_mha = float(B_MHA_E);
    b_ma2 = float(B_MA2_E);
    break;

case 2: //Glycine
    ka1 = float(KA1_G);
    ka2 = float(KA2_G);
    b_ma = float(B_MA_G);
    b_mha = float(B_MHA_G);
    b_ma2 = float(B_MA2_G);
    break;

case 3: //Phthalate

```

```

        ka1 = float(KA1_P);
        ka2 = float(KA2_P);
        b_ma = float(B_MA_P);
        b_mha = float(B_MHA_P);
        b_ma2 = float(B_MA2_P);
        break;

    case 4: //Salicylate
        ka1 = float(KA1_S);
        ka2 = float(KA2_S);
        b_ma = float(B_MA_S);
        b_mha = float(B_MHA_S);
        b_ma2 = float(B_MA2_S);
        break;

    case 5: //Citrate
        ka1 = float(KA1_C);
        ka2 = float(KA2_C);
        ka3 = float(KA3_C);
        b_ma = float(B_MA_C);
        b_mha = float(B_MHA_C);
        b_mh2a = float(B_MH2A_C);
        break;

    default:
        exit(1);
}
//Equations used in calculation

c_moh2 = float(B_MOH2 * pow(KW/h,2));

c_mha = b_mha * h / ka2;

c_ha = h/ka2;

c_h2a = h*h/ka1/ka2;

fprintf(infile,"a_t ,f_moh,f_moh2,f_ma,f_mha,f_ma2,f_m
    \n");

//Iteration for calculating a

for(j=1; j<=100; j++)
{
    a_t = a_t_max /100 * j;
    low =0;

```

```

high = m_t;

c_moh = float(B_MOH * KW /h);

for(i = 1; i <= 50; i ++)
{
    m = (low + high)/2;

    bba = b_ma * m + c_mha *m+ c_h2a +c_ha +1;

    if(code ==5)
        a = a_t / (1+h/ka3+h*h/ka2/ka3+(b_ma+b_mha*h/ka3+
            b_mh2a*h*h/ka2/ka3)*m);
    else
    {
        if(b_ma2 == 0)
            a = a_t/bba;
        else
            a = float((sqrt(bba*bba + 8*b_ma2 * a_t*m)
                - bba)/(4*b_ma2*m));
    }

    if(code == 5)
        m_t2 = float((1+c_moh+ c_moh2)*m +
            (b_ma+b_mha*h/ka3+b_mh2a*h*h/ka2/ka3)*m*a);
    else
        m_t2 = float((1+c_moh+ c_moh2)*m +
            (b_ma+ c_mha)*m*a+b_ma2*m*a*a);

    delt = (m_t2 - m_t)/m_t;

    if(delt > 0)
        high = m;
    else
        low = m;

    if(delt<0.001 && delt >-0.001)
        break;
}

```

//Equation used in calculation

```

f_moh = c_moh *m *100/m_t;

f_moh2 = c_moh2 *m * 100/m_t;

f_ma = b_ma *m *a*100/m_t;

if(code == 5)
{
    f_mha = b_mha*m*h*a/ka3*100/m_t;
    f_ma2 = b_mh2a*h*h*m*a/ka2/ka3*100/m_t;
}
else
{
    f_ma2 = b_ma2*m*a*a*100/m_t;
    f_mha = c_mha *m*a*100/m_t;
}

f_m = m*100/m_t;

//Display results on screen

printf("%.2e,%.1f,%.1f,%.1f,%.1f,%.1f,%.1f,%.1f,%.1f,\n",
        a_t, f_moh,f_moh2,f_ma,f_mha,f_ma2, f_m);

//Output results into file "species"

fprintf(infile,"%.2e,%.1f,%.1f,%.1f,%.1f,%.1f,%.1f,%.1f,%.1f,\n",
        a_t, f_moh,f_moh2,f_ma,f_mha,f_ma2, f_m);

}
fclose(infile);

}

```

Appendix 4

Macro Program for ICP/MS Data Treatment

```

'
'
Sub Macro
  Dim threshold As Double
  ActiveCell.Offset(3, 2).Range("A1").Select
  ok = MsgBox("is the element cell on the active cell?", vbYesNo + vbCritical +
vbDefaultButton2)
  If ok = vbYes Then
    bg = InputBox("number of background cells", , 30)
    For i = 0 To bg - 1
      bg2 = bg2 + ActiveCell.Offset(i, -2).Value
    Next i
    bg2 = bg2 / bg
    For i = 0 To bg - 1
      bg4 = bg4 + (bg2 - ActiveCell.Offset(i, -2).Value) ^ 2
    Next i
    bg3 = 3 * Sqr(bg4 / (bg - 1))
    threshold = bg2 + bg3
    default = Str(threshold)
    t = InputBox("threshold", , default)
    threshold = Val(t)
    peak = 0
    j = 0
    i = 0
    n = 0
    Do Until IsEmpty(ActiveCell.Offset(i, -2))
      If ActiveCell.Offset(i, -2).Value > threshold Then

```



```
peak = peak + ActiveCell.Offset(i, -2).Value
n = n + 1

Else
If peak > 0 Then
peak = peak - n * bg2
n = 0
ActiveCell.Offset(j, 0).Value = peak
ActiveCell.Offset(j + 1, 0).Clear
j = j + 1
peak = 0
End If
End If
i = i + 1
Loop
End If
End Sub
```

Appendix 5

Data for Figures

The data used in composing the experimental Figures within this thesis are given in this appendix. The figure number is given at the end of each table caption.

Table A5.1 Data for Figure 2.5.

C_{MeOH} (g/mL)	γ_{MeOH}	C_{THF} (g/mL)	γ_{THF}
0	1.8680	0	20.2383
0.00275	1.8635	0.00205	20.1034
0.00672	1.8571	0.00299	20.0417
0.01490	1.8439	0.00405	19.9726
0.03367	1.8138	0.01083	19.5361
0.05023	1.7873	0.01549	19.2422
0.06786	1.7594	0.03501	18.0548
0.07023	1.7556	0.07401	15.8974
0.2152	1.5345	0.1313	13.1853
0.2510	1.4827	0.2050	10.3557
0.3941	1.2916	0.3535	6.3465
0.4258	1.2532	0.5123	3.7364
0.5336	1.1379	0.7160	1.8570
0.7310	1.0096		

Table A5.2 Data for Figure 2.6.

$C_{\text{MeOH}} \text{ (g/mL)}$	$\chi_{\text{MeOH, mol}}$	$C_{\text{THF}} \text{ (g/mL)}$	$\chi_{\text{THF, mol}}$
0	0	0	0
0.00275	0.00090	0.00205	0.00046
0.00672	0.00324	0.00299	0.00070
0.01490	0.00807	0.00405	0.00097
0.03367	0.01929	0.01083	0.00270
0.05023	0.02935	0.01549	0.00390
0.06786	0.04024	0.03501	0.00903
0.07023	0.04172	0.07401	0.01977
0.2152	0.1400	0.1313	0.03684
0.2510	0.1672	0.2050	0.06161
0.3941	0.2930	0.3535	0.1246
0.4258	0.3258	0.5123	0.2244
0.5336	0.4565	0.6820	0.4119
0.7310	0.8322	0.7160	0.4693
0.7864	0.9969	0.8811	1.000

Table A5.3 Data for Figure 3.6.

Loading Time (min.)	Signal from Eluate
0	0
10	67.8
20	72.5
30	74.2
40	73.8
60	73.5

Table A5.4 Data for Figure 3.7.

Loading Time (min.)	Signal from Eluate
0	0
10	69.2
20	71.5
40	75.0
60	74.2
80	74.2

Table A5.5 Data for Figure 3.8.

Loading Time (min.)	Particle Diameter (div.)
0	208.5
2	217.5
5	216.5
20	217.3
60	217.7
120	217.2

Table A5.6 Data for Figure 4.1.

MeOH		THF	
Activity	$V_{\text{MeOH},S}$ (mL/g)	Activity	$V_{\text{THF},S}$ (mL/g)
0.00172	$0.00188 \pm 4.47 \times 10^{-5}$	0.00923	$0.00937 \pm 6.55 \times 10^{-5}$
0.00605	$0.00392 \pm 1.92 \times 10^{-4}$	0.0140	$0.0109 \pm 5.88 \times 10^{-4}$
0.0149	$0.00508 \pm 4.65 \times 10^{-4}$	0.0193	$0.0154 \pm 1.30 \times 10^{-4}$
0.0351	$0.00871 \pm 7.50 \times 10^{-4}$	0.0528	$0.0269 \pm 2.96 \times 10^{-3}$
0.0526	$0.0107 \pm 1.07 \times 10^{-3}$	0.0750	$0.0356 \pm 4.94 \times 10^{-4}$
0.0708	$0.0152 \pm 1.22 \times 10^{-3}$	0.163	$0.0522 \pm 7.42 \times 10^{-3}$
0.0733	$0.0146 \pm 1.59 \times 10^{-3}$	0.314	$0.0717 \pm 4.92 \times 10^{-3}$
0.214	$0.0344 \pm 5.13 \times 10^{-3}$	0.485	$0.0998 \pm 5.10 \times 10^{-3}$
0.247	$0.0401 \pm 6.01 \times 10^{-3}$	0.637	0.115 ± 0.0110
0.378	$0.0668 \pm 9.26 \times 10^{-3}$	0.788	0.142 ± 0.0117
0.408	0.0705 ± 0.0104	0.831	0.170 ± 0.0174
0.520	0.0915 ± 0.0128	0.848	0.203 ± 0.0251
0.839	0.122 ± 0.0176	0.855	0.207 ± 0.0269
0.997	0.131 ± 0.0212	1.00	0.233 ± 0.0310

Table A5.7 Data for Figure 4.2.

MeOH		THF	
Activity	ΔV_p (mL/g)	Activity	ΔV_p (mL/g)
0.00621	0	0	0
0.0141	$0.00664 \pm 4.68 \times 10^{-5}$	0.0132	$0.00420 \pm 5.08 \times 10^{-5}$
0.0241	$0.00932 \pm 5.01 \times 10^{-5}$	0.0266	$0.0108 \pm 1.39 \times 10^{-4}$
0.0474	$0.0178 \pm 1.48 \times 10^{-4}$	0.0679	$0.0356 \pm 6.59 \times 10^{-4}$
0.0863	$0.0213 \pm 1.50 \times 10^{-4}$	0.127	$0.0461 \pm 7.70 \times 10^{-4}$
0.214	$0.0378 \pm 3.36 \times 10^{-4}$	0.261	$0.0767 \pm 2.01 \times 10^{-3}$
0.320	$0.0464 \pm 2.96 \times 10^{-4}$	0.353	$0.0922 \pm 2.21 \times 10^{-3}$
0.411	$0.0548 \pm 5.01 \times 10^{-4}$	0.516	$0.103 \pm 2.11 \times 10^{-3}$
0.522	$0.0593 \pm 7.44 \times 10^{-4}$	0.776	$0.112 \pm 1.70 \times 10^{-3}$
0.625	$0.0596 \pm 7.07 \times 10^{-4}$	0.812	$0.116 \pm 1.86 \times 10^{-3}$
0.827	$0.0653 \pm 6.82 \times 10^{-4}$	0.832	$0.120 \pm 1.90 \times 10^{-3}$
0.946	$0.0648 \pm 3.10 \times 10^{-4}$	0.878	$0.125 \pm 1.64 \times 10^{-3}$
		1.00	$0.127 \pm 6.48 \times 10^{-4}$

Table A5.8 Data for Figure 4.3.

$V_{\text{MeOH},s}$ (mL/g)	ΔV_p (mL/g)
0	0
0.00389	$0.00664 \pm 4.68 \times 10^{-5}$
0.00609	$0.00932 \pm 5.01 \times 10^{-5}$
0.0100	$0.0178 \pm 1.48 \times 10^{-4}$
0.0162	$0.0213 \pm 1.50 \times 10^{-4}$
0.0366	$0.0378 \pm 3.36 \times 10^{-4}$
0.0545	$0.0464 \pm 2.96 \times 10^{-4}$
0.0700	$0.0548 \pm 5.01 \times 10^{-4}$
0.0875	$0.0593 \pm 7.44 \times 10^{-4}$
0.102	$0.0596 \pm 7.07 \times 10^{-4}$
0.123	$0.0653 \pm 6.82 \times 10^{-4}$
0.132	$0.0648 \pm 3.10 \times 10^{-4}$

Table A5.9 Data for Figure 4.4.

$V_{\text{THF,S}}$ (mL/g)	ΔV_p (mL/g)
0	0
0.0107	$0.00420 \pm 5.08 \times 10^{-5}$
0.0182	$0.0108 \pm 1.39 \times 10^{-4}$
0.0330	$0.0356 \pm 6.59 \times 10^{-4}$
0.0453	$0.0461 \pm 7.70 \times 10^{-4}$
0.0627	$0.0767 \pm 2.01 \times 10^{-3}$
0.0727	$0.0922 \pm 2.21 \times 10^{-3}$
0.0911	$0.103 \pm 2.11 \times 10^{-3}$
0.121	$0.107 \pm 2.21 \times 10^{-3}$
0.138	$0.112 \pm 1.70 \times 10^{-3}$
0.155	$0.116 \pm 1.86 \times 10^{-3}$
0.177	$0.120 \pm 1.90 \times 10^{-3}$
0.203	$0.124 \pm 2.01 \times 10^{-3}$
0.217	$0.125 \pm 1.64 \times 10^{-3}$
0.229	$0.127 \pm 6.48 \times 10^{-4}$

Table A5.10 Data for Figure 4.5(A): Sorption isotherm of naphthalene on PRP- ∞ from 7/3 MeOH/H₂O adopted from Ells.⁴

Concentration (mL _{NA} /mL _{solution})	V _{NA,S} (mL/g PRP- ∞)
8.426×10^{-8}	$(7.45 \pm 0.74) \times 10^{-6}$
8.426×10^{-7}	$(7.94 \pm 0.27) \times 10^{-5}$
6.888×10^{-6}	$(7.47 \pm 0.25) \times 10^{-4}$
1.694×10^{-5}	$(1.78 \pm 0.08) \times 10^{-3}$
8.458×10^{-5}	$(5.59 \pm 0.10) \times 10^{-3}$
1.561×10^{-4}	$(8.27 \pm 0.24) \times 10^{-3}$
7.709×10^{-4}	$(2.84 \pm 0.08) \times 10^{-2}$
1.547×10^{-3}	$(3.97 \pm 0.08) \times 10^{-2}$
2.866×10^{-3}	$(4.98 \pm 0.15) \times 10^{-2}$
3.674×10^{-3}	$(5.42 \pm 0.15) \times 10^{-2}$

⁴ Ells, B. In *Role of the Matrix in Bandbroadening on Polymeric HPLC Packings*, Ph.D. thesis, University of Alberta, Edmonton, 1998.

Table A5.11 Data for Figure 4.5(B): Sorption isotherm of naphthalene on PRP- ∞ from 0.2/6.8/3 THF/MeOH/H₂O adopted from Ells.⁴

Concentration (mL _{NA} /mL _{solution})	V _{NA,S} (mL/g PRP- ∞)
1.041×10^{-7}	$(2.7 \pm 1.2) \times 10^{-5}$
1.041×10^{-6}	$(6.62 \pm 0.45) \times 10^{-5}$
5.206×10^{-6}	$(2.72 \pm 0.05) \times 10^{-4}$
1.041×10^{-5}	$(5.45 \pm 0.11) \times 10^{-4}$
1.650×10^{-4}	$(5.22 \pm 0.10) \times 10^{-3}$
8.040×10^{-4}	$(1.88 \pm 0.01) \times 10^{-2}$
1.961×10^{-3}	$(3.37 \pm 0.03) \times 10^{-2}$
3.367×10^{-3}	$(4.50 \pm 0.04) \times 10^{-2}$
3.961×10^{-3}	$(4.74 \pm 0.06) \times 10^{-2}$
4.391×10^{-3}	$(4.84 \pm 0.06) \times 10^{-2}$

Table A5.12 Data for Figure 4.5(C): Sorption isotherm of naphthalene on PRP- ∞ from 1/6/3 THF/MeOH/H₂O adopted from Ells.⁴

Concentration (mL _{NA} /mL _{solution})	V _{NA,S} (mL/g PRP- ∞)
7.882×10^{-7}	$(1.00 \pm 0.06) \times 10^{-4}$
7.882×10^{-6}	$(2.25 \pm 0.06) \times 10^{-4}$
7.930×10^{-5}	$(2.03 \pm 0.05) \times 10^{-3}$
3.965×10^{-4}	$(7.49 \pm 0.25) \times 10^{-3}$
7.480×10^{-4}	$(1.27 \pm 0.01) \times 10^{-2}$
1.821×10^{-3}	$(2.29 \pm 0.04) \times 10^{-2}$
1.192×10^{-3}	$(3.26 \pm 0.05) \times 10^{-2}$
4.982×10^{-3}	$(4.06 \pm 0.034) \times 10^{-2}$
6.542×10^{-3}	$(4.54 \pm 0.04) \times 10^{-2}$
7.836×10^{-3}	$(4.52 \pm 0.09) \times 10^{-2}$

Table A5.13 Data for Figure 4.6: (A) 0/7/3 THF/MeOH/H₂O; (B) 0.2/6.8/3 THF/MeOH/H₂O; (C) 1/6/3 THF/MeOH/H₂O.

Loading Time (min.)	Fraction of equilibrium amount sorbed		
	0/7/3	0.2/6.8/3	1/6/3
0.50	0.055	0.152	0.213
1	0.124	0.218	0.293
3		0.390	
5	0.411		0.632
7		0.693	
10			0.713
15	0.628	0.783	
20	0.729	0.866	0.870
30	0.797	0.931	0.938
40		0.959	0.961
45	0.904		
60	0.936	0.974	0.999
85	0.946		
90		1.014	1.035

Table A5.14 Data for calculated perturbation factors with varying $\text{Log}(K_{f,ML2}[L]^2)$, when $V_o / V_{aq} = 2.00 \times 10^{-6}$, $C_{M, aq} = 5.00 \times 10^{-6} M$, $C_{X, aq} / C_{M, aq} = 0.500$, $\text{Log}K_{ML2} = 3.00$ (Figure 6.1).

Log $K_{f,ML2}'$	Log ($K_{f,ML2}[L]^2$)		
	0	0.7	1.0
-2	1.000	1.000	1.000
-1	1.000	1.000	1.000
0	1.000	1.000	1.000
1	1.000	1.000	1.000
2	1.000	1.000	1.000
3	1.002	1.001	1.000
4	1.020	1.011	1.020
5	1.132	1.067	1.150
6	1.287	1.101	1.380
7	1.128	1.031	1.210
8	1.019	1.004	1.040
9	1.002	1.000	1.004
10	1.000	1.000	1.000
11	1.000	1.000	1.000
12	1.000	1.000	1.000
13	1.000	1.000	1.000
14	1.000	1.000	1.000
15	1.000	1.000	1.000

Table A5.15 Data for calculated perturbation factors with varying $\text{Log } \kappa_{\text{ML}2}$, when $V_o/V_{\text{aq}} = 2.00 \times 10^{-6}$, $C_{\text{M, aq}} = 5.00 \times 10^{-6} \text{M}$, $C_{\text{X, aq}}/C_{\text{M, aq}} = 0.500$, $\text{Log } (K_{\text{f,ML}2}[\text{L}^{-2}] = 1.00$ (Figure 6.2).

Log $K_{\text{f,ML}2}$	Log $\kappa_{\text{ML}2}$		
	3	7	9
-2	1.000	1.000	1.000
-1	1.000	1.000	1.000
0	1.000	1.000	1.000
1	1.000	1.000	1.000
2	1.000	1.000	1.000
3	1.000	1.002	1.002
4	1.020	1.024	1.024
5	1.150	1.174	1.175
6	1.380	1.590	1.608
7	1.210	1.757	1.926
8	1.040	1.374	1.968
9	1.004	1.072	1.814
10	1.000	1.008	1.369
11	1.000	1.000	1.070
12	1.000	1.000	1.008
13	1.000	1.000	1.000
14	1.000	1.000	1.000
15	1.000	1.000	1.000

Table A5.16 Data for calculated perturbation factors with varying $C_{X, \text{aq}} / C_{M, \text{aq}}$, when $V_o / V_{\text{aq}} = 2.00 \times 10^{-6}$, $C_{M, \text{aq}} = 5.00 \times 10^{-6} \text{M}$, $\text{Log } \kappa_{\text{ML2}} = 3.00$, $\text{Log } (K_{f, \text{ML2}}[\text{L}]^2) = 1.00$ (Figure 6.3).

Log $K_{f, \text{MX}'}$	$C_{X, \text{aq}} / C_{M, \text{aq}}$				
	0.5	0.9	1.0	10	1000
-2	1.000	1.000	1.000	1.000	1.000
-1	1.000	1.000	1.000	1.000	1.000
0	1.000	1.000	1.000	1.000	1.004
1	1.000	1.000	1.000	1.000	1.045
2	1.000	1.000	1.000	1.000	1.435
3	1.002	1.004	1.004	1.050	4.125
4	1.020	1.039	1.043	1.420	9.208
5	1.150	1.277	1.309	3.880	10.80
6	1.383	1.919	2.085	8.920	11.00
7	1.214	2.210	2.823	10.80	11.00
8	1.036	1.669	3.152	11.00	11.00
9	1.004	1.147	3.266	11.00	11.00
10	1.000	1.018	3.302	11.00	11.00
11	1.000	1.002	3.314	11.00	11.00
12	1.000	1.000	3.318	11.00	11.00
13	1.000	1.000	3.319	11.00	11.00
14	1.000	1.000	3.319	11.00	11.00
15	1.000	1.000	3.319	11.00	11.00

Table A5.17 Data for calculated perturbation factors with varying $\text{Log}(1-\exp(-kt))$ for EDTA system, at constant values of $V_o / V_{\text{aq}} = 2.00 \times 10^{-6}$, $\text{pH} = 7.00$, $\kappa_{\text{CuL}_2} = 180$, $K_{\text{f, CuL}_2}' = 1.00 \times 10^{10}$, $[\text{L}^-] = 8.25 \times 10^{-9} \text{M}$, $K_{\text{f, CuEDTA}}' = 2.51 \times 10^{13}$. (Figure 6.4).

Log (1-exp(-kt))	$C_{\text{X, aq}} / C_{\text{M, aq}}$				
	0.2	0.4	0.6	0.8	0.9
0.000	1.00	1.00	1.00	1.00	1.00
-0.301	1.00	1.00	1.00	1.00	1.00
-1.00	1.00	1.00	1.00	1.00	1.00
-2.00	1.00	1.00	1.00	1.00	1.01

Table A5.18 Data for calculated perturbation factors with varying $\text{Log}(1-\exp(-kt))$ for glycine system, at constant values of $V_o / V_{\text{aq}} = 2.00 \times 10^{-6}$, $\text{pH} = 7.00$, $\kappa_{\text{CuL}_2} = 180$, $K_{\text{f, CuL}_2}' = 1.00 \times 10^{10}$, $[\text{L}^-] = 8.25 \times 10^{-9} \text{M}$, $K_{\text{f, CuGlycine}}' = 2.94 \times 10^5$. (Figure 6.5).

Log (1-exp(-kt))	$C_{\text{X, aq}} / C_{\text{M, aq}}$				
	0.2	0.4	0.6	1.2	2.0
0.000	1.12	1.26	1.59	1.98	2.87
-0.301	1.13	1.27	1.61	2.00	2.92
-1.00	1.13	1.27	1.62	2.02	2.96
-2.00	1.13	1.27	162	2.02	2.97

Table A5.19 Data for calculated perturbation factors with varying $\text{Log}(1-\exp(-kt))$ for phthalate system, at constant values of $V_o / V_{aq} = 2.00 \times 10^{-6}$, $\text{pH} = 7.00$, $K_{\text{CuL2}} = 180$, $K_{f, \text{CuL2}}' = 1.00 \times 10^{10}$, $[\text{L}^-] = 8.25 \times 10^{-9} \text{M}$, $K_{f, \text{CuPh}}' = 1.66 \times 10^3$, $K_{f, \text{Cu(Ph)}_2}' = 2.88 \times 10^5$. (Figure 6.6).

Log (1-exp(-kt))	$C_{X, \text{aq}} / C_{M, \text{aq}}$				
	200	400	800	1200	2000
0.000	1.33	1.65	2.29	2.95	4.15
-0.301	1.33	1.66	2.31	2.95	4.23
-1.00	1.33	1.66	2.32	2.98	4.30
-2.00	1.33	1.66	2.33	2.99	4.32

Table A5.20 Data for calculated perturbation factors with varying $\text{Log}(1-\exp(-kt))$ for citrate system, at constant values of $V_o / V_{aq} = 2.00 \times 10^{-6}$, $\text{pH} = 6.00$, $K_{\text{CuL2}} = 180$, $K_{f, \text{CuL2}}' = 1.00 \times 10^9$, $[\text{L}^-] = 8.32 \times 10^{-10} \text{M}$, $K_{f, \text{CuCit}}' = 6.02 \times 10^5$. (Figure 6.7).

Log (1-exp(-kt))	$C_{X, \text{aq}} / C_{M, \text{aq}}$		
	40	70	100
0.000	1.82	1.83	1.83
-0.301	2.63	2.64	2.64
-0.602	4.10	4.15	4.17
-0.921	7.49	7.68	7.76
-1.00	8.70	8.96	9.07
-1.25	14.1	14.8	15.1
-1.50	22.1	24.0	24.8
-1.75	33.8	38.6	40.9
-2.00	49.2	60.1	65.8

Table A5.21 Data for Figure 7.4

[Cu ²⁺] (M)	ICP/MS Peak Area Ratio of Cu to Ga
0	0
7.5 x 10 ⁻⁴	0.4292
1.0 x 10 ⁻³	0.5116
2.5 x 10 ⁻³	1.2206
5.0 x 10 ⁻³	2.4013
7.5 x 10 ⁻³	3.4521

Table A5.22 Data for the concentration of extracted CuL₂ /octane (M) in rate curves (Figure 7.5) with varying stirring speed.

Time (min.)	Stirring Speed (rpm)					
	200	400	600	700	850	1000
0	0	0	0	0	0	0
5	3.30x10 ⁻⁴	7.58x10 ⁻⁴	1.35x10 ⁻³		1.46x10 ⁻³	1.32x10 ⁻³
10	9.34x10 ⁻⁴	1.52x10 ⁻³	2.70x10 ⁻³	2.61x10 ⁻³	2.42x10 ⁻³	2.86x10 ⁻³

Table A5.23 Data for the concentration of extracted CuL_2 /octane (M) in rate curves (Figure 7.6) with varying organic drop size.

Time (min.)	Volume of Octane (μL)	
	0.6	1.1
0	0	0
5	1.46×10^{-3}	1.41×10^{-3}
10	2.42×10^{-3}	2.49×10^{-3}
20	4.04×10^{-3}	4.19×10^{-3}

Table A5.24 Data for Figure 7.7.

Experimental Condition		Initial Rates (M/min.)
Stirring Speed (with 0.6 μL octane)	200 rpm	6.60×10^{-5}
	400 rpm	1.52×10^{-4}
	600 rpm	2.70×10^{-4}
	700 rpm	2.61×10^{-4}
	850 rpm	2.92×10^{-4}
	1000 rpm	2.64×10^{-4}
Volume of Octane (with 850 rpm stirring speed)	0.6 μL	2.92×10^{-4}
	1.1 μL	2.82×10^{-4}

Table A5.25 Data for Figure 7.8.

Time (min.)	$[\text{CuL}_2]_{o,t}$ (M)
0	0
5	9.08×10^{-4}
10	1.79×10^{-3}
20	2.80×10^{-3}
30	4.28×10^{-3}
40	5.29×10^{-3}
50	5.64×10^{-3}
60	6.68×10^{-3}

Table A5.26 Data for Figure 7.9.

$[\text{Cu}^{2+}]_{\text{aq}}$ ($\text{M} \times 10^{-5}$)	$[\text{CuLix}]_o$ ($\text{M} \times 10^{-3}$)
0	0
0.005	0.009
0.010	0.019
0.025	0.066
0.050	0.128
0.075	0.180
0.100	0.266
0.250	0.504
0.500	0.908
0.750	1.282
1.000	1.469
2.500	3.065
5.000	5.058

Table A5.27 Data for experimental points in Figure 8.1.

[EDTA] ($M \times 10^{-6}$)	$[Cu^{2+}]_{X=0} / [Cu^{2+}]_{X=0}$
0.00	1.000
1.00	0.743
2.00	0.619
3.00	0.410
4.00	0.156
4.50	0.064
5.00	0.000

Table A5.28 Data for calculated perturbation factors with varying $C_{EDTA, aq} / C_{Cu, aq}$ (Figure 8.2).

Log $K_{f, CuEDTA}'$	$C_{EDTA, aq} / C_{Cu, aq}$				
	0.2	0.4	0.6	0.8	0.9
1	1.000	1.000	1.000	1.000	1.000
2	1.000	1.000	1.000	1.000	1.000
3	1.002	1.002	1.003	1.004	1.004
4	1.010	1.017	1.025	1.034	1.038
5	1.060	1.116	1.176	1.238	1.268
6	1.113	1.250	1.463	1.714	1.857
7	1.070	1.117	1.292	1.240	2.088
8	1.005	1.017	1.055	1.226	1.586
9	1.000	1.002	1.005	1.031	1.124
10	1.000	1.000	1.000	1.003	1.015
11	1.000	1.000	1.000	1.000	1.001
12	1.000	1.000	1.000	1.000	1.000
13	1.000	1.000	1.000	1.000	1.000
14	1.000	1.000	1.000	1.000	1.000
15	1.000	1.000	1.000	1.000	1.000

Table A5.29 Experimental data (solid points) and corrected data (open points) by Perturbation Factor for glycine system. (Figure 8.3)

[Glycine] ($M \times 10^{-6}$)	$[Cu^{2+}]_{X \neq 0} / [Cu^{2+}]_{X=0}$	
	Observed	Corrected
0.0	1.000	1.000
1.0	1.012	0.910
2.0	1.050	0.840
4.0	0.958	0.619
6.0	1.048	0.550
10.0	1.039	0.385

Table A5.30 Data for calculated perturbation factors with varying $C_{\text{Glycine, aq}} / C_{\text{Cu, aq}}$ (Figure 8.4).

Log $K_{f, \text{Cugly}}'$	$C_{\text{Glycine, aq}} / C_{\text{Cu, aq}}$				
	0.2	0.4	0.8	1.2	2.0
2	1.000	1.000	1.000	1.000	1.000
3	1.000	1.000	1.000	1.002	1.010
4	1.010	1.014	1.033	1.051	1.090
5	1.062	1.127	1.267	1.413	1.720
6	1.155	1.366	1.996	2.923	5.170
7	1.088	1.252	2.267	6.422	1.380
8	1.006	1.026	1.321	8.999	7360

Table A5.31 Experimental data (solid points) and corrected data (open points) by Perturbation Factor for phthalate system. (Figure 8.5)

[Phthalate] ($M \times 10^{-4}$)	$[\text{Cu}^{2+}]_{x \neq 0} / [\text{Cu}^{2+}]_{x=0}$	
	Observed	Corrected
0.0	1.000	1.000
2.0	0.988	0.754
4.0	1.024	0.629
8.0	0.997	0.452
12.0	1.022	0.369
20.0	0.999	0.267

Table A5.32 Data for calculated perturbation factors with varying $C_{\text{Phthalate, aq}} / C_{\text{Cu, aq}}$ (Figure 8.6).

Log $K_{f, \text{CuPh}}$	$C_{\text{Phthalate, aq}} / C_{\text{Cu, aq}}$				
	200	400	800	1200	2000
1	1.002	1.000	1.008	1.012	1.018
2	1.018	1.039	1.071	1.110	1.156
3	1.150	1.381	1.760	2.130	2.827
4	2.905	4.722	8.080	11.11	16.26
5	16.68	27.19	40.20	47.80	55.95

Table A5.33 Experimental data (solid points) and corrected data (open points) by Perturbation Factor for citrate system. (Figure 8.7)

[Citrate] ($M \times 10^{-6}$)	$[Cu^{2+}]_{x \neq 0} / [Cu^{2+}]_{x=0}$	
	Observed	Corrected
0.0	1.000	1.000
4.0	0.689	0.336
7.0	0.517	0.224
10.0	0.421	0.169

Table A5.34 Data for calculated perturbation factors with varying $C_{\text{Citrate, aq}} / C_{\text{Cu, aq}}$ (Figure 8.8).

Log $K_{f, CuCit'}$	$C_{\text{Citrate, aq}} / C_{\text{Cu, aq}}$		
	40	70	100
2	1.000	1.000	1.000
3	1.000	1.002	1.002
4	1.010	1.016	1.022
5	1.140	1.128	1.084
6	2.922	3.198	3.129
7	6.399	5.782	5.030
8	7.546	6.376	5.392
9	7.688	6.444	5.432
10	7.702	6.450	5.436